

**VARIABLE-ANGLE ELECTRON SPECTROSCOPIC STUDIES OF VARIOUS
POLYATOMIC MOLECULAR SYSTEMS**

Thesis by
Charles Frederick Koerting

In Partial Fulfillment of the Requirements
for the Degree of
Doctor of Philosophy

California Institute of Technology
Pasadena, California

1985

(Submitted November 27, 1984)

© 1985

Charles Frederick Koerting

All Rights Reserved

To my parents, Kurt and Ruth

Acknowledgments

The work contained in this thesis required the cooperation and assistance of many individuals. At this time I would like to acknowledge their help. I owe a great deal to my research advisor Professor Aron Kuppermann. His constant attention to detail provided much insight into the interpretation of the experimental results in addition to helping solve some of the vexing experimental problems I have encountered. He has provided the necessary scientific atmosphere which has encouraged thoroughness and creativity.

I wish to thank Dr. David Edmonson who had the patience to introduce me to the nuts and bolts aspect of experimental chemical physics. Dave was always a ready source of information concerning the troubleshooting and operation of the electron optics he designed for EISIII. I also owe a social debt of gratitude to my co-workers Dorothy Flanagan and Kerry Walzl. Dorothy wrote the computer routines used to analyze the data from the photoelectron experiment and was of great assistance in taming the sometimes temperamental computer associated with that experiment. Kerry helped collect the data on all of the electron-impact experiments presented in this thesis. He has been ever so helpful in formulating and expressing the concepts used to explain the data. Kerry has truly been invaluable to me over the past four years.

I also owe a special thanks to Jerry "Beamer" Winniczek. Jerry has always been an endless source of knowledge concerning computer programming and also wrote the computer programs which allowed us to transfer our data to the chemistry department VAX. Jerry has accompanied me on numerous expeditions totaling thousands of miles of travel by foot, car, and boat. He has always been a party to discussions on a

myriad of topics both scientific and non-scientific.

I also wish to thank the other members of the Kuppermann group both past and present, Dave Moll, Jack Kaye, Jim Garvey, Diane Hood, Paul Hipes, Garth Parker, Joseph Wong, and Steve Cuccaro for their friendship over the years. I also acknowledge the friendship of some of the other students in the chemical physics program at Caltech, Francis Celii, Maureen Hanratty, and Bruce Schilling.

Professors Jack Beauchamp, William Goddard III, Harry Gray and Randy Sparks were all ready sources of ideas and advice concerning the experiments. I thank them for their help.

The work presented in this thesis would not have been possible were it not for the aid and assistance of the personnel of the chemistry department shops. I personally thank Bill Schuelke, Tony Stark, Guy Duremberg, Ray Garcia, and Delmer Dill for their cooperation in the construction, design, and maintenance of the instruments used in these studies. Jim Olsen and Jim Gangwer of the mechanics shop also deserve a hearty thanks for their efforts in keeping the pumping systems on the spectrometer in top condition. I also owe a great deal to Tom Dunn and Jack Guledjian of the electronics shop for the miracles they worked in keeping our electronics in operation.

I wish to thank our group secretaries, Heidi Tanciar and Adria McMillan for their ever-available assistance. I especially thank Heidi who did a great deal of the typing of this manuscript.

I wish to thank Sierra and her parents for their constant patience, understanding, and encouragement over the past five years. Finally I wish to thank my parents because without their help all of this would not have been possible.

Abstract

The complementary techniques of low-energy, variable-angle electron-impact spectroscopy and ultraviolet variable-angle photoelectron spectroscopy have been used to study the electronic spectroscopy and structure of several series of molecules. Electron-impact studies were performed at incident beam energies between 25 eV and 100 eV and at scattering angles ranging from 0° to 90°. The energy-loss regions from 0 eV to greater than 15 eV were studied. Photoelectron spectroscopic studies were conducted using a HeI radiation source and spectra were measured at scattering angles from 45° to 90°. The molecules studied were chosen because of their spectroscopic, chemical, and structural interest. The operation of a new electron-impact spectrometer with multiple-mode target source capability is described. This spectrometer has been used to investigate the spin-forbidden transitions in a number of molecular systems.

The electron-impact spectroscopy of the six chloro-substituted ethylenes has been studied over the energy-loss region from 0-15 eV. Spin-forbidden excitations corresponding to the $\pi \rightarrow \pi^*$, $N \rightarrow T$ transition have been observed at excitation energies ranging from 4.13 eV in vinyl chloride to 3.54 eV in tetrachloroethylene. Symmetry-forbidden transitions of the type $\pi \rightarrow np$ have been observed in trans-dichloroethylene and tetrachloroethylene. In addition, transitions to many states lying above the first ionization potential were observed for the first time. Many of these bands have been assigned to Rydberg series converging to higher ionization potentials. The trends observed in the measured transition energies for the $\pi \rightarrow \pi^*$, $N \rightarrow T$, and $N \rightarrow V$ as well as the $\pi \rightarrow 3s$ excitation are discussed and compared to those observed in the methyl- and fluoro-

substituted ethylenes.

The electron energy-loss spectra of the group VIb transition metal hexacarbonyls have been studied in the 0 eV to 15 eV region. The differential cross sections were obtained for several features in the 3-7 eV energy-loss region. The symmetry-forbidden nature of the ${}^1A_{1g} \rightarrow {}^1A_{1g}$, $2t_{2g}(\pi) \rightarrow 3t_{2g}(\pi^*)$ transition in these compounds was confirmed by the high-energy, low-angle behavior of their relative intensities. Several low-lying transitions have been assigned to ligand field transitions on the basis of the energy and angular behavior of the differential cross sections for these transitions. No transitions which could clearly be assigned to singlet \rightarrow triplet excitations involving metal orbitals were located. A number of states lying above the first ionization potential have been observed for the first time. A number of features in the 6-14 eV energy-loss region of the spectra of these compounds correspond quite well to those observed in free CO.

A number of exploratory studies have been performed. The $\pi \rightarrow \pi^*$, $N \rightarrow T$, singlet \rightarrow triplet excitation has been located in vinyl bromide at 4.05 eV. We have also observed this transition at approximately 3.8 eV in a cis-/trans- mixture of the 1,2-dibromoethylenes. The low-angle spectrum of iron pentacarbonyl was measured over the energy-loss region extending from 2-12 eV. A number of transitions of 8 eV or greater excitation energy were observed for the first time. Cyclopropane was also studied at both high and low angles but no clear evidence for any spin-forbidden transitions was found. The electron-impact spectrum of the methyl radical resulting from the pyrolysis of tetramethyl tin was obtained at 100 eV incident energy and at 0° scattering angle. Transitions observed at 5.70 eV and 8.30 eV agree well with the previous optical

results. In addition, a number of bands were observed in the 8-14 eV region which are most likely due to Rydberg transitions converging to the higher ionization potentials of this molecule. This is the *first* reported electron-impact spectrum of a polyatomic free radical.

Variable-angle photoelectron spectroscopic studies were performed on a series of three-membered-ring heterocyclic compounds. These compounds are of great interest due to their highly unusual structure. Photoelectron angular distributions using HeI radiation have been measured for the first time for ethylene oxide and ethyleneimine. The measured anisotropy parameters, β , along with those measured for cyclopropane were used to confirm the orbital correlations and photoelectron band assignments. No high values of β similar to those expected for alkene π orbitals were observed for the Walsh or Forster-Coulson-Moffit type orbitals.

Table of Contents

	Page
Acknowledgments	iv
Abstract	vi
Table of Contents	ix
CHAPTER 1: INTRODUCTION	1
References	4
CHAPTER 2: INTRODUCTION TO ELECTRON-IMPACT SPECTROSCOPY	5
References	12
Tables	15
CHAPTER 3: THEORY OF ELECTRON IMPACT	16
References	23
CHAPTER 4: EXPERIMENTAL ELECTRON-IMPACT SPECTROSCOPY	25
References	36
Tables	37
Figures	38
CHAPTER 5: ELECTRON-IMPACT SPECTROSCOPY OF THE	
CHLOROETHYLENES	46
References	74
Tables	81
Figures	117
CHAPTER 6: THE SPECTROSCOPY OF THE GROUP VIb TRANSITION METAL	
HEXACARBONYLS AS STUDIED BY ELECTRON-IMPACT	153
References	169
Tables	175
Figures	182

Table of Contents (continued)

	Page
CHAPTER 7: EXPLORATORY STUDIES	207
References	212
Tables	214
Figures	219
CHAPTER 8: INTRODUCTION TO VARIABLE-ANGLE	
PHOTOELECTRON SPECTROSCOPY	229
References	233
CHAPTER 9: THEORY OF PHOTOELECTRON ANGULAR DISTRIBUTIONS	235
References	247
Figures	249
CHAPTER 10: EXPERIMENTAL VARIABLE-ANGLE	
PHOTOELECTRON SPECTROSCOPY	252
References	263
Figures	264
CHAPTER 11: THE ANGLE RESOLVED PHOTOELECTRON SPECTROSCOPY	
OF CYCLOPROPANE, ETHYLENE OXIDE, AND ETHYLENEIMINE	273
References	285
Tables	289
Figures	292

CHAPTER 1

INTRODUCTION

Over the past 80 years, electron spectroscopy has proven itself an invaluable tool in the study of the electronic structures of atoms and molecules. The past 20 years have seen a renaissance occur within this field, primarily due to technological advances in vacuum techniques and methods of electron beam production, energy analysis and detection. Electron spectroscopy is a term which covers a broad range of types of measurements. Many of these techniques are reviewed in the excellent series of monographs on electron spectroscopy edited by C. R. Brundle and A. D. Baker.¹ The common feature in all of these techniques is that they all involve measurements of processes that are either induced by electrons incident upon a target or that involve electrons which are emitted by the target. The target may consist of atomic or molecular gases, solids, or atomic or molecular species adsorbed on surfaces.

The majority of electron spectroscopic techniques may be classified into two major types. In those of the first type, electrons are produced by the interaction of ionizing electromagnetic radiation (usually ultraviolet light \rightarrow x-ray) with the target. This type of electron spectroscopy is usually referred to as photoelectron spectroscopy (PES). In those of the second type of electron spectroscopy, the electrons themselves are used as the excitation source. This type is referred to as electron-impact spectroscopy (EIS). In this work, experiments involving variable-angle, low-energy electron-impact spectroscopy and variable-angle ultraviolet photoelectron spectroscopy will be described.

There are fundamental similarities and differences between both types of experiments. Both involve the measurement of the kinetic

energy of scattered electrons and utilize similar experimental techniques to accomplish this task. The major difference between them concerns the nature of the excitation sources involved. When a vacuum ultraviolet or x-ray photon interacts with a target, as occurs in PES, it is generally annihilated and does not scatter with a different energy than it came in with (the exceptions being Raman and Compton scattering which are not important processes in the experiments under consideration here). On the other hand, when an electron interacts with a target, it is not annihilated but usually scattered either with no change in its kinetic energy (elastic scattering) or with a kinetic energy which is different by a ΔE than its initial energy, where ΔE corresponds to the energy imparted to or removed from the target. Other differences exist in the nature of the information obtained from these experiments. Photoelectron spectroscopy probes the energetics of bound state to ionic state transitions while in the electron impact spectroscopy considered in this thesis, we probe the bound state to bound state excitations.

In spite of the differences between these two kinds of experiments, the information obtained from them is mutually complementary in that both involve the same initial state. One example of this interconnection involves the use of EIS to measure the positions and determine the nature of the Rydberg type excitations of a molecule. These in turn are used to confirm the location and nature of the ionic states observed in PES. Conversely, one can use the locations and band shapes observed in the PES spectrum to approximately predict the position of the Rydberg states of a molecule thereby facilitating the assignment of the states observed by EIS.

An added feature of the studies presented in this work, is the use of

the scattering angle, θ , as an experimental parameter. In the variable-angle, ultraviolet photoelectron spectroscopy experiment, θ is defined as being the angle between the incident photon beam and the ejected electron beam. In the low-energy variable-angle electron-impact spectroscopy experiment, θ is defined as the angle between the incident and the scattered electrons. The use of this variable in the experiments allows one not only to obtain additional information concerning the electronic structure of the target but also provides useful information about the dynamics involved in these processes. Thus the use of θ as an experimental parameter presents us with a "key" to deciphering some of the information contained in the electron kinetic energy spectrum produced by both experiments. In EIS, the measurement of the differential cross section (DCS) for a given excitation as a function of θ allows us to elucidate the nature of the transition and thus shed light on the initial and final states involved. In PES the variation of the DCS as a function of θ allows one to determine the asymmetry parameter, β , which in turn can help identify the initial states involved in addition to identifying whether or not such dynamical processes as shape resonances or autoionization are occurring.

The work which follows can be divided into two major sections. Chapters 2-7 deal with the technique of low-energy, variable-angle electron-impact spectroscopy and its application to the chloro-substituted ethylenes and the group VIb transition metal hexacarbonyls. Chapters 8-11 involve experiments using variable-angle, ultraviolet photoelectron spectroscopy. This technique is described along with its application to a series of three-membered ring heterocycles.

References

- 1) *Electron Spectroscopy, Theory, Techniques, and Applications*. Vols 1-4 edited by C. R. Brundle and A. D. Baker (Academic Press, New York 1977-1980).

CHAPTER 2

INTRODUCTION TO ELECTRON-IMPACT SPECTROSCOPY

The collision of an electron with a gas phase-atom or molecule may result in a number of possible outcomes. Some of these are transfer of translational energy, excitation or de-excitation of internal target states (electronic, vibrational, or rotational), ionization, negative ion formation, molecular fragmentation, or various combinations of these processes. Data from electron scattering experiments are useful not only for the study of the internal states of the target but also for gathering dynamical information about the electron-target interaction. The information gleaned from such experiments has direct application in the study and understanding of upper atmospheric processes,¹ electron beam transport in gases,² gaseous discharges,³⁻⁵ plasma chemistry and physics,⁶⁻⁸ electron beam pumped lasers,^{9,10} and astrophysics.¹¹ In this work, our primary concern is with the inelastic scattering of electrons by gas phase molecular systems. In particular, we will be dealing with the formation of electronic excited states of these systems by the electron-impact process. A knowledge of the energy and nature of these states is important in understanding photochemistry¹² and radiation chemistry and physics.¹³ The transition energies and cross section data also serve to provide "benchmarks" with which to compare *ab initio* electronic structure calculations and calculations of the dynamics of electron scattering. Conversely, accurate calculations may be used to help interpret the data obtained from electron-impact experiments.

In our case, studies of molecular systems are performed by making use of electron energy-loss spectroscopy. Such spectra are obtained by focusing a beam of mono-energetic electrons onto a gas target, usually

contained in a static gas cell or in an effusive molecular beam, and then measuring the energy of the scattered electrons at a given scattering angle, θ , and for a given incident electron energy, E_0 . Care must be taken to keep the gas pressure of the sample low enough so that an electron traversing the interaction region undergoes no more than a single collision otherwise inaccuracies will result in the measured cross-sections and energy losses for the observed transitions. The result of such a measurement is the energy-loss spectrum, and is the electron-impact analog of the optical spectrum. This type of measurement is not new; in fact, the first electron energy-loss spectra were recorded for atomic species by Franck and Hertz^{14,15} in the early 1900's.

Electron impact spectroscopy has several advantages and disadvantages when compared with optical spectroscopy. The major advantage of optical spectroscopy is its superior resolution in the infrared and visible regions of the spectrum. Rotational resolution is not difficult to achieve in this region and is several orders of magnitude better than the typical 20-30 meV resolution achieved with today's state-of-the-art electron-impact spectrometers. Another major advantage of optical spectroscopy is that the theory of optical absorption is much easier than that of low-energy electron-impact spectroscopy and has been the subject of many detailed studies over the past 80 years. Much theoretical work on the interpretation of optical spectra exists and the selection rules are generally well-defined.¹⁶⁻¹⁸ Theoretical work of this type has generally lagged behind somewhat in the field of electron-impact. Even though efforts are being made to rectify this situation, the difficulty of theory involved is still a serious stumbling block.

There are several major advantages to using electron-impact spec-

troscopy over optical spectroscopy. The first of these is that with a single instrument one has the capability of obtaining spectra whose energy-loss extends from the infrared (several meV) clear through the x-ray region of the spectrum (several hundred eV) with a constant energy resolution over the entire range. This capability does not exist for optical spectroscopy, which would require several instruments to scan the same energy-loss range. The advantages of using electron-impact spectroscopy become readily apparent in the spectral region beyond the LiF cutoff frequency (about 12 eV). Very little optical work has been performed in the energy-loss region of 10-20 eV due to the complex instrumentation required for such studies. Using the electron-impact method, it is as easy to study energy-loss regions at 20 eV as it is to study them at 2 eV. The spectral region from 10 to 20 eV is especially interesting in that it contains transitions to super-excited states which lie above the first ionization potentials of the molecules. An understanding of the nature of these states is important to understand the physics and chemistry occurring in this little-studied spectral region. In this region the resolution of electron-impact spectroscopy equals or exceeds that available with typical vacuum-ultraviolet monochromators. The electron-impact method also avoids some of the complications such as line saturation effects which must be contended with when using optical spectroscopy to obtain accurate oscillator strengths for transitions within this region.¹⁹

Electron-impact also has the advantage of possessing two variables in addition to the energy-loss for determining the nature of the excited states of the target. These are the incident energy, E_0 , and the scattering angle, θ , which have no optical analog. It is by varying these two parameters that one can observe and assign transitions forbidden by the

optical selection rules.^{20,21} These include both spin-forbidden and symmetry-forbidden transitions. To see why this occurs, we must first discuss the two modes of excitation which exist in electron-impact spectroscopy. The first mechanism is referred to as the direct or Coulomb excitation. In this case the target sees a rise in the electric field due to the passing electron's charge. The target may absorb energy from this field in a similar manner to which it can be thought to absorb energy from a light wave. By conservation of energy, the amount of energy the target absorbs shows up as an energy-loss experienced by the passing electron. Transitions which are primarily excited by this mechanism see a slow increase in intensity as the incident electron energy increases from threshold to 50-100 eV above threshold after which they show a slow decrease as one goes to higher incident energies.²² Transitions excited by this mechanism also exhibit a marked intensity peak at 0° scattering angle, dropping off by one to two orders of magnitude as the scattering angle is increased from $0-90^\circ$.^{20,21} This is due to the relatively long-range nature of the electrostatic force which drives these excitations, as a result of which the electron does not have to pass very close to the target for the latter to "feel" that charge. This results in the majority of the electrons undergoing little or no change in direction after interacting with the target. At high energies and low scattering angles, where the Born approximation holds,²³ this mechanism of excitation obeys the optical selection rules.^{24,25}

The second mechanism of excitation has no optical analog and involves the electron exchange process. This process, first discussed by Oppenheimer^{26,27} involves the physical exchange between the incident electron and a target electron. This type of interaction may have three

possible outcomes. First, an electron in the target may exchange with an incident electron of identical spin and then leave the target carrying with it the same amount of energy the incident electron came in with. Second, the electron may exchange with an electron of identical spin and leave the target with an energy-loss corresponding to an excitation energy of the target. Third, the electron may exchange with an electron of opposite spin and leave the target in an excited state, the outgoing electron leaving with an energy-loss corresponding to the spin forbidden excitation energy. It is this last possible outcome that circumvents the conservation of spin selection rule of optical spectroscopy. One must remember, however, that this $\Delta S=0$ selection rule is not violated for the electron plus target system since the spin of the entire system does not change even though the spin multiplicity of the target changes. Excitations involving the exchange mechanism exhibit rapid intensity decreases as one moves from incident energies near threshold to higher incident electron energies.²⁸ Transitions excited by this mechanism exhibit a nearly uniform intensity as one increases the scattering angle from 10° to 90° . This is due to the scrambling of the directional information carried by the incident electron during the exchange process. It is this trait of spin-forbidden transitions which permits their essentially unambiguous identification in electron-impact spectroscopy in systems for which spin-orbit coupling is small.

Another advantage to using the electron impact method is that it not only allows one to measure transition energies to the excited states of the target that it also permits one to investigate the dynamics of the electron-target collision process. This is usually done by measuring the scattering angle and incident electron energy dependence of the inten-

sity of a given feature in the electron impact spectrum. As mentioned previously, these experimental parameters have no optical analog since photoabsorption is a resonant process in which the photon is annihilated. The measured quantity which is the primary carrier of the dynamical information is known as the cross section. The cross section is defined as being the number of events per unit time per target divided by the number of incident electrons per unit time per unit area²⁹ thus giving the cross section the dimensions of an area per target. There are two kinds of cross sections referred to in describing the collision process. The first is the differential cross section (DCS) which is just the cross section per unit solid angle for scattering into a given direction defined by the spherical polar angles Θ and Φ . In our experiments in the gas phase, the target molecules are randomly oriented with respect to the incident electron beam and thus the Φ dependence of the DCS will vanish.²¹ The other is the integral cross section and is just the differential cross section integrated over all scattering directions. Again, experiments measuring the angular dependence of the DCS for inelastic electron scattering are not new, the first having been performed by Dymond in 1927.³⁰

The angular dependence of the DCS for a given transition in the energy-loss spectrum has proven to be useful in determining the nature of the excited state involved.^{20,21} The DCS of a spin-forbidden transition is generally approximately isotropic and usually remains constant to within a factor of 2 over the angular range of 10° to 90° . As described previously, this is due to the nature of the exchange excitation mechanism. In contrast to this, spin-allowed transitions and elastic scattering display strongly forward peaked DCS's which fall off by one to two orders

of magnitude as the scattering angle is increased from 10° to 90° . Again, this is due to the nature of the excitation process. Spin-allowed but symmetry-forbidden transitions present an intermediate case. DCS's for these transitions do not fall off quite as rapidly as a function of angle as do the fully allowed transitions nor do they remain as constant over the angular range as do spin-forbidden transitions.³¹ Examples of this type of transition occur in both the chloroethylenes and the transition metal hexacarbonyls and makes the identification of the symmetry-forbidden transitions in these compounds a rather straightforward task. It is this ability to observe and assign optically forbidden transitions that makes electron impact spectroscopy the powerful tool that it is. Table 1 shows examples of the enhancements of both types of forbidden transitions as observed in the spectrum of helium.

In this work we will be applying these principles to the study of a series of chlorinated ethylenes and the group VIb transition metal hexacarbonyls (chapters 5 and 6, respectively). In chapter 3 a brief introduction to the theoretical foundations of the concepts presented in this chapter will be presented. In chapter 4 the instrument used in these studies will be described. At this point those readers who desire further material concerning electron impact spectroscopy are referred to some of the many reviews that exist on this subject.^{19-21,24,31-35}

References

- 1) K. Takayanagi and Y. Itikawa, *Space Science Reviews* **11**, 380 (1970).
- 2) P. H. de Haan, R. N. Singh, H. J. Hopman, G. C. A. M. Janssen, E. H. A. Granneman, and P. S. Strelkov, *J. Phys. E* **14**, 373 (1981).
- 3) L. G. H. Huxley and R. W. Crompton, *The Diffusion and Drift of Electrons in Gases*, (John Wiley and Sons, New York 1974).
- 4) A. Gilardini, *Low Energy Electron Collisions in Gases; Swarm and Plasma Methods Applied to Their Study*, (John Wiley and Sons, New York 1972).
- 5) E. W. McDaniel, *Collision Phenomena in Ionized Gases*, (John Wiley and Sons, New York 1964).
- 6) T. Taniguchi, H. Tagashira, and Y. Sakai, *J. Phys. D* **10**, 2301 (1977).
- 7) P. D. Edgley and A. von Engel, *Proc. Roy. Soc.* **1370**, 375 (1980).
- 8) A. Kh. Mnatsakanyan, *High Temp.* **12**, 745 (1974).
- 9) C. S. Willett, *Introduction to Gas Lasers: Population Inversion Mechanisms*, (Pergamon Press, New York 1974).
- 10) C. Brau in *Topics in Applied Physics*, vol 30, *Excimer Lasers* (Springer-Verlag, Berlin 1979), p 87.
- 11) J. H. Black, *Astrophys. J.* **222**, 125 (1978).
- 12) J. G. Calvert and J. N. Pitts Jr. *Photochemistry*, (John Wiley and Sons, New York 1966).
- 13) V. I. Makarov and L. S. Polak, *High Energy Chem. (USSR)* **4**, 1 (1970).
- 14) J. Franck and G. Hertz, *Verh. der Phys. Ges.* **16**, 457 (1914).
- 15) J. Franck and G. Hertz, *Z. Physik.* **17**, 409 (1916).

- 16) G. Herzberg, *Infrared and Raman Spectra*, (Van Nostrand, New York 1945).
- 17) G. Herzberg, *Spectra of Diatomic Molecules*, (Van Nostrand, New York 1950).
- 18) G. Herzberg, *Electronic Spectra of Polyatomic Molecules*, (Van Nostrand, New York 1966).
- 19) R. S. Celotta and R. H. Huebner in *Electron Spectroscopy: Theory, Techniques, and Applications*, vol 3 edited by C. R. Brundle and A. D. Baker, (Academic Press 1979), pp 41-125.
- 20) A. Kuppermann, J. K. Rice, and S. Trajmar, *J. Phys Chem*, **72**, 3894 (1968).
- 21) S Trajmar, J. K. Rice, and A. Kuppermann, *Adv. Chem. Phys.* **18**, 15 (1970).
- 22) H. S. W. Massey and E. H. S. Burhop, *Electronic and Ionic Impact Phenomena*, 2nd ed., vol 3 (Oxford University Press, London 1969), pp437, 880, 968.
- 23) N. F. Mott and H. S. W. Massey, *The Theory of Atomic Collisions*, 3rd ed., (Oxford University Press, London 1965), p87.
- 24) E. N. Lassette and A. Skerebele in *Inelastic Electron Scattering, Methods Experimental Physics*, vol 3 (Academic Press, New York 1974),pp 868-951.
- 25) E. N. Lassette, A. Skerebele, and M. A. Dillon Jr., *J. Chem Phys.* **50**, 1829 (1969).
- 26) J. R. Oppenheimer, *Phys Rev* **29**, 433 (1927).

- 27) J. R. Oppenheimer, Phys. Rev. **32**, 361 (1928).
- 28) D. C. Cartwright and A. Kuppermann, Phys. Rev. **163**, 86 (1967).
- 29) A. Messiah, *Quantum Mechanics* vol 2 (John Wiley and Sons, New York 1961) p 833.
- 30) E. G. Dymond, Phys. Rev. **29**, 433 (1927).
- 31) M. A. Dillon in *Creation and Detection of the Excited State*, vol 1 (Dekker, New York 1971), pp 375-427.
- 32) E. N. Lassette in *Chemical Spectroscopy and Photochemistry in the Vacuum Ultraviolet* edited by C. Sandorfy, P. Ausloss, and M. B. Robin (D. Reidel Publ. Co., Dordrecht, Holland 1974), pp 43-73.
- 33) D. E. Golden, Adv. Atom. and Molec. Phys., **14**, 1, (1978).
- 34) S. J. Trajmar, Accts. Chem. Res., **13**, 14, (1980).
- 35) A. Kuppermann, W. M. Flicker, and O. A. Mosher, Chem. Rev **79**, 77 (1979).
- 36) G. Herzberg, *Atomic Spectra and Atomic Structure* (Dover Publications, New York 1944)
- 37) M. S. Yurev, Opt. Spectry., **25**, 157 (1968).
- 38) D. R. Bates, and A. Fundaminsky, J. W. Leech, and H. S. W. Massey, Trans. Roy. Soc., **A243**, 93 (1950).
- 39) J. D. Jobe and R. M. St. John, Phys. Rev., **164**, 117 (1967).
- 40) J. K. Rice, A. Kuppermann, and S. Trajmar, J. Chem. Phys., **48**, 945 (1968).

Table 1.

A Comparison of Some Relative Electron-Impact Excitation Probabilities in Helium with Typical Optical Transition Probabilities. P_{opt} is the Relative Optical Excitation Probability; P_{elec}^T is the Relative Electron-Impact Excitation Probability for an Incident Energy of 35 eV; and $P_{elec}(\theta)$ is the Relative Probability for Electrons to Scatter at an Angle θ After Causing the Excitation for an Incident Energy of 35 eV.

Transition	Transition Type	P_{opt}	P_{elec}^T	$P_{elec}(\theta)^f$	
				$\theta = 0^\circ$	$\theta = 70^\circ$
$1^1S \rightarrow 2^1P$	Electric dipole allowed.	1^a	1^a	1^a	1^a
$1^1S \rightarrow 2^1S$	Electric dipole forbidden, electric quadrupole allowed	$10^{-5} - 10^{-8}^b$	0.18^d	0.40	0.21
$1^1S \rightarrow 2^3P$	Spin forbidden, electric dipole allowed.	$\sim 10^{-10}^c$	0.12^e	0.023	1.3

a) The relative probability of this excitation is taken to be unity.

b) Ref. 36

c) Ref. 37

d) Ref. 38

e) Ref. 39

f) Ref. 40

CHAPTER 3

THE THEORY OF ELECTRON IMPACT

In this chapter, we will not attempt any rigorous derivation of the quantum mechanical formalisms of the electron scattering problem. Rather, we will present the results of such derivations with the major emphasis placed on their physical interpretation and their implications for the experimental results. A more detailed theoretical treatment is given in the appropriate reviews on the subject.¹⁻⁵

The theoretical descriptions which follow may be divided into two separate approaches to the interpretation of the electron scattering problem. The first approach makes use of potential scattering theory in order to determine the general behavior of the differential cross section (DCS) for both the direct (Coulomb scattering) and exchange scattering processes. The second approach involves the use of the first Born approximation to show the relation between optical spectroscopy and electron-impact spectroscopy.

We will now show how the general behavior of the DCS for the various processes can be obtained from basic potential scattering theory. The argument presented here will generally follow that presented by Trajmar et al.⁶ in their review on electron-impact spectroscopy.

The wave function of the incident electron, when far away from the target molecule⁷, is a plane wave of the form

$$\psi_{inc} = \exp(i\mathbf{p}\cdot\mathbf{r}/\hbar) = \exp(i\mathbf{k}\cdot\mathbf{r}) \quad (1)$$

where the \mathbf{r} is the electron's position vector and \mathbf{k} its wave-number vector. If we orient the z axis along the incident electron direction, equation 1 becomes

$$\psi_{inc} = \exp(ikz) \quad (2)$$

If we now introduce a central field scattering potential, which interacts with the plane wave, the scattered electrons can be thought to emanate from the scattering center as a spherical wave which, as $r \rightarrow \infty$ has the form

$$\psi_{sc} = f(\theta) \frac{\exp(ikr)}{r} \quad (3)$$

where $f(\theta)$ is the amplitude for the electron scattering into the direction making an angle, θ , with the direction of the incident electron. The asymptotic behavior of the electron's total wave function is given by

$$\psi = \exp(ikz) + f(\theta) \frac{\exp(ikr)}{r} \quad (4)$$

and the expression relating the scattering amplitude to the DCS is

$$\frac{d\sigma}{d\Omega} = |f(\theta)|^2 \quad (5)$$

If one applies partial wave analysis¹ to this problem, one can express the incident wave as sum of products of radial and angular functions

$$\exp(ikz) = \sum_{l=0}^{\infty} (2l+1) i^l j_l(kr) P_l(\cos\theta) \quad (6)$$

where j_l is now the spherical Bessel function of order l . One can now think of the scattering process as distorting the plane wave by introducing phase shifts, η_l , in the different angular momentum terms of the incident wave. We can then relate the scattering amplitude to these phase shifts, η_l , by realizing that the wave function must asymptotically reduce to the form of equation 4. This leads to,

$$f(\theta) = \frac{1}{k} \sum_{l=0}^{\infty} (2l+1) \exp(i\eta_l) \sin\eta_l P_l(\cos\theta) \quad (7)$$

l to the DCS. from which we get,⁵

$$\frac{d\sigma}{d\Omega} = \frac{1}{4k^2} \left| \sum_{l=0}^{\infty} (2l+1) (\exp(2\eta_l) - 1) (P_l(\cos\theta)) \right|^2 \quad (8)$$

where each term in the expansion is called a contribution of partial wave l to the DCS. If η_l is small then it can be shown, using a perturbation approach, that⁸

$$\eta_l \cong -\frac{\pi}{2} \int_0^{\infty} [J_{l+\frac{1}{2}}(kr)]^2 U(r) r dr \quad (9)$$

where $U(r)$ is the electron- molecule interaction potential and $J_{l+\frac{1}{2}}$ is a Bessel function.

We now make the assumption that $r^2 U(r)$ has an effective range r_{\max} and that within that range it never exceeds some finite value⁶. Thus we can state the following,

$$r^2 |U(r)| \leq a \quad 0 < r \leq r_{\max} \quad (10a)$$

$$= 0 \quad r_{\max} < r \quad (10b)$$

With a low enough impact energy such that $\frac{k r_{\max}}{2} \ll 1$ we can use the small argument form of $J_{l+\frac{1}{2}}$.⁹ When applied to equation 9, this gives

$$|\eta_l| < \frac{\pi}{2} \frac{a}{[\Gamma(l+\frac{1}{2})]} \int_0^{r_{\max}} \left(\frac{kr}{2}\right)^{2l+1} \frac{dr}{r} = \frac{2\pi a}{(2l+1)^3} \left(\frac{k r_{\max}}{2}\right)^{2l+1} \frac{1}{[\Gamma(l+\frac{1}{2})]} \quad (11)$$

For small η_l equation 8 can be written as

$$\frac{d\sigma}{d\Omega} \cong \frac{i}{k^2} \left| \sum_{l=0}^{\infty} (2l+1) \eta_l P_l(\cos\theta) \right|^2 \quad (12)$$

We can now obtain a feel for the behavior of the DCS as a function of excitation mechanism. In chapter 2 we discussed the mechanisms of excitation in electron-impact phenomena and pointed out that the range of the direct or Coulomb interaction mechanism is much larger than that

of the exchange interaction. From equation 11 one can see that many more partial waves will contribute to the DCS expressed in equation 12 for the direct mechanism than for the exchange mechanism based purely on the effective range of the interaction potential. Due to the nature of the Legendre polynomials, the more of them that are included in the expansion, the more forward peaked the DCS will become. For the exchange mechanism, less terms are needed and thus the DCS will display a more isotropic behavior. One can also see from equation 11 that if one lowers k (lower incident electron energy) that again fewer partial waves are needed and that the DCS should become more isotropic. Both of these general trends have been verified experimentally.⁶

At higher incident electron energies, we may approach the problem from a different perspective. We will now present the basic arguments used by Celotta and Huebner¹⁰ in relating optical results to electron scattering results in their review of electron-impact spectroscopy. For a detailed discussion on the theory of high energy electron scattering, the works of Bethe¹¹ and Inokuti³ are recommended.

At sufficiently high incident energies one may use the first Born approximation. From it one can write the differential cross section for the scattering of an electron off a ground state target to produce an excited state with an excitation energy of E_n as

$$\frac{d\sigma}{d\Omega} = 4a_0^2 \frac{k'}{k} K^{-4} |\epsilon_n(\mathbf{K})|^2 \quad (13)$$

where \mathbf{K} is the momentum transfer vector $\mathbf{K} = \mathbf{k} - \mathbf{k}'$. One can relate the magnitude of \mathbf{K} to the incident and scattered electron momenta, \mathbf{k} and \mathbf{k}' , and the corresponding kinetic energies T and T' , where $T' = T - E_n$, by the following expression,

$$\begin{aligned} (Ka_0)^2 &= (ka_0)^2 + (k'a_0)^2 - 2kk'a_0^2 \cos\theta \\ &= \frac{T}{R} + \frac{T - E_n}{R} - 2 \frac{[T(T - E_n)]^{1/2}}{R} \cos\theta \end{aligned} \quad (14)$$

The quantity $|\varepsilon_n(\mathbf{K})|$ in equation 13 is defined as the transition matrix element between the initial state ψ_0 and final state ψ_n of the target and can be written as

$$\varepsilon_n(\mathbf{K}) = \langle \psi_n | \sum_{j=1}^N \exp(i\mathbf{K} \cdot \mathbf{r}_j) | \psi_0 \rangle \quad (15)$$

where N is the total number of electrons in the target and \mathbf{r}_j is the position vector of the j th electron. $\varepsilon_n(\mathbf{K})$ is often referred to as the inelastic-scattering form factor and contains the properties of the target. If this expression is summed over all molecular orientations and all degenerate substates, ε_n becomes a function of the magnitude of \mathbf{K} and will be written as $\varepsilon_n(K)$ from now on.

Bethe¹⁰ has introduced the concept of the generalized oscillator strength (GOS) as

$$f_n(K) = \left(\frac{E_n}{R}\right) (Ka_0)^{-2} |\varepsilon_n(K)|^2 \quad (16)$$

We can then use this relation along with equation 13 to obtain the following expression for the DCS in the first Born approximation.

$$\frac{d\sigma}{d\Omega} = \frac{4a_0^2}{T/R} \frac{kk'}{K^2} \frac{f_n(K)}{(E_n/R)} \quad (17)$$

Equation 17 can now be used to introduce the concept of an apparent GOS, $f_n(k, T)$, based on the DCS, whether or not the first Born approximation is valid. It is defined as

$$f_n(K, T) = \frac{1}{4a_0^2} \left(\frac{T}{R}\right) \frac{K^2}{kk'} \frac{E_n}{R} \frac{d\sigma}{d\Omega} \quad (18)$$

where $\frac{d\sigma}{d\Omega}$ is the correct DCS. Defining γ by

$$\gamma^2 = \left(1 - \frac{E_n}{T}\right)^{-1/2} \left[1 - \left(1 - \frac{E_n}{T}\right)^{1/2}\right]^2 \quad (19)$$

we can express K^2/kk' in terms of it as

$$\frac{K^2}{kk'} = \gamma^2 + 4\sin^2\frac{\theta}{2} \quad (20)$$

Equation 18 applies to transitions between discrete states but Inokuti³ has discussed the modification of this expression to include transitions to continuum final states. This is done by replacing σ by $d\sigma/dE$ and $f_n(K)$ by $df(K,E)/dE$. $df(K,E)/dE$ is just the energy-loss density of GOS and is usually summed over all possible discrete and continuum states. This results in

$$\frac{df(K,E)}{dE} = \sum_n \left(\frac{E_n}{R}\right) \left[\frac{|\varepsilon_n(K)|^2}{(Ka_0)^2}\right] \delta(E_n - E) \quad (21)$$

where $\delta(E_n - E)$ is the delta function of energy transfer and \sum_n denotes a sum over discrete states and an integral over continuous ones. Lassetre¹² has shown that the GOS can be obtained from the electron impact spectra regardless of whether or not the Born approximation is valid by extrapolating to $k=0$.

One can now expand the operator in the right-hand side of equation 15 using a power series expansion in the same manner one would expand the optical operator. This yields,

$$\begin{aligned} \varepsilon_n(K) &= \sum_{m=1}^{\infty} \frac{(iKa_0)^m}{m!} \langle \psi_n | \sum_{j=1}^{\infty} \left(\frac{F_j}{a_0} \cdot \mathbf{q}\right)^m | \psi_0 \rangle \\ &= \sum_{m=1}^{\infty} \frac{(iKa_0)^m}{m!} \varepsilon_{n,m} \end{aligned} \quad (22)$$

where \mathbf{q} is a unit vector in the direction of \mathbf{K} . Since only the square of the absolute value of $\epsilon_n(\mathbf{K})$ appears in the expression for the GOS, only the even powers of \mathbf{K} survive. One can see from the power series expansion, that for small \mathbf{K} only the dipole term is important. At large enough \mathbf{K} higher order terms become important and thus by altering \mathbf{K} (which is a function of incident electron energy and scattering angle) one can observe dipole forbidden transitions. This is an important consequence of equation 22.

Now one can relate the GOS to the optical oscillator strength f_n by

$$\lim_{K \rightarrow 0} f_n(K) = \frac{E_n}{R} |\epsilon_{n,1}|^2 = f_n \quad (23)$$

and therefore the optical oscillator strength can be obtained from electron scattering measurements

The importance of the electron exchange process in electron scattering was first pointed out by Oppenheimer^{13,14} in 1928. He pointed out that as the energy of the incident electron decreases the cross section for exchange increases. Furthermore, Goddard¹⁵ and Read and Whitehead¹⁶ have used symmetry arguments to predict the behavior of the DCS for certain types of symmetry-forbidden transitions.

Exact calculations involving the electron scattering problem are at best an extremely difficult if not impossible task involving the solution of an infinite set of coupled integro-differential equations.¹⁷ To circumvent this problem a number of approximate methods have been used to solve these equations or to reformat the problem into a more tractable form. We will not discuss any of these methods at the present time; however, those who are interested are referred to the appropriate reviews¹⁸⁻²¹ and the references they contain.

References

- 1) H. S. W. Massey and E. H. S. Burhop, *Electronic and Ionic Impact Phenomena* Vol 1 (Oxford University Press, London 1969).
- 2) A. Messiah, *Quantum Mechanics* Vol 2 (John Wiley and Sons , New York 1961) pp 833.
- 3) M. Inokuti, Rev. Mod. Phys **43**,297 (1971).
- 4) M. L. Goldberger and K. M. Watson, *Collision Theory*, (John Wiley and Sons, New York 1964).
- 5) N. F. Mott and H. S. W. Massey, *The Theory of Atomic Collisions*, 3rd ed. (Clarendon Press, Oxford 1952).
- 6) S. Trajmar, J. K. Rice , and A. Kuppermann Adv. Chem. Phys **18**,15 (1970).
- 7) D. Saxon, *Elementary Quantum Mechanics* Vol 2 (Holden-Day, San Francisco 1969) pp 352.
- 8) ref 5 pp. 28
- 9 H. S. W. Massey in *Handbuch Der Physik* Vol. 36 edited by S. Flugge (Springer-Verlag, Berlin 1956) pp 240.
- 10) R. J. Celotta and R. H. Huebner *Electron Spectroscopy, Theory, Techniques and Applications* Vol. 3 edited by C. R. Brundle and A. D. Baker (Academic Press, New York 1979) pp 45 - 121.
- 11) H. A. Bethe Ann. Physik **5**, 325 (1930).
- 12) E. N. Lassette, A. Skerebele, M. A. Dillon J. Chem. Phys. **50**, 1829 (1969).
- 13) J. R. Oppenheimer Proc. Nat. Acad. Sci. **14**, 261 (1928).

- 14) J. R. Oppenheimer Phys. Rev. **32**, 361 (1928).
- 15) W. A. Goddard III, D. L. Hustis, D. C. Cartwright, and S. Trajmar Chem. Phys. Lett. **11**, 329 (1971).
- 16) F. H. Read and G. L. Whiterod Proc. Phys. Soc. **82**, 435 (1963).
- 17) I. C. Percival and M. J. Seaton, Proc. Cambridge Soc. **53**, 654 (1957).
- 18) P. G. Burke and W. G. Robb Adv. Atom and Molec. Phys. **11**, 143 (1975).
- 19) N. F. Lane Rev. Mod. Phys. **52**, 29 (1980).
- 20) D. W. Norcorss and L. A. Collins Adv. Atom. and Molec. Phys. **18**, 36 (1982).
- 21) *Electron and Photon-Molecule Collision Processes*, edited by T. Rescigno, V. McKoy, and B. Schneider (Plenum, New York 1979).

CHAPTER 4

EXPERIMENTAL ELECTRON-IMPACT SPECTROSCOPY

The results presented in this thesis were obtained using a modified version of the Model III electron-impact spectrometer (EISIII) which has been described in the Ph.D. theses of W. M. Flicker¹, R. P. Frueholz² and R. Rianda.³ In this chapter we will present a brief description of the experimental apparatus with emphasis being placed on the changes made in the instrument over the past five years. The instrumentation will be discussed in the following sections and a review of the data handling procedures will also be included.

a) Vacuum system

The vacuum system used in these studies has been described previously by Rice⁴ and Flicker⁵ and consists of a #304 stainless steel enclosure of about 70 liters in internal volume (figure 1). The chamber is connected to the pumping system via an 8" diameter flexible metal bellows assembly. The pumping system consists of a 10" pneumatically controlled gate valve, 9" diameter 304 stainless steel elbow, 9" liquid nitrogen trap, 9" freon baffle, and a 9" 1500 liters/second mercury diffusion pump. The speed of the pumping system has been measured to be between 300 and 350 liters/second at the inlet to the main chamber. The diffusion pump is backed by a 500 liter/minute mechanical pump with a 2" diameter freon baffle at its inlet. The freon baffle prevents mercury from the diffusion pump from contaminating the oil in the backing pump. The base pressure of this system under typical operating conditions varies from 1×10^{-7} to 3×10^{-7} torr.

In addition to the main chamber pumping, two additional pumps are mounted on the spectrometer. The electron optics enclosures are

differentially pumped with respect to the main chamber. In the original design,¹ this pumping was to have been provided by a 30 liter/second ion pump. However, this was found to cause problems due to the magnetization of some of the spectrometer parts and was replaced by a 30 liter/second mercury diffusion pump stack consisting of a 2" gate valve, 2" liquid nitrogen trap, and a 2" mercury diffusion pump backed by a 60 liter/minute mechanical pump. The base pressure of this pumping system after several days of pumping varies from 5×10^{-7} to 1×10^{-6} torr. This pumping system can maintain a pressure differential of two orders of magnitude between the electron optics enclosures and the main chamber. This is important, especially when the molecular beam source is used, for maintaining clean electron optics to ensure reliable operation of the spectrometer. The pressure in the optics chamber is usually maintained between 1×10^{-6} and 4×10^{-6} torr. The enclosures around the electron optics also reduce the instrumental noise by shielding them from stray background electrons.

The third source of pumping consists of a liquid nitrogen cooled cryotrap.¹ Though initially designed as a beam dump, it was found that for condensable materials, the pressure in the main chamber was lowered by a factor of 2 to 5 when this pump was used.

The entire vacuum system is under the control of a vacuum interlock system described by Mosher.⁵ This system shuts the gate valve and turns off the diffusion pump in case of an over-pressure. The pressures are monitored at the foreline and at several places on the spectrometer. There is also a vacuum switch on the foreline which shuts down the instrument when the pressure rises above 1 torr. This interlock system also turns off the filament in the electron gun and the high voltage to the

detector in order to prevent damage to these components. The clock circuit which controlled the filling of the 9" cryotrap has been replaced by a liquid nitrogen level sensing Torr Vacuum Products Cryomiser which has proven to be more reliable than the clocks previously used. The 2" diffusion pump trap and the cryopump must be filled manually at approximately 8 hour intervals.

b) R.F. and magnetic shielding

The spectrometer and its associated electronics are contained within a specially designed RF shielded enclosure manufactured by Topatron Inc. This room provides 100 dB attenuation of electromagnetic frequencies in the range of 10^4 to 10^{11} hz. All of the electrical and mechanical feedthroughs into this room are designed to minimize RF transmittance. It had been thought that such shielding was necessary for high resolution work⁴ but we have found that for the resolutions used in this work (30 - 100 meV), that keeping the entrance door to the enclosure open or closed made no difference in the operation of the spectrometer.

Magnetic shielding is very important in ensuring proper operation of this instrument. The magnetic shielding used consists of a single .050" μ -metal shield which reduces the ambient magnetic field within the spectrometer to about 5 milligauss. Even with this shielding, care must be taken not to introduce any highly magnetic materials or objects into the vicinity of the spectrometer. It was found that LN₂ dewars and some tools had a visible effect on the electron beam when brought into the vicinity of the instrument. This was especially true at the lower incident energies (15 - 25 eV).

c) Electron optics

The electron optics form the heart of any electron impact spectrometer since the operating characteristics of the instrument are determined by them. There are two sets of electron optics which may be used with this instrument. The first set is that described in the Ph.D. thesis of W. M. Flicker¹ and was initially tried with negative results. Negligible current was measured at the scattering center (in addition to being difficult to tune) leading to the design of a new set of electron optics. This set was designed by Dr. David Edmonson and is briefly described in the thesis of R. Rianda. For a more detailed discussion of the design parameters used, the reader is referred to laboratory notebook #4377, pp. 11-79. While showing better characteristics than the original optics, this set also proved to have problems in ease of tuning and maintaining a usable electron current at the scattering center. A number of modifications were made before reliable operation was attained. We will thus proceed to describe this last set of optics with the design changes included since it is this set which was used in the collection of all the data presented in this thesis.

The overall optical design, shown in figure 2, is loosely based on that used by Chutjian⁶ with the electron gun used being very similar in design to that described by Mosher.⁵ The electrons are emitted from a heated tungsten electron microscope filament and are extracted through a .050" aperture located in a Pierce element (M9) which is biased at a slightly negative voltage as measured relative to the center of the filament. The electrons are then accelerated through a .035" aperture located in the anode (M7). The anode (M7), condenser (M5), and (M3) form a condensing lens of ratios 2:6:1 which serves to illuminate the entrance window of the analyzer with the image formed at the anode and subsequently translated

to the decelerator lens. Originally two deflecting plates located at 90° with respect to one another were located in the anode. This arrangement was changed to a symmetric configuration using four deflector plates. This change resulted in greatly increased current at the scattering center in addition to simplifying the tuning of the instrument.

The 12:1 decelerator is formed by lens elements M3 and HM1. It is here that the image sizes, pencil angles, and energy of the electron beam are set prior to energy analysis. In the initial design, the window object and pupil were composed of .040" and .030" molybdenum apertures, respectively. These have been changed to two .020" apertures which resulted in slightly lower beam currents as measured at the hemispherical analyzer but increased the beam current transmitted through the analyzer by at least a factor of five as well as providing an increase of a factor of two in the energy resolution. There are four deflector plates located between these two apertures which are used to maximize current transmission and to counter surface potential effects. There is a .1" diameter spatter aperture located in HM1 which serves to prevent stray electrons from entering the hemispherical analyzer. The electron energy analyzers in both the monochromator and analyzer sections of the instrument consist of hemispherical sectors with a mean radius of 2.25". The theoretical $\Delta E/E$ of these analyzers is 1%.

Electrons leaving the monochromator hemispheres are imaged onto a 1:12 accelerator formed by the lens elements HM2 and M4. The window in M4 has a diameter of .040". Lens elements M4, M6 focus, and M6 field form a variable ratio field lens which has been designed to operate over an electron energy range of 10 eV to 200 eV. The M6 field lens element operates at a 3:1 voltage ratio to the M6 focus lens element and also con-

tains four deflector plates for final beam steering. The electrons leave the monochromator optics through a .030" aperture in the exit snout and enter the scattering region. The exit snout, scattering chamber, and entrance snout form a field free region for the electrons to traverse. The apertures in both snouts serve to perform additional collimation of the electron beam as well as separating the main vacuum chamber from the differentially pumped optics chambers. The beam divergence angle has been measured to be about 1.5 degrees. Ideally the interaction region is to be free of both electric and magnetic fields but in practice we have found that in using incident energies below 20 eV is difficult and requires very careful removal of all stray magnetic fields.

Two apertures (.030" and .015") within the exit snout define the 2° acceptance angle of the analyzer system. Electrons traveling through the snout are accelerated by the adder (A11) which serves to add in the energy the electron lost in its interaction with the target gas. This lens is designed to be a "weak" lens in that the focal properties of the electron beam passing through it are not significantly changed. The focus lens (A9) functions over a wide voltage range and focuses the beam onto a 4:1:4 Einzel lens formed by the lens elements A7, A5, and A3. A7 contains another set of 4 deflectors which permit fine beam steering. This Einzel lens translates the image to a 35:1 decelerator formed by lens elements A3 and HA2. The electrons are again energy analyzed by a hemispherical sector analyzer identical to that used in the monochromator.

The detector stage optics are not those originally designed for this set but rather those designed for the original electron optics by W. M. Flicker.¹ The actual differences between the two are minor and they are functionally identical. Basically HA2 and A4 form a 35:1 accelerator

which translates the electrons leaving the hemispheres onto the front cone of a Gallileo 4219 spiral electron multiplier. There is a .030" aperture located in HA2 which functions as the energy resolving aperture. This was changed from the .050" aperture in the initial design. There is a set of deflectors located in A4 in order to prevent "bore sighting" in the electron multiplier but these are not used at present and are just electrically connected to A4. The theoretical voltages for the lens elements are listed in table 1. These voltages only represent good starting points, the actual voltages vary according to the operating conditions and cleanliness of the electron optics.

As mentioned earlier, two of the problems encountered with both sets of optics were the lack of usable current at the scattering center and ease of tunability. It was found in the case of the second set of optics that the asymmetric deflectors were the primary cause of this trouble. The deflectors were changed to symmetric sets in both sets of optics even though the Flicker design was not used in these studies. The instrument wiring has been changed (see pages 154 and 162 of lab book #5000) to accommodate both sets of optics in a way that interchanging them should be an easy task.

Changes were also made to the control panel wiring described in Lab book #4377, pages 140-141. The accelerator and decelerator lens elements on both the analyzer and monochromators were wired together but this was changed such that all the elements were individually adjustable. This has made tuning easier and allows for more complete compensation of surface potential effects.

The monochromator is mounted on a rotating table such that it may be rotated from -15° to $+110^{\circ}$ about the pivot axis with respect to the

analyzer (see figure 3). The actual scattering angle varies from -15° to 100° due to the fact that the analyzer and monochromator are located at an angle of 20° with respect to the horizontal plane (figure 4). This is somewhat less than the 135° maximum scattering angle achievable with the Flicker design. Initially this 20° angle caused difficulty in aligning the optics however the mounting brackets on the front flange were modified so that the entire spectrometer assembly can be tilted -20° with respect to the horizontal plane such that one has a straight line-of-sight through the optics for alignment. As mentioned previously both the analyzer and monochromator optics assemblies are enclosed in differentially pumped housings which maintain pressures below 5×10^{-6} torr during spectrometer operation. The entire spectrometer is mounted on a wheeled cart so that it can be easily removed for servicing (figure 5).

Typical beam currents as measured at the scattering center range from 1 to 20 nanoamps. System resolutions are typically between 50 and 100 meV FWHM as measured for the elastically scattered beam. High resolution spectra have been taken at 30 meV FWHM under optimal conditions.

d) Target source

In the thesis of W. M. Flicker¹, a dual mode target source was described which could either be used as a static gas cell or, with the removal of a cap, a capillary-array molecular beam source. This was all designed into two stainless steel blocks which also contained the electron optics he designed. With the new electron optics, this system could not be used so a new target source had to be devised. A new source was devised in such a way that it would be easy to convert from a static gas cell to a molecular beam target. The static gas cell (figure 6) consists of a

tube of an OFHC copper tube which has a slot of .060" width milled 120° around its circumference at a 20° angle to the horizontal. There are two .060" holes drilled opposite the slot at 0° and 55° which allow the electron beam to exit into the analyzer and Faraday cup assemblies, respectively. The Faraday cup consists of a short length of OFHC copper tubing that is sealed at one end. The tube slides onto a 3/8" OD copper tube and is held in place by three set screws. The 3/8" tube functions as the gas inlet and passes through the differential pumping stand in the center of the table via a rotary seal assembly. In all other respects the sample inlet system closely resembles that described by Flicker.¹

Initially the molecular beam capillary array described by Flicker was tried but it was found to load down the vacuum system without producing a sufficient intensity at the scattering center. A new effusive source was constructed using a #316 stainless steel hypodermic needle of .050" ID and length-to-diameter ratio of 6 (figure 6). This assembly is press fit onto the gas inlet tube and was found to provide adequate gas density at the scattering center without overloading the pumping system. The pressure in the main chamber is approximately a factor of two greater when using the beam source as compared to the static gas cell. DCS measurements using well-known systems were made using both sources to ensure that no artifacts due to surface effects were present.

The third target source which may be used with this instrument is the heated pyrolysis tube (figure 7). This consists of a 1/4" OD quartz tube which is constricted at one end to form a 1/8" OD, .060" ID, .3" long capillary. Around this capillary is wrapped one layer of #316 stainless steel sheathed heater wire (manufactured by Semco Industries) which can generate temperatures up to 1000° C. The heater assembly is

wrapped with a single layer of .005" tantulum foil which acts as a radiation shield. Thermocouples located on the heater assembly are used to monitor the temperature. Temperatues in excess of 800° C have been attained with this source. The characteristics of this source are very similar to the capillary source described previously. The gas inlet line for this source is a #316 stainless steel flexible hose which connects to the normal inlet system at the front flange feedthrough. The flexline permits free rotation over the full angular range of the instrument. Preliminary results (see Chapter 7 of this thesis) indicate this type of source can be used to provide a usable density of free radicals at the scattering center.

There are, however, several problems which must be addressed in future revisions of this design. The major problem incurred is the magnetic field generated by the current flowing through the heater wire. At the maximum heater current a decrease of 20% in the electron beam current at the scattering center was observed. This may cause problems when accurate DCS measurements are desired.

e) Detection and data collection system

Electron detection is accomplished by a Gallileo SEM 4219 electron multiplier. The multiplier is connected into the circuit described by R. Rianda³ with the exception to his design being the replacement of the preamplifier he described by a Mechtronics Nuclear Model 509 NIM preamplifier. This proved to be much more reliable and less noisy. The computer system consists of a MSC 8001, Z80 based single board computer and is fully described in R. Rianda's thesis.³ This computer functions as a programmable multichannel scaler which collects the counts from the electron multiplier and stores them in memory. The computer also sweeps the voltages of the electron energy analyzer while increment-

ing the storage locations in its memory. This results in the collection of the spectrum under study. The computer also displays the spectrum being accumulated on an oscilloscope and can plot the spectrum on an X-Y recorder. The spectra accumulated are stored on floppy disk for transfer to a mainframe computer for further data analysis.

f) Data handling

The data handling programs written by R. Rianda¹ were not used in this work due to the removal of the computer for which they were written. These programs were rewritten so that they would run on the chemistry department VAX 11/780. The floppy disk operating system on the spectrometer computer uses a different storage format than that used by the VAX. To remedy this a translation program was written by J. W. Winniczek which converts data from one storage format to the other. Once the data is transferred, it may be further analyzed by a set of programs based on the series of data analysis programs described by W. M. Flicker¹ and R. Rianda.³ The data resulting from this analysis may either be plotted or stored on magnetic tape.

References

1. W. M. Flicker, Ph.D. Thesis, California Institute of Technology, Pasadena, CA. (1976).
2. R. P. Frueholz, Ph.D. Thesis, California Institute of Technology, Pasadena, CA. (1978).
3. R. Rianda, Ph.D. Thesis, California Institute of Technology, Pasadena, CA. (1981).
4. J. K. Rice, Ph.D. Thesis, California Institute of Technology, Pasadena, CA. (1969).
5. O. A. Mosher, Ph.D. Thesis, California Institute of Technology, Pasadena, CA. (1975).
6. A. Chutjian, *J. Chem. Phys.* **61**, 4279 (1974).

Table 1.
Lens Element Voltages

Monochromator^a

Anode	Condenser	M3	HM1, HM2	M4	M6 Field	M6 Focus
40	200	24	2	24	175	60

Analyzer^b

E ₀	A9 Focus	A4, A3, A7	A5	HA1, HA2
30	100	80	20	3
50	175	110	28	4
70	240	140	35	5
90	300	170	42	6

a) Voltages referenced to the filament center voltage.

b) Voltages referenced to analyzer power bus.

Figure Captions

- Figure 1. Schematic diagram of the electron-impact spectrometer vacuum system. CB1: 9" freon baffle, CB2: 2" freon baffle, CT: 9" LN₂ cryotrap, DP: 9" mercury diffusion pump, E: stainless steel elbow, EL: mechanical pump exit line, FL: foreline, GV: 10" pneumatic gate valve, G1, G2: ionization gages, MP: 500 liter/minute mechanical pump, T1, T2: thermocouple gages, V1: foreline valve, V2: roughing valve, V3: chamber vent valve, V4: foreline vent valve.
- Figure 2. Schematic diagram of the electron optics (set #2).
- Figure 3. Schematic diagram showing the rotation of the monochromator relative to the analyzer about the pivot axis.
- Figure 4. Schematic diagram showing the orientation of the electron energy analyzers to the parting plane and the rotating table.
- Figure 5. Schematic diagram showing the flange cart with the spectrometer mounting table and flange indicated by the dashed lines.
- Figure 6. Schematic diagram showing a) the effusive molecular beam source, b) the static gas cell. AES: analyzer entrance snout, CAP: hypodermic needle capillary, EA: exit aperature, ES: entrance slot, GI: gas inlet, MES: monochromator exit snout.
- Figure 7. Schematic diagram showing the free radical beam source. GI: gas inlet, H: heater, QT: quartz tube, SL: swagelock fitting, TS: tantalum shield.

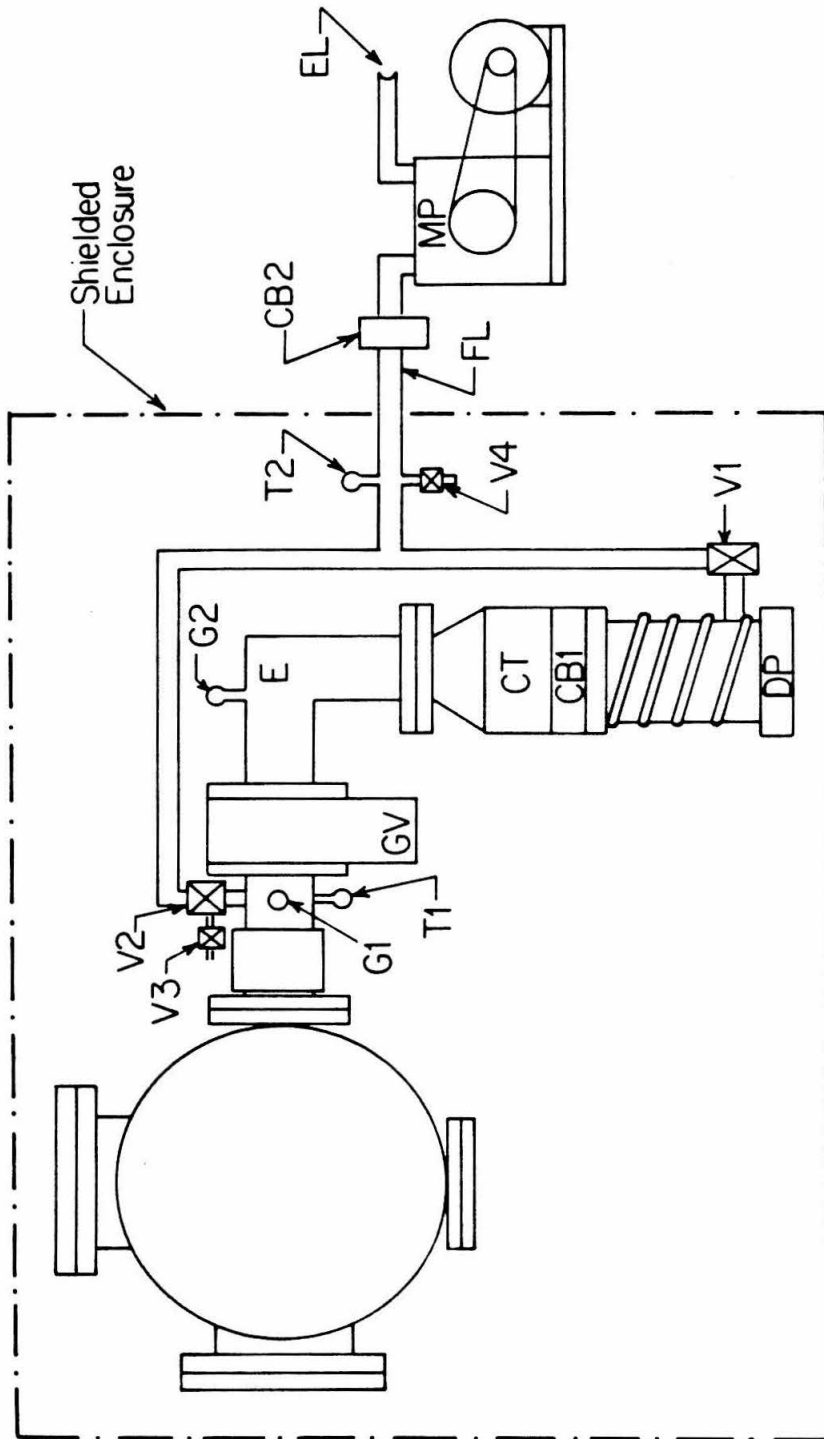


Figure 1.

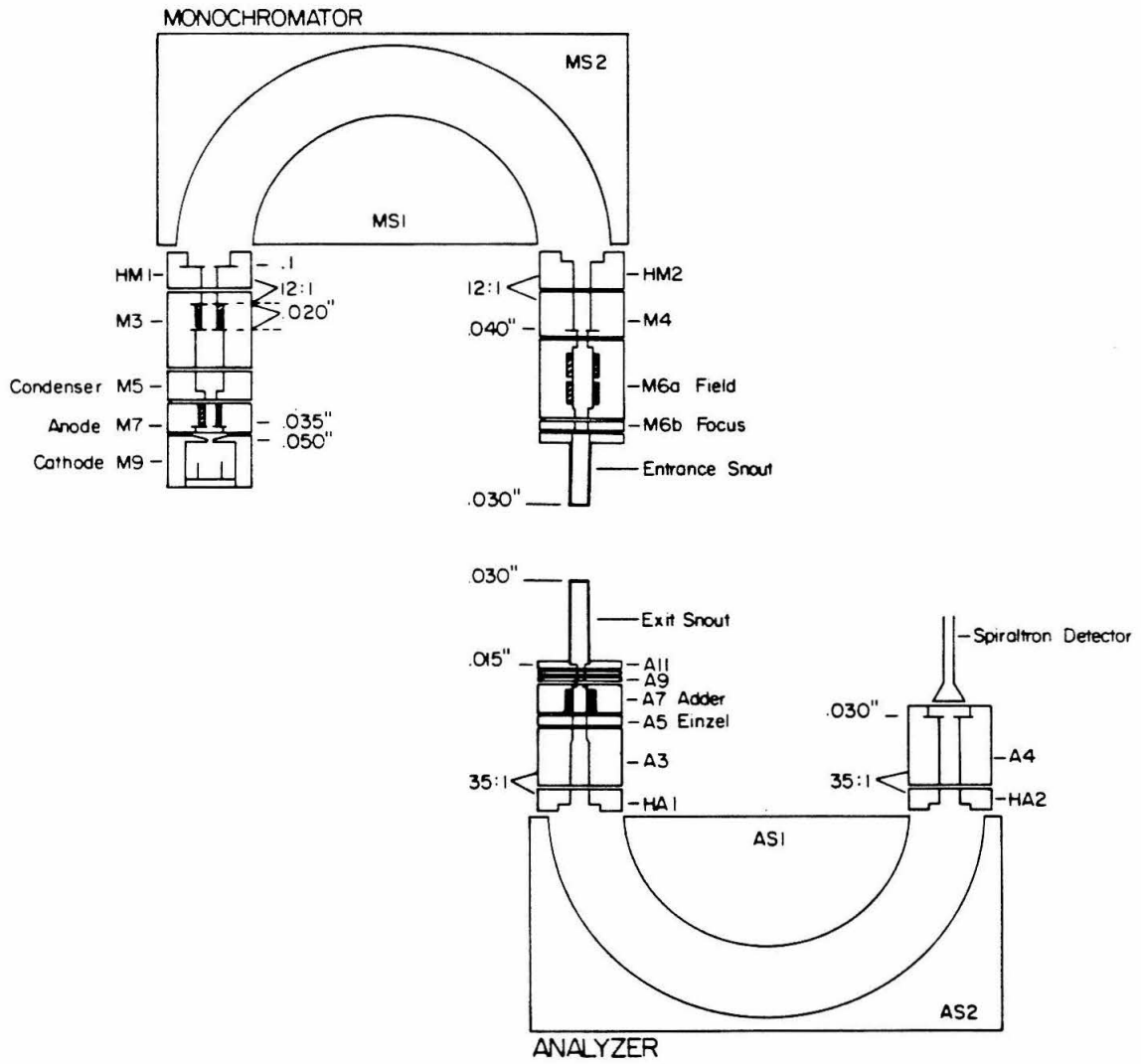
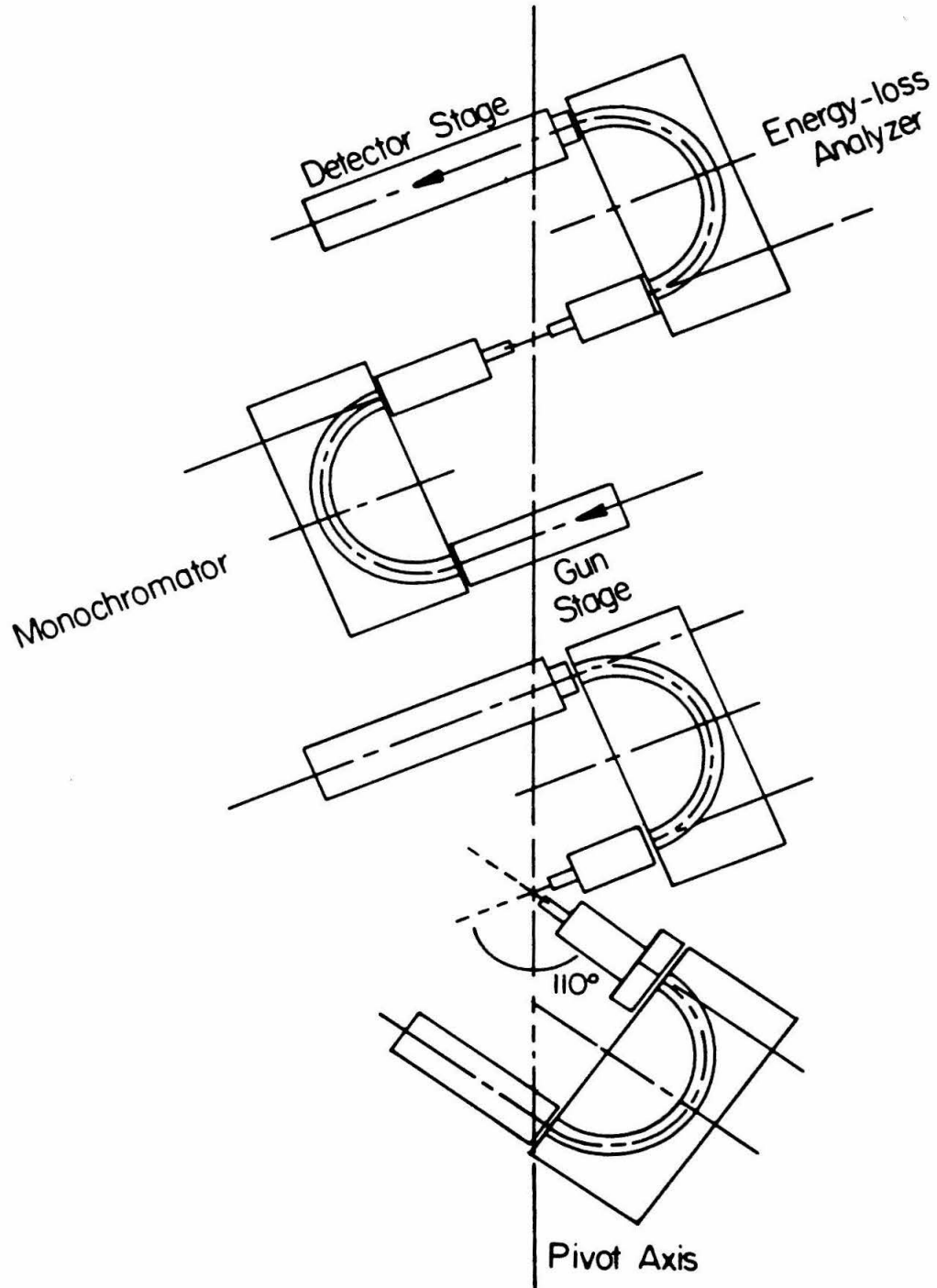


Figure 2.



SPECTROMETER ORIENTATION

Figure 3.

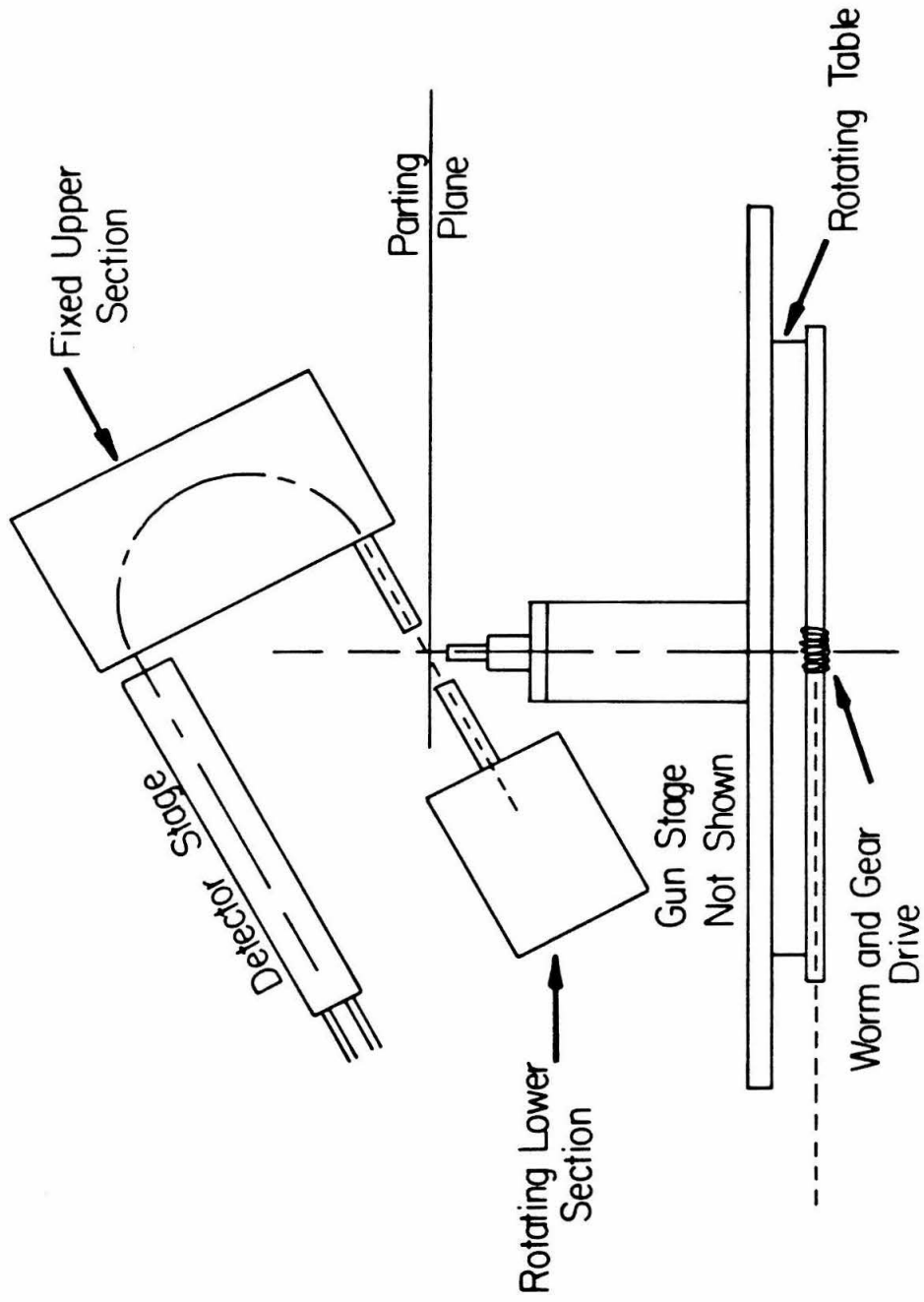
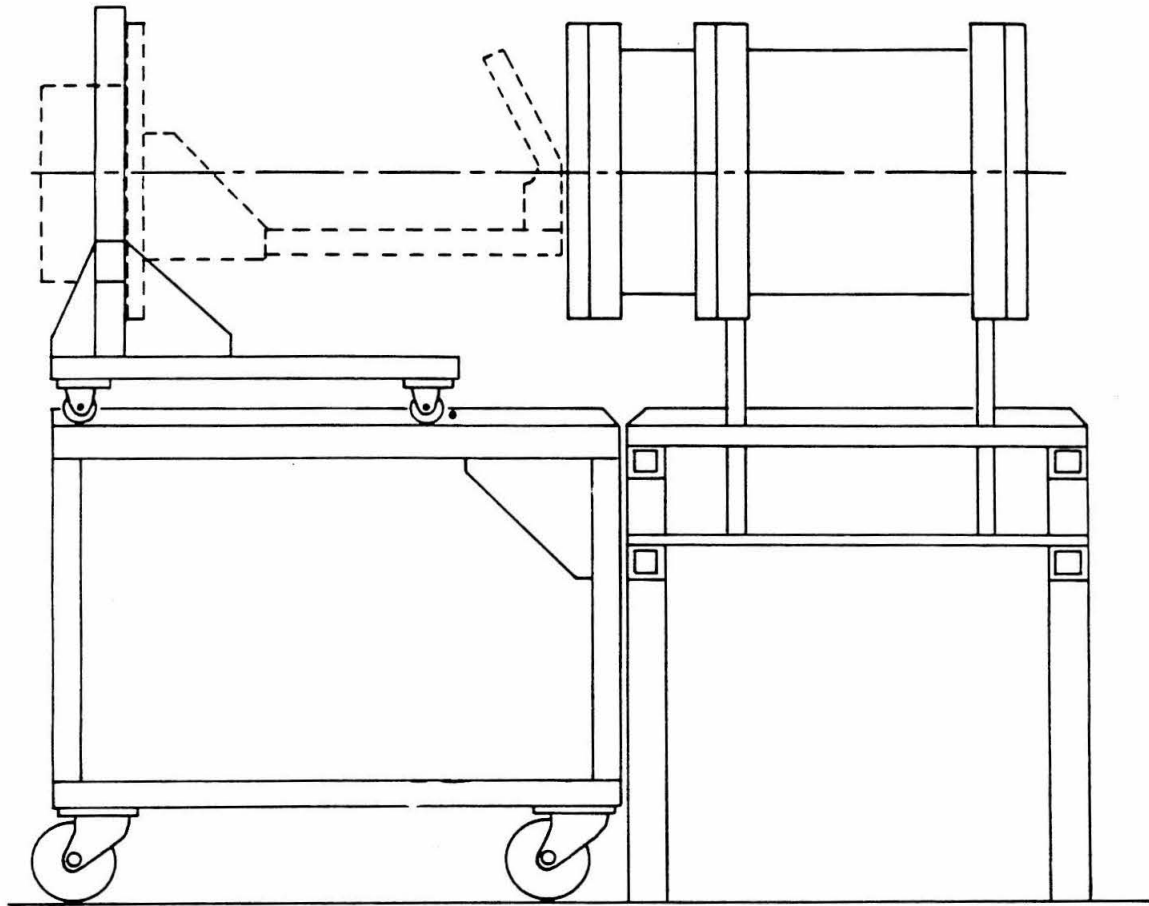


Figure 4.

ORIENTATION OF ENERGY ANALYZERS



ROLLING CART

Figure 5.

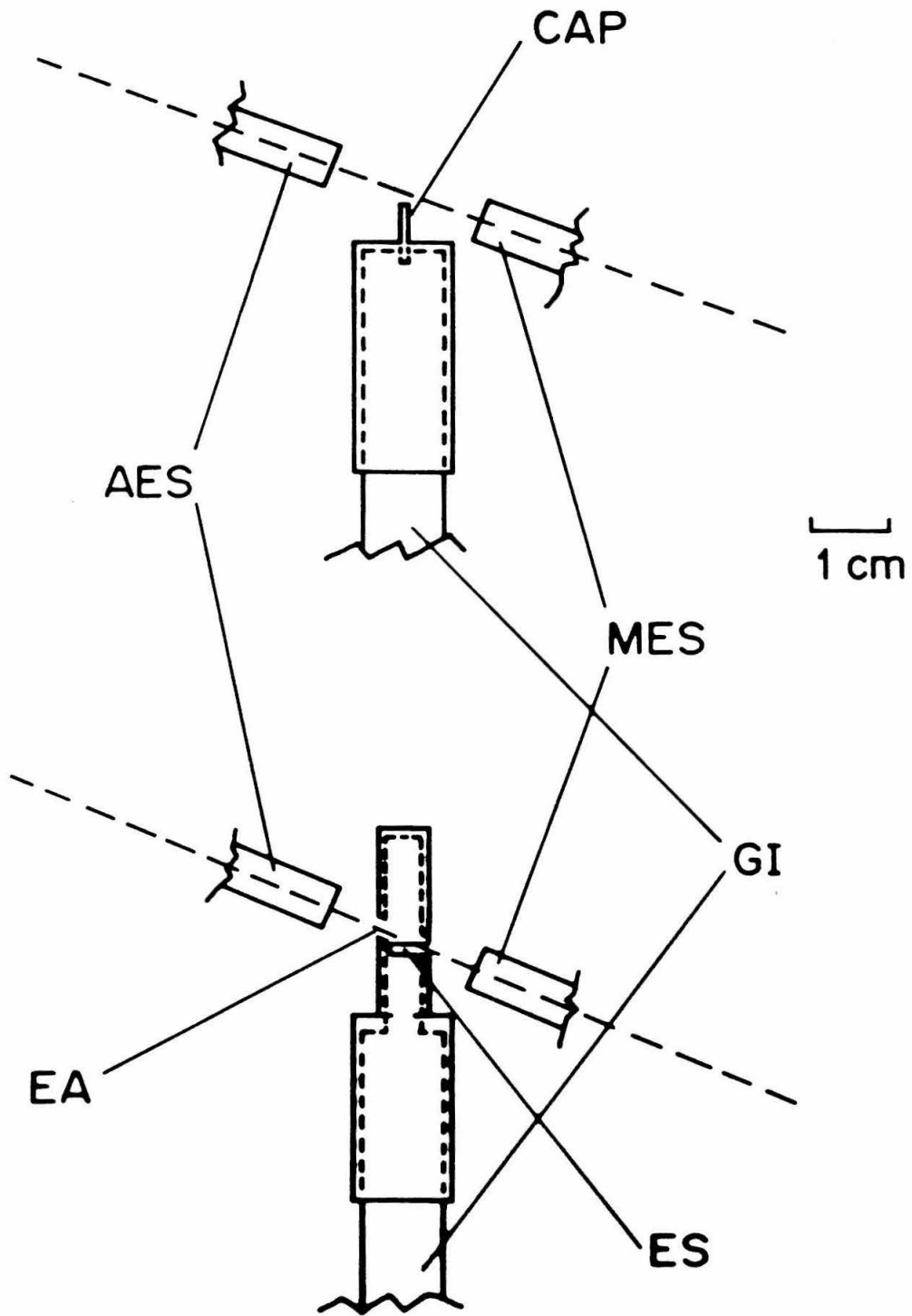


Figure 6.

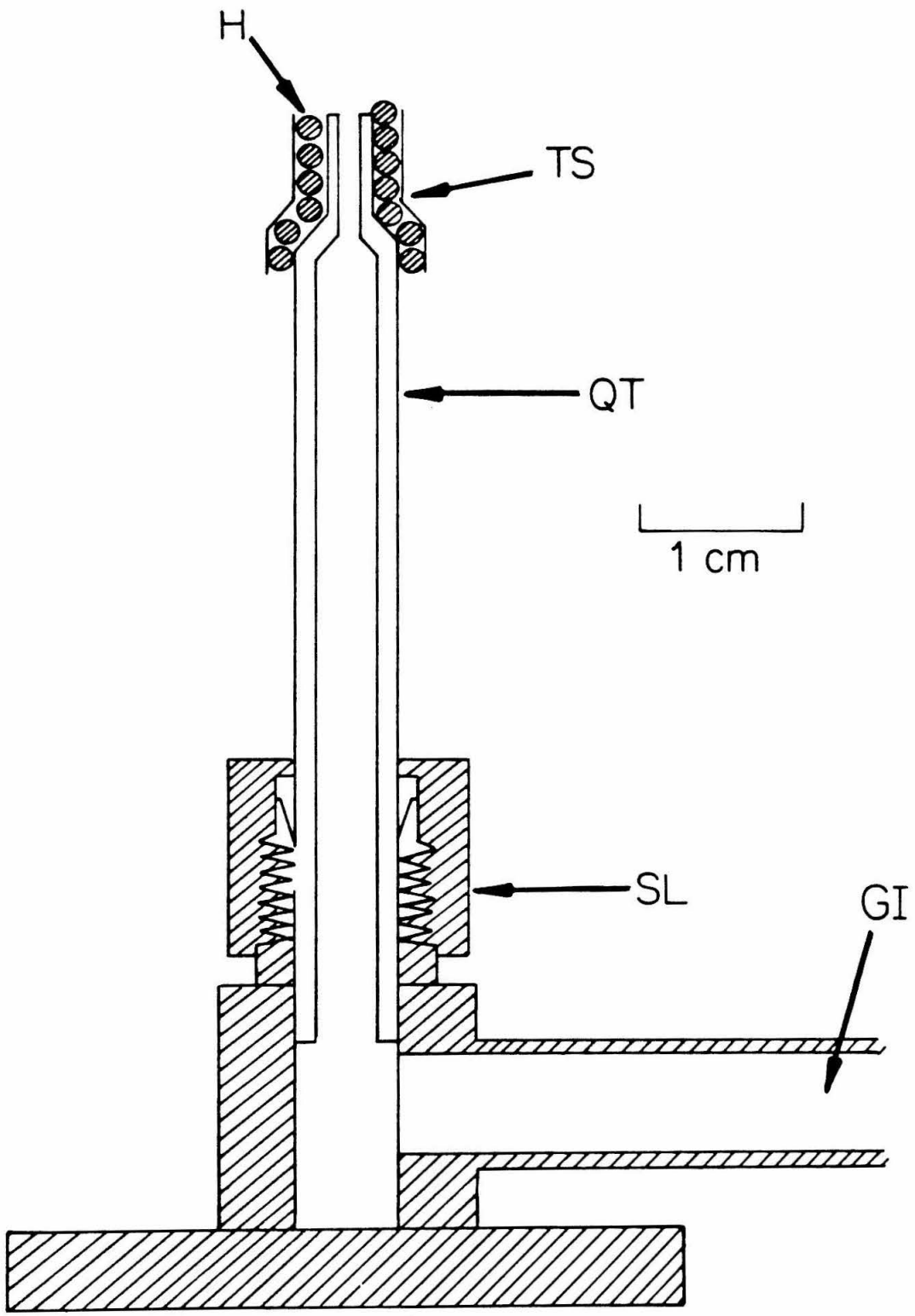


Figure 7.

CHAPTER 5

Paper I:

Electron-Impact Spectroscopy of the Chloroethylenes

Electron-Impact Spectroscopy of the Chloroethylenes

C. F. Koerting^a, K. N. Walzl and A. Kuppermann

Arthur Amos Noyes Laboratory of Chemical Physics,^b

California Institute of Technology, Pasadena, California 91125 USA

Electron-impact spectra of the six chloroethylenes have been obtained at impact energies of 25, 50, and 100 eV and at scattering angles from 0° to 90°. The angular and energy dependence of the relative differential cross sections was obtained for several features in the energy-loss region from 0-11 eV. The behavior of the differential cross section was used to identify transitions as being spin-forbidden, symmetry-forbidden, or fully allowed. In each molecule the lowest transition was identified as being analogous to the N → T transition in ethylene. The position of the excitation maxima for these transitions decreases from 4.13 eV in vinyl chloride to 3.54 eV in tetrachloroethylene. Symmetry-forbidden features were also observed in trans-dichloroethylene and tetra-chloroethylene. Transitions to many states, lying above the first ionization potential, were observed for the first time and assigned as belonging to Rydberg series converging to higher ionization potentials by using the term value method.

^a Work performed in partial fulfillment of the requirements for the Ph.D. degree in chemistry at the California Institute of Technology.

^b Contribution No. ---

I. INTRODUCTION

An extensive quantity of both theoretical and experimental work has been devoted to the study of the electronic structure and spectroscopy of ethylene.¹ By virtue of its being the simplest olefin, ethylene and its derivatives are frequently studied in order to understand the nature of the carbon-carbon double bond and its interaction with substituents. In the present work we have employed the technique of low-energy, variable angle electron-impact spectroscopy^{2,3,4} to study the excited states of the chloro-substituted ethylenes. Previous electron-impact studies of methyl-⁵ and fluoro-⁶ substituted ethylenes have yielded much information concerning the effects of these substituents on the electronic structure of these compounds. Previous optical work on the chloroethylenes⁷⁻²⁰ has focused mainly on the optically allowed transitions in the 5-10 eV excitation energy region. The use of electron-impact spectroscopy not only allows the study of optically allowed states but also permits the study of transitions forbidden by quantum mechanical selection rules.^{3,4} Electron-impact spectroscopy has several distinct advantages over other techniques used for the study of these excitations in that the nature of a transition can usually be uniquely determined by the variance of the cross section as a function of scattering angle, θ , and incident electron energy, E_0 , for cases in which spin-orbit coupling effects are small. Electron-impact spectroscopy also permits easy access to states whose excitation energy is greater than 10 eV. In this work we have undertaken a study of all six of the chloro-substituted ethylenes with this technique. This allows us to observe and study the effect of chlorine substitution on the olefinic bond in both the optically allowed and optically forbidden transitions.

We have obtained electron energy-loss spectra with incident electron energies of 25 eV and 50 eV and at scattering angles at 10° intervals between 10° and 90° . Higher resolution energy-loss spectra were measured at 100 eV incident energy and 0° scattering angles so as to approximate "optical" spectra.¹

In the following sections we shall attempt to summarize the previous experimental and theoretical work on the chloroethylenes. The experimental details of this work will be described and results presented and discussed on a molecule-by-molecule basis. In the case of valence-type excitations, the assignments of the various transitions are made with reference to those in ethylene. For Rydberg transitions the term value approach is used. The relevance of this work to the photochemistry of the chloroethylenes will be discussed, as well as the trends observed in transition energies as a function of substitution. These trends will also be discussed in light of those for other substituents.^{5,6}

II. PREVIOUS WORK

a) *Experimental*

Optical spectroscopic studies of the complete set of the chloroethylenes have been performed by Walsh⁷ and Berry⁸ in the 4 to 10 eV energy region. Walsh and other workers^{9-20,22-26} have also studied individual members of this series. Qualitatively, the spectra of all the chloroethylenes look very similar with the lowest optically allowed transition, analogous to the $N \rightarrow V$, $\pi \rightarrow \pi^*$ excitation in ethylene, occurring as a broad band with some very diffuse structure. The first members of the $\pi \rightarrow nl$ Rydberg series are usually superimposed on the high energy side of this band. Generally one does not see $n \rightarrow \pi^*$, $n \rightarrow \sigma^*$ or $\pi \rightarrow \sigma^*$ type

valence transitions below the first ionization potential (IP) but their presence has been inferred from various shoulders appearing on the $N \rightarrow V$ transition.⁶ The remainder of the spectrum consists mainly of sharp bands which are $Cl3p \rightarrow nl$ Rydberg-type transitions converging to the various ionization potentials of the molecules. Moore²² has previously studied the $N \rightarrow T$, $\pi \rightarrow \pi^*$, singlet \rightarrow triplet excitations in vinyl chloride, 1,1-dichloroethylene, and tetrachloroethylene using ion scattering techniques. This transition occurs as a broad structureless band extending between 2.5 and 4.5 eV.

A large number of photoelectron and photoionization studies have been performed on various members of this series of compounds.²⁷⁻⁴⁷ In the tables of transitions for each molecule we will refer exclusively to the works of Lake and Thompson²⁷ and Von Niessen et al.²⁸

b) *Theoretical*

No high quality, *ab initio* type calculations exist for any of the chloroethylenes. However, semi-empirical MO-type calculations have been performed on this system by several groups. Pellegatti et al.,⁴⁸ and Rajzmann and Pouzard⁴⁹ have calculated $\pi \rightarrow \pi^*$, $N \rightarrow V$ excitation energies while Kato et al.⁵⁰ have not only calculated the positions of $N \rightarrow V$ transitions but have also calculated the positions of the $N \rightarrow T$ excitations. Favani and Simonetta,⁵¹ Howe et al.,⁵² and Fueno and Yamaguchi⁵³ have performed similar calculations on the dichloroethylenes. The results of these calculations will be listed in the tables of transitions for each molecule.

III. EXPERIMENTAL

The apparatus used in this study is basically a new instrument, similar to the Simpson-Kuyatt^{54,55} type electron-impact spectrometers used

previously in our group.^{2,3,56} The major difference between this instrument and our previous ones are

- a) introduction of differentially pumped electron optics,
- b) interchangeable target sources, i.e., static gas cell or effusive molecular beam sources,
- c) larger hemispherical analyzers,
- d) the monochromator and analyzer reside at 20° angles with respect to the horizontal plane.

In brief, it consists of an electron monochromator, which can be rotated about the scattering center from -15° to +100° with respect to the electron energy analyzer. The electron optical schematic is shown in figure 1. The heart of both the monochromator and analyzer systems are two identical 2.25" mean radius hemispherical sector electron energy analyzers. The electron optics themselves are based on the design used by Chutjian.⁵⁷ The target in these experiments can consist of either a static gas cell or an effusive molecular beam. Electrons are emitted from a tungsten hairpin filament, focused onto the plane of the hemispherical analyzer, energy selected, and then focused onto the target. Scattered electrons are then focused onto a second hemispherical analyzer, once again energy analyzed, and then focused onto the front cone of a spiral-tron electron multiplier. The electron optical assemblies are enclosed in housings which are differentially pumped with respect to the main chamber. This keeps the sample gas from contaminating the electron optics. During operation the main chamber pressure range was from $1-2 \times 10^{-5}$ torr with the pressure in the electron optic chambers varying from 1×10^{-6} to 3×10^{-6} torr. Typical beam currents ranged from 1 to 20 nanoamps as measured at the scattering center.

The output pulses from the electron multiplier are amplified and stored in the memory of an MSC 8001, Z80 based microcomputer. This microcomputer is set up to function as a programmable multichannel scaler which also provides a ramp voltage to sweep the electron optics. The resulting spectra may be plotted on an X-Y recorder and stored on floppy disk for transfer to a mainframe computer for further analysis.

The typical resolution used in these studies was set to be between 60 meV and 90 meV as measured by the FWHM of the elastically scattered signal. Higher resolution spectra were taken at resolutions of 30 meV to 45 meV FWHM at 100 eV incident energy for comparison to optical results.

The vinyl chloride used in this study was obtained from Matheson Gas Products and had a stated purity of 99%. The rest of the chlorinated ethylenes were obtained from the Aldrich Chemical Company and had stated purities of better than 97%. All samples were subjected to liquid nitrogen freeze-pump-thaw cycles and a vacuum distillation prior to use to provide some additional purification.

IV. RESULTS AND DISCUSSIONS

a) *Vinyl Chloride*

The transitions observed in vinyl chloride are listed in table 1 along with our tentative assignments. In cases where two or more assignments are possible for one band, all are listed.

The first observed transition (figure 2) occurs as a broad band extending from 3.4 eV to 5.2 eV with a maximum at 4.13 eV. The behavior of the differential cross section (DCS) of this transition as a function of angle (see figures 3,4) immediately reveals that this is a spin-forbidden type of excitation. We assign this transition as being the singlet \rightarrow triplet, N \rightarrow T transition corresponding to the $\pi \rightarrow \pi^*$ excitation. The observed

position of the transition maximum agrees well with the values of 4.08 eV and 4.1 eV obtained by previous electron-impact⁵⁸ and ion impact²² spectroscopic studies, respectively.

Extending from approximately 5.8 eV to 7.5 eV is a strong, broad band, as seen in Figure 5. Examination of a version of that figure with that energy region expanded a few fold reveals that the structure seen consists of some sharp and some diffuse features. Walsh⁷ and Sood and Watanbe²⁰ observed this band optically and found that the maximum of the band with diffuse structure occurred at 6.70 eV with a vibrational spacing of 0.17 eV which corresponds to the excited state C=C stretching frequency. The observed extent and diffuseness of this band was ascribed to a large geometry change in the excited state. Both of these groups assigned this band to the $\pi \rightarrow \pi^*$, N \rightarrow V excitation. In our spectra we observe diffuse shoulders at 6.61 eV and 6.77 eV which we assign to N \rightarrow V bands with the latter being the band maximum. The sharp structure on this band is most likely a $\pi \rightarrow 3s$ Rydberg excitation with a vertical transition energy of 6.72 eV. The remainder of the vinyl chloride spectrum can be ascribed to a multitude of Rydberg series converging to various IP's, which are listed in table 1. The high resolution, low angle spectrum agrees well with the appearance of the spectrum published by Berry⁹ even though he does not list any transition energies or assignments. Walsh⁸ studied the spectrum of vinyl chloride from 5 eV to 10 eV and observed two Rydberg series, $\pi \rightarrow ns$, $\delta = 0.85$ and $\pi \rightarrow nd'$, $\delta = .05$ converging to an IP of 10.00 eV. Sood and Watanbe²¹ confirmed these series and assigned two additional series, $\pi \rightarrow np$, $\delta = 0.58$ and $\pi \rightarrow nd$, $\delta = 0.13$. At 7.82 a structured band appears which Walsh assigned as belonging to an as yet unidentified Rydberg series. Sood and Watanbe also observed

this band and could not assign it to a particular Rydberg series.

It has been shown by previous work⁵⁹ on norboradiene that the intensity ratio of valence to Rydberg transitions changes as a function of incident electron energy. We measured similar ratios for these vinyl chloride "Walsh" bands and found no significant change in the ratio of the intensities of these bands to those of known Rydberg transitions, over the range of 25 eV to 100 eV incident electron energies. This tends to confirm that these bands are predominantly Rydberg in character. There are several other unassigned transitions in the 7 eV to 10 eV energy region which also are probably Rydberg-type excitations.

Reinke et al.¹⁹ have studied the photoabsorption and photoionization of vinyl chloride in the region from 10 eV to 23 eV. They observed 3 Rydberg series converging to an IP of 11.65 eV with quantum defects of $\delta = 0.82, 0.48$ and 0.17 . We observed these bands in our study and have assigned them to $Cl3p \rightarrow nL$ type excitations as did Reinke. However, since Reinke only studied the spectral region of energy >10 eV, we feel that he did not observe the true origins of these series. In Table 2 we list our three series (which agree with his but include additional transitions below 10 eV) as well as three new $Cl3p \rightarrow nL$ series convergent to IP's of 11.78 and 13.56 eV. Robin⁶⁰ and Walsh⁷ have assigned the band at 8.48 eV as being a $Cl3p \rightarrow 4p$ "D" band with a term value of approximately 3.2 eV. We believe that the additional $Cl3p \rightarrow 4p$ type transitions are located at 9.52 eV and 9.62 eV with term values of 2.2 eV and 2.1 eV, respectively. These are lower than but closer to the "normal" term values of 2.5 eV reported for these types of transitions.⁶⁰ Again we must emphasize that our assignments are based on the magnitude of the defects and that they are tentative.

b) *1,1-Dichloroethylene*

With the addition of a second chlorine atom, the spectrum becomes more complicated. The spectrum for $E_0 = 100\text{eV}$ and $\theta = 0^\circ$ shown in figure 6 resembles that published by Berry.⁸ As in vinyl chloride, the first broad band at 3.75 eV is identified as the $N \rightarrow T, \pi \rightarrow \pi^*$ triplet excitation. The enhancement of this transition with respect to the allowed transitions seen in going from 10° to 90° (figure 7) and the behavior of the DCS as a function of angle (figures 8,9) verify that this is a spin-forbidden type of excitation. The value of 3.75 eV obtained for the position of the maximum of this band is somewhat lower than the value of 3.9 eV which was obtained by ion scattering.²²

The $N \rightarrow V, \pi \rightarrow \pi^*$ transition has its maximum at 6.42 eV and numerous shoulders superimposed on both sides of the band. Most of these have not been assigned but most likely represent various vibrational components of the $N \rightarrow V$ transitions. The diffuseness and broadness of this band indicates a large geometry change with respect to the ground state.

The remainder of the spectrum consists mainly of Rydberg excitations to the first five ionization potentials. Walsh et al.¹⁷ identified a $\pi \rightarrow ns(\delta = 0.95)$, two $\pi \rightarrow np(\delta = 0.56, 0.52)$, and a $\pi \rightarrow nd(\delta = 0.18)$ Rydberg series converging to the first IP at 9.86 eV. Teegan and Walsh¹⁶ also noted that the spectrum between 5 eV and 10 eV could be divided into two types of bands. The "a" bands, as they refer to them, consist of groups of transitions which are sharp and have very definite vibrational patterns. The second type or "b" bands are more diffuse and do not exhibit any vibrational structure. The "a" bands were supposed by Walsh et al.¹⁷ to belong to the Rydberg series converging to the first IP while the "b" bands were surmised to belong to a series convergent to higher IP's.

Table 3 lists the components of both types of these bands which we have observed.

Since the VUV work¹⁷ work only extended to 10 eV, the transition energies for 1,1 dichloroethylene above that value presented in Tables 3 and 4 have not been previously measured. In 1,1-dichloroethylene there are four ionization potentials due to electrons from chlorine 3p lone pairs. One thus expects a number of Rydberg series converging to these IP's. Indeed we do observe a number of series convergent to the second, third and fourth IP's. In addition two members of a Cl3p \rightarrow ns($\delta=0.98$) Rydberg series converging to the fifth IP are identified. The assignments again are based on the magnitude of the defect and are tentative.

c) Cis- dichloroethylene

The high energy, low angle electron energy-loss spectrum (figure 10) of cis-dichloroethylene agrees quite well with Berry's⁸ work. As expected the first observed band maximum at 3.94 eV corresponds to the N \rightarrow T, $\pi \rightarrow \pi^*$ triplet excitation. This assignment is supported by the angular behavior of the DCS for this transition (figures 11-13).

The first optically allowed transition is observed as a broad band extending from approximately 5.4 eV to 7.2 eV. The maximum of this band, which we assign as the $\pi \rightarrow \pi^*$, N \rightarrow V singlet transition, occurs at 6.60 eV. Again, as in the other chloroethylenes, numerous shoulders are observed on this band. Most of this structure is diffuse and is most likely associated with various vibrational components of the N \rightarrow V transition. We have assigned some of these shoulders to $\pi \rightarrow 3s$ Rydberg transitions. The apparent diffuseness of this Rydberg excitation is in agreement with the observations of Robin.⁶⁰

As in all the chloroethylenes, the remainder of the observed spectrum is almost exclusively due to Rydberg type excitations convergent upon the various IP's of the molecule. Walsh et al.^{7,18} have identified a $\pi \rightarrow ns$ and a $\pi \rightarrow ns$ Rydberg series from $\delta=0.95$ and $\delta=0.09$ respectively. Walsh and Warsop¹⁸ have also postulated the existence of a $\pi \rightarrow np$ series which we have confirmed with an observed defect of $\delta=0.54$ converging to an IP of 9.65 eV. We did not confirm the two Rydberg series, $\delta=0.05$ and $\delta=0.01$, observed by Mahncke and Noyes²⁶ in their study.

The observed transition energies along with our tentative assignments are listed in table 5. Table 6 consists of a compilation of the observed Cl3p-nl Rydberg series converging to the second and third IPs. In addition to the aforementioned Rydberg series are two bands, one at 12.8 eV and the other at 13.5 eV which we tentatively assign to $\sigma \rightarrow \pi^*$ -type transitions.

d) Trans- dichloroethylene

Interpretation of the spectra of trans-dichloroethylene is more difficult than that of the other members of this series. Walsh⁷ has noted that on the whole the optical spectrum was far more diffuse than that of the other chloroethylenes. The results of our work are compiled in Table 8 along with our tentative spectral assignments. The 100 eV, 0° spectrum is shown in figure 14.

In our studies the $\pi \rightarrow \pi^*$, N \rightarrow T triplet transition occurs as a broad band ranging from 2.9 eV to 4.8 eV with the vertical maximum at 3.84 eV. This assignment is again confirmed by the angular behavior of the DCS for this excitation (Figures 15-17). From 5.5 eV to 7 eV a broad band appears with a large number of diffuse shoulders. This we assign to the N \rightarrow V, $\pi \rightarrow \pi^*$ singlet excitation and is the first optically allowed

transition in the spectrum of this compound. The shoulders on both sides of the 6.36 eV maximum of this band most likely are vibrational components of either the $N \rightarrow V$ transition or of the $\pi \rightarrow 3s$ Rydberg transition, which is assigned to the shoulder appearing at 6.40 eV.

The remainder of the spectrum of this compound is mainly Rydberg in nature. Walsh and Warsop¹⁴ studied the band extending from approximately 8.1 eV to 8.6 eV in detail and assigned it as belonging to either a $\pi \rightarrow ns$ - or $\pi \rightarrow nd$ -type Rydberg series. Earlier Walsh⁷ assigned a number of bands to a series ($\delta=0.72$) converging to an IP of 9.91 eV, which is about 0.3 eV too high. Goto¹⁵ and Mahncke and Noyes²⁶ did not assign any Rydberg series in their studies of this molecule.

In this study we have tentatively assigned various transitions to three Rydberg series, $\pi \rightarrow ns$, $\delta = 0.93$, $\pi \rightarrow np$, $\delta = 0.69$, and $\pi \rightarrow np'$, $\delta = 0.43$. In trans-dichloroethylene the $\pi \rightarrow np$ transitions are forbidden by symmetry selection rules. However, using the fact that the ratios of symmetry-forbidden transitions to fully allowed ones change as a function of incident energy and scattering angle,³ we can use variable angle electron impact spectroscopy to locate and assign these transitions. Figure 18 shows the electron energy-loss spectra taken at several incident energies and angles in the energy-loss region of 7 eV to 9 eV. One can see from observing the relative intensities of the peaks indicated by the vertical arrows that as the incident electron energy is lowered or the scattering angle increased these transitions are enhanced with respect to the other peaks, which correspond to fully allowed transitions. Judging by the apparently different amounts of enhancement of these symmetry-forbidden peaks to the optically allowed one occurring at 8.55 eV, they seem to form two distinct band systems. In both of Walsh's^{7,14} studies

only a very diffuse, continuous absorption was observed in this region. Goto¹⁵ did observe several very weak, diffuse bands which most likely were due to these forbidden transitions. Additional forbidden type bands occur at 8.55, 8.72 and 8.82 eV. These we assign to higher members of the Rydberg series whose $n=3$ members appear in the 7 eV to 8 eV energy-loss region. In figure 19 we now look at the 9 eV to 11 eV energy-loss region. Again we can see enhanced transitions at 9.15, 9.63, 10.58 and 10.79 eV (indicated by arrows) with respect to the optically allowed one at 9.27 eV as the scattering angle is increased from 0° to 10° . The band at 9.15 eV is again assigned as being a higher member of one of the previously mentioned Rydberg series. The band at 9.63 eV and the overall enhancement of the 9.5 to 9.8 eV region with respect to the 9.27 eV peak is probably due to the congestion caused by the large number of Rydberg transitions which converge to the first IP.

The remaining bands at 10.58 eV and 10.79 eV lie above the first IP and are surely due to forbidden $Cl3p \rightarrow nl$ type transitions. As in the other chloroethylenes, these excitations dominate the spectrum above the first IP. The observed $Cl3p-nl$ Rydberg series are summarized in Table 9.

Using the symmetry arguments of Read and Whiterod⁶¹ one expects that there will be no p-type Rydberg series converging to the third IP of this molecule. In our studies, a strong band appears at 9.27 eV which Robin⁶⁰ has assigned to $Cl3p \rightarrow 4p$, "D" band type transition. This implies that either this assignment is incorrect or that the chlorine lone pair orbital, from which the excitation originates, is somehow causing the symmetry constraints to be relaxed. Such apparent violations of symmetry selection rules are also observed in the $Br4p \rightarrow nl$ Rydberg series

in the optical spectra of cis- and trans-dibromoethylene^{62,63} and may be due to a breakdown in the $\delta \rightarrow l$ correspondence.

In addition to the $Cl3p \rightarrow nl$ excitations, there occur two bands, one at 10.68 eV and one at 15.5 eV, which we have tentatively assigned to $\sigma_{C-Cl} \rightarrow 3s$ and $\sigma_{C-H} \rightarrow \pi^*$ transitions respectively.

e) *Trichloroethylene*

With the addition of the third chlorine substituent the spectrum becomes substantially more complex (figure 20). As expected, the first transition is assigned to the $\pi \rightarrow \pi^*$, $N \rightarrow T$, singlet \rightarrow triplet excitation. This is born out by the angular behavior of the DCS (Figures 21-23). This transition occurs as a broad band, extending between 3.0 eV and 4.7 eV, with a maximum at 3.70 eV.

The first optically allowed transition occurs between 5.2 eV and 7.0 eV. This transition is broad and has a maximum at 6.33 eV. It also has a large number of superimposed diffuse shoulders, following the pattern observed in the other chloroethylenes. Again, these are most likely due to vibrational components of the $N \rightarrow V$ transition. Some of these shoulders have been assigned to the $\pi \rightarrow 3s$ Rydberg transition. As mentioned in the previous section, Robin⁶⁰ has noted that the $\pi \rightarrow 3s$ transitions in the chloroethylenes are usually quite diffuse. The possibility that some of the diffuse structure and shoulders seen on the $N \rightarrow V$ band are due to underlying transitions originating from σ or n type orbitals cannot be ignored.

The region between 7.3 and 8.6 eV has been studied in detail by Walsh et al.^{7,13} He assigned the 1686 Å band as coming from three distinct $\pi \rightarrow 3p$ Rydberg transitions. The quantum defects for these transitions are $\delta=0.45$, 0.42 and 0.38. The 1553 Å transition was assigned to either a $\pi \rightarrow ns$ - or $\pi \rightarrow nd$ -type of Rydberg transition. We assign this band to the

$\pi \rightarrow 4s$ transition with a defect of $\delta=0.98$.

No detailed optical spectroscopic studies have been performed above 8.5 eV. This is the region in which one expects the "D" band $Cl3p \rightarrow 4p$ transitions to dominate. We have assigned as "D" bands those occurring at 8.94 eV, 9.27 eV, 9.62 eV, 9.82 eV, 9.90 eV, and 11.35 eV which correlated well with the second through seventh IP's of this molecule. The region of the spectrum beyond the first IP has a large amount of diffuse structure, which is mostly due to Rydberg series converging to the chlorine lone pair IP's. The series we have identified in this work are listed in table 10.

f) Tetrachloroethylene

Tetrachloroethylene has been studied more than any other member of this series. The first band observed in this work appears as a broad, diffuse band extending from 2.6 eV to 4.5 eV with a maximum at 3.54 eV (figure 24). This transition is assigned to the $\pi \rightarrow \pi^*$, $N \rightarrow T$ excitation, and again this assignment is confirmed by the behavior of the DCS as a function of angle (figures 25,26). The value of 3.54 eV for the maximum is substantially lower than the value of 4.2 eV obtained for this transition using ion scattering.²² The $E_0 = 100\text{eV}$ $\theta = 0^\circ$ spectrum from 5 eV to 10 eV energy-loss (figures 27) resembles closely the published optical spectra in this energy range.^{7,8,11,12} The most prominent feature is again the $\pi \rightarrow \pi^*$ $N \rightarrow V$ excitation occurring between 4.7 and 7.2 eV with the maximum at 6.22 eV. Tetrachloroethylene is different from the other members of this series in that there is a large amount of vibrational structure which is discernible on this band. In particular, one can follow the C=C stretch on both sides of the band. Tetrachloroethylene also has a strong $n=3$ member of a $\pi \rightarrow ns$ Rydberg series ($\delta = 0.91$) superimposed

on the short wavelength side of the $N \rightarrow V$ feature. This feature was analyzed in detail by Dauber and Brith¹⁰ who examined the $N \rightarrow V$ transition in the gas phase, solid phase, and in rare gas matrices. Their work also confirmed the presence of a second valence transition at 7.69 eV which was assigned to an $n \rightarrow \pi^*$ type transition.

The remainder of the spectrum consists of Rydberg series converging on the various IP's. Since tetrachloroethylene is a centro-symmetric molecule all $\pi \rightarrow np$ Rydberg series convergent on the first IP are forbidden by symmetry selection rules. Figure 28 compares the electron $E_0 = 100\text{eV}$ energy-loss spectra between 7 and 9 eV at 0° scattering angle, where one expects optical selection rules to hold, with that at 10° scattering angle where symmetry-forbidden transitions are expected to show enhancement with respect to fully allowed excitations.⁶⁵ One does observe excitations showing such behavior, as indicated by the arrows in that figure. Most of these bands can be assigned to the $n=3$ and $n=4$ members of a $\pi \rightarrow np$ Rydberg series ($\delta=0.49$) converging to the first IP. Such symmetry forbidden behavior was also observed in higher energy-loss regions as a changing background but was not clear enough to permit analysis.

At energy losses above 9.5 eV the spectrum consists almost exclusively of $Cl3p \rightarrow nl$ type transitions. Several prominent "D" band $Cl3p \rightarrow 4p$ -type transitions were observed converging and a number of Rydberg series assigned (table 12). $Cl3p \rightarrow 4p$ transitions were also observed to several IP's where, by symmetry, they should have been forbidden. This behavior was also noted in trans-dichloroethylene. These transitions may become more allowed through electronic or vibronic coupling involving the Cl lone pair states in these molecules. Such vibronic

coupling has been invoked by Potts et al.⁴⁷ in their study of this region in the tetrachloroethylene photoelectron spectrum. It is possible that this may be occurring with other members of this series of compounds.

V. PHOTOCHEMISTRY

The chloroethylenes have an interesting and varied photochemical behavior. The photoreactions of these compounds can be classified into three major types: C-Cl bond scission with subsequent radical formation, HCl elimination, and cis-trans isomerization. The type of reaction which is most probable in these systems depends both on the number of chlorine substituents and on the specific electronic state excited.

The cis-trans photoisomerization reaction of the 1,2-dichloroethylenes has been studied by a number of methods. Olson and Maroney²⁵ studied photolyzed compounds with light of $\lambda > 2643 \text{ \AA}$ (4.7 eV). Grabowski and Bylino⁶⁶ studied this same reaction in high pressures of added oxygen⁶⁷ and noted absorption in the 3 to 4 eV energy range. Photosensitized isomerization reactions of the 1,2-dichloroethylenes with $\text{SO}_2(^3\text{B}_1)$,⁶⁸ benzaldehyde,⁶⁹ and 2-butene⁷⁰ have also been studied. These reactions are believed to occur through triplet-triplet energy transfer and the results are consistent with the location of the triplet states in the 1,2-dichloroethylenes. The quenching of triplet ketones by chloroethylenes has also been studied⁷² and is again consistent with the known locations of the triplet states.

Irradiation of the chloroethylenes with UV light ($\lambda < 2400 \text{ \AA}$) results in a large amount of HCl elimination. This HCl is vibrationally "hot" and has been utilized as the lasing species in a photodissociation chemical laser system.⁷²⁻⁷⁶ The photolysis of vinyl chloride has been studied using

direct irradiation^{77,78} and Hg 6(³P₁) sensitization.⁷⁹ Fujimoto et al.⁷⁷ concluded that one excited state was responsible for both the radical reactions and the HCl elimination they observed. They also concluded that the Hg 6(³P₁) photosensitized reaction results were identical with theirs and thus the same excited states were involved in both cases. Ausloss et al.⁷⁸ studied the photochemistry of vinyl chloride in the far UV ($h\nu > 10$ eV) and concluded that a substantial amount of the reactions observed occurred through the ions formed by this irradiation. M. H. J. Wignen and co-workers,⁸⁰⁻⁸³ have concluded from their studies of the dichloroethylenes that two states are involved in the photochemistry of these compounds. Warren et al.⁸⁴ and Tyerman⁸⁵ indicate that the $n \rightarrow \sigma^*$ state may be involved in both its singlet and triplet forms although the initial excitation in the above reaction is undoubtedly the $N \rightarrow V$, $\pi \rightarrow \pi^*$ excitation. Walsh⁸ noted that the spectrum in this region seemed quite diffuse and predissociative, and it is not unreasonable to assume that some crossing into a $N \rightarrow \sigma^*$ state is occurring. This state was not directly identified in our spectra but may be the cause of some of the long wavelength shoulders of the $N \rightarrow V$ band. Certainly more study of the photochemistry of these compounds is needed.

VI. DISCUSSION OF TRENDS IN THE TRANSITION ENERGIES

In a previous publication, we offered a tentative explanation of the transition energy shifts in the $N \rightarrow T$ and $N \rightarrow V$ transitions of the chloroethylenes.⁸⁶ At this point we will look at the trends observed in the $N \rightarrow T$, $N \rightarrow V$, and $\pi \rightarrow 3s$ transition energies (see table 13) not only as a function of the number of substituents but also as a function of the type of substituent. To be specific, we will compare the effects of chloro, fluoro, and methyl substitution on ethylene as compared to ethylene

itself. We will also speculate on the cause of the observed effects.

In figures 25-31 we plot the shift in transition energies (with respect to ethylene) as a function of the number of substitutions, for the $N \rightarrow T$, $N \rightarrow V$ and $\pi \rightarrow 3s$ transition respectively. One sees from these figures that the transition energy shifts for the $N \rightarrow T$ transition are typically one-third to one-half as great in magnitude as those for the $N \rightarrow V$ and $\pi \rightarrow 3s$ transitions. One can also see, from figure 29, that the shift is a linear function of the number of substituents for methyl substitution, and is successively less linear for chloro and fluoro substitution. The relatively low sensitivity of the $N \rightarrow T$ transitions to Cl atom substitution indicates that the substituent effects on the π^* triplet state are nearly the same as their effect on the ground state. Calculation by Dunning et al.⁸⁷ on ethylene showed that the electron spatial distribution in the T state was very similar to that of the N ground state. Assuming, in addition, that the $\sigma-\pi$ separation approximation⁸⁸, so often used in calculating properties of excited olefins is valid, one can rationalize this low substituent sensitivity.

There are two main mechanisms of interaction with the substituent. The first are delocalization effects which in general are stabilizing and the second are repulsive effects which are usually destabilizing. The variations of the transition energy shifts with substituents (figure 29) show that the interaction of methyl groups with the T state is very slight while that of chloro and fluoro groups is much stronger. Thus for methyl groups these two effects would seem to nearly balance one another with delocalization over the CH_3 p orbitals becoming relatively larger with increasing substitution. This is also demonstrated by the minor (0.03 eV) variation for the shifts of the di-substituted isomers with respect to each

other.

With chlorine, the 3p lone pairs in the plane of the π bond can have a significant effect on the T state. This is pointed out by the steep slope of the N \rightarrow T transition energy shift with increasing substitution. The variation among the di-substituted isomers is much greater (0.19 eV) than with the methyl groups. Interestingly enough, the 1,1 isomer seems to show the greatest relative stabilization in the T state. From the analysis of the vibrational structure of some of the Rydberg excitations, Walsh and co-workers^{11,13,14,17,18} have concluded that removal of the π electron results in a strengthening of the C-Cl bond with a consequent increase in the C-Cl stretching frequency and a decrease in the C-C-Cl bond angle. This opening of the Cl-C-Cl bond angle may provide enough relief for the Cl-Cl repulsion to the point where the system is stabilized below the cis and trans isomers. These observations have been theoretically studied by Coulson and Luz.⁸⁹ They argued that removal of a π electron in ionization results in a slight positive charge on the carbon atoms which in turn polarizes the substituent, pulling its electrons closer. This may also occur on excitation to the π^* state. The slight withdrawal of electron density from the Cl may allow the π^* orbital to be delocalized over the Cl to a greater extent. Possible resonance-type interactions of the two chlorines through the common carbon may also contribute to the stabilization of this state. It may be that the lack of such an interaction and the decrease of the C-C-Cl angle will increase the repulsion in the triplet states of cis and trans dichloroethylene in a manner that does not allow them to stabilize to the same extent. If the T state geometry has the end groups perpendicular to each other one would expect these two isomers to share a common triplet state. This assumption is born out by the pho-

tochemical isomerization reactions.^{25,66} Since it is expected that the trans isomer would be the more stable one in the ground state, due to the lack of Cl-Cl repulsion, it should have a higher transition energy. However, this is not what is observed. The cis and trans forms are equally stable to within ± 0.086 eV in the ground states as shown by thermodynamic data⁹⁰ and the adiabatic ionization potentials²⁷ which are the same to within ± 0.02 eV. The fact that the cis isomer has the larger transition energy indicates that the difference may be almost entirely due to the Franck-Condon factors for the transitions.

With fluorine substitution one sees a slight increase in the N \rightarrow T transition energy with increasing substitution. This may be due to the predominance of the repulsive over the delocalization effects. Fluorine is a much "harder" substituent with a lower polarizability than chlorine or methyl, and this type of behavior is therefore expected. In the disubstituted isomer, the 1,1 isomer's transition energy is now substantially higher than for either the cis or trans isomer and the spread among the transition energy shifts is much larger (0.45 eV) than for the corresponding chloroethylenes. The 1,1 isomer's apparent destabilization may be explained in part by looking at the first band of the photoelectron spectra. Lake and Thompson²⁷ have analyzed this band for tetrafluoroethylene and found that the C-F vibrational frequency decreases over that of the neutral molecule. This indicates that removal of the π electron weakens the C-F bond, thus destabilizing the system. One can also possibly say that resonance interactions of the F-C-F type will be substantially reduced over those of the corresponding chloroethylenes since the F 2p lone pairs will not conjugate with the p orbital on the carbon atom as well as with the Cl 3p lone pairs. The

difference in the cis and trans isomer transition energies is again most likely due to Franck-Condon effects since the adiabatic ionization potentials differ by only about 0.1 eV.⁹² The general increase in repulsive over delocalization effects is noted as a slight rise in the transition energies on going from mono- to tetra-substitution.

Characterizing the trends of the $N \rightarrow V$ transitions is at best a difficult task. The general trends are very similar but the magnitudes of the energy shifts are a factor of 2 to 3 greater than the $N \rightarrow T$ transition energy shifts. If one can again assume that the shifts are in part due to repulsive and delocalization interactions, one would expect these shifts to be larger than those for the $N \rightarrow T$ transition since calculations for ethylene show the $N \rightarrow V$ to have a larger spatial distribution than the $N \rightarrow T$ state.⁸⁷ Consequently, one expects that this state would tend to "feel" the substituents to a greater degree than the $N \rightarrow T$ states. This is indeed what one observes, but this picture is clouded by the occurrence of Rydberg-valence mixing. This effect has been shown to be important in describing the V state in ethylene in theoretical studies of that system.⁹² The amount of mixing depends on the symmetry of the mixing states, presence of vibronic coupling, and the energy separation of these states, and should affect the intensity and positions of the observed $N \rightarrow V$ transitions. This effect would tend to mask some of the trends evident in the $N \rightarrow T$ transition. Nevertheless from figure 30 one can see that the order of the stabilization, $Cl > CH_3 > F$, is the same as that observed for the $N \rightarrow T$ transition. The slopes of the transition energy shifts are now markedly non-linear when compared to the $N \rightarrow T$ shifts. The biggest change seems to occur with the initial substitution while additional substituents change the transition energy less. One anomaly is the large

jump in the transition energy on going from tri- to tetrafluoroethylene. Salahub^{94,95} has suggested that the jump is due to the replacement of low energy C-H σ orbital configurations by higher energy C-F σ orbital configurations. However, this does not entirely account for the large observed shift. Mulliken⁹⁶ has pointed out the importance of σ - π mixing in describing the V state of ethylene. This may account for the remainder of the observed shift. Such a model repudiates the validity of the σ - π separation approximation⁸⁸ for the V state for the substituted ethylenes. Burrow, Jordan and co-workers⁹⁷⁻⁹⁹ have studied trends in the electron affinities (EA's) of the fluoro-, methyl- and chloro-substituted ethylenes. Jordan¹⁰⁰ has used the expression

$$\omega(\pi \rightarrow \pi^*) = IP - EA - (\text{coulomb} + \text{exchange terms}) + \\ (\text{residual correlation and reorganization terms})$$

where ω and EA are the vertical excitation energy and the electron affinity, respectively, to suggest that one may find a simple relationship between the $\pi \rightarrow \pi^*$ transition energies and the quantity IP-EA. This has been done for methyl⁹⁷ and fluoro⁹⁸ substituted ethylenes and it was found that the $\pi \rightarrow \pi^*$, N \rightarrow T transitions when plotted versus the IP-EA were reasonably linear. When one plots the $\pi \rightarrow \pi^*$ N \rightarrow T transition energies from this study versus the quantity IP-EA using Burrow's et al.⁹⁹ EA's one also observes a linear variation with chlorine substitution. This agrees with our observations on the transition energy trends themselves. However, when one plots the $\pi \rightarrow \pi^*$, N \rightarrow V transition energies versus the quantity IP-EA the trends are definitely non-linear.^{99,100} This was explained as being due to $\pi \rightarrow \pi^*$, π^{*2} configuration mixing¹⁰⁰ in the assymmetrically (mono-, 1,1- and tri-) substituted compounds which contributes to an additional lowering of transition energies in these molecules.

Mixing since no mixing of this type can not occur in the symmetrically substituted species. However, this trend does not seem to hold equally well for chloro- substitution as seen in figure 32, thus indicating that other processes or types of mixing may be becoming important in the chloro-ethylenes.

In the $\pi \rightarrow 3s$ state the picture becomes even less clear. The $\pi \rightarrow 3s$ transition may be contrasted with the $N \rightarrow V$ and $N \rightarrow T$ ones since the former is considered an extravalence transition while the latter are intravalence transitions. State mixing must also be considered a very definite possibility in this transition. One would also suspect that due to the spatial diffuseness of the 3s Rydberg orbital, the transition energies will not be as affected by substituents as are the valence transitions. This seems to be born out by the measured transition energy shifts (figure 31). In the case of this transition the stabilization order has changed to $CH_3 > Cl > F$. The chloro and fluoro-ethylenes display the same general trend while transition energy shifts for the methyl substituted ethylenes have a much more linear behavior. No detailed explanation of the observed trends can be offered at this time although the ones for the π -3s transition generally follow, as expected, the trends in the first IP's of these compounds.

One would, on the basis of these $N \rightarrow T$ and $N \rightarrow V$ energy shift trends, like to develop the capability for making reasonably accurate predictions concerning the spectroscopy of the substituted ethylenes based solely on the properties of the substituent. We will choose as an example bromine. This atom is very similar to chlorine in that it has 4p lone pairs which can interact with the π^* states much the same as the chlorine 3p lone pairs. One would expect this interaction to be slightly greater in bromine than

in chlorine due to the larger spatial diffuseness of the 4p lone pair orbitals. The $N \rightarrow T$ transitions of vinyl bromide and a mixture of cis and trans dibromoethylene have been measured¹⁰¹ and found to be approximately 4.0 eV and 3.8 eV, respectively. Both these values are slightly lower than the corresponding chloroethylene values and seem to follow a similar trend. The $N \rightarrow V$ transitions have been measured at approximately 6.4 eV for vinyl bromide and at 5.93 eV⁶³ and 6.22 eV⁶² for cis and trans-dibromoethylene, respectively. These are shifted to the red by about 0.2 eV with respect to the corresponding chloroethylenes and also seem to follow the general trend of the chloroethylenes.

VII. SUMMARY AND CONCLUSIONS

These are the first electron energy loss spectroscopic studies of the chloroethylenes reported so far. We have located the maxima and observed the band shapes for the $\pi \rightarrow \pi^*$, $N \rightarrow T$ transitions in all six of these molecules. In addition several symmetry-forbidden, $\pi \rightarrow np$ Rydberg transitions were identified in trans-dichloroethylene and tetrachloroethylene. A large number of transitions lying above the first IP's of these molecules were observed, most of them for the first time, and tentatively assigned to $Cl3p \rightarrow nl$ -type Rydberg series. We have also looked at the trends observed in the transition energies as a function of both the number of H atoms substituted and the nature of the substituent. The following conclusions can be drawn based on our observations.

- a) The substituent effects on the $N \rightarrow T$ transition energy can be interpreted in terms of the interaction of the substituents with the π^*, T state.

- b) A similar interpretation for the $N \rightarrow V$ transitions is obscured by the presence of valence-Rydberg and other mixing effects in the π^*, V state.
- c) Effects attributable to deviations from the $\sigma-\pi$ separation approximation seem to be present for both the T and the V states.

Our study suggests some future work which would help clarify the spectroscopy of these compounds. First, the need for high quality *ab initio* calculations in this area is great. Such calculations might help sort out substituent effects from mixing effects in the V and 3s states. Calculations concerning high-lying Rydberg states would also be helpful. Second, there is need for studies of the condensed phase optical spectroscopy of these compounds in the 5 to 10 eV transition energy region. In most cases, the valence transitions in these compounds are broad and relatively structureless. Usually only the $N \rightarrow V$ and $N \rightarrow T$ transitions have been positively identified. Many $n \rightarrow \pi^*$ and $n \rightarrow \sigma^*$ states are predicted to exist in this energy region but have not been observed due to strongly overlapping Rydberg absorptions. Condensed phase work would suppress or eliminate¹¹ Rydberg absorptions and possibly allow the valence states to be detected and studied. Third, high resolution optical studies at energies >9 eV would be useful. This would help with the assignments of the $Cl3p \rightarrow nL$ Rydberg series. Finally, one would like to see more complete studies of substituted ethylenes to provide a larger data base for comparing trends and making predictions, in particular, the bromo and iodo ethylenes and substituents other than halogens such as $-C\equiv N$, and $-OCH_3$, should be investigated. Studies of mixed substituents would in addition provide information concerning substituent-substituent interac-

tions.

REFERENCES

- 1) A. J. Merer and R. S. Mulliken, Chem. Rev. **69**, 639 (1969), and references therein.
- 2) A. Kuppermann, J. K. Rice and S. Trajmar, J. Phys. Chem. **72**, 3894 (1968).
- 3) S. Trajmar, J. K. Rice and A. Kuppermann, Adv. Chem. Phys. **18**, 15 (1970).
- 4) A. Kuppermann, W. M. Flicker and O. A. Mosher, Chem. Rev. **79**, 77 (1979).
- 5) W. M. Flicker, O. A. Mosher and A. Kuppermann, Chem. Phys. Lett. **36**, 56 (1975).
- 6) M. J. Coggiola, W. M. Flicker, O. A. Mosher and A. Kuppermann, J. Chem. Phys. **65**, 2655 (1976).
- 7) A. D. Walsh, Trans. Farad. Soc. **41** 35 (1945).
- 8) M. J. Berry, J. Chem. Phys. **61**, 3114 (1974).
- 9) J. R. Lacher, L. E. Hummel, E. F. Bohmfalk and J. D. Park, J. Amer. Chem. Soc. **72**, 5486 (1950).
- 10) P. Dauber and M. Brith, Chem. Phys. **11** 143 (1975).
- 11) C. M. Humphries, A. D. Walsh and P. A. Warsop, Trans. Farad. Soc. **63**, 513 (1967).
- 12) K. Goto, Sci. Light **11**, 119 (1962).
- 13) A. D. Walsh and P. A. Warsop, Trans. Farad. Soc. **64**, 1425 (1968).
- 14) A. D. Walsh and P. A. Warsop, Trans. Farad. Soc. **63**, 524 (1967).
- 15) K. Goto, Sci. Light **9**, 104 (1960).

- 16) J. P. Teegan and A. D. Walsh, *Trans. Farad. Soc.* **47**, 1 (1951).
- 17) A. D. Walsh, P. A. Warsop and J. A. B. Whiteside, *Trans. Farad. Soc.* **64**, 1432 (1968).
- 18) A. D. Walsh and P. A. Warsop, *Trans. Farad. Soc.* **64**, 1418 (1968).
- 19) D. Reinke, R. Kroessig and J. Baumgärtel, *Z. Naturforsch* **28**, 1021 (1973).
- 20) S. P. Sood and K. Watanbe, *J. Chem. Phys.* **45**, 2913 (1966).
- 21) E. N. Lassetre, A. Skerebele, and M. A. Dillon, *J. Chem. Phys.* **50**, 1829 (1969).
- 22) J. H. Moore, *J. Phys. Chem.* **76**, 1130 (1972).
- 23) Y. Takagi, Y. Udagawa, N. Mikomi, K. Kaya and M. Ito, *Chem. Phys. Lett.* **17**, 227 (1972).
- 24) Y. Hukumoto, *J. Chem. Phys.* **3**, 164 (1935).
- 25) A. R. Olson and W. Maroney, *J. Amer. Chem. Soc.* **56**, 1320 (1934).
- 26) H. E. Mahncke and W. A. Noyes, *J. Chem. Phys.* **3**, 536 (1935).
- 27) R. F. Lake and H. Thompson, *Proc. Roy. Soc. A* **315**, 323 (1970).
- 28) W. Von Niesen, L. Åsbrink and G. Bieri, *J. Elect. Spect.* **26**, 173 (1982).
- 29) J. S. Sandhu, *Indian J. Chem.* **10**, 667 (1972).
- 30) K. Gregson and G. G. Hall, *Mol. Phys.* **17**, 49 (1969).
- 31) K. Wittel and H. Bock, *Chem. Ber.* **107**, 317 (1974).
- 32) R. Bralsford, P. V. Harris, and W. C. Price, *Proc. Roy. Soc.* **A2581** 459 (1960).
- 33) J. Momigny, *Nature* **191**, 1089 (1961).

- 34) J. Momigny, *Nature* **199**, 1179 (1963).
- 35) N. Jonathan, K. Ross, and V. Tomlinson, *Int. J. Mass. Spec and Ion Phys.* **4**, 51 (1970).
- 36) M. Klasson and R. Manne in *Electron Spectroscopy*, edited by D. A. Shirley (North Holland, Amsterdam-London, 1972), p. 471.
- 37) M. B. Robin, N. A. Kuebler, and C. R. Brundle in *Electron Spectroscopy*, edited by D. A. Shirley (North Holland, Amsterdam-London, 1972), p. 351.
- 38) D. W. Turner, C. Baker, A. D. Baker and C. R. Brundle, *Molecular Photoelectron Spectroscopy*, (Wiley Interscience, 1970).
- 39) A. Berndtsson, E. Basilier, U. Gelius, J. Hedman, M. Klasson, R. Nilsson, C. Nordling, and S. Svensson, *Phys. Scr.* **12**, 235 (1975).
- 40) K. Kimura and S. Katsumata, *Monogr. Ser. Res. Inst. Appl. Electr., Hokkaido Univ.*, **25** (1978).
- 41) J. C. Bunzli, D. C. Frost, F. G. Herring and C. A. McDowell, *J. Electron Spectrosc. Relat. Phenom.* **9**, 289 (1976).
- 42) T. Yamazaki and K. Kimura, *Bull. Chem. Soc. Jap.* **48**, 1065 (1975).
- 43) W. Lohr, H. W. Jochims, and H. Baumgärtel, *Ber. Bunsenges. Phys. Chem.* **79**, 901 (1975).
- 44) H. Bock and K. Wittel, *J. Chem. Soc. Chem. Commun.* 602 (1972).
- 45) A. Katrib, T. P. Debies, R. J. Colton, T. H. Lee and J. W. Rabalais, *Chem. Phys. Lett.* **22**, 196 (1973).
- 46) G. W. Mines and H. W. Thompson, *Spectrochimica Acta* **29A** 485 (1975).
- 47) A. W. Potts, I. Novak, and M. L. Lyus, *J. Electron Spectrosc. Relat. Phenom.* **31**, 57 (1982).

- 48) A. Pellegatti, J. C. Pieribattesti, and M. Benard, *J. Chim. Phys.* **68**, 1708 (1971).
- 49) M. Rajzmann, and G. Pouzard, *Theoret. Chim. Acta* **32**, 135 (1973).
- 50) M. Kato, K. Hirao, H. Konishi, and T. Yonezawa, *Bull. Chem. Soc. Jap.* **44**, 2062 (1971).
- 51) G. Favini, and M. Simonetta, *Il Nuovo Cimento* **9**, 1058 (1958).
- 52) J. A. Howe, J. S. Muirhead, and S. H. Goldstein, *J. Chem. Phys.* **36**, 841 (1962).
- 53) T. Fueno and K. Yamaguchi, *Bull. Chem. Soc. Jap.* **45**, 3290 (1972).
- 54) J. A. Simpson, *Rev. Sci. Instrum.* **35**, 1698 (1964).
- 55) C. E. Kuyatt and J. A. Simpson, *Rev. Sci. Instrum.* **38**, 103 (1967).
- 56) O. A. Mosher, W. M. Flicker, and A. Kuppermann, *J. Chem. Phys.* **62**, 2600 (1975).
- 57) A. Chutjian, *J. Chem. Phys.* **61**, 4279 (1974).
- 58) W. M. Flicker, Ph. D. Thesis, California Institute of Technology, Pasadena, CA (1975).
- 59) J. P. Doering and R. McDiarmid, *J. Chem. Phys.* **75**, 87 (1981).
- 60) M. B. Robin, *Higher Excited States of Polyatomic Molecules*, vol. II, (Academic Press 1974) p. 50-68.
- 61) F. H. Read and G. L. Whiterod, *Proc. Phys. Soc.* **9**, 434 (1963).
- 62) K. Wittel, W. S. Felps, L. Klansinc and S. P. McGlynn, *J. Chem. Phys.* **65**, 3698 (1976).
- 63) W. S. Felps, K. Wittel, and S. P. McGlynn, *J. Molec. Spect.* **71**, 101 (1978).

- 64) M. B. Robin, *Higher Excited States of Polyatomic Molecules*, vol. I (Academic Press 1974) p. 13.
- 65) A. Skerebele and E. Lassetre, *J. Chem. Phys.* **55**, 424 (1971).
- 66) Z. R. Grablowski and A. Bylino, *Trans. Farad. Soc.* **60** 1131 (1964).
- 67) D. Evans, *J. Chem. Soc.* 1735 (1960).
- 68) F. B. Wampler and J. W. Böttenheim, *Int. J. Chem. Kin.* **8**, 585 (1976).
- 69) G. R. DeMare', M. C. Fontaine, G. Huybrechts, and M. Termonia, *J. Photochem.* **12**, 289 (1972).
- 70) R. B. Cundall and D. G. Milne, *J. Amer. Chem. Soc.* **83**, 3902 (1961).
- 71) U. Maharaj and M. A. Winnik, *Tett. Lett.* **23**, 3035 (1982).
- 72) M. J. Berry and G. C. Pimentel, *J. Chem. Phys.* **51**, 2274 (1969).
- 73) M. J. Berry and G. C. Pimentel, *J. Chem. Phys.* **53**, 3453 (1970).
- 74) M. J. Molina and G. C. Pimentel, *J. Chem. Phys.* **56**, 3988 (1972).
- 75) M. J. Berry, *J. Chem. Phys.* **61**, 3114 (1974).
- 76) R. Becerra, M. Castillejo, J. M. Figuera and M. Martin, *Chem. Phys. Lett.* **100**, 340 (1983).
- 77) T. Fujimoto, A. M. Rennart, and M. H. J. Wijnen, *Ber. Bunsenges Phys. Chem.* **74**, 282 (1970).
- 78) P. Ausloos, R. E. Rebbert, and M. H. J. Wijnen, *J. Res. Nat. Bureau Stand.* **77A**, 243 (1973).
- 79) M. G. Bellas, J. K. S. Wan, W. F. Allen, O. P. Strausz and H. E. Gunning, *J. Phys. Chem.* **68**, 2170 (1964).
- 80) M. H. J. Wijnen, *J. Amer. Chem. Soc.* **83**, 4109 (1961).
- 81) R. Ausubel and M. H. J. Wijnen, *J. Photochem.* **4**, 241 (1975).

- 82) R. Ausubel and M. H. J. Wijnen, *Int. J. Chem. Kin.* **7**, 739 (1975).
- 83) R. Ausubel and M. H. J. Wijnen, *J. Photochem.* **5**, 233 (1976).
- 84) J. A. Warren, G. R. Smith and W. Guillory, *J. Photochem.* **7**, 263 (1977).
- 85) W. J. R. Tyerman, *Trans. Farad. Soc.* **65**, 2948 (1969).
- 86) C. F. Koerting, K. N. Walzl, and A. Kuppermann, *Chem. Phys. Lett.* **109** 140 (1984).
- 87) T. H. Dunning, Jr., W. J. Hunt, and W. A. Goddard, *Chem. Phys. Lett.* **4**, 147 (1969).
- 88) R. G. Parr, *Quantum Theory of Molecular Electronic Structure* (W. A. Benjamin, Inc., 1964) pp. 41-45.
- 89) C. A. Coulson and Z. Luz, *Trans. Farad. Soc.* **64**, 2884 (1968).
- 90) J. D. Cox and G. Pilcher, *Thermochemistry of Organic and Organometallic Compounds* (Academic Press, 1970) p. 404.
- 91) A. J. Gordon and R. A. Ford, *The Chemists Companion, A Handbook of Practical Data, Techniques, and References* (Wiley Interscience, New York 1972) pp. 152-153.
- 92) J. A. Sell and A. Kuppermann, *J. Chem. Phys.* **71**, 4703 (1979).
- 93) R. J. Buenker and S. D. Peyerimhoff, *Chem. Phys. Lett.* **36**, 415 (1975).
- 94) D. R. Salahub, *Theor. Chim. Acta* **22**, 330 (1971).
- 95) D. R. Salahub, Ph. D. Thesis, University of Montreal, Montreal, Canada (1970).
- 96) R. S. Mulliken, *Chem. Phys. Lett.* **25**, 305 (1974).
- 97) N. S. Chiu, P. D. Burrow and K. D. Jordan, *Chem. Phys. Lett.* **68**, 121 (1979).

- 98) K. D. Jordan and P. D. Burrow, J. Amer. Chem. Soc. **102**, 6882 (1980).
- 99) P. D. Burrow, A. Modelli, N. S. Chiu and K. D. Jordan, Chem. Phys. Lett., **82**, 270 (1981).
- 100) K. D. Jordan, Int. J. Quant. Chem. **15**, 331 (1981).
- 101) C. F. Koerting, K. N. Walzl, and A. Kuppermann, unpublished results.

Table 1. Electronic transition energies in Vinyl chloride (eV)

Assignment	Present Results	Previous Work
$\pi \rightarrow \pi^*$, N \rightarrow T	4.13 (3.4-5.1) ^a	4.0 ^b , 4.08 ^c , 4.17 ^d
$\pi \rightarrow \pi^*$, N \rightarrow V	6.61 sh ^e	
$\pi \rightarrow 3s_1$ ^f	6.72	6.72 ^f , 6.72 ^g
$\pi \rightarrow \pi^*$, N \rightarrow V (vert)	6.77 sh ^e	6.9 ^b , 6.68 ^f 6.74 ^g , 6.23 ^h , 6.65 ⁱ , 6.70 ^j
	6.84	6.83 ^c
$\pi \rightarrow 3s_1 + \nu_1$ ^k	6.88	6.89 ^g
	6.99	
$\pi \rightarrow 3s_1 + 2\nu_1$	7.22	7.23 ^g , 7.28 ^j
	7.36 sh ^e	
$\pi \rightarrow 3p_1$	7.64	7.63 ^g , 7.61 ^j
"Walsh"	7.82	7.81 ^c , 7.82 ^{g,j}
	7.95	7.95 ^g
"Walsh" + ν_1	7.99	7.97 ^c , 8.00 ^g , 7.99 ^j
"Walsh" + $2\nu_1$	8.16	8.13 ^c , 8.18 ^g , 8.16 ^j
$\pi \rightarrow 3d_1'$	8.34	8.33 ^g , 8.32 ^j
Cl3p \rightarrow 4p ₂	8.52	8.53 ^c , 8.48 ^g , 8.49 ^j
$\pi \rightarrow 3d_1' + \nu_1$	8.59	8.58 ^g , 8.57 ^j
$\pi \rightarrow 4s_1$	8.64	8.63 ^g , 8.67 ^j
$\pi \rightarrow 3d_1' + 2\nu_1$	8.73	8.73 ^{g,j}
	8.77	8.75 ^g
$\pi \rightarrow 4p_1$, Cl3p \rightarrow 4p ₂ '	8.85	8.84 ^g
$\pi \rightarrow 4p_1 + 3\nu_2$	8.96	8.99 ^g
$\pi \rightarrow 4p_1 + \nu_1$	9.02	9.02 ^g
$\pi \rightarrow 4d_1$	9.15	9.12 ^c , 9.13 ^{g,j}

Assignment	Present Results	Previous Work
	9.26	9.25 ^c , 9.24 ^g
$\pi \rightarrow 5p_1$	9.31 sh ^e	9.31 ^g
	9.38	9.38 ^c , 9.36 ^g
$\pi \rightarrow 5d_1, \pi \rightarrow 5d_1'$	9.43 sh ^e	9.45 ^g , 9.43 ^g , 9.44 ^j
$Cl3p \rightarrow 4p_2'', \pi \rightarrow 6s_1$	9.52 sh ^e	9.49 ^{g,j}
$\pi \rightarrow 6p_1$	9.55 sh ^e	9.54 ^g
$\pi \rightarrow 6d_1, \pi \rightarrow 6d_1', Cl3p \rightarrow 4d_2$	9.62	9.61 ^{g,j}
$\pi \rightarrow 7p_1, \pi \rightarrow 7s_1$	9.68	9.67 ^g , 9.65 ^j
$\pi \rightarrow 7d_1, \pi \rightarrow 7d_1'$	9.73	9.72 ^{g,j}
$\pi \rightarrow 9s_1$	9.80	9.80 ^{g,j}
$\pi \rightarrow 8d_1$	9.83	9.83 ^{g,j}
$\pi \rightarrow 11d_1$	9.87	9.88 ^j
	9.92	
$Cl3p \rightarrow 4d_2'$	10.06	10.06 ^c
	10.17	10.19 ^c
IP1		10.18(10.00) ^{l,m} 10.2(10.0) ⁿ ,
$Cl3p \rightarrow 5p_2$	10.23	
$Cl3p \rightarrow 5_2'$	10.30	10.31 ^c , 10.28 ^o
	10.37 sh ^e	
	10.43	10.42 ^c
$Cl3p \rightarrow 5d_2$	10.58	10.54 ^{c,o}
$Cl3p \rightarrow 5p_2''$	10.62 sh ^e	
$Cl3p \rightarrow 5d_2'$	10.75	10.77 ^c , 10.72 ^o
$Cl3p \rightarrow 6p_2, Cl3p \rightarrow 6p_2'$	10.88	10.88 ^c , 10.86 ^o
$Cl3p \rightarrow 6d_2$	11.00	10.98 ^o

Assignment	Present Results	Previous Work
Cl3p → 6d ₂ ' , Cl3p → 6p ₂ ''	11.08	11.05 ^o
Cl3p → 7p ₂ '	11.15	11.15 ^o
Cl3p → 7d ₂ ' , Cl3p → 7p ₂ ''	11.24	11.25 ^o
Cl3p → 8p ₂ '	11.30	11.29 ^o
Cl3p → 9p ₂ '	11.39	
Cl3p → 4p ₄	11.46	
	11.53	11.55 ^c
	11.60	
	11.67	
IP2		11.72 ^m , 11.7 ⁿ
Cl3p → 5p ₄	12.5	
Cl3p → 6p ₄	12.9	12.87 ^c
IP3		13.14 ^m , 13.2 ⁿ
IP4		13.56 ^m , 13.6 ⁿ
	14.8	

^a Uncertainty ±.05 eV for this band, ±.02 for all other bands. Extent of Franck-Condon envelope indicated by numbers in parentheses.

^b Ref. 22.

^c Ref. 58.

^d Ref. 50.

^e shoulder

^f Subscript denotes IP to which Rydberg series is converging; i.e., 1 = first IP, 2 = second IP, etc.

- g Ref. 20.
- h Ref. 48.
- i Ref. 49.
- j Ref. 7.
- k For definitions of vibrational modes see ref. 21.
- l Vertical IP (adiabatic in parentheses).
- m Ref. 27.
- n Ref. 28.
- o Ref. 20.

**Table 2. Electronic Transition Energies in Vinyl Chloride
for the Cl3p → n*l* Rydberg Series (eV)**

<i>l</i>	n	observed	calculated
p	4	8.52	8.42
	5	10.23	10.24
	6	10.88	10.88
	$\infty = 11.72$		$\delta = 1.97$
p'	4	8.85	8.84
	5	10.30	10.32
	6	10.88	10.88
	7	11.15	11.15
	8	11.30	11.30
	9	11.39	11.39
	$\infty = 11.65$		$\delta = 1.80$
p''	4	9.52	9.51
	5	10.62	10.60
	6	11.08	11.04
	7	11.24	11.27
	$\infty = 11.72$		$\delta = 1.52$
d	4	9.62	9.61
	5	10.58	10.59
	6	11.00	11.00
	$\infty = 11.65$		$\delta = 1.42$
d'	4	10.06	10.00
	5	10.75	10.74
	6	11.08	11.08
	7	11.24	11.26
	$\infty = 11.65$		$\delta = 1.13$
p	4	11.46	11.48
	5	12.5	12.49
	6	12.9	12.91
	$\infty = 13.56$		$\delta = 1.44$

Table 3. Electronic Transition Energies in 1,1 - Dichloroethylene (eV)

Assignment	Present Results	Previous Work
$\pi \rightarrow \pi^*, N \rightarrow T$	3.75 (3.2-5.1) ^a 6.02 sh ^d	3.9 ^b , 3.95 ^c
$\pi \rightarrow \pi^*, N \rightarrow V$	6.42 6.47 6.51 6.54 sh ^d 6.57 sh ^d	6.9 ^b , 6.44 ^c , 6.46 ^f , 5.92 ^g , 6.6 ^h , 6.49 ⁱ , 6.42 ^e
$\pi \rightarrow 3s_1^j$	6.65 sh ^d	
$\pi \rightarrow 3s_1 + \nu_2^k$	6.77 sh ^d	
$\pi \rightarrow 3s_1 + \nu_2 + \nu_4$	6.86 sh ^d	
$\pi \rightarrow 3s_1 + 2\nu_2$	6.97 7.01	
$\pi \rightarrow 3s_1 + 2\nu_s + \nu_4$	7.05	
$\pi \rightarrow 3s_1 + 3\nu_2$	7.13 sh ^d 7.28 sh ^d 7.35 sh ^d	
$\pi \rightarrow 3p_1 + \nu_4$	7.56	7.59 ^e
$\pi \rightarrow 3p_1 + \nu_2$	7.65	7.66 ^e
$\pi \rightarrow 3p_1 + \nu_2 + \nu_4$	7.72	7.75 ^e
$\pi \rightarrow 3p_1 + 2\nu_2$	7.82	7.83 ^e
$\pi \rightarrow 3p_1 + 2\nu_2 + \nu_4$	7.89	7.91 ^e
$\pi \rightarrow 3p_1 + 3\nu_2, \pi \rightarrow 3p_1' + \nu_4$	7.96	7.94 ^e , 7.99 ^e
$\pi \rightarrow 3p_1 + 3\nu_2 + \nu_4$	8.06	8.07 ^e

Assignment	Present Results	Previous Work
$\pi \rightarrow 3d_1 + \nu_4, \pi \rightarrow 3p_1' + 2\nu_2$	8.20	8.18 ^e , 8.22
$\pi \rightarrow 3p_1' + 2\nu_2 + \nu_4^0$	8.25 sh ^d	
$\pi \rightarrow 3d_1 + \nu_2 + \nu_4$	8.36	8.38 ^e 8.36
$\pi \rightarrow 3d_1 + 2\nu_2, \pi \rightarrow 4s_1 + \nu_4$	8.45	8.47 ^e
$\pi \rightarrow 3d_1 + 2\nu_2 + \nu_4, \pi \rightarrow 4s_1 + \nu_2$	8.53	8.55 ^e
	8.80	
$\pi \rightarrow 3d_1 + 3\nu_2, \pi \rightarrow 4s_1 + \nu_2 + \nu_4$	8.67 sh ^d	8.63 ^e , 8.64 ^{e,f}
$\pi \rightarrow 4p_1 + \nu_4$	8.76	
$\pi \rightarrow 4p_1 + \nu_2, Cl3p \rightarrow 4s_3$	8.84	
$\pi \rightarrow 4d_1$	8.93	8.93 ^{e,f}
$\pi \rightarrow 4p_1 + 2\nu_2, \pi \rightarrow 4d_1 + \nu_4$	8.99	8.96 ^e , 8.98 ^e
$\pi \rightarrow 4d_1 + \nu_2, Cl3p \rightarrow 4p_3'$	9.08	9.09 ^e
$\pi \rightarrow 5p_1, Cl3p \rightarrow 4p_2$	9.22	9.19 ^{e,f} , 9.24
$\pi \rightarrow 4d_1 + 2\nu_2 + \nu_4, \pi + 6p_1$	9.36 sh ^d	9.33 ^e
$\pi \rightarrow 6d_1$	9.47	
$\pi \rightarrow 7d_1$	9.58	
$Cl3p \rightarrow 4p_3$	9.67 sh ^d	9.69 ^e , 9.66 ^f
	9.75	
	9.82 sh ^d	
$Cl3p \rightarrow 4p_4$	9.96	10.01 ^e
$Cl3p \rightarrow 4d_2$	9.99	
IP1		10.00(9.83) ^{l,m} , 10.00(9.83) ⁿ
$Cl3p \rightarrow 4d_3$	10.30 sh ^d	
$\sigma(C-Cl), 3b_2 \rightarrow 3s_5$	10.36 sh ^d	

Assignment	Present Results	Previous Work
	10.39	
	10.43	
Cl3p → 5p ₂	10.51	
	10.59	
Cl3p → 5s ₃	10.68	
Cl3p → 5d ₂	10.75	
Cl3p → 5p ₃ '	10.79	
	10.85 sh ^d	
Cl3p → 6p ₂ , Cl3p → 5p ₃	10.96	
	11.05 sh ^d	
Cl3p → 4p ₅ , Cl3p → 6d ₂	11.10	
Cl3p → 7p ₂ , Cl3p → 5d ₃	11.20	
Cl3p → 6s ₃ , Cl3p → 5p ₄	11.31	
Cl3p → 6p ₃	11.37	
Cl3p → 6p ₃	11.45	
Cl3p → 6d ₃	11.55	
Cl3p → 7s ₃	11.63	
Cl3p → 7p ₃	11.68	
IP2		11.67(11.46) ^m , 11.7 ⁿ
Cl3p → 7d ₃	11.75	
Cl3p → 8s ₃ , Cl3p → 6p ₄	11.80	
IP3		12.17(12.06) ^m , 12.2 ⁿ
σ(C-Cl), 3b ₂ → 4s ₅	12.2	
IP4		12.51 ^m , 12.5 ⁿ
	12.7	

Assignment	Present Results	Previous Work
	13.4	
IP5		13.7 ^m , 13.8 ⁿ ,
	14.2	
IP6		14.24 ^m , 14.3 ⁿ
(3a ₁ → π*, Cσ 2s → π*)	15.1	
IP7		15.89 ^m , 15.4-16.8 ⁿ
	16.3	

- a) Uncertainty ±.05 eV for this band, ±.02 eV for all other bands. Extent of Franck Condon envelope indicated by numbers in parentheses.
- b) Ref. 22.
- c) Ref. 50.
- d) shoulder
- e) Ref. 17.
- f) Ref. 16.
- g) Ref. 48.
- h) Ref. 49.
- i) Ref. 52.
- j) Subscript denotes IP to which Rydberg series is converging; i.e., 1 = first IP.
- k) For definition of vibrational modes see ref. 18.
- l) Vertical IP's (adiabatic in parentheses).
- m) Ref. 27.

n) Ref. 28.

Table 4. Electronic Transition Energies in 1,1 - Dichloroethylene for the Cl3p → n*l* Rydberg Series (eV)

<i>l</i>	n	observed	calculated
p	4	9.22	9.27
	5	10.51	10.48
	6	10.96	10.96
	7	11.20	11.20
	∞ = 11.67		δ = 1.62
d	4	9.99	10.01
	5	10.75	10.76
	6	11.10	11.09
	∞ = 11.67		δ = 1.14
s	4	8.84	8.87
	5	10.68	10.69
	6	11.31	11.33
	7	11.63	11.63
	8	11.80	11.80
	∞ = 12.17		δ = 1.97
p	4	9.67	9.69
	5	10.96	10.95
	6	11.45	11.45
	7	11.68	11.69
	∞ = 12.17		δ = 1.66
p'	4	9.08	9.14
	5	10.79	10.77
	6	11.37	11.37
	∞ = 12.17		δ = 1.88
p	4	10.30	10.30
	5	11.20	11.18
	6	11.55	11.55
	7	11.75	11.75
	∞ = 12.51		δ = 1.65

Table 5. Electronic Transition Energies in Cis-dichloroethylene (eV)

Assignment	Present Results	Previous Work
$\pi \rightarrow \pi^*$, N \rightarrow T	3.94(3.0-5.2) ^a 6.23 sh ^d 6.43 sh ^d	3.82, ^b 3.98 ^c
$\pi \rightarrow 3s_1$ ^e	6.54 sh ^d	
$\pi \rightarrow \pi^*$, N \rightarrow V	6.60	6.53 ^{f,g} , 6.70 ^h , 6.13 ^b 5.76 ⁱ , 6.40 ^j 7.43 ^k , 6.27 ^c
$\pi \rightarrow 3s_1 + \nu_2$	6.72 sh ^d	
$\pi \rightarrow 3s_1 + 3\nu_2$	7.07 sh ^d 7.18 sh ^d 7.38 sh ^d	7.16 ^h 7.33 ^f
$\pi \rightarrow 3p_1$	7.42	7.41 ^{f,g}
$\pi \rightarrow 3p_1 + \nu_4$	7.50	7.51 ^{f,g,h}
$\pi \rightarrow 3p_1 + \nu_2$, $\pi \rightarrow 3p_1 + 2\nu_4$	7.60	7.58 ^{f,g,h} , 7.61 ^f
$\pi \rightarrow 3p_1 + \nu_2 + \nu_4$	7.69 sh ^d	7.68 ^{f,g,h}
$\pi \rightarrow 3p_1 + 2\nu_2$, $\pi \rightarrow 3p_1 + \nu_2 + 2\nu_4$	7.78	7.76 ^{f,g,h} , 7.78 ^f
$\pi \rightarrow 3p_1 + 2\nu_2 + \nu_4$	7.86	7.86 ^f
$\pi \rightarrow 3p_1 + 3\nu_2$, $\pi \rightarrow 3p_1 + 2\nu_2 + 2\nu_4$	7.95	7.93 ^f , 7.96 ^f
$\pi \rightarrow 3p_1 + 3\nu_2 + \nu_4$	8.05 sh ^d 8.11	8.03 ^f , 8.06 ^h 8.08 ^{f,g} , 8.10 ^h
$\pi \rightarrow 3d_1$	8.19	8.17 ^{f,g} , 8.19 ^h
$\pi \rightarrow 3d_1 + \nu_4$	8.28	8.27 ^{f,g,h} , 8.26 ^h , 8.28 ^h
$\pi \rightarrow 3d_1 + \nu_2$	8.38	8.34 ^{f,g,h} , 8.36 ^h
$\pi \rightarrow 3d_1 + 2\nu_2$	8.49	8.51 ^{f,g} ,

Assignment	Present Results	Previous Work
		8.45 ^g , 8.49 ^h
Cl3p → 4p ₂ , π → 4p ₁		
π → 4p ₁ + ν ₂ , Cl3p → 4s ₃	8.71	8.69 ^{f,h}
π → 4d ₁	8.80	8.77 ^{f,g,h} , 8.80 ^{g,h}
π → 5s ₁	8.83 sh ^d	8.83 ^{g,h}
π → 4d ₁ + ν ₂	8.94	8.95 ^f , 8.94 ^{g,h}
π → 5p ₁	8.98	8.98 ^{f,g,h}
π → 4d ₁ + ν ₂ + ν ₄	9.05	9.09 ^g , 9.04 ^h
π → 6s ₁	9.14	9.13 ^g , 9.12 ^h
π → 6p ₁	9.21	9.20 ^h
π → 6d ₁ , π → 7s ₁ , π → 7p ₁	9.32	9.28 ^f , 9.29 ^g , 9.30 ^h
π → 7d ₁ , π → 8p ₁	9.40	9.38 ^f
	9.53 sh ^d	
Cl3p → 4p ₄	9.67	9.68 ^h
Cl3p → 4p ₃ Cl3p → 4p' ₄	9.79	
IP1		9.8(9.65) ^{l,m} , 9.83(9.65) ⁿ
Cl3p → 4d ₂	9.91 sh ^d	
Cl3p → 5p ₄	10.11	
Cl3p → 5p ₂	10.26	10.28 ^o
	10.30	
	10.35	
	10.53	10.50 ^o
Cl3p → 5s ₃	10.60	
Cl3p → 5d ₂	10.76	10.74 ^o
Cl3p → 6p ₂	10.89	

Assignment	Present Results	Previous Work
Cl3p → 5p ₃	10.97	
Cl3p → 5p ₄ , Cl3p → 6d ₂	11.11	
Cl3p → 6s ₃ , Cl3p → 5p' ₄	11.27	
Cl3p → 6p ₃	11.42	
	11.55	
	11.63	
IP2		11.9 ^l , 11.71 ⁿ
	11.88	
Cl3p → 7p' ₄	12.03	
IP3		12.0 ^l , 12.09 ⁿ
Cl3p → 8p ₄	12.15	
	12.24 sh ^d	
	12.37 sh ^d	
IP4		12.6 ^l , 12.51 ⁿ
Cl3p → 5p ₆ ,	12.8	
4a ₁ → 2a ₂ (σ → π*)	13.2	
3a ₁ → 2a ₂ (σ → π*)	13.5	
IP5		13.9 ^l , 13.72 ⁿ
IP6		14.2 ^l , 14.1 ⁿ
	14.6	
	15.3	
IP7		15.8 ^l , 15.66 ⁿ

^a Uncertainty ±.05 eV for this band, ±.02 eV for all other bands. Numbers in parentheses indicate extent of Franck-Condon envelope.

- b Ref. 50.
- c Ref. 51.
- d sh = shoulder
- e Subscript denotes IP to which Rydberg series is converging, i.e., 1 = first IP, 2 = second IP, etc.
- f Ref. 14.
- g Ref. 7.
- h Ref. 26.
- i Ref. 48.
- j Ref. 49.
- k Ref. 9.
- l Ref. 28.
- m Vertical IP's. (adiabatic in parentheses)
- n Ref. 27.
- o Ref. 34.

Table 6. Electronic Transition Energies in Cis-dichloroethylene for the Cl3p → n*l* Rydberg Series (eV)

<i>l</i>	n	observed	calculated
p	4	8.49	8.57
	5	10.26	10.28
	6	10.89	10.89
	$\infty=11.71$	$\delta=1.92$	
d	4	9.91	9.92
	5	10.76	10.75
	6	11.11	11.11
	$\infty=11.71$	$\delta=1.24$	
s	4	8.71	8.74
	5	10.60	10.61
	6	11.27	11.26
	$\infty=12.11$	$\delta=1.56$	
p	4	9.67	9.57
	5	11.11	11.14
	6		11.72
	7		11.99
	8	12.15	12.15
	$\infty=12.51$	$\delta=1.85$	
p'	4	9.79	9.92
	5	11.27	11.25
	6		11.77
	7	12.03	12.02
	$\infty=12.51$	$\delta=1.71$	

Table 7. Electronic Transition Energies in Trans-dichloroethylene (eV)

Assignment	Present Results	Previous Work
$\pi \rightarrow \pi^*, N \rightarrow T$	3.84(2.9-4.8) ^a 5.98 sh ^d 6.02 sh ^d 6.06 sh ^d 6.09 sh ^d	3.81 ^b 4.12 ^c
$\pi \rightarrow \pi^*, N \rightarrow V$	6.36	6.21 ^b , 8.63 ^c , 6.30 ^e , 6.33 ^f , 5.82 ^g , 7.43 ^h , 6.36 ^{i,j,k} , 6.28 ^l
$\pi \rightarrow 3s_1^m$	6.40 6.84 sh ^d 6.93 sh ^d	6.92 ^l
$\pi \rightarrow 3p_1$	7.09	
$\pi \rightarrow 3p_1 + \nu_2$	7.25	7.29 ^l
$\pi \rightarrow 3p_1 + 2\nu_2$	7.41	7.41 ^l
$\pi \rightarrow 3p'$	7.57	7.57 ^l
$\pi \rightarrow 3p'_1 + \nu_2$	7.73	7.72 ^l
$\pi \rightarrow 3p'_1 + 2\nu_2$	7.90 8.04 sh ^d	7.93 ^l 8.07 ^k
$\pi \rightarrow 4s_1 + \nu_5$	8.19	8.16 ^{i,j,k} , 8.20 ^k
$\pi \rightarrow 4s_1 + \nu_2 + \nu_5$	8.35	8.34 ^{i,k} , 8.33 ^j
$\pi \rightarrow 4s_1 + \nu_2 + 2\nu_5,$ $\pi \rightarrow 4p_1$	8.38	8.38 ^{j,k}
$\pi \rightarrow 4s_1 + \nu_2 + \nu_4 + \nu_5$	8.45	8.47 ^{j,k}
$\pi \rightarrow 4s_1 + 2\nu_2 + \nu_5$	8.51	8.51 ^{i,j,k}
$\pi \rightarrow 4p'_1$	8.55	
$\pi \rightarrow 4p'_1 + \nu_2$	8.71	

Assignment	Present Results	Previous Work
$Cl3p \rightarrow 4p_2$	8.75	8.69 ^{i,j,k}
$\pi \rightarrow 4p_1' + \nu_2 + \nu_4$	8.82	
$\pi \rightarrow 5s_1$	8.87	8.83 ⁱ , 8.80 ^k
	9.00	8.95 ⁱ
$\pi \rightarrow 6p_1$	9.15	
$Cl3p \rightarrow 4p_3$	9.27	9.20 ⁱ , 9.21 ^k
	9.40	9.46 ⁱ
	9.54	
	9.58	9.58 ^l
	9.61	
	9.63 sh ^d	9.63 ^l
	9.67 sh ^d	9.06 ^l
	9.70 sh ^d	9.70 ^l
	9.77 sh ^d	9.75 ^l
IP1		9.81(9.64) ^{n,o} , 9.84 ^p ,
$Cl3p \rightarrow 4p_4$	9.87	9.81 ^{i,k}
	9.98	
	10.01 sh ^d	
	10.09 sh ^d	
	10.25 sh ^d	10.17 ^k
	10.28	
	10.33 sh ^d	
$Cl3p \rightarrow 5p_2$, $Cl3p \rightarrow 4p_4'$	10.39	10.38 ^k
	10.51 sh ^d	
	10.58	10.59 ⁱ

Assignment	Present Results	Previous Work
C-Cl σ \rightarrow 3s	10.68	10.61 ^{l,k}
	10.79	
	10.88 sh ^d	10.89 ^l
	10.98	10.97 ^l
Cl3p \rightarrow 6p ₂	11.02	11.02 ^l
	11.06	
Cl3p \rightarrow 4p ₆	11.20	11.28 ^l
Cl3p \rightarrow 7p ₂ , Cl3p \rightarrow 5p ₄	11.33	11.38 ^l
	11.43	11.45 ^l
Cl3p \rightarrow 8p ₂ , Cl3p \rightarrow 5p ₄ '	11.50	11.49 ^l
	11.56	
	11.70	
	11.80	
		11.86 ⁿ , 11.9 ^p
IP2		
Cl3p \rightarrow 6p ₄ '	12.02	
IP3		12.06 ⁿ , 12.1 ^p
Cl3p \rightarrow 7p ₄	12.13	
IP4		12.61 ⁿ , 12.7 ^p
IP5		13.85 ⁿ
	14.2	
IP6		14.2 ^{n,p} ,
	15.1	
	15.3	
2b ₀ \rightarrow 2b _g , (σ C-H \rightarrow π^*)	15.5	

Assignment	Present Results	Previous Work
IP7		16.23 ⁿ , 16.3 ^p

- ^a Uncertainty ± 0.05 eV for this band, ± 0.02 eV for all other bands. Extent of Franck-Condon envelope indicated by numbers in parentheses.
- ^b Ref. 50.
- ^c Ref. 51.
- ^d sh = shoulder
- ^e Ref. 48.
- ^f Ref. 52.
- ^g Ref. 49.
- ^h Ref. 53.
- ⁱ Ref. 14.
- ^j Ref. 7.
- ^k Ref. 26.
- ^l Ref. 15.
- ^m Subscript denotes IP to which Rydberg series is converging, i.e., 1 = first IP, 2 = second IP, etc.
- ⁿ Ref. 27.
- ^o Vertical IP's (adiabatic in parentheses).
- ^p Ref. 28.

Table 8. Electronic Transition Energies in Trans-dichloroethylene for the Cl3p → n'l Rydberg Series (eV)

<i>l</i>	n	observed	calculated
p	4	8.75	8.65
	5	10.39	10.41
	6	11.02	11.03
	7	11.33	11.33
	8	11.50	11.49
	∞=11.86		δ=1.94
p	4	9.87	9.85
	5	11.33	11.33
	6		11.89
	7	12.13	12.16
	∞=12.66		δ=1.80
p'	4	10.39	10.37
	5	11.50	11.50
	6	12.02	11.97
	∞=12.66		δ=1.56

Table 9. Electronic Transition Energies in Trichloroethylene (eV)

Assignment	Present Results	Previous Work
$\pi \rightarrow \pi^*N \rightarrow T$	3.70(3.0-4.7) ^a	3.99 ^b
	5.22 sh ^c	
	5.29 sh ^c	
	5.40 sh ^c	
	5.57 sh ^c	
	5.65 sh ^c	
	5.76 sh ^c	
	5.84 sh ^c	
	5.98 sh ^c	
	6.04 sh ^c	
$\pi \rightarrow 3s_1$ ^d	6.12 sh ^c	
$\pi \rightarrow 3s_1 + \nu_2$ ^e	6.29 sh ^c	
$\pi \rightarrow \pi^*, N \rightarrow V$	6.33	6.31 ^b , 6.33 ^{f,g} 5.58 ^h , 6.20 ^{i,j}
$\pi \rightarrow 3s_1 + 2\nu_2$	6.45 sh ^c	
	6.58 sh ^c	
	6.76 sh ^c	
	6.86 sh ^c	
	6.93 sh ^c	
	7.04	
	7.21	
$\pi \rightarrow 3p_1$	7.38	7.35 ^{f,g}
$\pi \rightarrow 3p_1'$	7.44	7.40 ^{f,g}
$\pi \rightarrow 3p_1''$	7.50 sh ^c	7.51 ^{f,g}
$\pi \rightarrow 3p + \nu_2$	7.54	7.53 ^{f,g}

Assignment	Present Results	Previous Work
$\pi \rightarrow 3p'' + \nu_2$	7.66 sh ^c	7.68 ^{f,g}
$\pi \rightarrow 3p + 2\nu_2$	7.73	7.70 ^{f,g}
$\pi \rightarrow 3p' + 2\nu_2$	7.78 sh ^c	7.78 ^{f,g} , 7.75 ^{f,g}
$\pi \rightarrow 3p + 3\nu_2$	7.85	7.87 ^{e,f}
$\pi \rightarrow 3p' + 3\nu_2$	7.94	
$\pi \rightarrow 4s$	8.00	7.98 ^{f,g}
$\pi \rightarrow 4s + \nu_2$	8.04 sh ^c	8.03 ^{f,g}
	8.10 sh	
$\pi \rightarrow 4s + \nu_2$	8.16	8.16 ^{f,g}
$\pi \rightarrow 4s + 2\nu_2$	8.36	8.33 ^{f,g}
$\pi \rightarrow 4s + 3\nu_2$	8.50 sh	8.50 ^{f,g}
$\pi \rightarrow 4s + 3\nu_2 + \nu_7$	8.56	8.56 ^f , 8.58 ^f
	8.69	
	8.88 sh ^c	
Cl3p \rightarrow 4p ₂	8.94	
	9.00 sh ^c	
	9.18	
Cl3p \rightarrow 4p ₃	9.27	
	9.55 sh ^c	
Cl3p \rightarrow 4p ₄	9.62	
IP1		9.65(9.48) ^{k,l} , 9.6 ^m
	9.74	
Cl3p \rightarrow 4p ₄	9.82	
Cl3p \rightarrow 4p ₆	9.90	
Cl3p \rightarrow 4p _{3'}	10.02	

Assignment	Present Results	Previous Work
	10.13	
	10.19	
	10.27	
C13p \rightarrow 5p ₂ , C13p \rightarrow 4d ₃	10.38	
	10.48 sh ^c	
	10.60	
	10.69	
	10.78	
C13p \rightarrow 5p ₄ , C13p \rightarrow 5p ₃ '	11.08 sh ^c	
	11.17	
C13p \rightarrow 5d ₃	11.25	
	11.32	
C13p \rightarrow 8p ₂ , C13p \rightarrow 4p ₇	11.35	
	11.47	
C13p \rightarrow 5p ₆ , C13p \rightarrow 6d ₃	11.59	
C13p \rightarrow 7p ₃	11.69	
IP2		11.73 ^k , 11.7 ^m
C13p \rightarrow 7p ₃ '	11.75 sh ^c	
C13p \rightarrow 7p ₄	11.90 sh ^c	
	12.01 sh ^c	
C13p \rightarrow 9p ₄	12.14	
IP3		12.18 ^k , 12.2 ^m ,
	12.30	

Assignment	Present Results	Previous Work
IP4		12.4 ^m ,
Cl3p → 8p ₆	12.60	
IP5		12.72 ^k , 12.7 ^m
	12.77	
	12.92	
IP6		12.96 ^k , 12.9 ^m ,
	13.08	
	13.48	
	13.67	
	13.86	
	14.11	
IP7		14.40 ^{k,m}

- ^a Uncertainty ± 0.05 eV for this band, $\pm .02$ for all other bands. Extent of Franck-Condon envelope indicated by the numbers in parentheses.
- ^b Ref. 50.
- ^c Shoulder.
- ^d Subscript denotes IP to which Rydberg series is converging, i.e., 1 = first, 2 = second, etc.
- ^e For definitions of vibrational modes see ref. 14.
- ^f Ref. 13.
- ^g Ref. 7.
- ^h Ref. 49.

- i Ref. 48.
- j Ref. 50.
- k Ref. 27.
- l Vertical IP (adiabatic in parentheses)
- m Ref. 28.

Table 10. Electronic Transition Energies in Trichloroethylene for the $Cl3p \rightarrow nl$ Series (eV)

l	n	observed	calculated
p	4	8.94	8.95
	5	10.38	10.40
	6		10.95
	7		11.21
	$\infty=11.71$		$\delta=1.78$
p'	4	10.02	10.02
	5	11.08	11.09
	6		11.53
	7	11.75	11.75
	$\infty=12.20$		$\delta=1.50$
d	4	10.38	10.39
	5	11.25	11.23
	6	11.59	11.59
	$\infty=12.20$		$\delta=1.26$
p	4	9.62	9.64
	5	11.08	11.09
	6		11.64
	7	11.90	11.90
	8		12.05
	9	12.14	12.15
	$\infty=12.40$		$\delta=1.78$
p	4	9.90	9.99
	5	11.59	11.58
	6		12.17
	7		12.45
	8	12.60	12.60
$\infty=12.96$		$\delta=1.86$	

Table 11. Electron Transition Energies in Tetrachloroethylene (eV)

Assignment	Present Results	Previous Work
$\pi \rightarrow \pi^*, N \rightarrow T$	3.54(2.6-4.5) ^a	4.2 ^b , 3.12 ^c , 4.38 ^d
$\pi \rightarrow \pi^*, N \rightarrow V$	5.29 sh ^e	
	5.35 sh ^e	
$\pi \rightarrow \pi^*, N \rightarrow V$	5.46 sh ^e	
$\pi \rightarrow \pi^*, N \rightarrow V$	5.63 sh ^e	
$\pi \rightarrow \pi^*, N \rightarrow V$	5.78 sh ^e	
	5.84 sh ^e	
$\pi \rightarrow \pi^*, N \rightarrow V$	5.91 sh ^e	5.90 ^f
	5.96 sh ^e	
$\pi \rightarrow \pi^*, N \rightarrow V$	6.07 sh ^e	6.06 ^f
$\pi \rightarrow \pi^*, N \rightarrow V$ (vert)	6.22	5.71 ^c , 6.46 ^d , 6.20 ^f 6.29 ^{g,h} , 5.80 ^j , 5.39 ^k
$\pi \rightarrow 3s_1^1$	6.27	6.25 ^f
$\pi \rightarrow 3s_1 + \nu_2^m$	6.33	6.30 ^f
$\pi \rightarrow 3s_1 + 2\nu_2$	6.37	6.35 ^f
$\pi \rightarrow \pi^*, N \rightarrow V$	6.40	
$\pi \rightarrow 3s_1 + \nu_1$	6.43	6.41 ^f
$\pi \rightarrow 3s_1 + 2\nu_1$	6.58	6.59 ^f
$\pi \rightarrow 3s_1 + 3\nu_1$	6.77	6.75 ^f
$\pi \rightarrow 3s_1 + 4\nu_1$	6.94	6.92 ^f
$\pi \rightarrow 3s_1 + 4\nu_1 + \nu_2$	6.97 sh ^e	6.97 ^f
$\pi \rightarrow 3s_1 + 4\nu_1 + 2\nu_2$	7.03	7.01 ^f
$\pi \rightarrow 3s_1 + 5\nu_1$	7.10	7.07 ^f
$\pi \rightarrow 3p$	7.19	
$\pi \rightarrow 3s + 6\nu_1$	7.23	7.25 ^f

Assignment	Present Results	Previous Work
$\pi \rightarrow 3s + 6\nu_1 + \nu_2$	7.27	7.28 ^f
$\pi \rightarrow 3p + \nu_1$	7.33	
$\pi \rightarrow 3p + \nu_1 + \nu_2$	7.41	
$\pi \rightarrow 3s + 8\nu_1$	7.46	7.43 ^f
$\pi \rightarrow 3p + 2\nu_1$	7.52	
	7.58	
	7.66 sh ^e	
$n(Cl3p) \rightarrow \pi^*$	7.69	7.68 ^f
$\pi \rightarrow 3p + 3\nu_1 + \nu_2$	7.75	
	7.81	
$\pi \rightarrow 4s$	7.90	7.88 ^{g,h,i}
$\pi \rightarrow 3p + 4\nu_1 + \nu_2$	7.93	
$\pi \rightarrow 4s + \nu_2$	7.95	
	8.02 sh ^e	
$\pi \rightarrow 4s + \nu_1$	8.05 sh ^e	8.05 ^{g,h,i}
	8.10	
$\pi \rightarrow 4s + \nu_1 + \nu_2$	8.12	8.11 ^{g,h} , 8.10 ⁱ
	8.21	
$\pi \rightarrow 4s + 2\nu_1$	8.23	8.21 ^{g,h,i}
$\pi + 4p$	8.26 sh	
$\pi \rightarrow 4s + 2\nu_1 + \nu_2$	8.28	8.27 ^{g,h,i}
	8.33 sh ^e	8.32 ^h , 8.33 ⁱ
$\pi \rightarrow 4s + 3\nu_1$	8.39	8.38 ^{g,h,i}
$\pi \rightarrow 4p + \nu_1$	8.43 sh ^e	
$\pi \rightarrow 4s + 3\nu_1 + \nu_2$	8.46	8.44 ^{g,h,i}

Assignment	Present Results	Previous Work
$\pi \rightarrow 4s + 4\nu_1, \pi \rightarrow 5s$	8.53	8.54 ^{g,h} , 8.52 ^g , 8.55 ⁱ
$\pi \rightarrow 5s + \nu_2$	8.60 sh ^e 8.63	8.58 ^g , 8.60 ^{h,i}
$\pi \rightarrow 5s + \nu_1$	8.70 sh ^e 8.73	8.69 ^{g,h,i} 8.72 ^{h,i}
$\pi \rightarrow 5s + \nu_1 + \nu_2$	8.76 sh ^e	8.75 ^{g,h,i}
$\pi \rightarrow 6s$	8.83 sh ^e	8.81 ^{g,h,i}
$\pi \rightarrow 5s + 2\nu_1$	8.88	8.86 ^{g,h,i}
$\pi \rightarrow 6s + \nu_1$	8.96 sh ^e	8.98 ^g , 8.96 ^{h,i}
$\pi \rightarrow 5s + 3\nu_1$	9.00 sh ^e	9.02 ^{g,h,i}
$\pi \rightarrow 6s + 2\nu_1$	9.15	9.14 ⁱ
$\pi \rightarrow 6s + 2\nu_1 + \nu_2, Cl3p \rightarrow 4p_2$	9.19 9.24 sh ^e	9.19 ⁱ 9.24 ⁱ
$\pi \rightarrow 6s + 3\nu_1$	9.30	9.29 ⁱ
$\pi \rightarrow 6s + 3\nu_1 + \nu_2$	9.36 sh ^e 9.43 sh ^e	9.34 ⁱ 9.44 ⁱ
$\pi \rightarrow 6s + 4\nu_1, Cl3p \rightarrow 4p_3$	9.48	9.47 ⁱ
IP1	9.53	9.51(9.34) ^{n,o} , 9.5 ^p 9.52 ⁱ
$Cl3p \rightarrow 4p_4$	9.62	9.61 ⁱ
$Cl3p \rightarrow 4s_6$	9.66 9.74 sh ^e	9.68 ⁱ 9.72 ⁱ
$Cl3p \rightarrow 4p_5$	9.77 9.86 sh ^e 9.90 sh ^e 9.98 sh ^e	9.76 ⁱ 9.88 ⁱ 9.92 ⁱ 9.99 ⁱ

Assignment	Present Results	Previous Work
	10.03	10.05 ⁱ
Cl3p → 4p ₄ '	10.10 sh ^e	10.11 ⁱ
	10.15	
Cl3p → 5p ₂	10.28 sh ^e	
Cl3p → 4p ₈	10.40	10.42 ⁱ
	10.62 sh ^e	10.64 ⁱ
	10.67	10.67 ⁱ
Cl3p → 6p ₂	10.72	10.72 ⁱ
	10.80	10.80 ⁱ
Cl3p → 7p ₂ , Cl3p → 5p ₃	10.92	10.93 ⁱ
	11.00	11.00 ⁱ
Cl3p → 8p ₂ , Cl3p → 5p ₄	11.07 sh ^e	11.09 ⁱ
	11.12	11.13 ⁱ
Cl3p → 5p ₅	11.20 sh ^e	11.21 ⁱ
Cl3p → 5p ₄ '	11.26 sh ^e	
Cl3p → 4p ₉ , Cl3p → 5s ₆	11.31	
IP2		11.38 ⁿ , 11.40 ^p
	11.42 sh ^e	
Cl3p → 6p ₃	11.45	
Cl3p → 4p ₁₀	11.49	
	11.60	
Cl3p → 6p ₄	11.64 sh ^e	
Cl3p → 7p ₃ , Cl3p → 5p ₈ , Cl3p → 6p ₄ '	11.70	
Cl3p → 6p ₅	11.76 sh ^e	
Cl3p → 7p ₄ , Cl3p → 6s ₆	11.90	

Assignment	Present Results	Previous Work
Cl3p → 9p ₃ , Cl3p → 7p ₄ '	11.95	
Cl3p → 7p ₅	11.99	
	12.12	
Cl3p → 6p ₈ , Cl3p → 7s ₆	12.18	
IP3		12.18 ⁿ , 12.2 ^p
	12.25	
Cl3p → 8s ₆	12.34	
IP4		12.44 ⁿ , 12.4 ^p
	12.5	
IP5		12.54 ⁿ , 12.5 ^p
IP6		12.67 ⁿ , 12.7 ^p
IP7		12.77 ⁿ , 12.8 ^p
IP8		12.91 ⁿ , 13.0 ^p
	13.0	
	13.5	
IP9		13.48 ⁿ , 13.5 ^p
	14.1	
IP10		14.68 ⁿ , 14.7 ^p
	15.0	
IP11		15.10 ^{n,p}

^a Uncertainty ±0.05 eV for this band, ±0.02 eV for all other bands. Extent of Franck-Condon envelope indicated by numbers in parentheses.

^b Ref. 22.

- c Ref. 51.
- d Ref. 50.
- e sh indicates shoulder
- f Ref. 10.
- g Ref. 11.
- h Ref. 7.
- i Ref. 12.
- j Ref. 48.
- k Ref. 49.
- l Subscript denotes IP to which Rydberg series converges, i.e., 1 = first IP, 2 = second IP, etc.
- m For definitions of vibrational modes see ref. 12.
- n Ref. 27.
- o Vertical IP (adiabatic in parentheses).
- p Ref. 28.

Table 12. Electronic Transition Energies in Tetrachloroethylene for the Cl3p → n'l Rydberg Series (eV)

<i>l</i>	<i>n</i>	observed	calculated
p	4	9.19	9.19
	5	10.28	10.28
	6	10.72	10.72
	7	10.92	10.94
	8	11.07	11.08
	∞ = 11.40		δ = 1.52
p	4	9.48	9.49
	5	10.92	10.90
	6	11.45	11.44
	7	11.70	11.70
	8	-	11.85
	9	11.95	11.94
	∞ = 12.20		δ = 1.76
p	4	9.62	9.61
	5	11.07	11.08
	6	11.64	11.63
	7	11.90	11.90
	∞ = 12.40		δ = 1.79
p'	4	10.10	10.10
	5	11.26	10.24
	6	11.70	11.71
	7	11.95	11.94
	∞ = 12.40		δ = 1.57
p	4	9.77	9.79
	5	11.20	11.20
	6	11.76	11.74
	7	11.99	12.00
	∞ = 12.50		δ = 1.76
s	4	9.66	9.70
	5	11.31	11.31
	6	11.90	11.90
	7	12.18	12.18
	∞ = 12.70		δ = 1.87

<i>l</i>	n	observed	calculated
p	4	10.40	10.40
	5	11.70	11.68
	6	12.18	12.18
$\infty = 12.91$		$\delta = 1.67$	

Table 13. Vertical Transition Energy/eV

Chemical Structure	x=H ^a			x=F ^b			x=Cl			x=CH ₃ ^{a,b}		
	N+T	N+V	π+3B	N+T	N+V	π+3B	N+T	N+V	π+3B	N+T	N+V	π+3B
	4.32	7.60	7.11	4.40	7.50	7.02	4.13	6.77	6.72	4.28	7.17	6.60
	-	-	-	4.63	7.50	6.95	3.75	6.42	6.65	4.22	6.60	6.15
	-	-	-	4.43	7.82	6.52	3.94	6.60	6.54	4.21	7.10	6.03
	-	-	-	4.18	7.39	6.44	3.84	6.36	6.40	4.24	6.95	6.15
	-	-	-	4.43	7.65	6.50	3.70	6.33	6.12	4.16	6.84	5.76
	-	-	-	4.68	8.84	6.62	3.54	6.22	6.27	4.10	6.57	5.55

^aRef. 6

^bRef. 5

^cRef. 58

Figure Captions.

- Figure 1. Schematic diagram of electron impact spectrometer (hemispherical analyzers not to scale).
- Figure 2. Low angle (10°) and high angle (90°) spectra of vinyl chloride with $E_0 = 25$ eV.
- Figure 3. DCS plot of vinyl chloride $E_0 = 25$ eV. Elastic scattering: ■ , $N \rightarrow V$: ▲, $N \rightarrow T$: ●. The same arbitrary units are used for all three curves. The X0.1 for the elastic scattering is the factor by which the corresponding DCS was multiplied before plotting.
- Figure 4. DCS plot of vinyl chloride $E_0 = 50$ eV. Elastic scattering: ■ , $N \rightarrow V$: ▲ $N \rightarrow T$: ●. See caption for figure 3 for scale explanation.
- Figure 5. High resolution electron energy-loss spectrum of vinyl chloride $E_0 = 100$ eV $\theta = 0^\circ$ resolution = 35 meV FWHM.
- Figure 6. High resolution electron energy-loss spectrum of 1,1 dichloroethylene $E_0 = 100$ eV, $\theta = 0^\circ$ resolution = 35 meV FWHM.
- Figure 7. Low angle (10°) and high angle (90°) spectra of 1,1 dichloroethylene with $E_0 = 25$ eV.
- Figure 8. DCS plot of 1,1 dichloroethylene $E_0 = 25$ eV. Elastic scattering: ■ , $N \rightarrow V$: ▲, $N \rightarrow T$: ●. See caption for figure 3.
- Figure 9. DCS plot of 1,1 dichloroethylene $E_0 = 50$ eV. Elastic scattering: ■ , $N \rightarrow V$: ▲ $N \rightarrow T$: ● See caption for figure 3.

- Figure 10. High resolution electron energy-loss spectra of cis-dichloroethylene $E_0 = 100$ eV, $\theta = 0^\circ$, resolution = 45 meV FWHM.
- Figure 11. Low angle (10°) and high angle (90°) spectra of cis-dichloroethylene with $E_0 = 25$ eV.
- Figure 12. DCS plot of cis-dichloroethylene $E_0 = 25$ eV. Elastic scattering: ■, N → V: ▲ N → T: ●. See caption for figure 3.
- Figure 13. DCS plot of cis-dichloroethylene $E_0 = 50$ eV. Elastic scattering: ■, N → V: ▲ N → T: ●. See caption for figure 3.
- Figure 14. High resolution electron energy-loss spectra of trans-dichloroethylene $E_0 = 100$ eV, $\theta = 0^\circ$ resolution = 40 meV FWHM.
- Figure 15. Low angle (10°) and high angle (90°) spectra of trans-dichloroethylene with $E_0 = 25$ eV.
- Figure 16. DCS plot of trans-dichloroethylene $E_0 = 25$ eV. Elastic scattering: ■, N → V: ▲, N → T: ●. See caption for figure 3.
- Figure 17. DCS plot of trans-dichloroethylene $E_0 = 50$ eV. Elastic scattering: ■, N → V: ▲, N → T: ●. See caption for figure 3.
- Figure 18. Plot of the electron energy-loss spectra in the 7 eV to 9 eV energy-loss region taken at various incident energies (E_0) and at various angles (θ) to illustrate the dependence of the symmetry forbidden transitions (shown by arrows) on these two parameters. Tick marks on the Y axis indicate the baselines of the successive spectra. The arbitrary units for each spectrum are different and are chosen so that the displayed height of the intensity of the 8.75 eV transition is the same

for all displayed spectra.

Figure 19. Plot of the electron energy-loss spectra in the 9 eV to 11 eV energy loss region at incident energy $E_0=100$ eV with $\theta=0^\circ$ and 10° to show emergence of symmetry forbidden transitions. Tick marks on the Y axis indicate the baselines of the successive spectra. The arbitrary units for each spectrum are different and are chosen so that the displayed height of the intensity of the 9.27 eV transition is the same for all displayed spectra.

Figure 20. High resolution electron energy-loss spectrum of trichloroethylene $E_0 = 100$ eV, $\theta = 0^\circ$, resolution = 40 meV FWHM.

Figure 21. Low angle (10°) and high angle (90°) energy-loss spectra at trichloroethylene with $E_0 = 25$ eV.

Figure 22. DCS plot of trichloroethylene $E_0 = 25$ eV Elastic scattering: \blacksquare , N \rightarrow V : \blacktriangle , N \rightarrow T : \bullet . See caption for figure 3.

Figure 23. DCS plot of trichloroethylene $E_0 = 50$ eV. Elastic scattering: \blacksquare , N \rightarrow V : \blacktriangle , N \rightarrow T : \bullet . See caption for figure 3.

Figure 24. Low angle (10°) and high angle (90°) energy-loss spectra of tetrachloroethylene with $E_0 = 25$ eV.

Figure 25. DCS plot of tetrachloroethylene $E_0 = 25$ eV. Elastic scattering: \blacksquare , N \rightarrow V : \blacktriangle , N \rightarrow T : \bullet . See caption for figure 3.

Figure 26. DCS plot of tetrachloroethylene $E_0 = 50$ eV. Elastic scattering: \blacksquare , N \rightarrow V : \blacktriangle , N \rightarrow T : \bullet . See caption for figure 3.

Figure 27. High resolution electron energy-loss spectrum of tetrachloroethylene $E_0 = 100$ eV, $\theta = 0^\circ$, resolution = 35 meV

FWHM.

- Figure 28. Plot of the electron energy-loss spectra in the 7 eV to 9 eV energy-loss region of incident energy $E_0 = 100$ eV with $\theta = 0^\circ$ and 10° to show emergence of symmetry forbidden transitions. Tick marks on the Y axis indicate the baselines of the successive spectra. Arbitrary units for each spectra are different and chosen so that the displayed height for the intensity of the 7.69 eV transition is the same for all displayed spectra.
- Figure 29. Transition energy shifts for the $N \rightarrow T$ transition as compared to ethylene ($n=0$) fluorine : ●, chlorine : ■, and methyl : ▲.
- Figure 30. Transition energy shifts for the $N \rightarrow V$ transition as compared to ethylene ($n=0$) fluorine : ●, chlorine : ■, and methyl : ▲.
- Figure 31. Transition energy shifts for the $\pi \rightarrow 3s$ transition as compared to ethylene ($n=0$) fluorine : ●, chlorine : ■, and methyl : ▲.
- Figure 32. Plot of transition energies versus the quantity IP-EA for the chloroethylenes. ■ : $N \rightarrow V$, ● : $N \rightarrow T$.

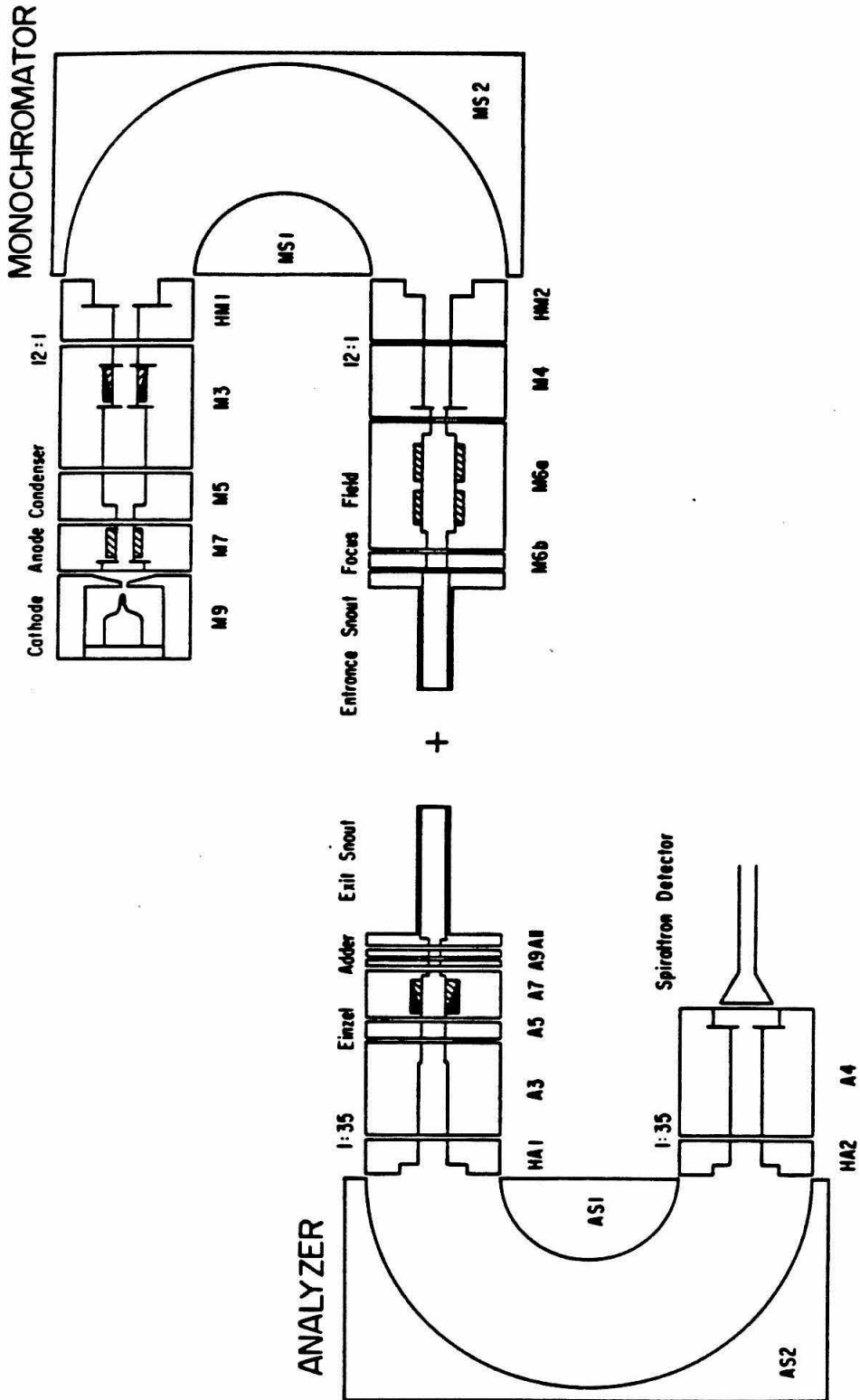


Figure 1.

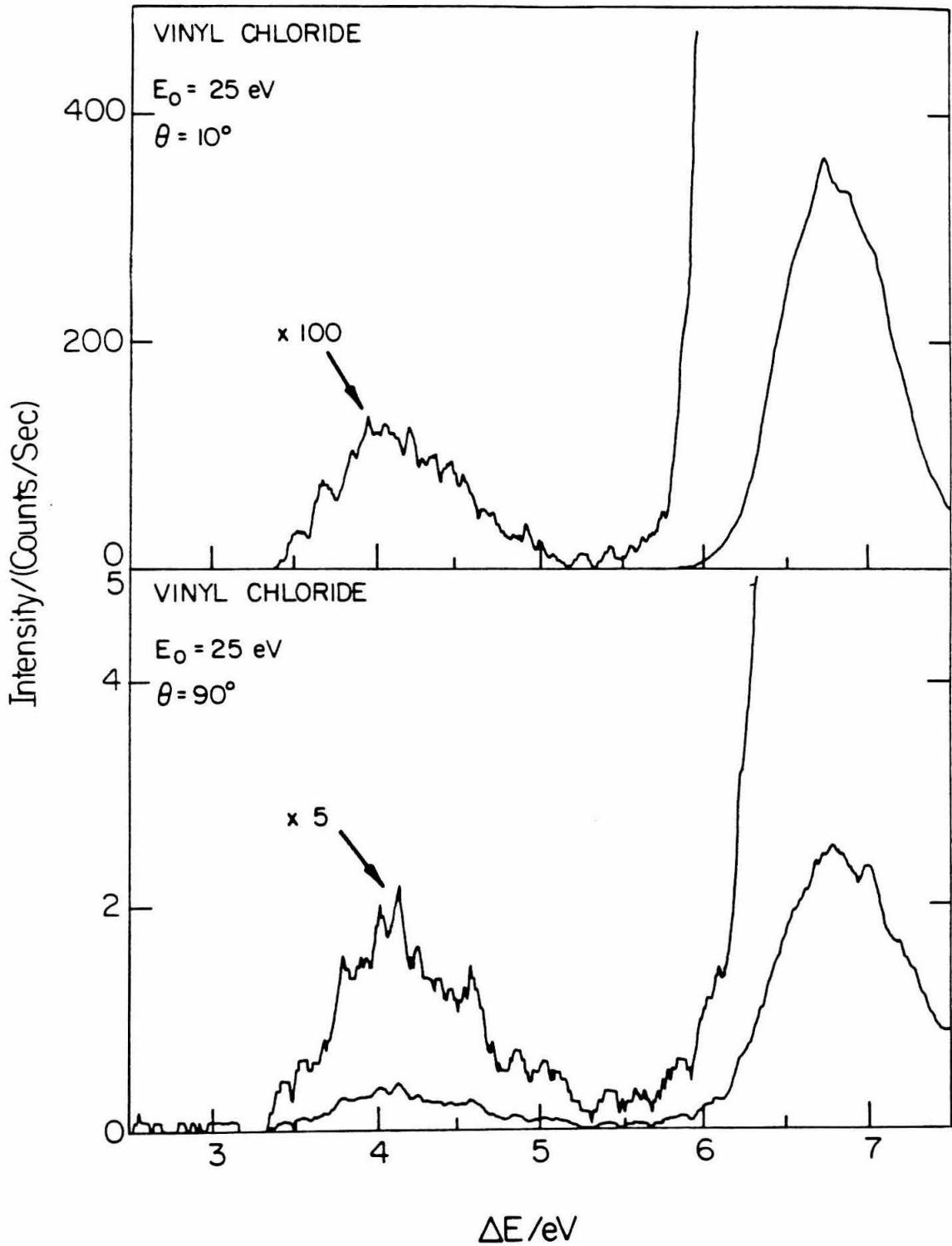


Figure 2.

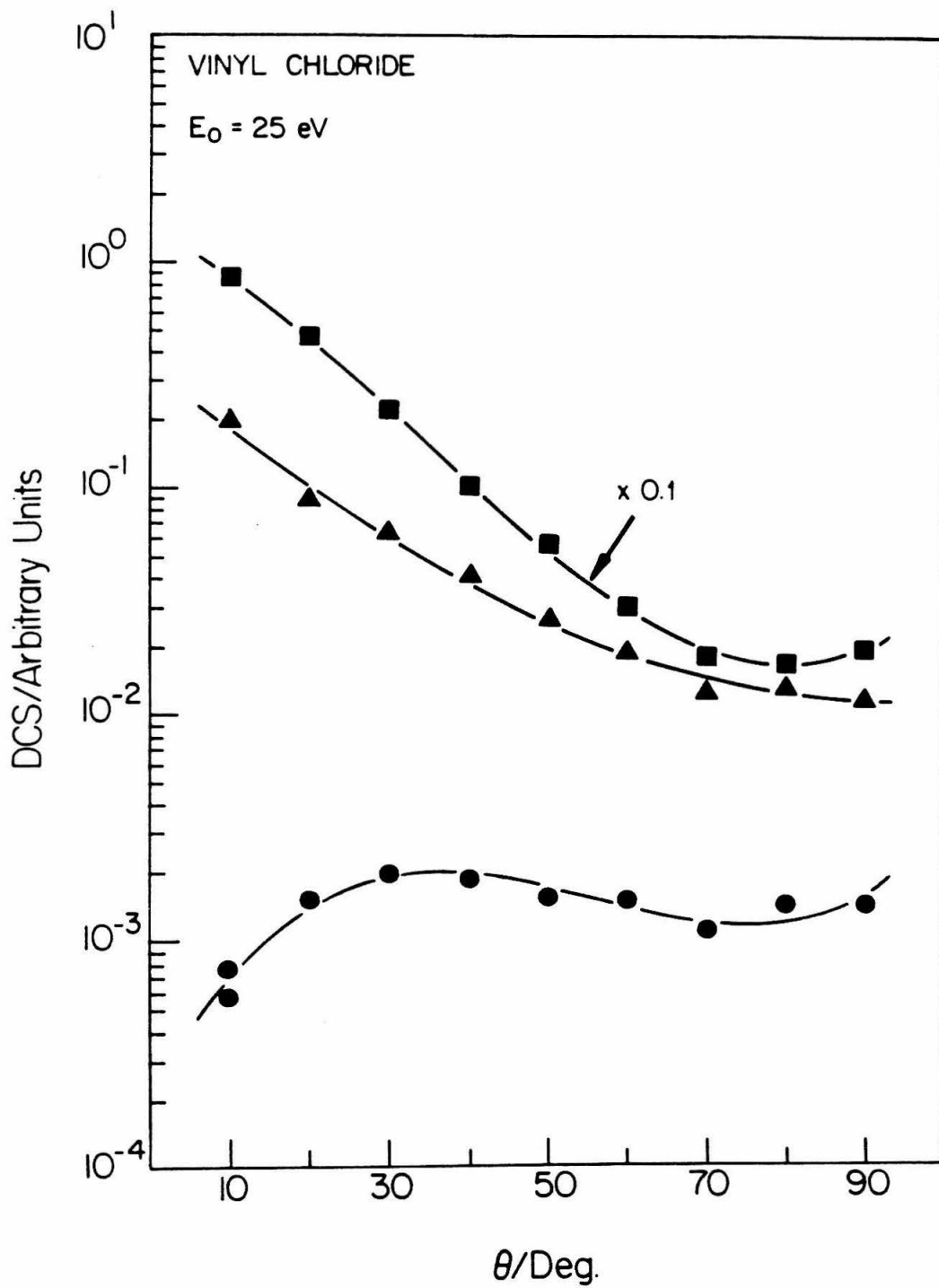


Figure 3.

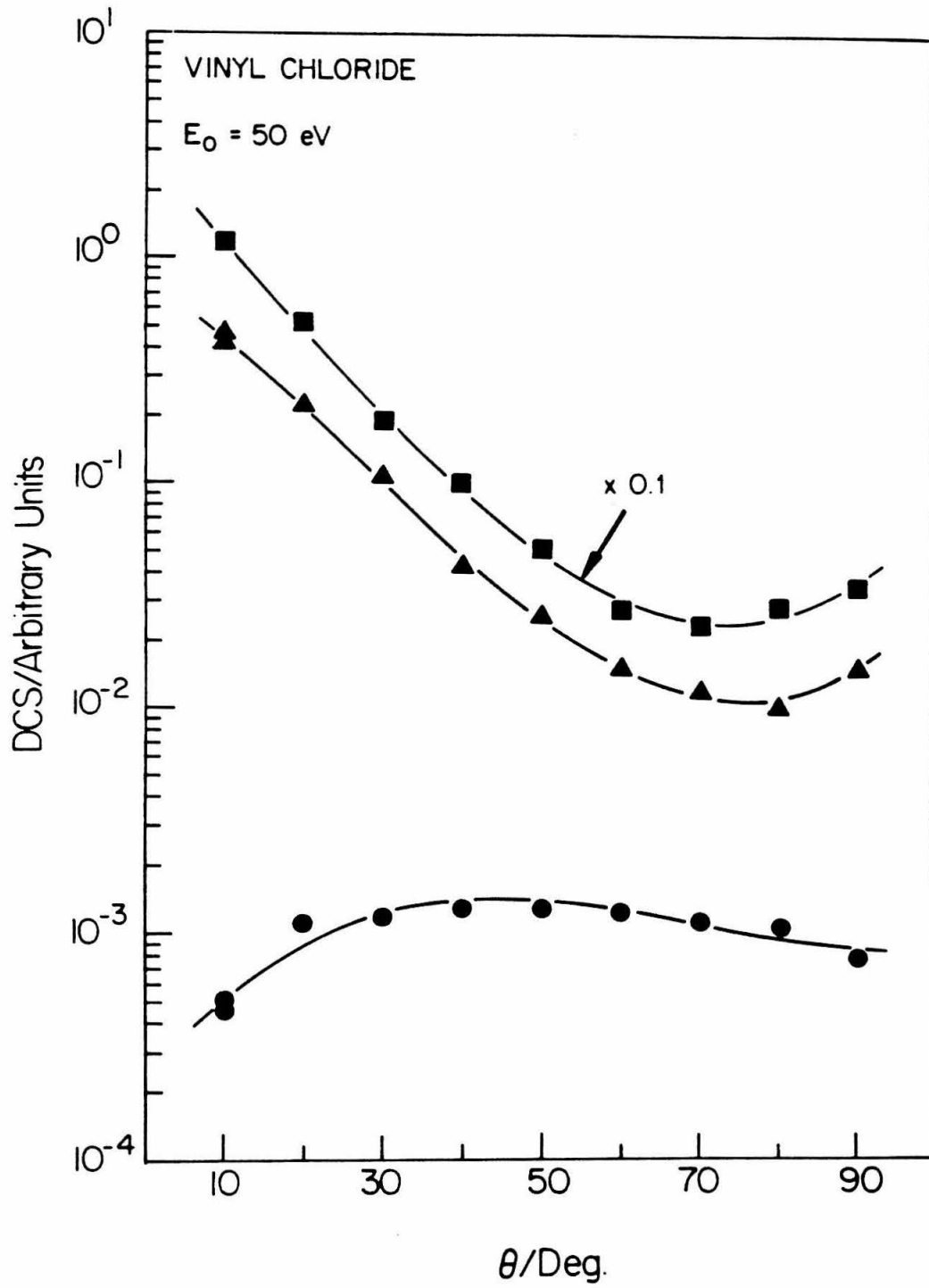


Figure 4.

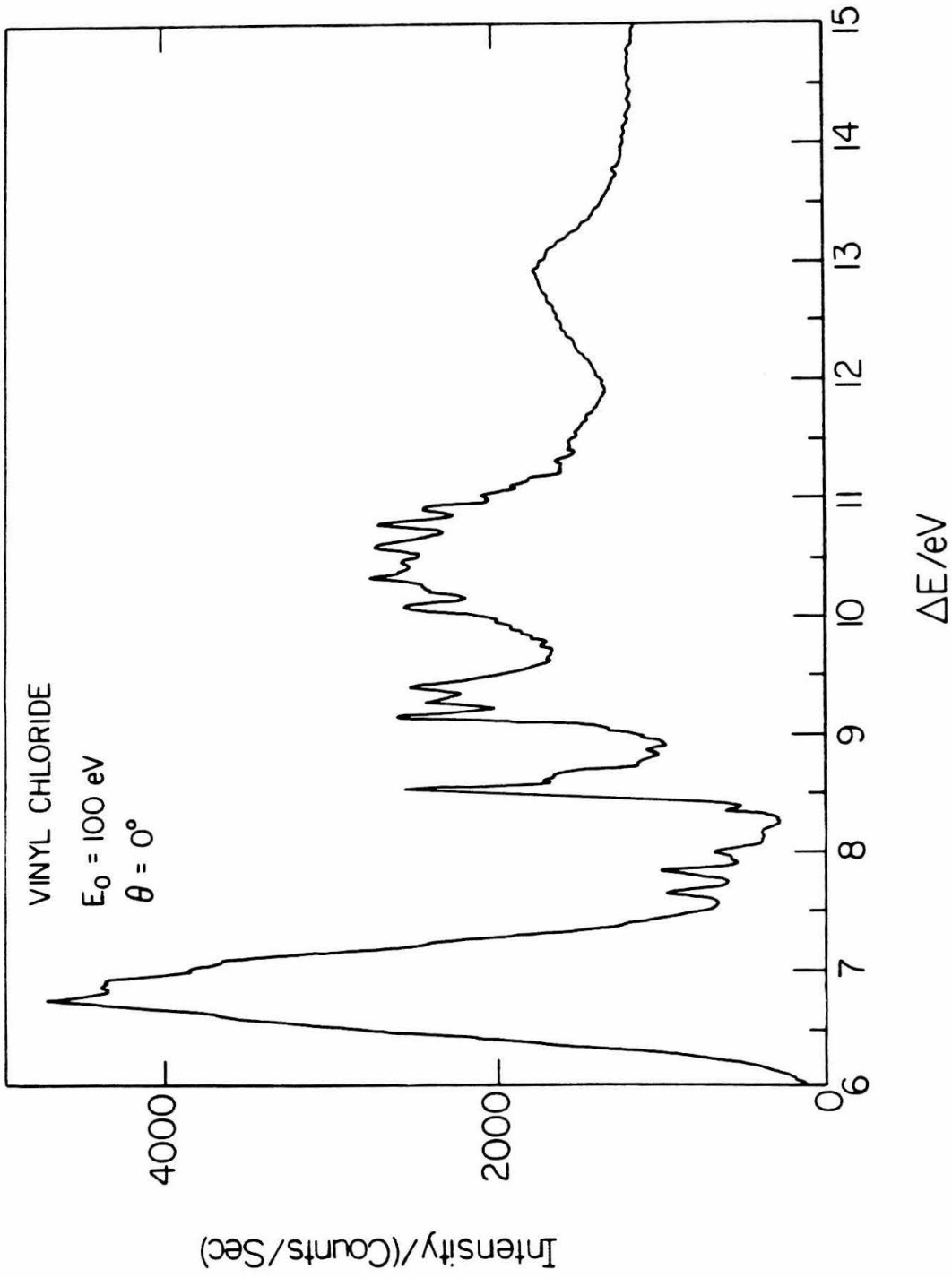


Figure 5.

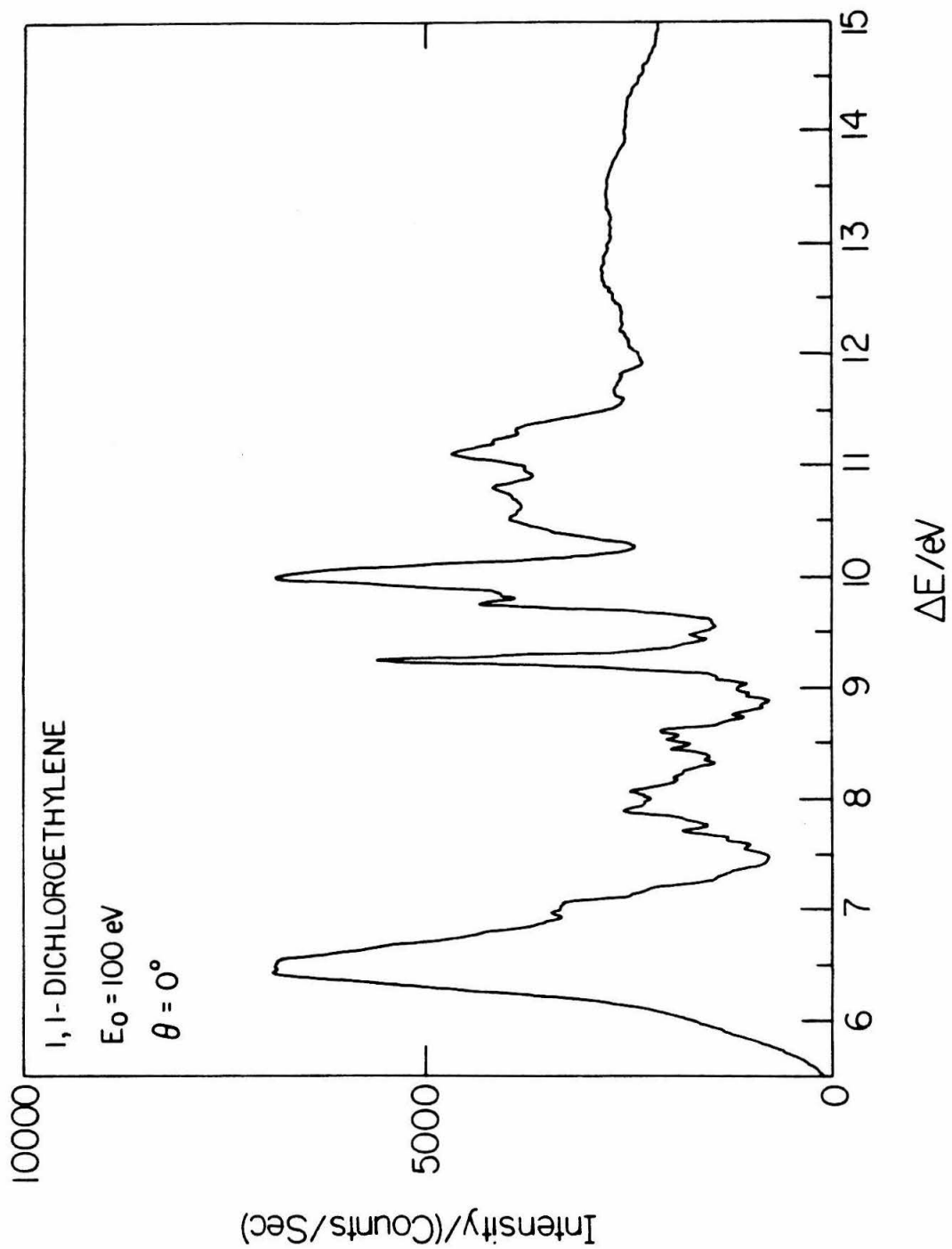


Figure 6.

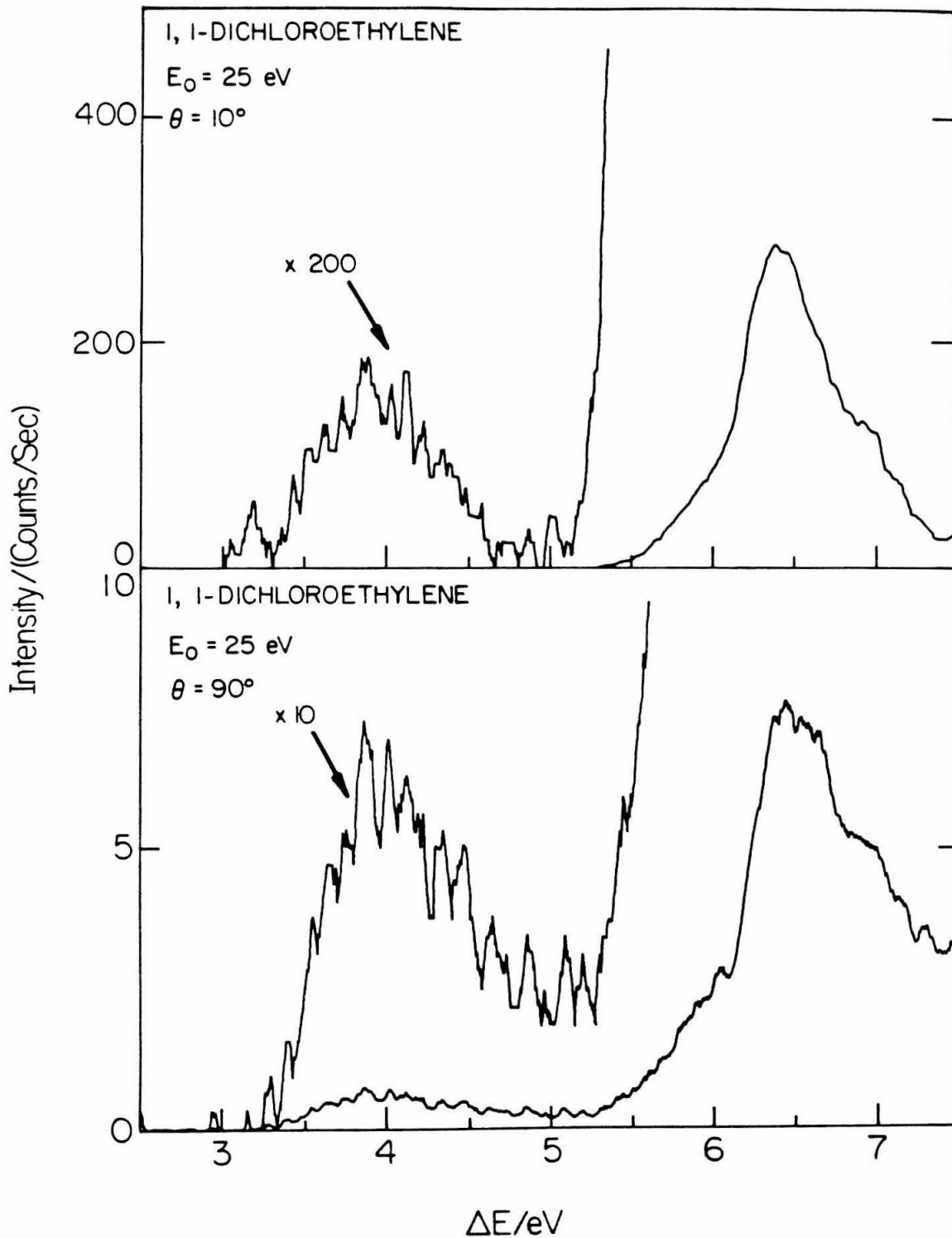


Figure 7.

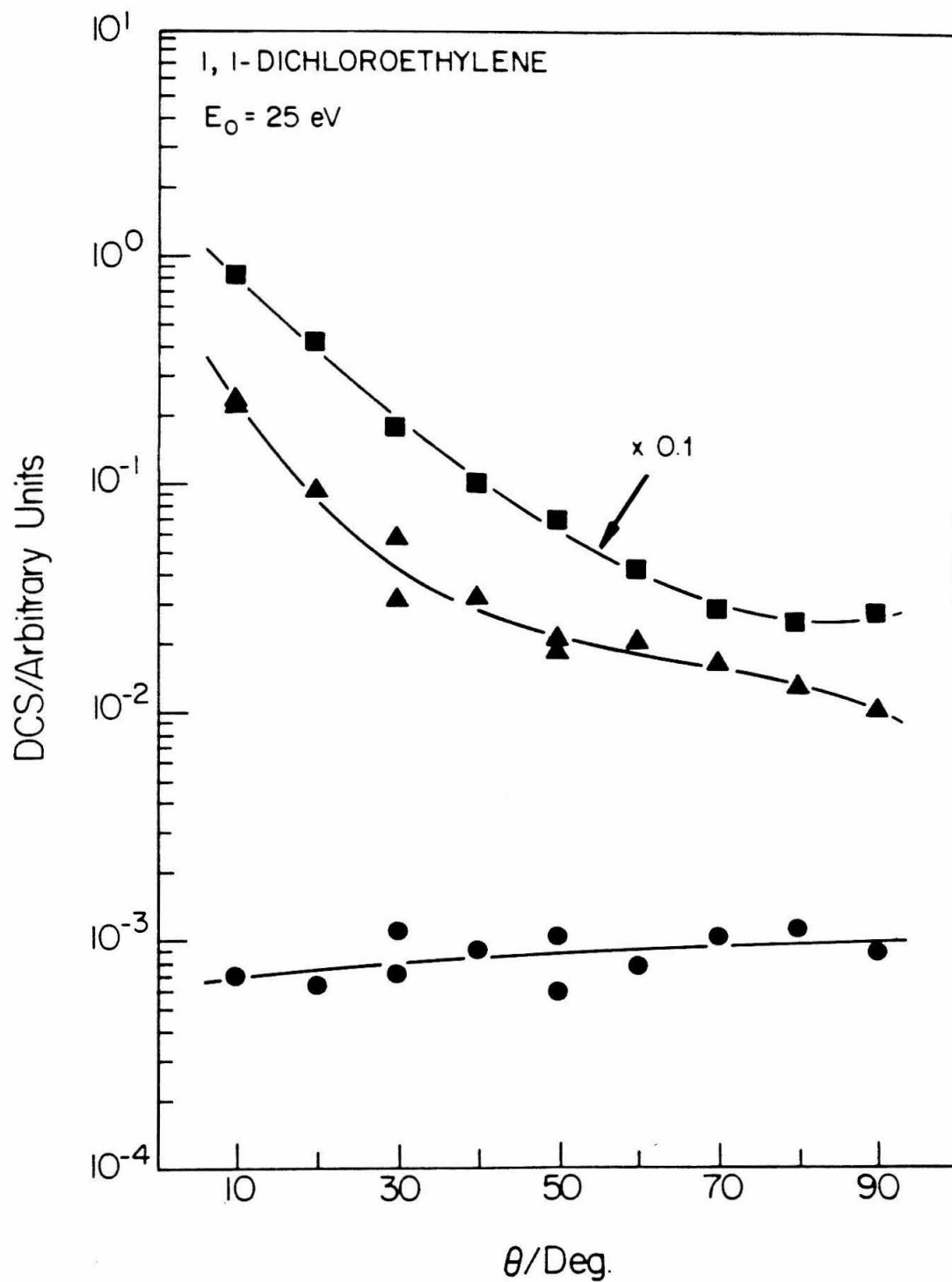


Figure 8.

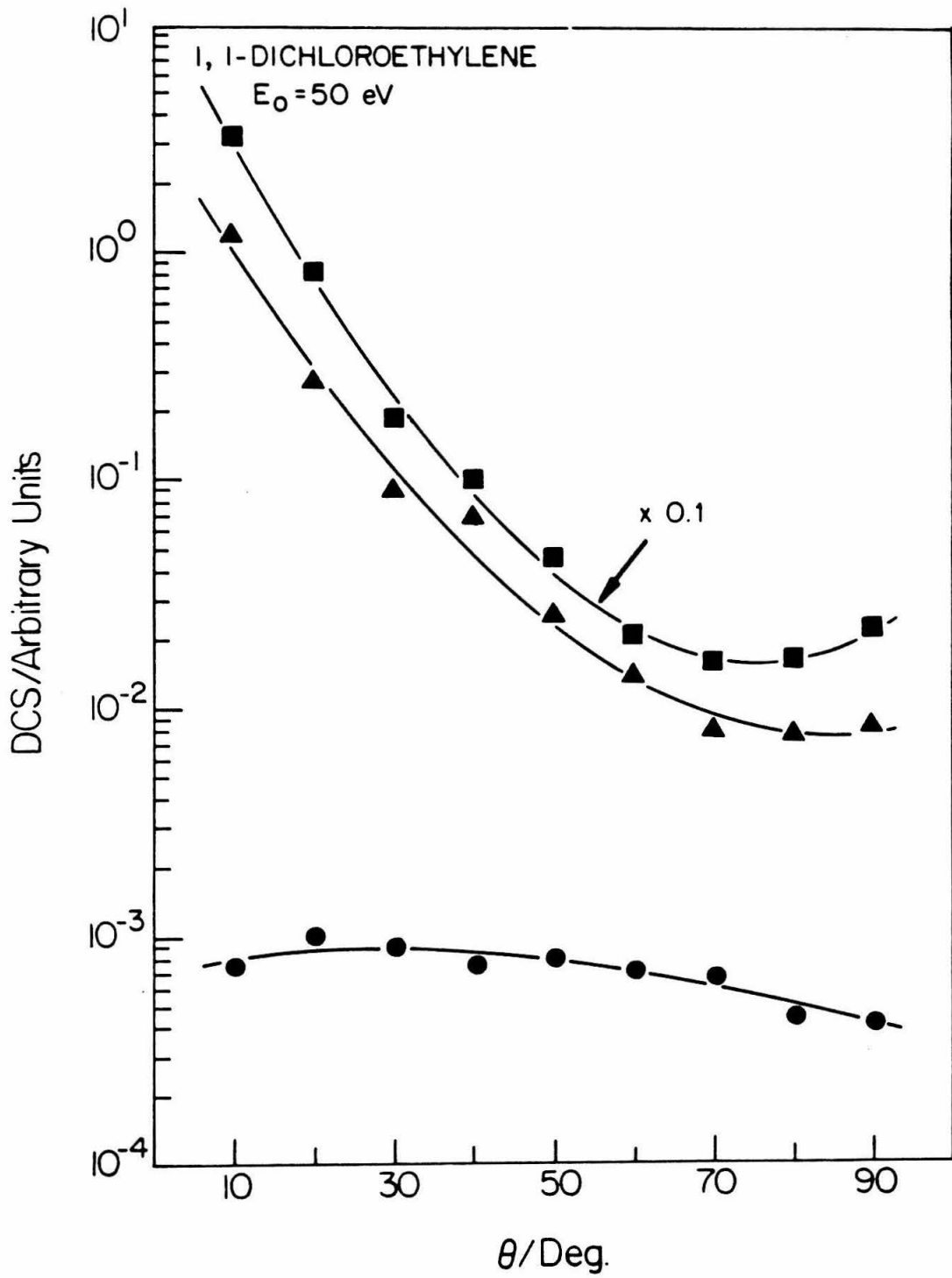


Figure 9.

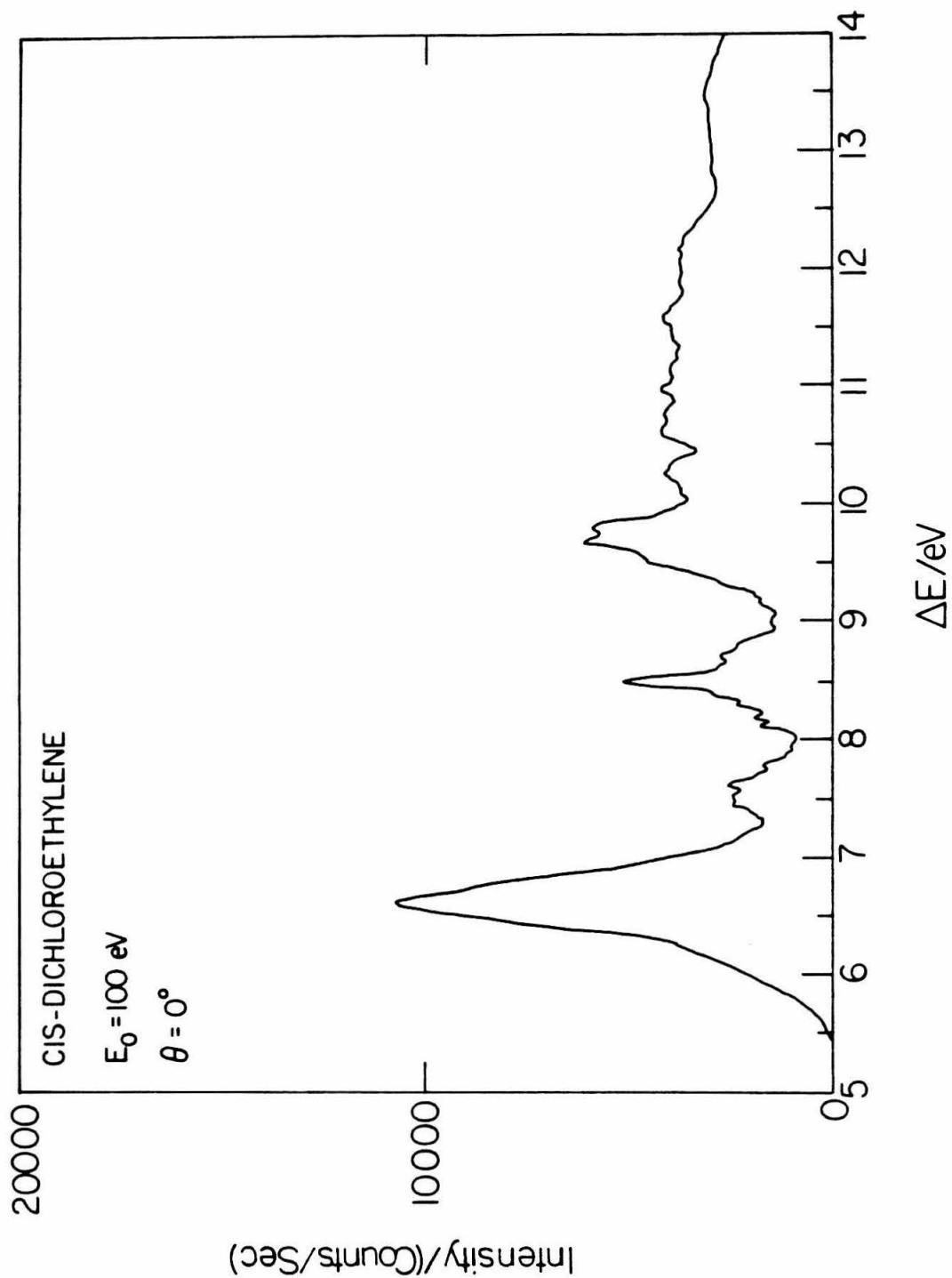


Figure 10.

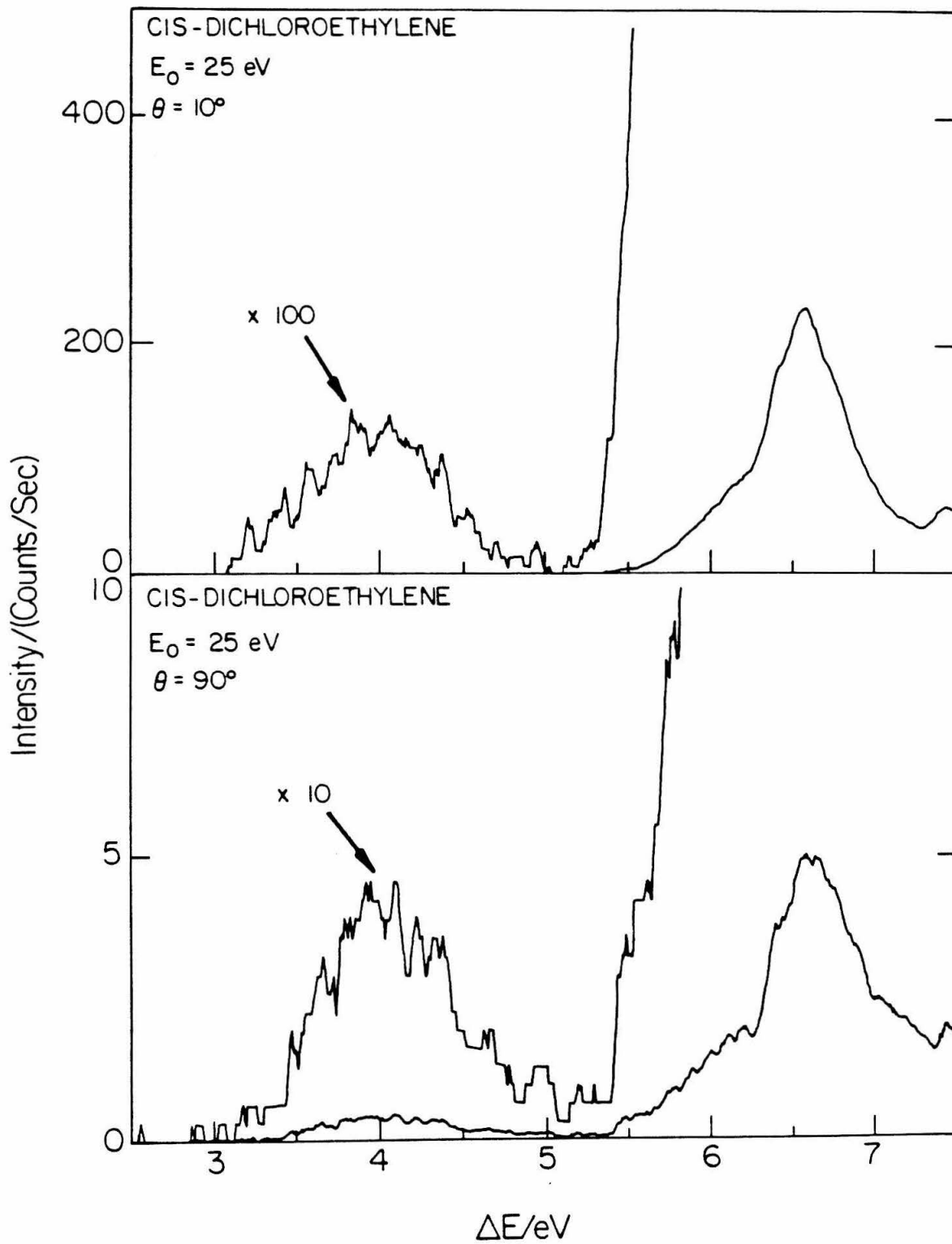


Figure 11.

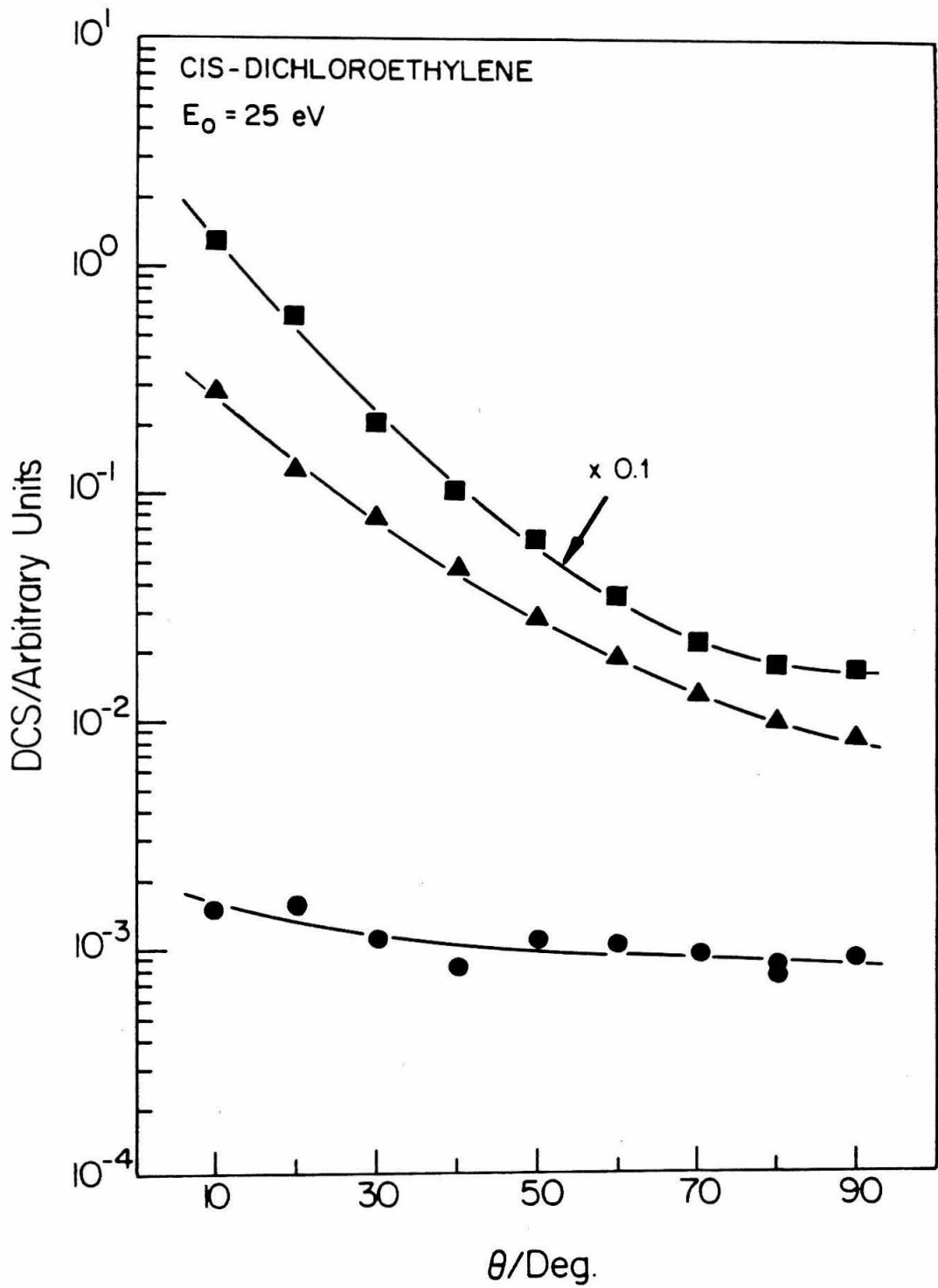


Figure 12.

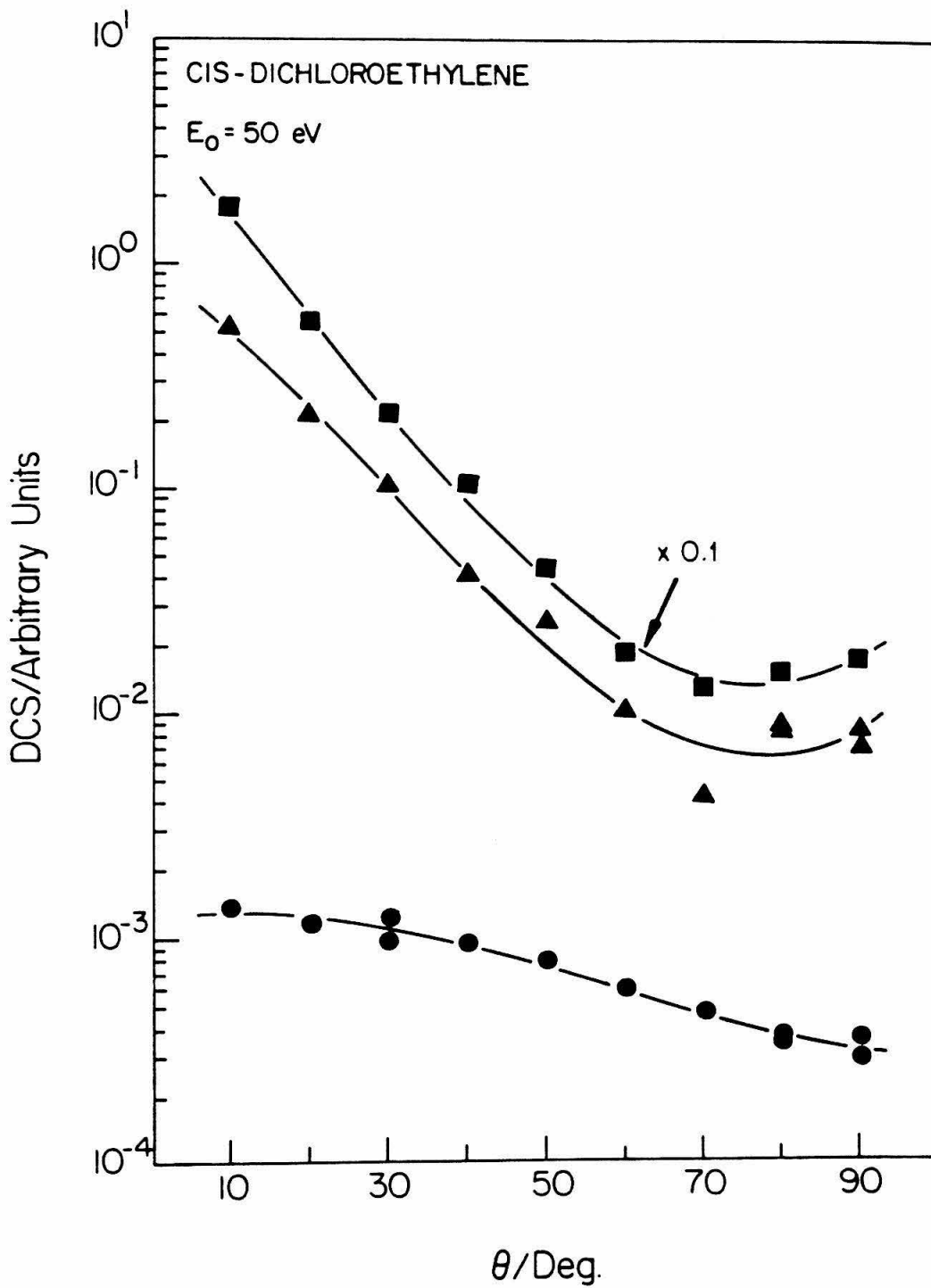


Figure 13.

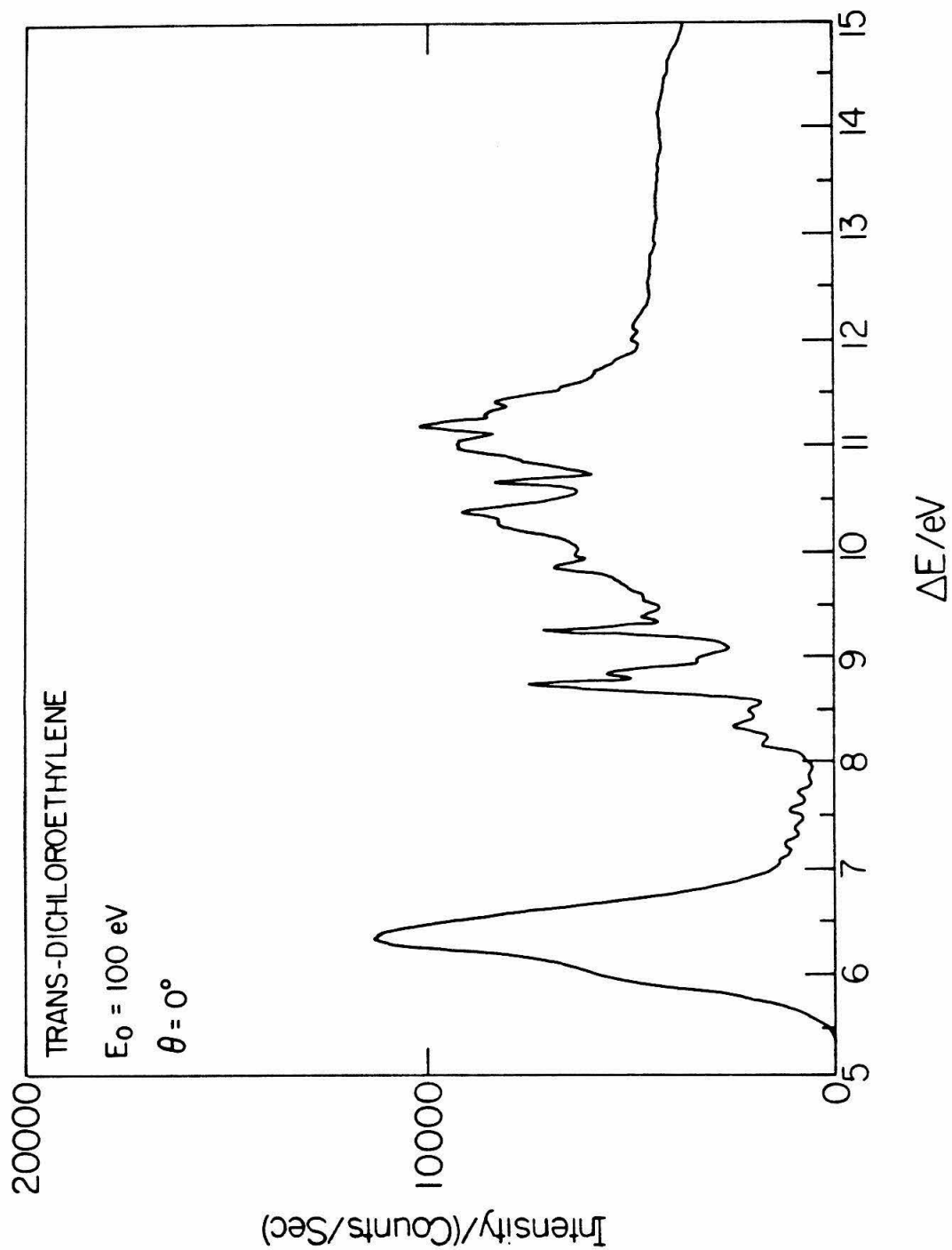


Figure 14.

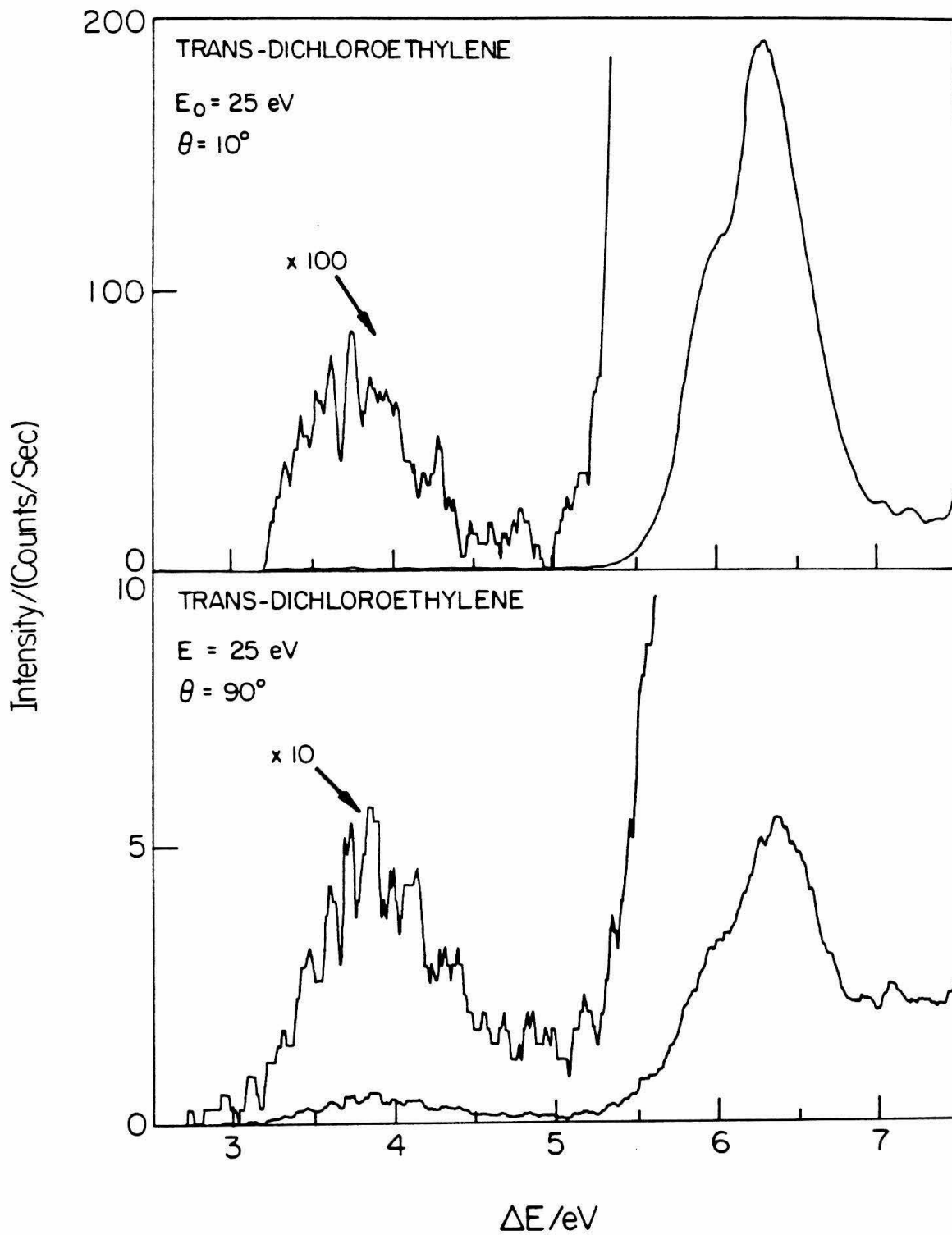


Figure 15.

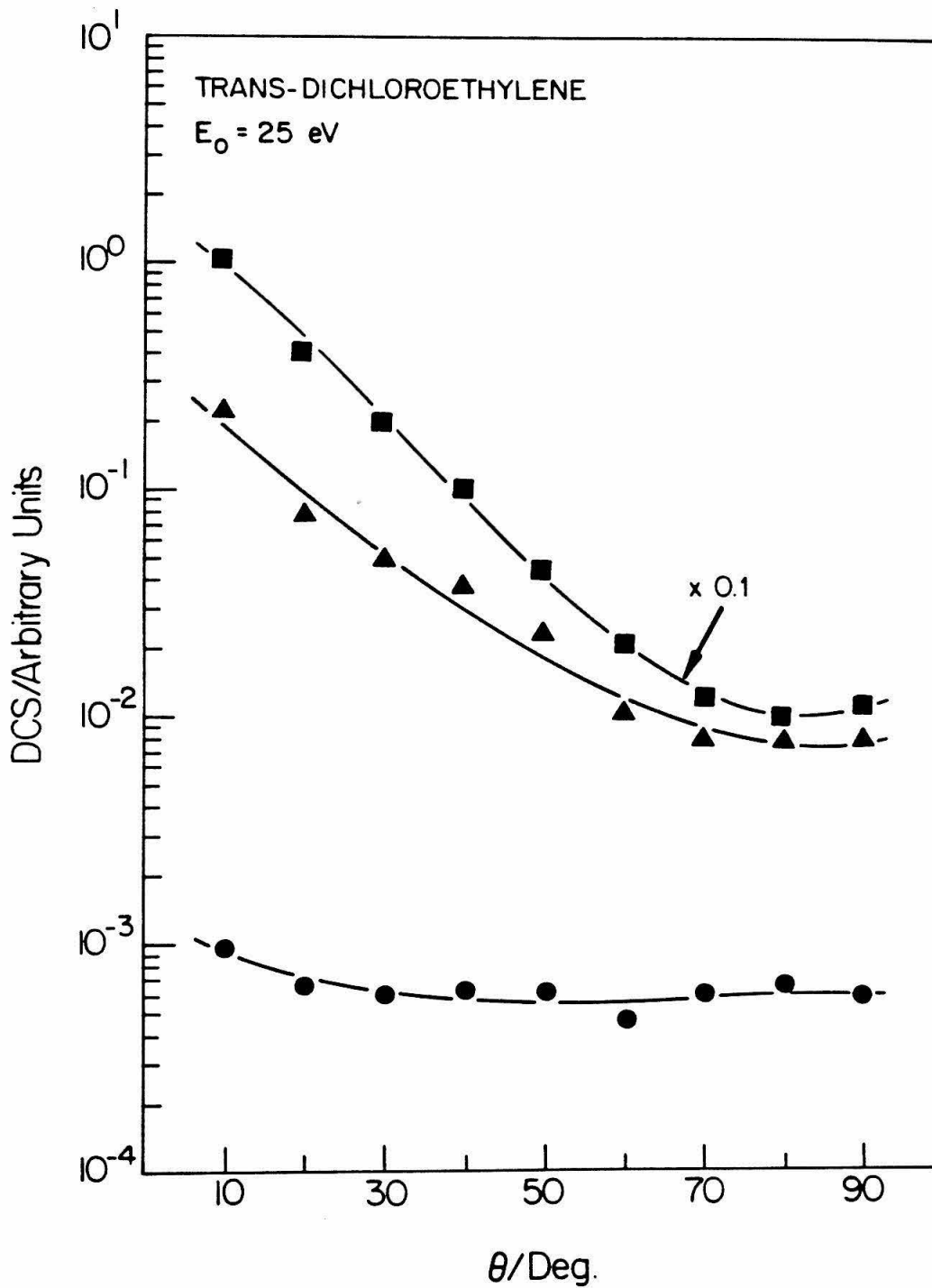


Figure 16.

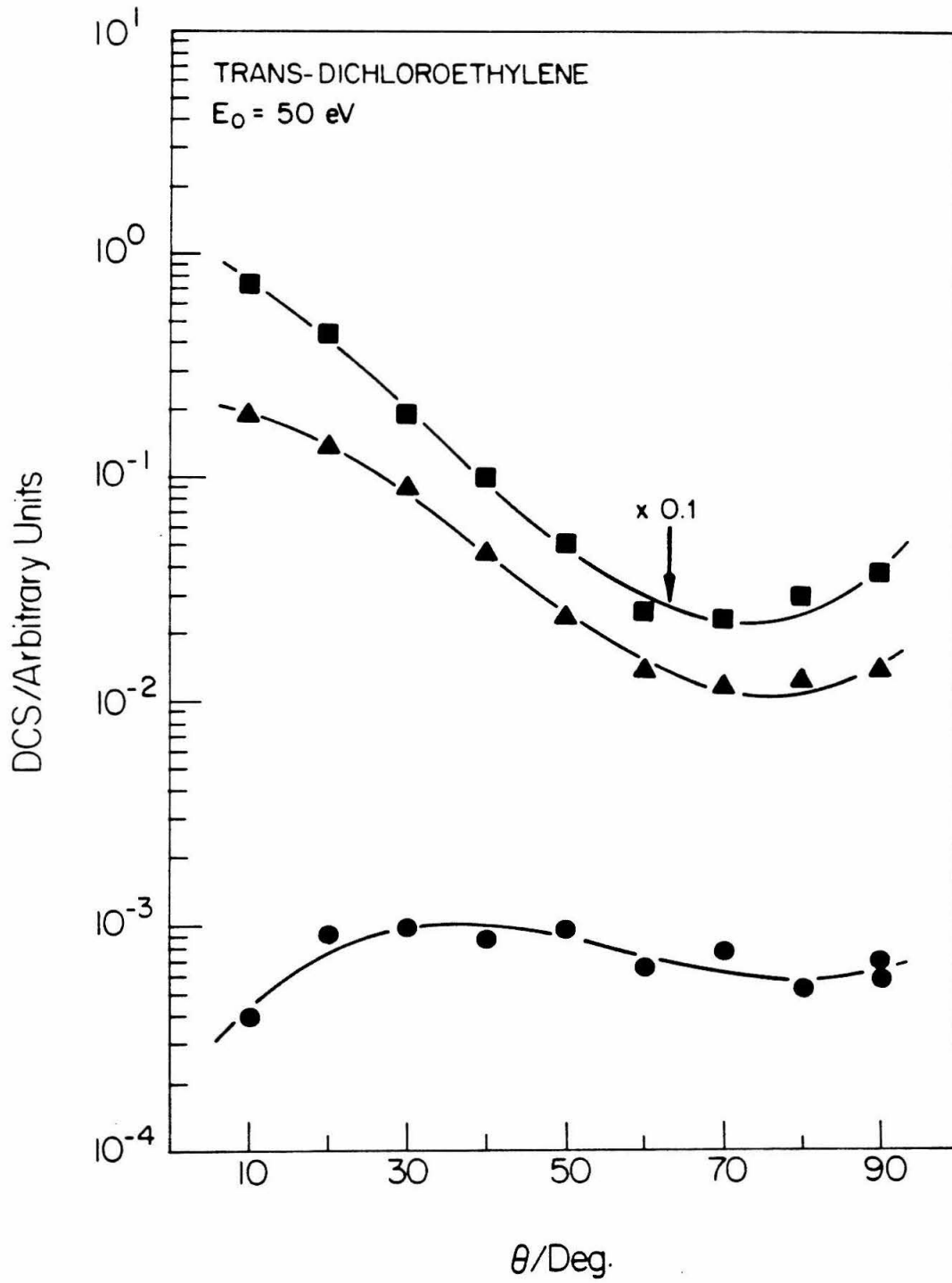


Figure 17.

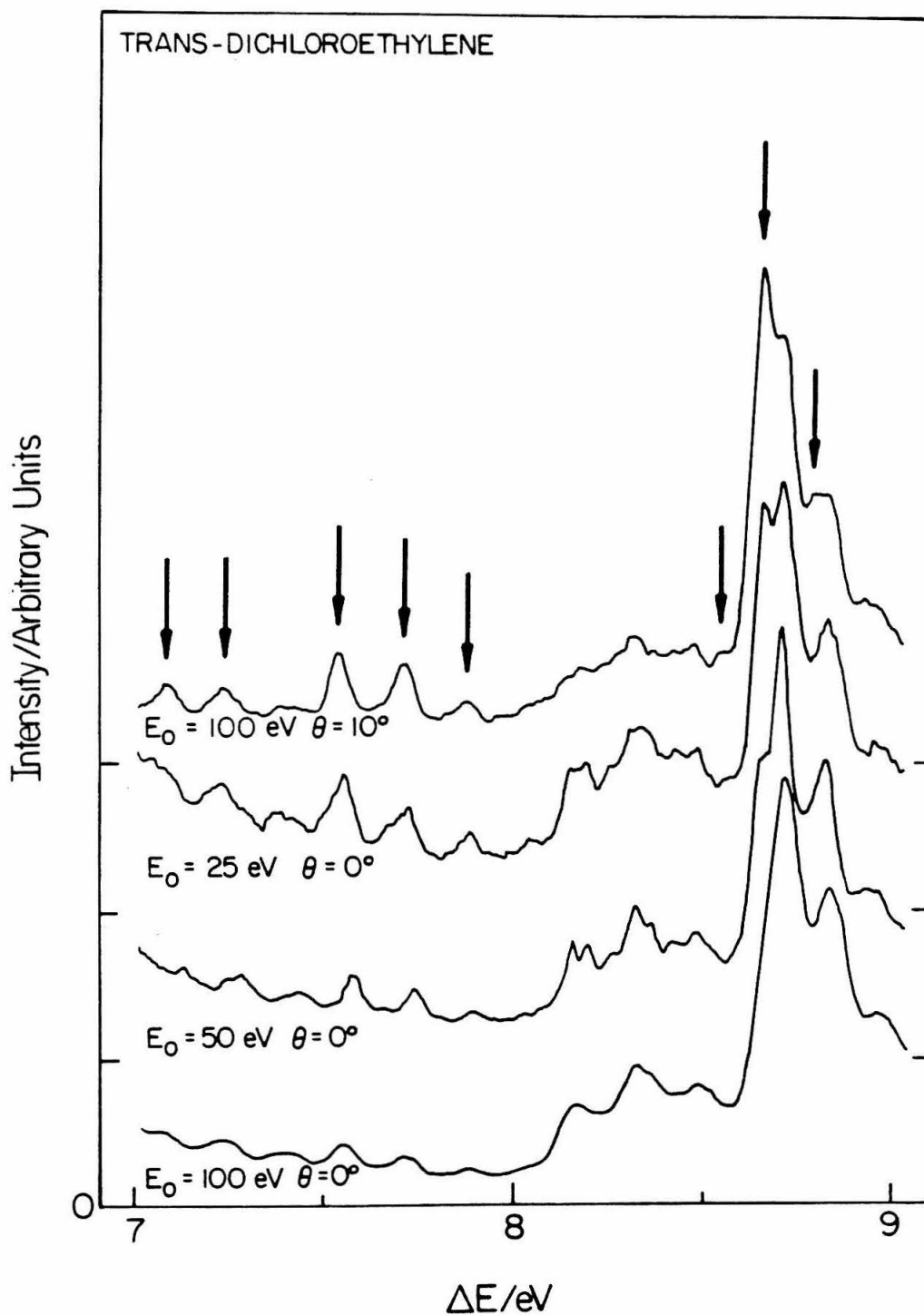


Figure 18.

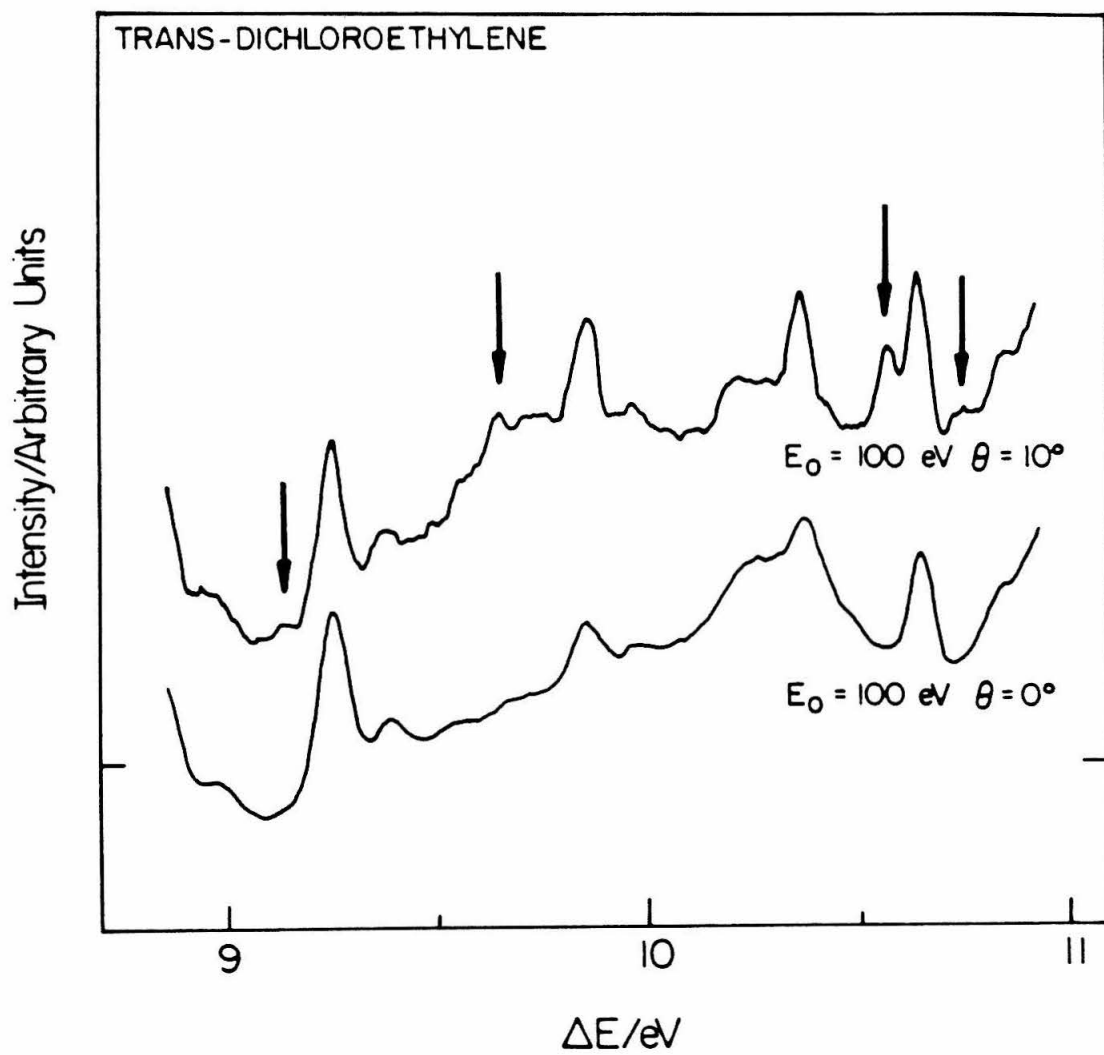


Figure 19.

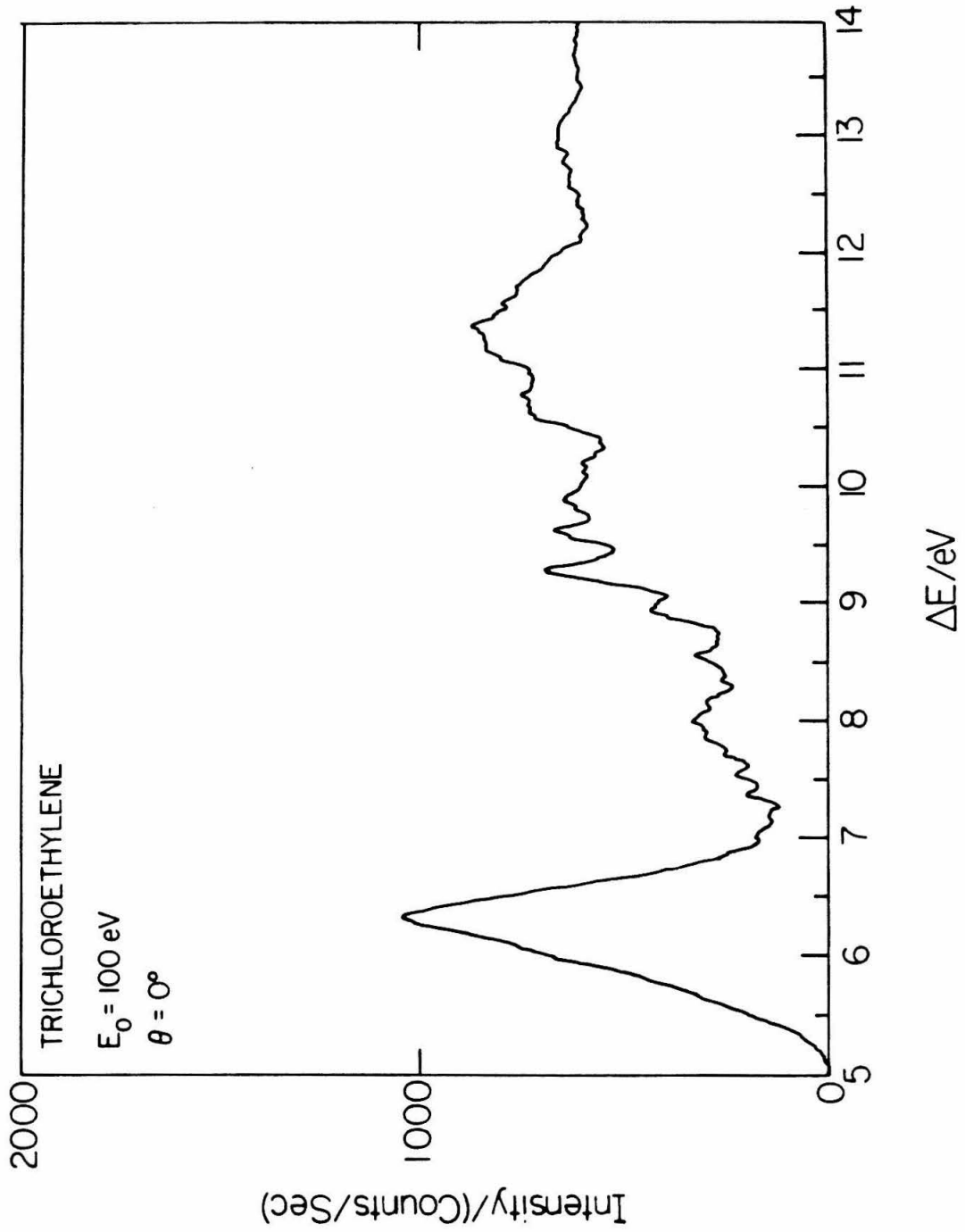


Figure 20.

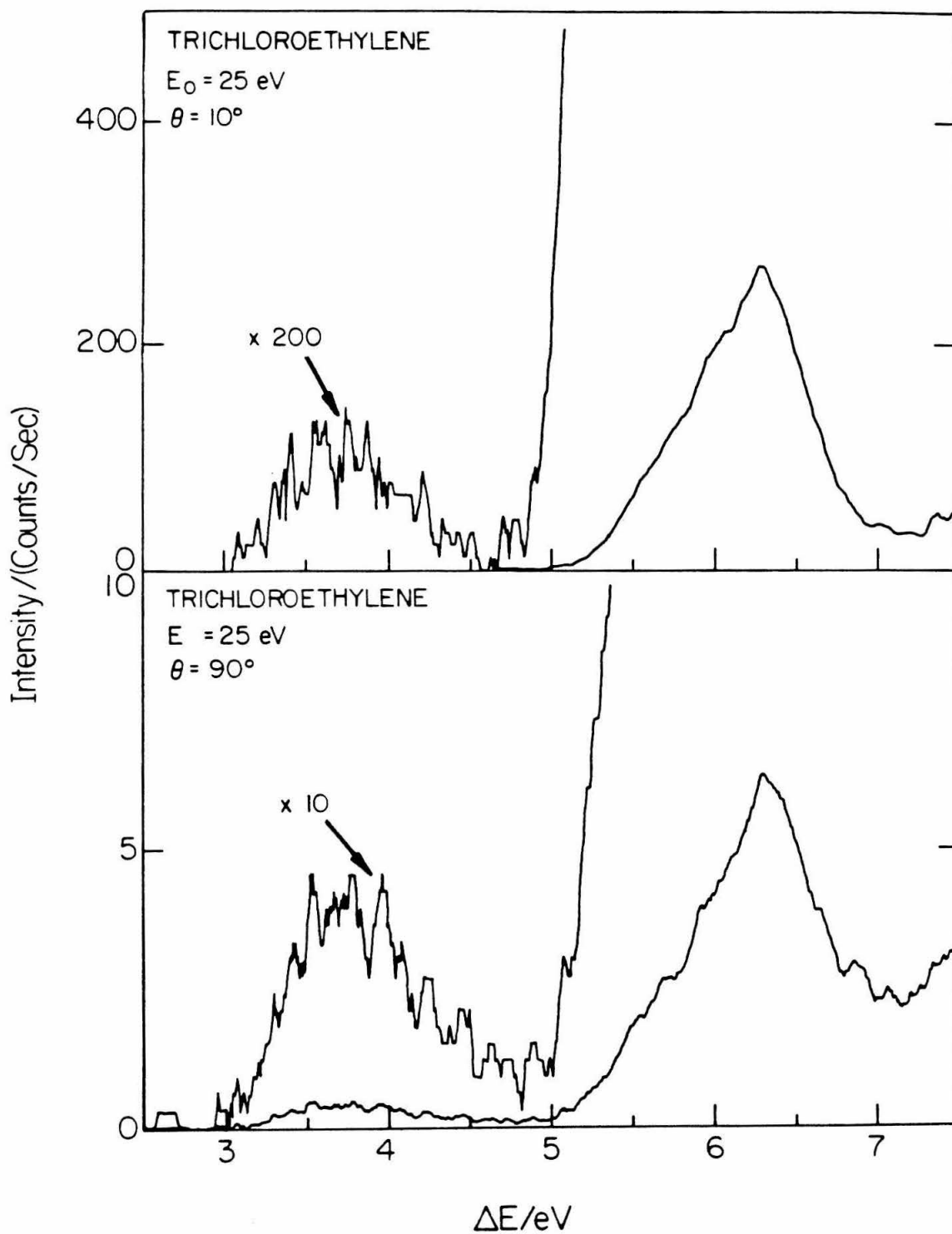


Figure 21.

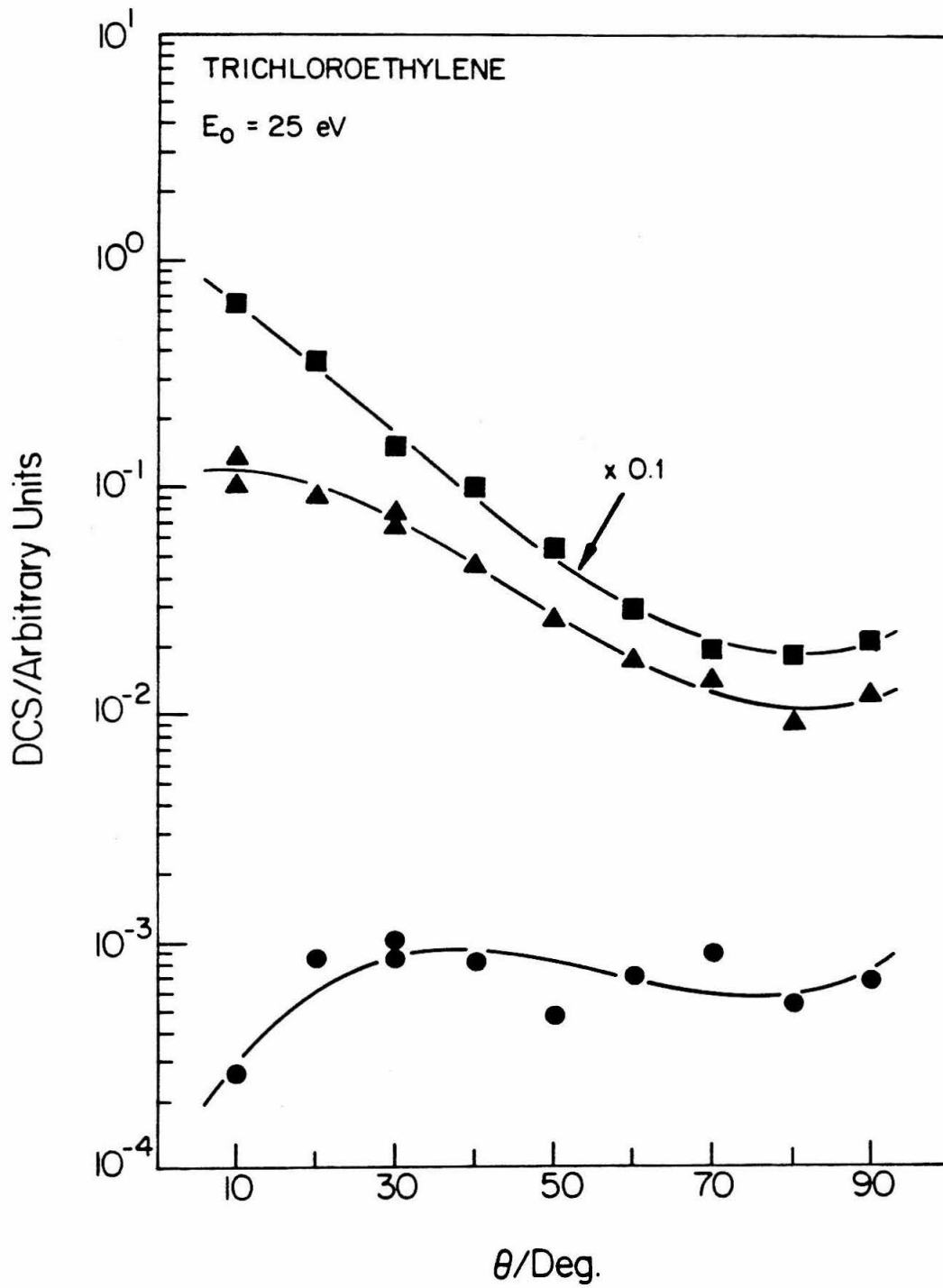


Figure 22.

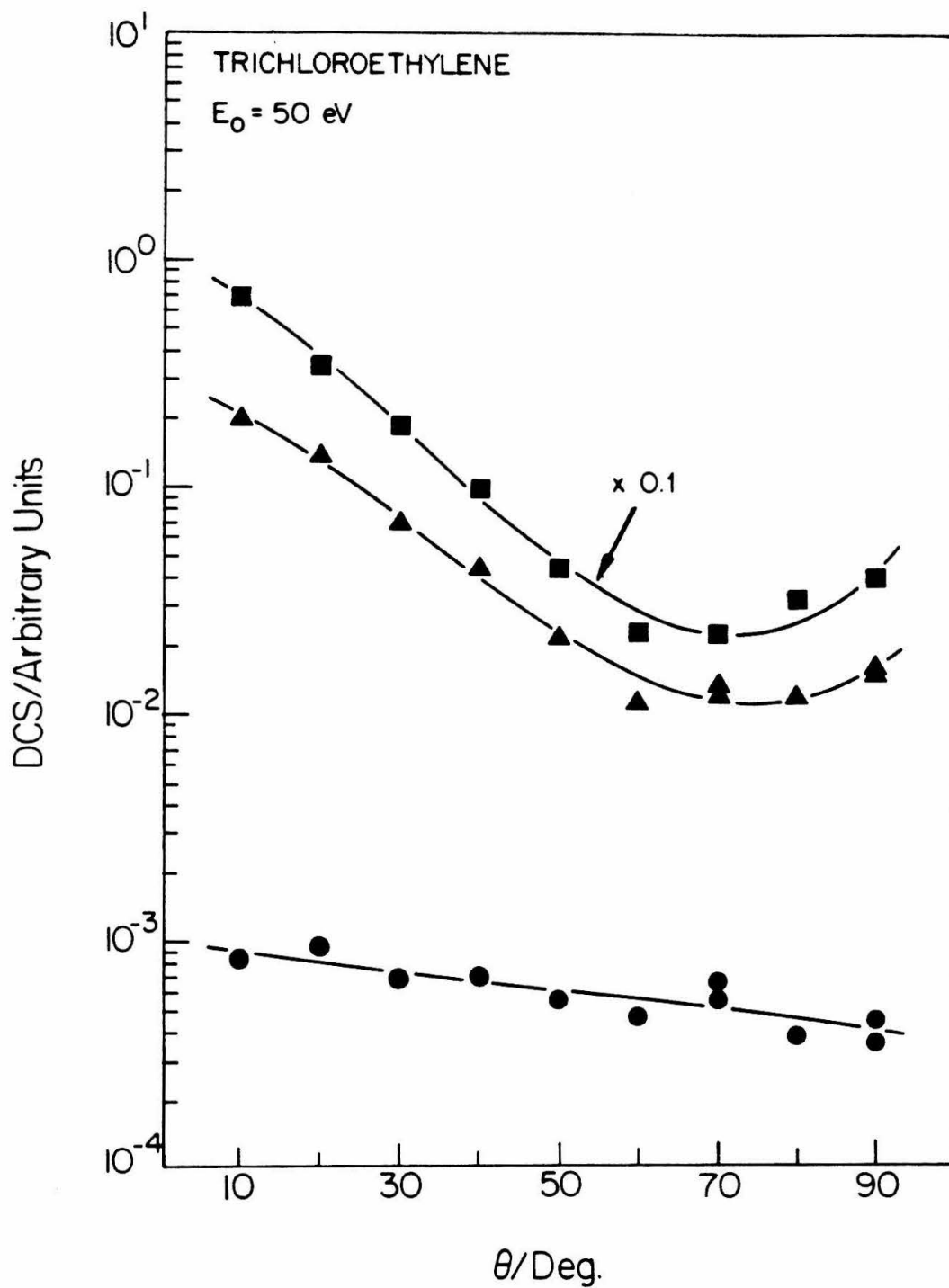


Figure 23.

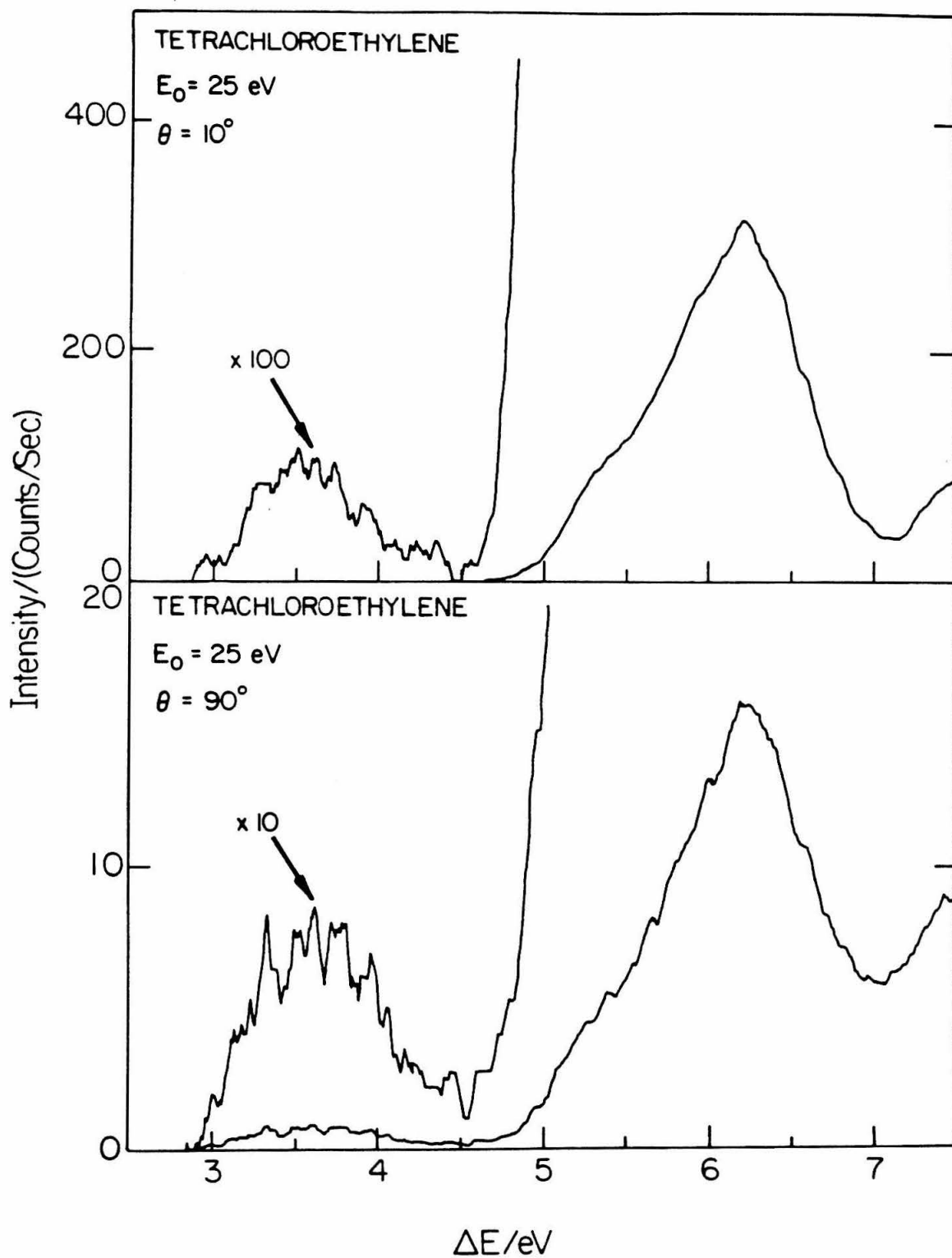


Figure 24.

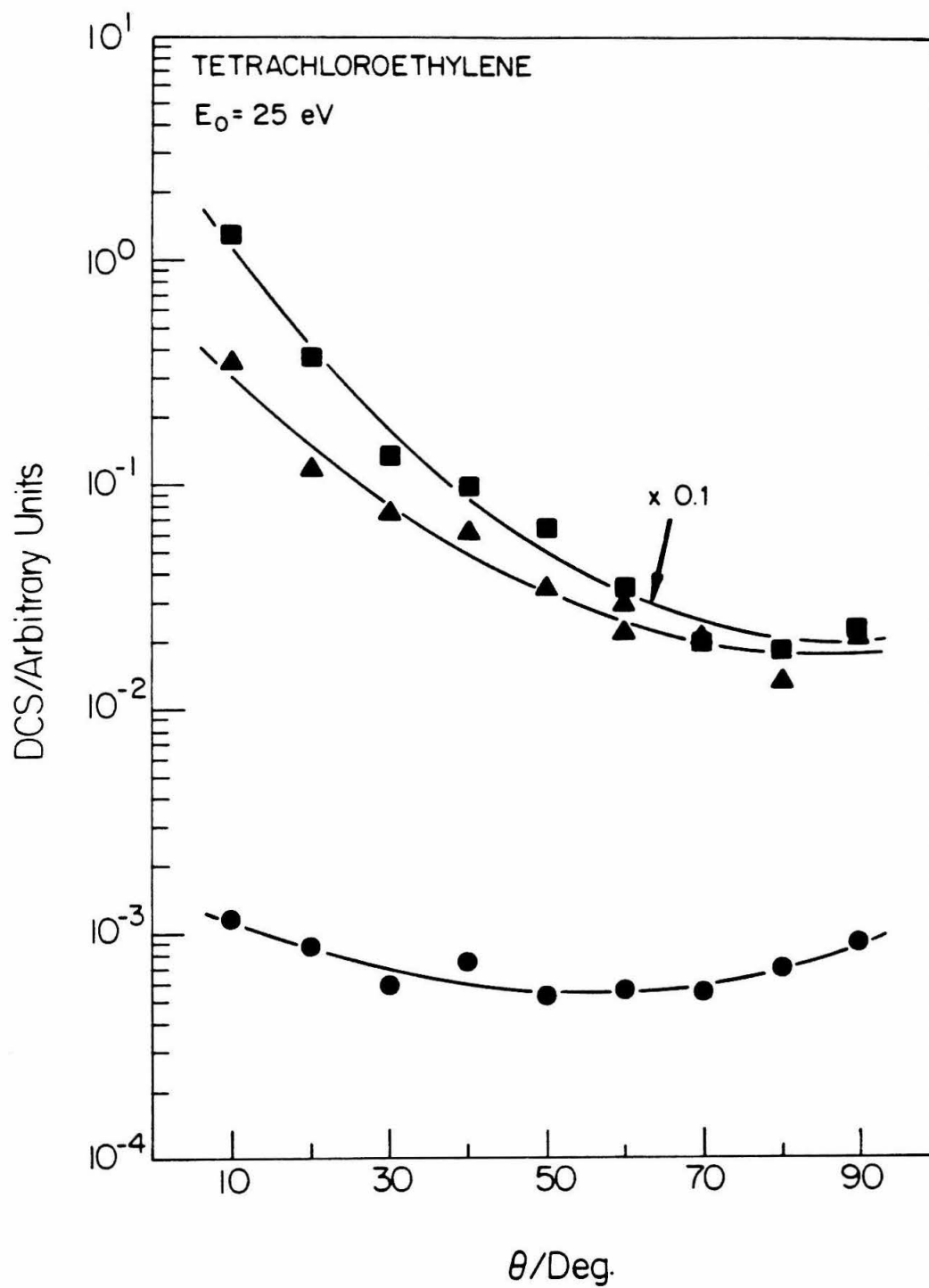


Figure 25.

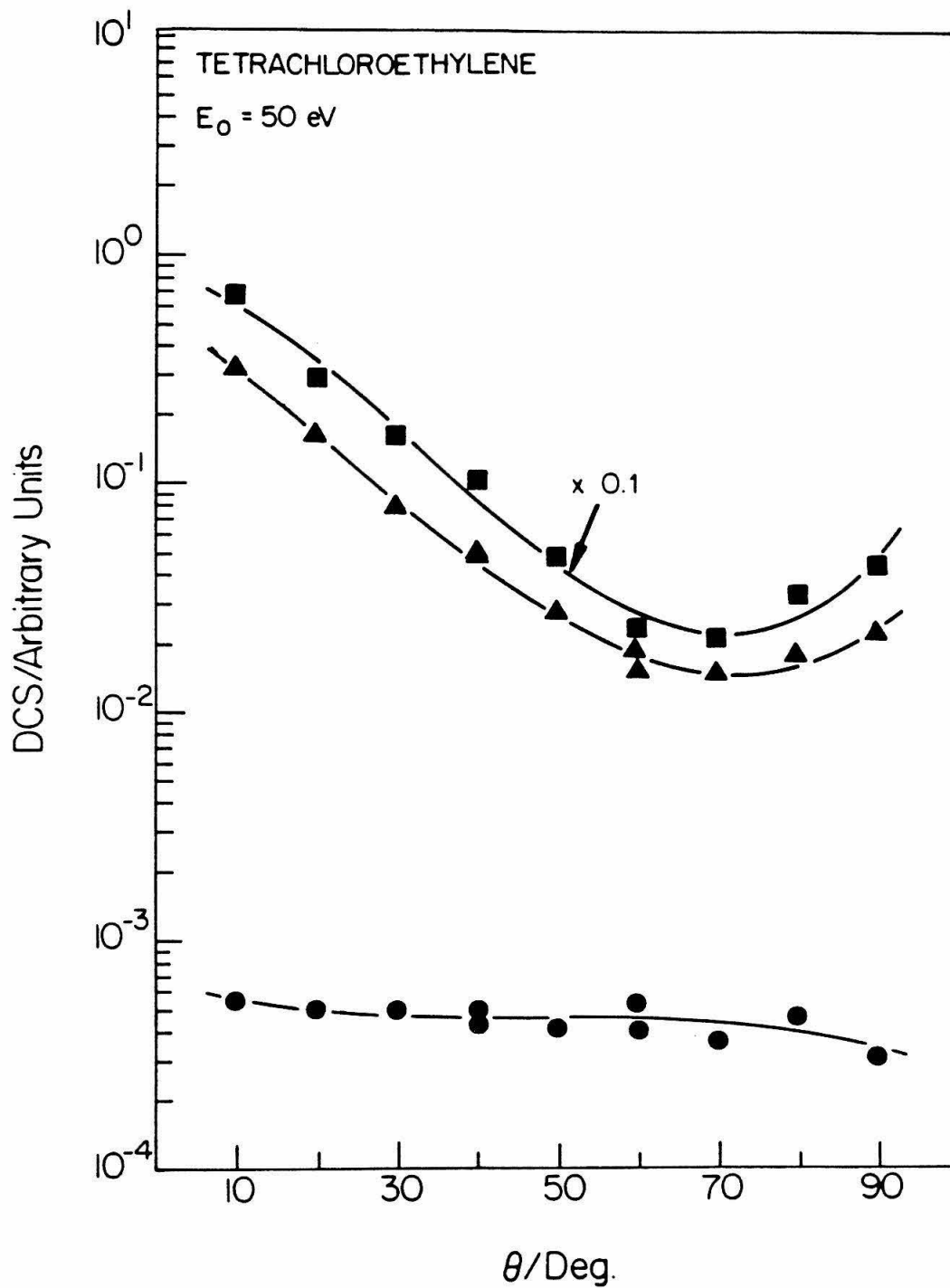


Figure 26.

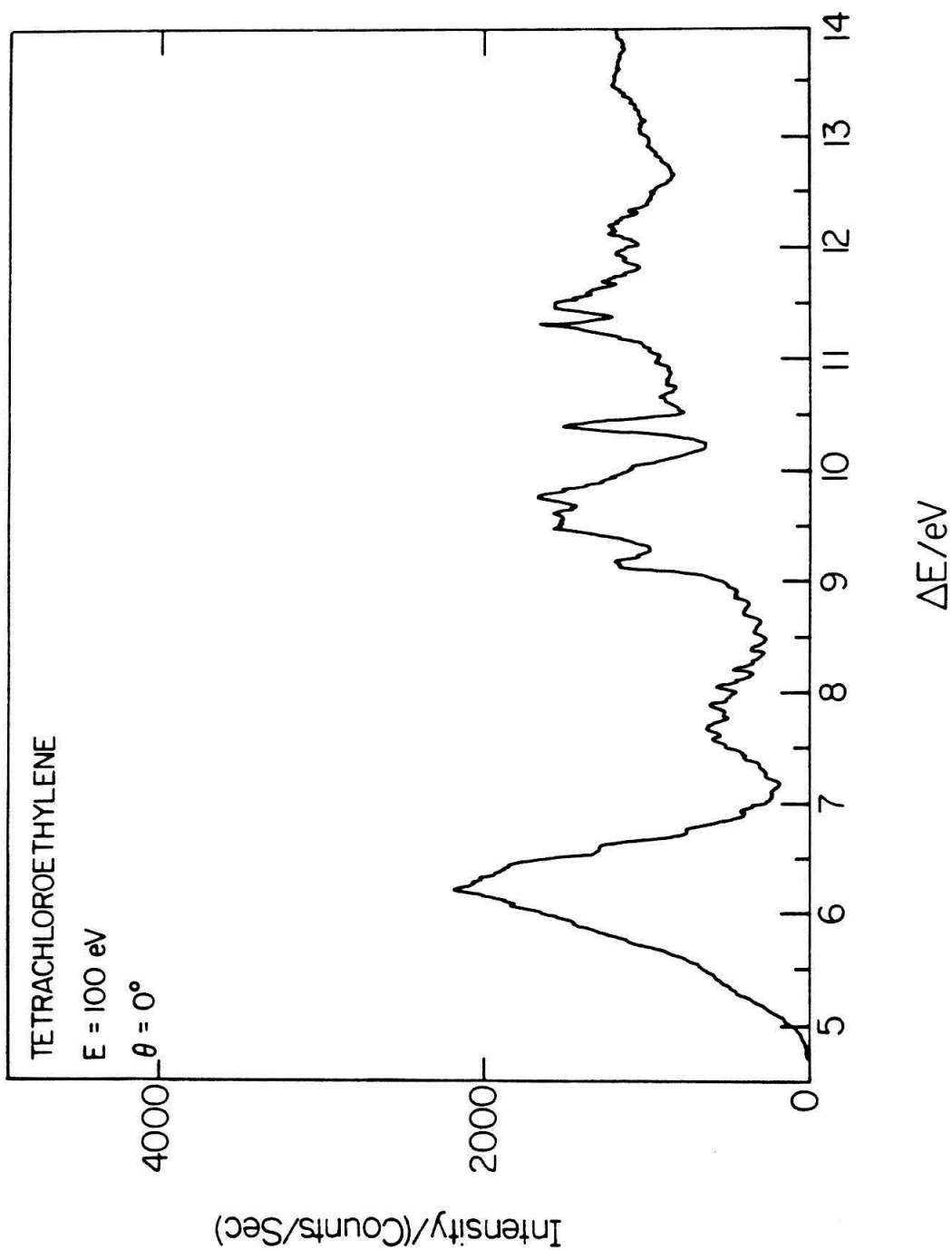


Figure 27.

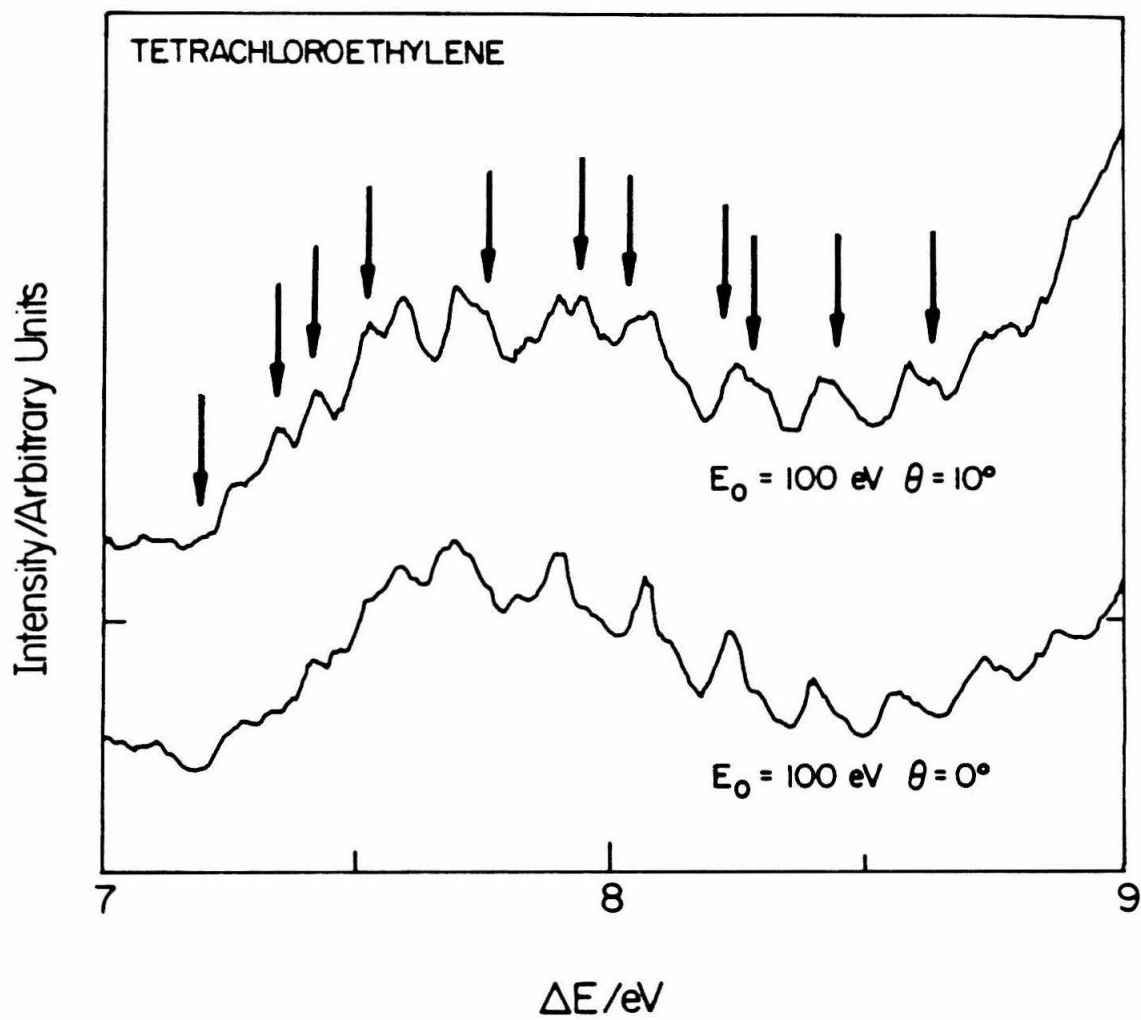


Figure 28.

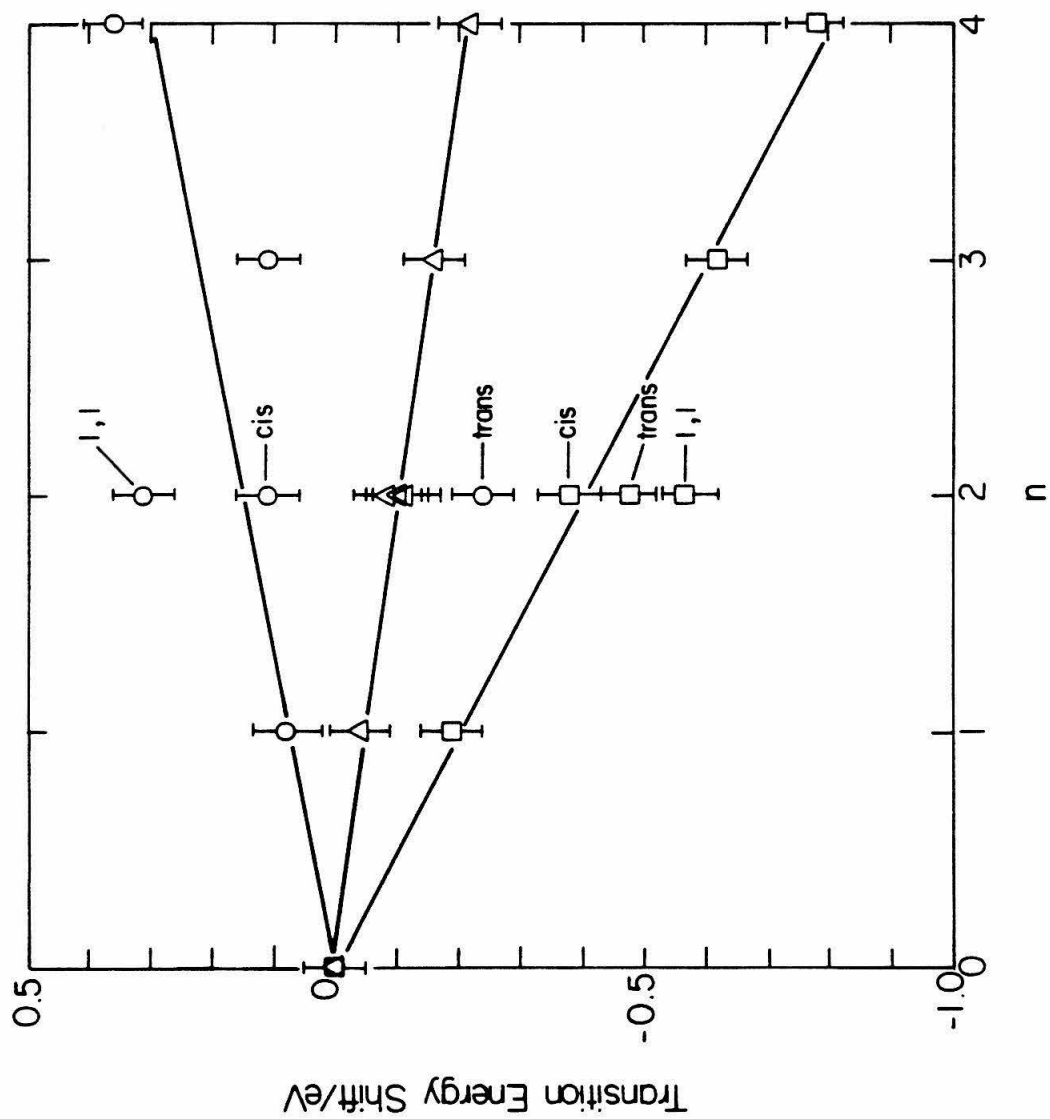


Figure 29.

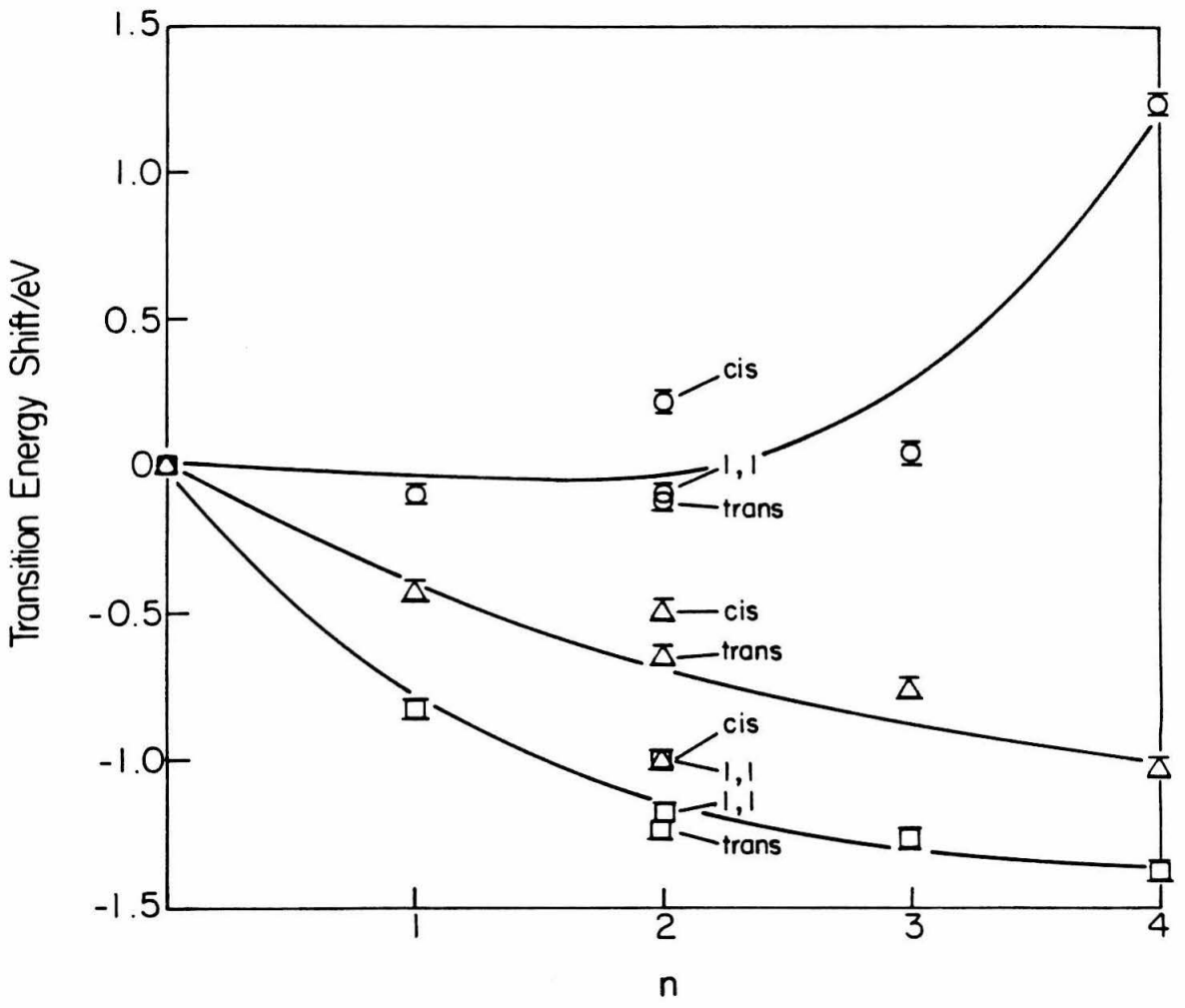


Figure 30.

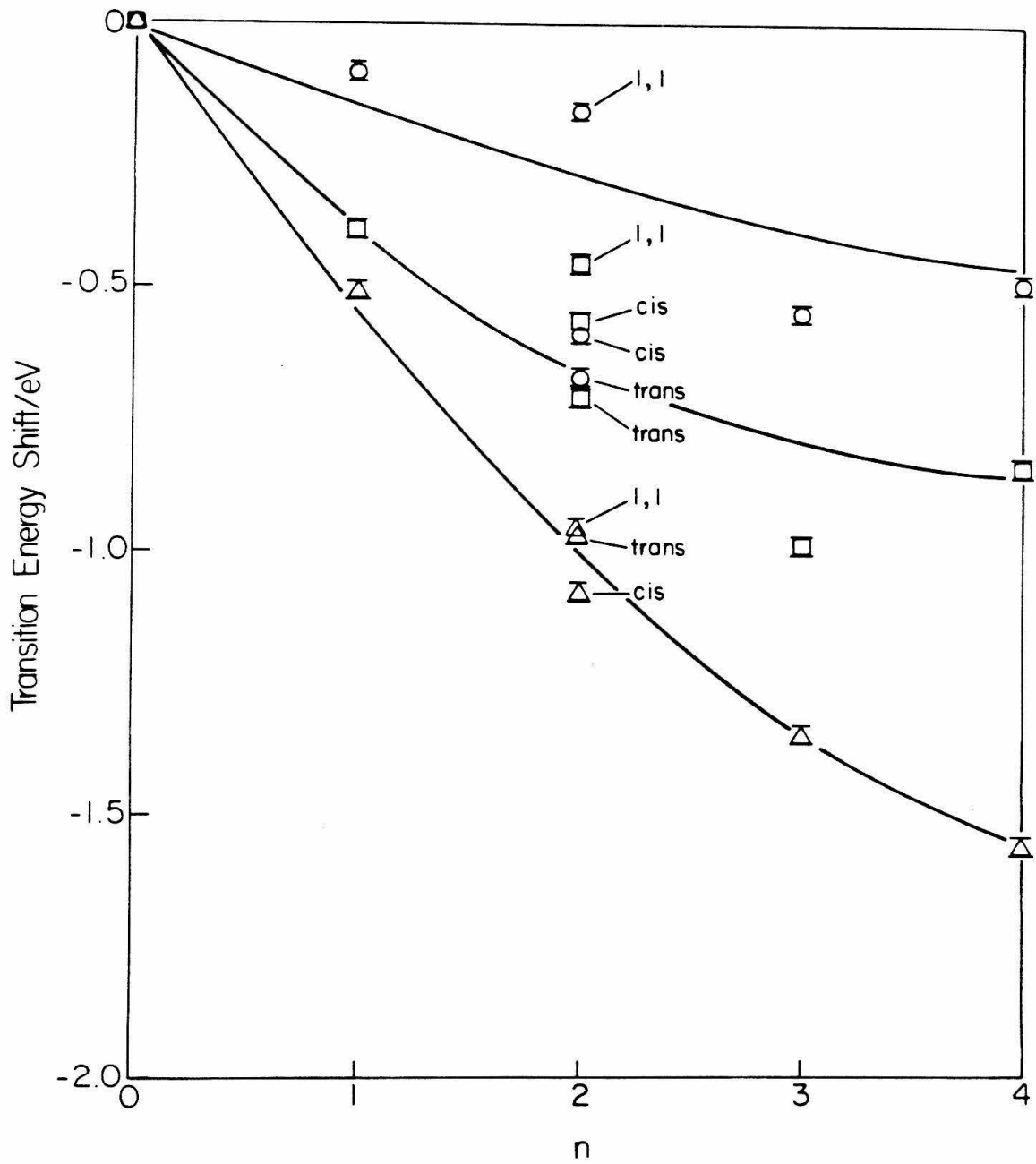


Figure 31.

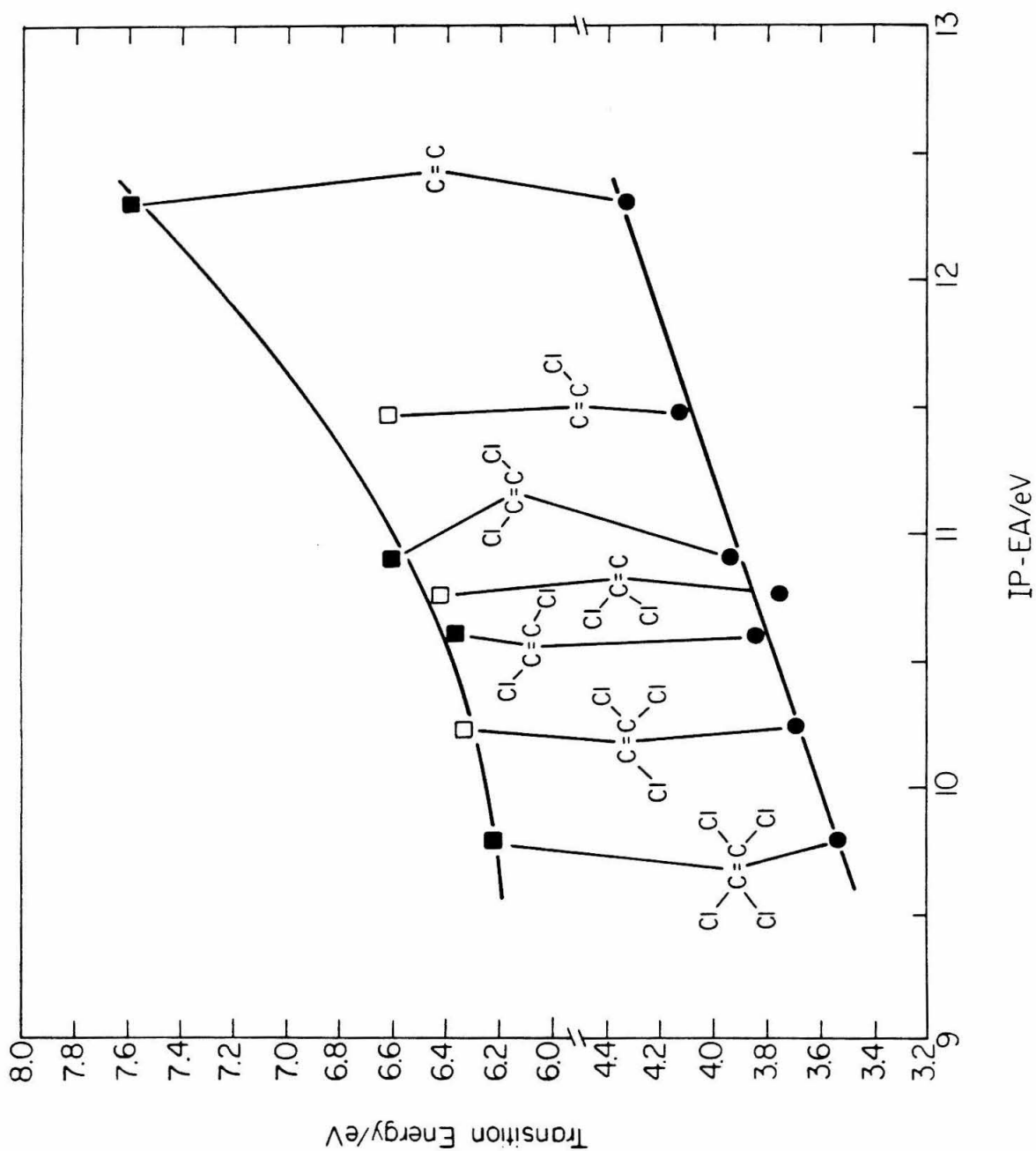


Figure 32.

CHAPTER 6

Paper II:

**The Spectroscopy of the Group VIb Transition Metal Hexacarbonyls
Using the Electron-Impact Method**

**The Spectroscopy of the Group VIb Transition Metal Hexacarbonyls
Using the Electron Impact Method^a**

C. F. Koerting,^b K. N. Walzl, and A. Kuppermann

Arthur Amos Noyes Laboratory of Chemical Physics,^c

California Institute of Technology, Pasadena, CA 91125

(received)

The electron energy-loss spectra of $\text{Cr}(\text{CO})_6$, $\text{Mo}(\text{CO})_6$, and $\text{W}(\text{CO})_6$ were measured at impact energies of 25, 50 and 100 eV and at scattering angles from 0° to 90° . The differential cross sections (DCS's) were obtained for several features in the 3-7 eV energy-loss region. The symmetry-forbidden nature of the $^1A_{1g} \rightarrow ^1A_{1g}$, $2t_{2g}(\pi) \rightarrow 3t_{2g}(\pi^*)$ transition in these compounds was confirmed. Several low energy excitations were assigned to ligand field transitions on the basis of the energy and angular behavior of their associated DCS's. No transitions which could clearly be assigned to singlet \rightarrow triplet excitations involving metal orbitals were located in these molecules. In addition, a number of states lying above the first ionization potential were observed for the first time. Several of these excitations seem to correspond quite well to some of the transitions observed in free CO.

^a This work was supported in part by the U. S. Department of Energy, contract No. DE-AM03-76F00767; Project Agreement No. DE-AT03-76ER72004.

^b Work performed in partial fulfillment of the requirements for the Ph.D. degree in Chemistry at the California Institute of Technology.

^c Contribution No. ---

I. Introduction

The group VIb transition metal hexacarbonyls are currently the focus of a large amount of research which has been stimulated by the catalytic properties exhibited by these compounds.¹⁻⁷ These compounds have also been studied as models for the binding of CO on transition metal surfaces.⁸⁻¹⁰ Understanding the electronic structures and bonding of these systems is very important to understanding their reactivity and thus gaining insight into their catalytic activity.¹¹

The bonding of CO to a transition metal atom or surface is thought to occur through a combination of σ - and π -type bonding.¹² The lone pair electron density of the carbon atoms is thought to delocalize into empty metal d orbitals thus forming a σ -type of interaction. Back donation of metal "lone pair" d orbitals into the π^* orbital of CO forms the π interaction. It is this synergetic interaction which results in very little net charge transfer occurring between the metal and the CO thus allowing the metal to be coordinated in relatively low oxidation states. Many theoretical studies have been performed on this system¹³ and large numbers of techniques and methods of experimentation have also been used to ascertain the exact nature of this bonding.

In this study we have applied the technique of low-energy, variable-angle, electron-impact spectroscopy^{14,15} to the group VIb transition metal carbonyls. This technique has been applied with great success to a large number of small organic molecules¹⁶ and more recently to inorganic systems.¹⁷ It not only provides information on excited states optically accessible from the ground state but also on those states which are optically inaccessible from the ground state.^{14,15} The behavior of the measured differential cross section (DCS) as a function of scattering

angle, θ , and incident electron energy, E_0 , permit identification of the nature of various transitions in the electron energy loss spectra of these compounds. Electron impact also allows easy access to the high energy, >10 eV, region of the spectrum. This is important in that many of the intra-ligand absorptions occur in this region of the spectrum. Such transitions are important in determining the nature of the metal-CO bond and can also be compared with electron energy-loss measurements of CO adsorbed on metal surfaces.²⁰

We have obtained electron energy-loss spectra with incident electron energies of 25 eV and 50 eV and at scattering angles at 10° intervals from 10° to 90° . High resolution energy-loss spectra were also measured at 100 eV incident energy and low scattering angles ($<10^\circ$) in order to produce spectra comparable to optical spectra.²¹

II. Previous Work

a) Experimental

For a series of compounds whose photochemistry has been studied as much as the group VIb metal hexacarbonyls, little attention has been given to the electronic spectroscopy of these compounds. Most of the previous studies have been performed in solution or solid matrices and were almost always done in the energy region below the quartz cutoff frequency (approximately 7 eV).²²⁻²⁸ Some work has been done in the gas phase,²⁹⁻³¹ with one VUV study reported by Iverson and Russell.³²

Photoionization studies of the transition metal hexacarbonyls have been performed by Vilesov and Kurbatov³³ and Lloyd and Schlag.³⁴ A number of UV photoelectron spectroscopic studies of this series have also been reported.³⁵⁻³⁸ Plummer and co-workers^{39,40} have studied the UV and x-ray photoelectron spectroscopy of the metal carbonyls in detail

and have also made some interesting comparisons with CO adsorbed on transition metal surfaces. Giordan et al.⁴¹ and Tossel et al.⁴² have used electron transmission spectroscopy to study the negative ion states of the transition metal hexacarbonyls.

b) *Theoretical*

A large number of theoretical studies, most of which use semi-empirical methods, have been performed on these compounds with the emphasis being on the metal-CO bonding in the ground state.⁴³⁻⁴⁶ There have also been a number of semi-empirical calculations performed to determine the energy levels of the excited states of these complexes.^{31,47-53} Hillier and Saunders⁵⁴ and Moncrieff et al.⁵⁵ report the only *ab initio* study of a member of this series, done on the Cr compound.

III. Experimental

The apparatus used in these studies has been described previously^{56,57} and is an updated version of the Simpson-Kuyatt^{58,598} type electron impact spectrometer. Briefly, it consists of an electron gun - 2.25" mean radius hemispherical electron energy analyzer-detector system. The monochromator can be rotated from -15° to +100° with respect to the analyzer system. The sample may be contained in a static gas cell or be in an effusive molecular beam. The entire experiment is under the control of a microcomputer which sweeps the electron energy-loss and accumulates the energy-loss spectrum. The sample pressure is maintained at a few millitorr, in the pressure regime free of multiple scattering events.

The entire inlet system may be heated to approximately 150° C for working with substances which have low vapor pressures. Careful

monitoring of the electron-impact spectra was done in order to avoid decomposition of the hexacarbonyls. This was accomplished by looking for the strong, sharp CO bands in the 6-9 eV energy-loss region. Sample inlet conditions were adjusted to avoid CO contamination. The samples of $\text{Cr}(\text{CO})_6$, $\text{Mo}(\text{CO})_6$, and $\text{W}(\text{CO})_6$ all came from the Aldrich Chemical Co. and had stated purities of 99%. The solid samples were degassed and admitted into the instrument without further purification.

IV. Results

The spectra of all of the group VIb transition metal hexacarbonyls are very similar in appearance. One can divide these spectra into two regions. The first one extends from 3.5 to 7.0 eV and consists primarily of metal to ligand charge transfer (MLCT) bands and metal d to d, ligand field (LF) bands. The region above 7.0 eV most likely consists of ligand to ligand, ligand to metal, and Rydberg-type excitations. We will discuss the results on a molecule-by-molecule basis. The tentative assignments given in tables 1-3 are based on those of Beach and Gray.³¹

a) *Chromium hexacarbonyl*

The high energy (100 eV incident electron energy) and low angle (0°) spectrum of $\text{Cr}(\text{CO})_6$ is shown in figure 1. The appearance of the energy-loss spectrum agrees quite well with the vapor-phase optical spectra of Gray and Beach⁹ and Iverson and Russell.³² Attempts to measure the DCS's for the various transitions were complicated due to severe overlapping of the various bands. After attempts at using various deconvolution procedures had failed, the approach of simply dividing the spectrum into regions and measuring the DCS of a particular energy loss range was adopted.⁶⁰ It was hoped that this procedure might indicate the presence of any possible spin-forbidden transitions which may be present. The

exception to this was the excitation present at 6.35 eV which was deconvoluted using a procedure similar to that described previously.^{61,62} The results of the DCS measurements are displayed in figures 2 and 3. The angular dependence of most of these DCS's are similar and no evidence for the presence of spin-forbidden transitions is apparent in all of the bands studied with one exception.

It has been found helpful in the past¹⁵ to plot the ratios of the DCS's for a given transition to that of a known, totally allowed transition as a function of scattering angle. It has been previously determined that, for systems with no significant spin-orbit coupling, the DCS ratio of spin-forbidden to spin-allowed transitions increases by one to two orders of magnitude as the scattering angle is increased from 10° to 90°. DCS ratios are plotted in figures 4 and 5 and with one exception, no case can be made for the presence of spin-forbidden transitions. Spectra taken at $E_0 = 25$ eV and $\theta = 10^\circ$ and 90° are shown in figure 6. Careful observation of these spectra and of others at intermediate angles shows the presence of two reproducible shoulders at 3.78 and 4.73 eV. The intensities of these features seem to be very slightly enhanced in going from 10° to 90° when compared with that of the 4.46 eV transition which has been assigned to a fully allowed MLCT type of excitation. This may indicate the presence of some forbidden character in these bands.

The shoulder at 3.78 eV has been previously assigned to a LF type transition³¹ while the bands observed at 4.46 and 5.51 eV correspond to the MLCT transitions. The 5.51 eV band has a much larger intensity than the 4.46 eV band. This has been explained³¹ as being due to a larger change in the M-CO bond dipole moment associated with the ${}^1A_{1g} \rightarrow {}^1T_{1u}^{(1)}$, $2t_{2g} \rightarrow 2t_{2u}$ transition as compared to that associated with the ${}^1A_{1g} \rightarrow {}^1T_{1u}^{(2)}$,

$2t_{2g} \rightarrow 4t_{1u}$ transition. The 4.73 shoulder has been assigned to a second LF band and also shows a similar enhancement with angle as does the shoulder at 3.78 eV. A shoulder is observed on the high energy side of the 5.51 eV band with a maximum at 6.35 eV. This band has been previously assigned³¹ as a LF ${}^1A_{1g} \rightarrow {}^1A_{1g}, t_{2g}(\pi) \rightarrow t_{2g}(\pi^*)$ symmetry-forbidden transition. This is confirmed by the behavior of the intensity of this transition, as shown in figure 7, which increases significantly as one goes from 0° to 6° scattering angle using 100 eV incident electrons. This type of behavior is characteristic of such symmetry-forbidden excitations.³¹ The interesting observation is made that the DCS's and their ratios to the intense MLCT band at 5.51 eV for this particular transition (figures 2, 3, 4, 5) display characteristics expected for spin-forbidden excitations at 25 eV incident energy. At 50 eV incident energy, this spin-forbidden behavior vanishes. This energy-dependence of the DCS indicates the possible presence of an underlying spin-forbidden transition, possibly due to a CO intra-ligand absorption. The transitions at 7.46 and 7.71 eV have not been assigned but may be due to components of the $d \rightarrow p$ metal-metal bands terminating in the $5t_{1u}$ orbital. A number of bands are observed above 7 eV energy-loss. One can turn to the work on CO bound to metal surfaces to possibly explain some of these transitions. Avouris et al.²⁰ have recently studied the electronic excitations of CO bound to various metal substrates. In all the cases they studied, they found adsorbate bands in the 5-6 eV and 8-9 eV energy-loss regions. These were assigned to triplet and singlet $5\sigma \rightarrow 2\pi^*$ CO-type transitions, respectively. Their findings indicated that the transition energies of bound CO were not significantly perturbed from those of free CO. In $\text{Cr}(\text{CO})_6$ the 5-6 eV band would be buried beneath the intense MLCT and LF bands but there is a band

observed at 8.80 eV which may correspond to the $5\sigma \rightarrow 2\pi^*$ singlet excitation. The triplet component of this excitation may be responsible for the anomalous behavior of the DCS for the 6.35 eV transition at $E_0 = 25\text{eV}$. The remainder of the spectrum consists of transitions to super-excited states (SES) at 10.8, 11.6, 12.4, 13.4 and 14.2 eV. These have not been assigned but may be due to Rydberg-type excitations or to other intra-ligand excitations.

b) Molybdenum hexacarbonyl

Figure 8 shows the 100 eV, 0° electron energy-loss spectrum of $\text{Mo}(\text{CO})_6$ in the energy-loss region from 3 to 13 eV. With the exception of the symmetry-forbidden transition DCS at 25 eV, the DCS's and their ratios (figures 9-12) do not indicate the presence of any spin-forbidden transitions. In figure 13 the 25 eV and 10° and the 25 eV and 90° spectra are compared. One can see that the transitions at 3.65, 3.82, and 4.65 eV are all enhanced by a factor of about 2 in going from 10° to 90° scattering angle. This is much less than the usual one to two orders of magnitude of enhancement observed for triplet states.¹⁵

The shoulder observed at 3.65 eV in the 25 eV 90° spectrum has been observed by Beach and Gray³¹ in solid state spectra at 77°K and has been assigned to the $^1A_{1g} \rightarrow ^3T_{1g}$ transition. The enhancement observed seems to indicate some amount of "forbiddenness" associated with this shoulder but it does not definitively confirm this assignment. The shoulders appearing at 3.82 and 4.65 eV also show an enhancement similar to that observed for the shoulder at 3.65 eV. As with $\text{Cr}(\text{CO})_6$, the two most intense features in the spectrum are the MLCT bands at 4.32 and 5.44 eV. In addition, LF bands are observed as shoulders at 3.82 and 4.65 eV. The shoulder at 6.33 eV has been assigned as the symmetry forbidden

${}^1A_{1g} \rightarrow {}^1A_{1g}$, $2t_{2g}(\pi) \rightarrow 3t_{2g}(\pi^*)$ transition on the basis of the angular behavior of its intensity (figure 14).

Additional bands have been observed at 7.08, 7.36, 7.65, 7.85, and 8.30 eV; some of them may belong to metal d-p type excitations. Transitions to states above the first IP occur at 9.65, 10.23, 11.43, 11.52, 12.19, 12.50, 12.83, and 13.26 eV. These, as in $\text{Cr}(\text{CO})_6$, are most likely due to Rydberg excitations or intra-ligand absorptions.

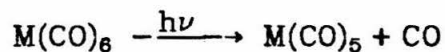
c) Tungsten hexacarbonyl

Figure 15 shows the 100 eV, 0° energy-loss spectrum of $\text{W}(\text{CO})_6$ between 3 and 13 eV. As is the case with the other two members of this series, the DCS's and their ratios (figures 16-19) show no forbidden behavior, the exception once again, being the symmetry-forbidden transition at 25 eV incident energy. Comparing the 25 eV and 10° spectrum to the 25 eV and 90° spectrum, one can see that the transitions at 3.61, 3.75, and 4.54 eV are, as was the case for $\text{Mo}(\text{CO})_6$, enhanced by about a factor of two with respect to the fully allowed transitions. As with $\text{Cr}(\text{CO})_6$ and $\text{Mo}(\text{CO})_6$, the two most intense transitions are assigned to MLCT type, ${}^1A_{1g} \rightarrow {}^1T_{1u}$ excitations. They occur at 4.32 and 5.55 eV, which are very close to the values of 4.46 and 5.51 eV observed for $\text{Cr}(\text{CO})_6$ and 4.32 and 5.44 eV observed for $\text{Mo}(\text{CO})_6$. The LF bands occur at 3.84 and 4.65 eV, which are also very close in energy to those seen in $\text{Cr}(\text{CO})_6$ and $\text{Mo}(\text{CO})_6$. The shoulder at 3.61 eV has been assigned by Beach and Gray³¹ to the ${}^1A_{1g} \rightarrow {}^3T_{1g}$ transition and the MCD measurements of Chastain et al.²⁸ seem to confirm that this assignment is correct. On the basis of our DCS measurements we can make no definitive statement confirming this assignment. Again at 6.24 eV occurs a symmetry-forbidden transition, as identified by the angular behavior of the intensity of this band relative to

the 5.55 eV band (figure 21). As with the other hexacarbonyls this is most likely the ${}^1A_{1g} \rightarrow {}^1A_{1g}$, $2t_{2g}(\pi) \rightarrow 3t_{2g}(\pi^*)$ transition. Other bands are observed below the first IP at 6.54, 7.66, and 8.38 eV. A number of transitions to SES states are observed at 8.80, 9.96, 10.38, 11.63 and 12.26 eV. These again are probably due to Rydberg or intra-ligand transitions.

IV. Photochemistry

The transition metal carbonyls probably have the most extensively studied photochemistry of any organometallic species.^{7,63,64} Recent work includes photodissociation in low temperature matrices and glasses,⁶⁵⁻⁶⁷ laser photodissociation,⁶⁸ multiphoton dissociation and ionization⁶⁹⁻⁷³, and picosecond laser studies.⁷⁴ Excitation of any of the LF or MLCT bands is known to cause photodissociation of the type



A number of studies have indicated that the energetically low-lying triplet states of these molecules are important in many of these processes.^{65,68,75} The work of Nasielski and Colas⁷⁵ indicates that the measured quantum yield for photodissociation of somewhat less than unity⁷⁶ may be accounted for by the radiationless decay of a relatively long-lived triplet state. Rest and Sodeau⁶⁵ have observed phosphorescence at 400 nm in mixed matrices of $Cr(CO)_6$ and have assigned it to the $Cr(CO)_6$, ${}^3T_{1g} \rightarrow {}^1A_{1g}$ transition. This places the triplet state for $Cr(CO)_6$ at about 3.1 eV. In this study we have found no band which is consistent with this assignment.

V. Discussion

We undertook this investigation with the hope of locating and definitively assigning the low-lying triplet states of these transition metal

hexacarbonyl compounds on the basis of the angular and energy dependence of the corresponding electron-impact DCSs. The major problem with using the DCS's to assign the transitions of these compounds involves the high atomic number of the metal atom. The rules correlating the behavior of the DCS with the transition type are based on a large body of data obtained from experiments with polyatomic molecules consisting primarily of first and second row elements. In these compounds the spin of the electron is considered to be a constant of the motion, i.e., a "good" quantum number. However, in the presence of the high electric fields experienced by the electron as it travels through an increased nuclear charge, as is the case with the heavier elements, the spin-orbit interaction becomes non-negligible.⁷⁷ This results in the spin angular momentum no longer being a good quantum number. The behavior of the DCS for transitions in systems involving various degrees of spin-orbit coupling is not known since only a few electron-impact studies involving compounds containing heavy nuclei have been performed.^{17-19,78-80}

From the DCS plots (figures 2,3,9,10,16,17) and ratio plots (figures 4,5,11,12,18, 19), the only transition which displays any forbidden character is the one assigned to the ${}^1A_{1g} \rightarrow {}^1A_{1g}, 2t_{2g}(\pi) \rightarrow 3t_{2g}(\pi^*)$ excitation. This excitation displays behavior characteristic of a symmetry-forbidden transition at incident energies of 100 eV (figures 7,14,21). The DCS for this transition at 25 eV incident energy behaves similarly as those observed for spin-forbidden transitions in light atom systems. Particularly interesting is the fact that this behavior essentially disappears as the incident energy is increased to 50 eV. This is also indicative of spin-forbidden type transitions and points out the possibility of there being an underlying spin-forbidden transition present which only contributes

significantly to the DCS at 25 eV. The plausibility of this argument is supported by the work of Avouris et al.²⁰ who, as mentioned earlier, studied the electronic excitations of CO bound to metal surfaces and found that some of the CO triplet and singlet transitions were not significantly perturbed from their gas phase values. If this holds true for the metal hexacarbonyls, the first CO triplet would fall within the region of the ${}^1A_{1g} \rightarrow {}^1A_{1g}$, $2t_{2g}(\pi) \rightarrow 3t_{2g}(\pi^*)$ transition for metal hexacarbonyls. One would expect that since this would be primarily an intra-ligand excitation, its DCS would behave similarly to that of free CO. This would also explain the presence of the transitions in the 8 to 9 eV range observed in all of these molecules. More work is clearly needed to confirm if this is indeed the case. In addition, a number of SES bands have been observed in all three compounds, which seem to correspond to the 10.78, 11.40, and 12.37 bands seen in free CO.⁸¹ These transitions differ from the free CO values by a few tenths of an eV. The presence of relatively unperturbed CO transitions is supported by the bands in the photoelectron spectra³⁵ which have been observed to be reasonably close in energy to those of free CO.

We have also noticed that the shoulders on the low-energy side of the first MLCT bands, which have been previously assigned as triplets in $\text{Mo}(\text{CO})_6$, and $\text{W}(\text{CO})_6$,³¹ all show the same relative degree of enhancement as a function of angle as do the bands assigned to the LF excitations. This indicates that all of these bands belong to a common type of transition. The question must be answered as to whether they belong to a spin-allowed LF transition or some type of LF or MLCT spin-forbidden transitions. The angular behavior of the DCS's for these bands indicates that they have the character of transitions in systems for which spin-orbit

coupling is small and thus, based on this information, no definite statement may be made either way. To further clarify this situation, we can look at the incident energy dependence of the ratio of the DCS of the bands in question to the DCS of the first MLCT band as a function of incident energy (table 4). For spin-forbidden transitions this ratio should rise dramatically as one approaches the threshold excitation energy.¹⁵ For spin-allowed transitions this ratio climbs slowly from threshold to peak at 5 to 10 eV above it and then slowly decreases as the incident energy is raised. The energy behavior of this ratio which we observe does not appear to indicate the presence of a spin-forbidden transition but rather a weak spin-allowed one.

From the evidence we have on the angular and energy behavior of these low-lying bands we tentatively assign them to LF bands. The LF bands are formally $g \rightarrow g$ symmetry-forbidden but they do not display the high energy, low angle intensity behavior characteristic of such transitions. This can be explained if the LF excited state is significantly distorted which would tend to remove some of the symmetry constraints on the transition. The symmetry forbiddenness of these bands might also explain the slight enhancement observed on increasing the scattering angle.

The lack of spin-forbidden behavior on the part of the DCS's may also be caused in part by the way in which they were obtained from the energy-loss spectra. The transitions for these compounds are so heavily overlapped that if the singlet-triplet splitting were small enough, and the triplet state intensity small enough compared to the overlapping singlet, then the singlet would dominate the behavior of the DCS of the combination of the two bands.

VI. Summary and conclusions

In summary, we have measured the electron energy-loss spectra of $\text{Cr}(\text{CO})_6$, $\text{Mo}(\text{CO})_6$, and $\text{W}(\text{CO})_6$ at incident energies of 25, 50 and 100 eV and at scattering angles from 10° to 90° . We have confirmed, on the basis of the low angle dependence of the differential cross section, the symmetry-forbidden nature of the $2t_{2g}(\pi) \rightarrow 3t_{2g}(\pi^*)$, ${}^1A_{1g} \rightarrow {}^1A_{1g}$ transitions located at 6.35, 6.33, and 6.24 eV for $\text{Cr}(\text{CO})_6$, $\text{M}(\text{CO})_6$, and $\text{W}(\text{CO})_6$, respectively. We have also tentatively assigned a number of low-lying ligand field bands on the basis of the energy and angular behavior of the DCSs. In addition a number of transitions to super-excited states were observed above 9 eV energy-loss, some of which corresponded quite well with transitions in free CO. No excitations were located which could confidently be assigned to singlet-triplet excitations involving metal orbitals.

The results of the present research point out the need for additional theoretical studies, especially on the electronic structures of these compounds and on the dynamics of electron scattering off strongly spin-orbit coupled species. The first area of additional study involves the electronically excited states of these compounds, and should also be extended to include the effects of binding to a metal on the CO to CO transitions. These studies would not only shed light on some of the problems encountered in the present work but also help explain results obtained on CO bound on metal surfaces.

The second area of theoretical study should involve the behavior of the DCS of low-energy electron scattering from targets with varying degrees of spin-orbit coupling. The calculations performed need not be exact since only qualitative trends are desired. They should be done for both direct and exchange scattering processes. It is hoped that the

present work will stimulate efforts in the previously mentioned areas since such studies would be useful for the interpretation of electron energy-loss spectra of organometallic compounds.

VII. Acknowledgments

We wish to thank Prof. Harry B. Gray for his stimulating discussions concerning the spectroscopy of the transition metal hexacarbonyls.

References

- 1) J. A. Huheey, *Inorganic Chemistry: Principals of Structure and Reactivity*, Harper and Row, New York, (1978) pp 524-536.
- 2) M. Wrighton, G. S. Hammond, and H. B. Gray, *J. Organomet. Chem.* **70**, 283 (1974).
- 3) E. Koerner van Gustorf and F. W. Guerals, *Fortsch. Chem. Forsch.* **13**, 366 (1969).
- 4) G. S. Lewandos and R. Pettit, *J. Amer. Chem. Soc.* **93**, 7087 (1971).
- 5) G. L. Leigh and E. O. Fischer, *J. Organometal. Chem.* **4**, 461 (1965).
- 6) E. O. Fischer and H. P. Fritz, *Angew. Chem.* **73**, 353 (1961).
- 7) M. Wrighton, *Chem. Rev.* **74**, 401 (1974) and references therein.
- 8) E. Muettterties, *Science* **194**, 1150 (1976).
- 9) E. Muettterties, *Science* **196**, 839 (1977).
- 10) E. W. Plummer, W. R. Saloneck, and J. S. Miller, *Phys. Rev. B* **18**, 1673 (1978).
- 11) J. N. Halpern, *Ann. Rev. Phys. Chem.* **16**, 103 (1965).
- 12) Ref 1 pp 526
- 13) D. E. Sherwood and M. B. Hall, *Inorg. Chem.* **22**, 93 (1983) and references therein.
- 14) A. Kuppermann, J. K. Rice, and S. Trajmar, *J. Phys. Chem.* **72**, 3894 (1968).
- 15) S. Trajmar, J. K. Rice, and A. Kuppermann, *Adv. Chem. Phys.* **18**, 15 (1970).
- 16) A. Kuppermann, W. M. Flicker, and O. A. Mosher, *Chem. Rev.* **79**, 77 (1979).

- 17) R. Rianda, R. P. Frueholz, and A. Kuppermann, *J. Chem. Phys.* **70**, 1056 (1979).
- 18) A. Chutjian, S. K. Srivastava, S. Trajmar, W. Williams, and D. C. Cartwright, *J. Chem. Phys.* **64**, 4791 (1976).
- 19) S. K. Srivastava, D. C. Cartwright, S. Trajmar, A. Chuthian, and W. Williams, *J. Chem. Phys.* **65**, 208 (1976).
- 20) Ph. Avouris, N. J. DiNardo, and J. E. Demuth, *J. Chem. Phys.* **80**, 491 (1984) and references therein.
- 21) E. N. Lassetre, A. Skerebele, and M. A. Dillon, *J. Chem. Phys.* **50**, 1829 (1969).
- 22) W. Strohmeier, K. Gerlach, *Zeit. für Phys. Chem.* **27**, 439 (1961).
- 23) R. T. Lundquist and M. Cais, *J. Org. Chem.* **27**, 1167 (1962).
- 24) H. Saito, J. Fuhita, and K. Saito, *Bull. Chem. Soc. Jap.* **41**, 359 (1968).
- 25) W. C. Trogler, S. R. Desjardins, and E. I. Solomon, *Inorg. Chem.* **18**, 2131 (1979).
- 26) L. Baraldi, G. Gottarelli, and B. Samori, *J. Phys. (Paris)* **40**, 204 (1979).
- 27) A. M. F. Hezemans, P. J. F. M. Van de Coulwijk, D. J. Stufhens, and G. Boxhoorn, *Chem. Phys. Lett.* **73**, 550 (1980).
- 28) S. K. Chastain, R. W. Mason, *Inorg. Chem.* **20**, 1395 (1981).
- 29) H. B. Gray and N. A. Beach, *J. Amer. Chem. Soc.* **85**, 2922 (1963).
- 30) D. S. Alderdice, *J. Molec. Spect.* **15**, 509 (1965).
- 31) N. A. Beach and H. B. Gray, *J. Amer. Chem. Soc.* **90**, 5713 (1968).
- 32) A. Iverson and B. R. Russell, *Chem. Phys. Lett.* **6**, 307 (1970).
- 33) F. E. Vilesov and B. L. Kurbatov, *Dokl. Acad. Nauk. SSSR* **140**, 1364 (1961).

- 34) D. R. Lloyd and E. W. Schlag, *Inorg. Chem.* **8**, 2544 (1969).
- 35) D. W. Turner, C. Baker, A. D. Baker, and C. R. Brundle, *Molecular Photoelectron Spectroscopy*, (Wiley Interscience, New York 1970) pp. 361-371.
- 36) B. R. Higgenson, D. R. Lloyd, P. Burroughs, D. M. Gibson, and A. F. Orchard, *J. Chem. Soc. Farad. Trans. 2* **69**, 1659 (1973).
- 37) D. S. Rajoria, L. Kovnat, E. W. Plummer, and W. R. Salaneck, *Chem. Phys. Lett.* **49**, 64 (1977).
- 38) J. L. Hubbard, D. L. Lichtenberger, *J. Amer. Chem. Soc.* **104**, 2132 (1982).
- 39) E. W. Plummer, W. R. Salaneck, J. S. Miller, *Phys. Rev. B* **18**, 1673 (1978).
- 40) G. Loubriel, E. W. Plummer, *Chem. Phys Lett.* **64**, 234 (1979).
- 41) J. C. Giordan, J. H. Moore, J. A. Tossell, *J. Amer. Chem. Soc.* **103**, 6632 (1981).
- 42) J. A. Tossell, J. H. Moore, and J. K. Olthoff, *J. Amer. Chem. Soc.* **106**, 823 (1984).
- 43) E. J. Baerends and P. Ros, *Mol. Phys.* **30**, 1735 (1975).
- 44) K. Tatsumi and J. Fueno, *Bull. Chem. Soc. Jap.* **49**, 939 (1976).
- 45) W. Heijser, E. J. Baerends, and P. Ros, *J. Mol. Struct.* **63**, 109 (1980).
- 46) D. Saddei, J. Freund, and G. Hohlneicher, *Chem. Phys.* **55**, 339 (1981).
- 47) M. I. Ba'n, Sz. Fenyi, M. Hegyhati, *Theory Struct. Complex Compounds Papers Symp*, Wroclaw, Poland (1964) pp. 195-202.
- 48) D. G. Carroll and S. P. McGlynn, *Inorg. Chem.* **7**, 1285 (1968).

- 49) K. G. Colton and R. F. Fenske, *Inorg. Chem.* **7**, 1273 (1968).
- 50) A. G. Schreiner and T. L. Brown, *J. Amer. Chem. Soc.* **90**, 3366 (1968).
- 51) J. B. Johnson and W. G. Klemperer, *J. Amer. Chem. Soc.* **99**, 7132 (1977).
- 52) B. E. Bursten, D. G. Freier and R. F. Fenske, *Inorg. Chem.* **19**, 1810 (1980).
- 53) C. Y. Yang, R. Arratia-Perez and J. P. Lopez, *Chem. Phys. Lett.* **107**, 112 (1984).
- 54) J. H. Hillier and V. R. Saunders, *Mol. Phys.* **22**, 1025 (1971).
- 55) D. Moncrieff, P. C. Ford, I. H. Miller, and V. R. Saunders, *J. Chem. Soc. Chem. Commun.* 1108 (1983).
- 56) C. F. Koerting, K. N. Walzl, and A. Kuppermann, *J. Chem. Phys.*, to be submitted.
- 57) C. F. Koerting, Ph. D. Thesis, California Institute of Technology (1985).
- 58) J. A. Simpson, *Rev. Sci. Instrum.* **35**, 1698 (1964).
- 59) C. E. Kuyatt and J. A. Simpson, *Rev. Sci. Instru.* **38**, 103 (1967).
- 60) L. Vuskovic and S. Trajmar, *J. Chem. Phys.* **78**, 4947 (1982)
- 61) R. P. Frueholz, R. Rianda, and A. Kuppermann, *J. Chem. Phys.* **68**, 775 (1978).
- 62) R. P. Frueholz, R. Rianda, and A. Kuppermann, *Chem. Phys.*, **30**, 315 (1978).
- 63) A. Vogler in *Concepts of Inorganic Photochemistry*, edited by A. W. Adamson and P. D. Fleishaur (Wiley, New York 1975) pp. 269-295.
- 64) G. L. Geoffry and M. S. Wrighton *Organometallic Photochemistry* (Academic Press, New York 1979) pp 68.

- 65) A. J. Rest and J. R. Sodeau, *J. Chem. Soc. Farad. Trans 2*, **73**, 1691 (1977).
- 66) M. J. Boylan, J. D. Black, and P. S. Braterman, *J. Chem. Soc. Dalton Trans.* **9**, 1646 (1980).
- 67) M. A. Graham, M. Poliakoff, and J. J. Turner *J. Chem. Soc. A* 2939 (1971).
- 68) T. R. Fletcher and R. N. Rosenfeld, *J. Amer. Chem. Soc.* **105**, 6359 (1983).
- 69) M. A. Duncan, T. G. Dietz, and R. E. Smalley, *Chem. Phys.* **44**, 415 (1979).
- 70) D. P. Gerrity, L. J. Rothberg, and V. Vaida, *Chem. Phys. Lett.* **74**, 1 (1980).
- 71) G. J. Fisanick, A. Gedanken, T. S. Eichelberger IV, N. A. Kuebler, and M. B. Robin, *J. Chem. Phys.* **75**, 5215 (1981).
- 72) D. P. Gerrity, L. J. Rothberg, and V. Vaida, *J. Chem. Phys.* **87**, 2222 (1983).
- 73) D. G. Leopold and V. Vaidi, *J. Amer. Chem. Soc.* **105**, 6809 (1983).
- 74) J. D. Simon and K. S. Peters, *Chem. Phys. Lett.* **98**, 53 (1983).
- 75) J. Nasielski and A. Colas, *Inorg. Chem.* **17**, 237 (1977).
- 76) J. Nasielski and A. Colas, *J. Organomet. Chem.* **101**, 215 (1975).
- 77) Gordon Baym, *Lectures in Quantum Mechanics* (W. A. Benjamin, Reading, Mass. 1969) pp. 460.
- 78) W. Williams, S. Trajmar, and A. Kuppermann, *J. Chem. Phys.* **62**, 3031 (1975).

- 79) W. Williams and S. Trajmar, Phys. Rev. Lett. **33**, 187 (1974).
- 80) S. Trajmar, W. Williams, and S. Srivistava, J. Phys. B. **10**, 3323 (1977).
- 81) G. Herzberg *Spectra of Diatomic Molecules* (Van Nostrand, New York 1950) pp. 521-522.

Table 1. Chromium Hexacarbonyl

Assignment ^a	Transition Energy/eV	
	Present Results	Previous Work
${}^1A_{1g} \rightarrow {}^1T_{1g}$	3.78 sh ^b	3.60 ^c
${}^1A_{1g} \rightarrow {}^1T_{1u}^{(1)}$	4.46	4.44 ^{c,f} , 4.37 ^d , 4.43 ^{g,l} , 4.44 ⁱ , 4.36 ⁱ , 4.35 ^l , 4.47 ^k , 2.95 ^l , 3.9 ^m , 3.99 ⁿ
${}^1A_{1g} \rightarrow {}^1T_{2g}$	4.73 sh	4.82 ^c
${}^1A_{1g} \rightarrow {}^1T_{1u}^{(2)}$	5.51	5.48 ^c , 5.39 ^d , 5.28 ^e , 5.51 ^f , 5.41 ^g , 5.54 ^h , 5.33 ⁱ , 5.58 ⁱ , 5.99 ^j , 5.27 ^k , 5.6 ^l , 5.52 ^l , 5.2 ^m , 4.8 ^m , 4.6 ^m
${}^1A_{1g} \rightarrow {}^1A_{1g}$ ($t_{2g}(\pi) \rightarrow t_{2g}(\pi^*)$)	6.35 sh	6.31 ^c , 6.36 ^f , 6.33 ^h , 6.38 ^l , 6.35 ^l , 5.9 ^m
	7.46	7.42 ^h
	7.71	7.70 ^h
IP1		8.40 ^{o,p}
SES	8.80	8.79 ^h
SES	10.8	
SES	11.6	
SES	12.4	
IP2		13.38 ^{o,p}
SES	13.4	
SES	14.2	

a Assignments based on ref. 31.

b sh indicates shoulder

c Ref. 31.

d Ref. 22.

e Ref. 23.

f Ref. 29.

g Ref. 30.

h Ref. 32.

i Ref. 28.

j Ref. 44.

k Ref. 48.

l Ref. 50.

m Ref. 51.

n Ref. 52.

o Ref. 36.

p Vertical IP's.

Table 2. Molybdenum Hexacarbonyl

Transition Energy/eV		
Assignment ^a	Present Results	Previous Work
$^1A_{1g} \rightarrow ^1T_{1g}$	3.65 sh ^b	3.64 ^d
$^1A_{1g} \rightarrow ^1T_{1g}$	3.82 sh	3.84 ^{c,d} , 3.89 ^{e,f} , 3.96 ^g 3.95 ^h , 3.78 ⁱ , 3.83 ⁱ
$^1A_{1g} \rightarrow ^1T_{1u}^{(1)}$	4.32	4.29 ^{c,i} , 4.33 ^d , 4.32 ^e 4.34 ^{f,h} , 4.2 [?] , 4.53 ^h 4.30 ⁱ , 4.35 ^j
$^1A_{1g} \rightarrow ^1T_{2g}$	4.65 sh	4.66 ^d , 4.67 ^e , 4.62 ^g 4.60 ⁱ , 4.69 ⁱ
$^1A_{1g} \rightarrow ^1T_{1u}^{(2)}$	5.44	5.39 ^{c,f,h} , 5.45 ^d , 5.44 ^{e,k} 5.32 ^g , 5.28 ^{j,i}
$^1A_{1g} \rightarrow ^1A_{1g}$ ($2t_{2g}(\pi) \rightarrow 3t_{2g}(\pi^*)$)	6.33	6.38 ^d , 6.42 ^{e,k}
	7.08 sh	
	7.36	7.47 ^k
	7.65	
	7.85	
	8.30	8.32 ^k
IP1		8.40 ^l
SES	9.65 sh	9.75 ^h
SES	10.23	
SES	11.43	
SES	11.52	
SES	12.19	
SES	12.50	12.39 ^h

Transition Energy/eV		
Assignment ^a	Present Results	Previous Work
SES	12.83	
IP2		13.32 ^l

a Assignments based on ref. 31.

b sh indicates shoulder

c Ref. 22.

d Ref. 31.

e Ref. 29.

f Ref. 24.

g Ref. 30.

h Ref. 25.

i Ref. 28.

j Ref. 23.

k Ref. 32.

l Ref. 36.

Table 3. Tungsten Hexacarbonyl

Transition Energy/eV		
Assignment ^a	Present Results	Previous Work
$^1A_{1g} \rightarrow ^1T_{1g}$	3.61 sh ^b	3.66 ^c , 3.52 ^e , 3.54 ^f 3.53 ⁱ , 3.56 ⁱ , 3.51 ⁱ
	3.75	3.77 ⁱ , 3.71 ⁱ
$^1A_{1g} \rightarrow ^1T_{1g}$	4.00 sh	4.04 ^d , 3.96 ^f , 3.93 ⁱ
$^1A_{1g} \rightarrow ^1T_{1u}^{(1)}$	4.32	4.28 ^c , 4.33 ^d , 4.27 ^e 4.30 ^{f,i} , 4.34 ^h , 4.38 ^j 3.75 ^j , 3.80 ^j , 4.39 ⁱ
$^1A_{1g} \rightarrow ^1T_{2g}$	4.54 sh	4.61 ^d , 4.51 ^e , 4.54 ^f 4.55 ⁱ
	4.86 sh	4.84 ^f , 4.15 ^g , 4.41 ^j 4.71 ⁱ , 4.79 ⁱ
$^1A_{1g} \rightarrow ^1T_{1u}^{(2)}$	5.55	5.41 ^c , 5.53 ^d , 5.44 ^e 5.56 ^g , 5.39 ^j , 5.43 ⁱ 5.55 ⁱ
$^1A_{1g} \rightarrow ^1A_{1g}$ ($2t_{2g}(\pi) \rightarrow 3t_{2g}(\pi^*)$)	6.24 sh	6.26 ^d , 6.24 ^f , 6.36 ^g
	6.54 sh	6.52 ^e , 6.55 ^f , 6.36 ^g
	7.66	7.65 ^g
	8.38	8.43 ^g
IP1		8.56 ^{k,l}
SES	8.80	
SES	9.96	
SES	10.38	
SES	11.63	
SES	12.26	

Transition Energy/eV		
Assignment ^a	Present Results	Previous Work
IP2		13.27 ^{k,l}

^a Assignments based on ref. 31.

^b sh indicates shoulder

^c Ref. 22.

^d Ref. 29.

^e Ref. 30.

^f Ref. 31.

^g Ref. 32.

^h Ref. 25.

ⁱ Ref. 28.

^j Ref. 53.

^k Ref. 36.

^l Vertical IP.

Table 4. Ratios of the area of the lowest MLCT band to that of the lowest energy shoulder as measured at 20° scattering angle.

	E_0 (eV)		
	100	50	25
$\text{Cr}(\text{CO})_6$	4.05	3.93	3.77
$\text{Mo}(\text{CO})_6$	4.83	4.82	4.23
$\text{W}(\text{CO})_6$	4.25	4.06	3.52

- Figure 1. High resolution electron energy-loss spectrum of $\text{Cr}(\text{CO})_6$, $E_0 = 100\text{eV}$, $\theta = 0^\circ$, resolution = 45 meV FWHM.
- Figure 2. DCS plot of $\text{Cr}(\text{CO})_6$, $E_0 = 25\text{ eV}$. Elastic scattering = \blacksquare ; P_1 (2.5 → 4.1 eV) = \bullet ; P_2 (4.1 → 4.8 eV) = \blacktriangle ; P_3 (4.8 → 7.2 eV) = \circ ; P_4 (6.35 eV symmetry-forbidden transition) = \square . The same arbitrary units are used for all curves.
- Figure 3. DCS plot of $\text{Cr}(\text{CO})_6$, $E_0 = 50\text{ eV}$. Elastic scattering = \blacksquare ; P_1 (2.5 → 4.1 eV) = \bullet ; P_2 (4.1 → 4.8 eV) = \blacktriangle ; P_3 (4.8 → 7.2 eV) = \circ ; P_4 (6.35 symmetry-forbidden transition) = \square . The same arbitrary units are used for all curves.
- Figure 4. Plot of the ratios of the DCS's of the various transitions of $\text{Cr}(\text{CO})_6$ to that of the transition P_3 (4.8 - 7.2 eV) at $E_0 = 25\text{ eV}$ $P_1/P_3 = \bullet$; $P_2/P_3 = \blacksquare$ $P_4/P_3 = \blacktriangle$. See caption for figure 2.
- Figure 5. Plot of the ratios of the DCS's of the various transitions of $\text{Cr}(\text{CO})_6$ to that of the transition P_3 (4.8 - 7.2 eV) at $E_0 = 50\text{ eV}$ $P_1/P_3 = \bullet$, $P_2/P_3 = \blacksquare$, $P_4/P_3 = \blacktriangle$. See caption for figure 2.
- Figure 6. Low angle (10°) and high angle (90°) spectra between 3.0 eV and 8.0 eV energy loss of $\text{Cr}(\text{CO})_6$ with $E_0 = \text{eV}$.
- Figure 7. Plot of the electron energy-loss spectra of $\text{Cr}(\text{CO})_6$ in the 3.5 eV to 7.5 eV energy-loss region at incident energy $E_0 = 100\text{ eV}$ with $\theta = 0^\circ, 3^\circ$ and 6° to show the emergence of symmetry-forbidden transitions. Tick marks on the Y axis

indicate the baselines of the successive spectra. The arbitrary units for each spectrum are different and are chosen so that the displayed height of the intensity of the 5.51 eV transition is the same for all displayed spectra.

- Figure 8. High resolution electron energy-loss spectrum of $\text{Mo}(\text{CO})_6$, $E_0 = 100$ eV, $\theta = 0^\circ$, resolution = 40 meV FWHM.
- Figure 9. DCS plot of $\text{Mo}(\text{CO})_6$, $E_0 = 25$ eV, Elastic scattering = ■, $P_1(2.5 \rightarrow 4.0$ eV) = ●, $P_2(4.0 \rightarrow 4.60$ eV) = ▲, $P_3(4.60 \rightarrow 4.85$ eV) = ○, $P_4(4.85 \rightarrow 6.5$ eV) = □, P_5 (6.33 eV symmetry-forbidden transition) = ◆. See caption for figure 2.
- Figure 10. DCS plot of $\text{Mo}(\text{CO})_6$, $E_0 = 50$ eV, Elastic scattering = ■, $P_1(2.5 \rightarrow 4.0$ eV) = ●, $P_2(4.0 \rightarrow 4.60$ eV) = ▲, $P_3(4.60 \rightarrow 4.85$ eV) = ○, $P_4(4.85 \rightarrow 6.5$ eV) = □, P_5 (6.33 eV symmetry-forbidden transition) = ◆. See caption for figure 2.
- Figure 11. Plot of the ratios of the DCS's of the various transitions of $\text{Mo}(\text{CO})_6$ to that of the transition $P_4(4.85 \rightarrow 6.5$ eV) at $E_0 = 25$ eV. $P_1/P_4 = \bullet$, $P_2/P_4 = \blacksquare$, $P_3/P_4 = \blacklozenge$, $P_5/P_4 = \blacktriangle$. See caption for figure 2.
- Figure 12. Plot of the ratios of the DCS's of the various transitions of $\text{Mo}(\text{CO})_6$ to that of the transition $P_4(4.85 \rightarrow 6.5$ eV) at $E_0 = 50$ eV. $P_1/P_4 = \bullet$, $P_2/P_4 = \blacksquare$, $P_3/P_4 = \blacklozenge$, $P_5/P_4 = \blacktriangle$. See caption for figure 2.
- Figure 13. Low angle (10°) and high angle (90°) spectra (between 3.0 and 8.0 eV energy-loss) of $\text{Mo}(\text{CO})_6$ with $E_0 = 25$ eV.

Figure 14. Plot of the electron energy-loss spectra of $\text{Mo}(\text{CO})_6$ in the 3.5 eV to 7.5 eV energy-loss region at incident energy $E_0 = 100$ eV with $\theta = 0^\circ, 3^\circ,$ and 6° to show the emergence of symmetry-forbidden transitions. Tick marks on the Y axis indicate the baselines of the successive spectra. The arbitrary units for each spectrum are different and are chosen so that the displayed height of the intensity of the 5.51 eV transition is the same for all displayed spectra.

Figure 15. High resolution electron energy-loss spectrum of $\text{W}(\text{CO})_6$, $E_0 = 100$ eV, $\theta = 0^\circ$, resolution = 40 meV FWHM.

Figure 16. DCS plot of $\text{W}(\text{CO})_6$, $E_0 = 25$ eV, Elastic scattering = \blacksquare , $P_1(2.5 \rightarrow 4.0 \text{ eV}) = \bullet$, $P_2(4.0 \rightarrow 4.60 \text{ eV}) = \blacktriangle$, $P_3(4.60 \rightarrow 5.1 \text{ eV}) = \circ$, $P_4(5.1 \rightarrow 6.4 \text{ eV}) = \square$, P_5 (symmetry-forbidden transition) = \blacklozenge . See caption for figure 2.

Figure 17. DCS plot of $\text{W}(\text{CO})_6$, $E_0 = 50$ eV, Elastic scattering = \blacksquare , $P_1(2.5 \rightarrow 4.0 \text{ eV}) = \bullet$, $P_2(4.0 \rightarrow 4.60 \text{ eV}) = \blacktriangle$, $P_3(4.60 \rightarrow 5.1 \text{ eV}) = \circ$, $P_4(5.1 \rightarrow 6.4 \text{ eV}) = \square$, P_5 (symmetry-forbidden transition) = \blacklozenge . See caption for figure 2.

Figure 18. Plot of the ratios of the DCS's of the various transitions of $\text{W}(\text{CO})_6$ to that of the transition $P_4(5.1 \rightarrow 6.4 \text{ eV})$ at $E_0 = 25$ eV. $P_1/P_4 = \bullet$, $P_2/P_4 = \blacksquare$, $P_3/P_4 = \blacklozenge$, $P_5/P_4 = \blacktriangle$. See caption for figure 2.

Figure 19. Plot of the ratios of the DCS's of the various transitions of $\text{W}(\text{CO})_6$ to that of the transition $P_4(5.1 \rightarrow 6.4 \text{ eV})$ at $E_0 = 50$ eV. $P_1/P_4 = \bullet$, $P_2/P_4 = \blacksquare$, $P_3/P_4 = \blacklozenge$, $P_5/P_4 = \blacktriangle$. See

caption for figure 2.

Figure 20. Low angle (10°) and high angle (90°) spectra (between 3.0 and 8.0 eV energy-loss) of $W(CO)_6$ with $E_0 = 25$ eV.

Figure 21. Plot of the electron energy-loss spectra of $W(CO)_6$ in the 3.5 eV to 7.5 eV energy-loss region at incident energy $E_0 = 100$ eV with $\theta = 0^\circ, 3^\circ$ and 6° to show the emergence of symmetry-forbidden transitions. Tick marks on the Y axis indicate the baselines of the successive spectra. The arbitrary units for each spectrum are different and are chosen so that the displayed height of the intensity of the 5.51 eV transition is the same for all displayed spectra.

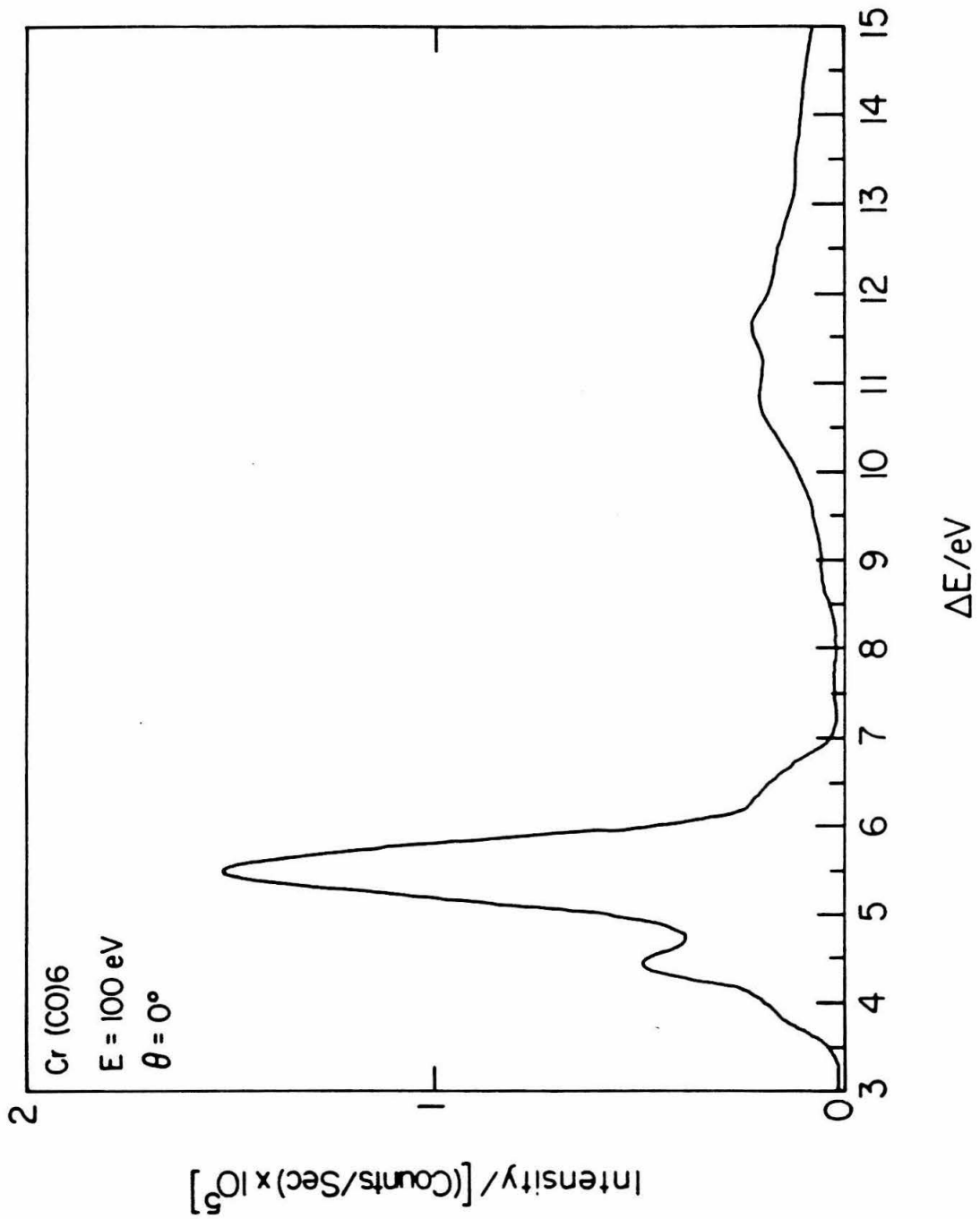


Figure 1.

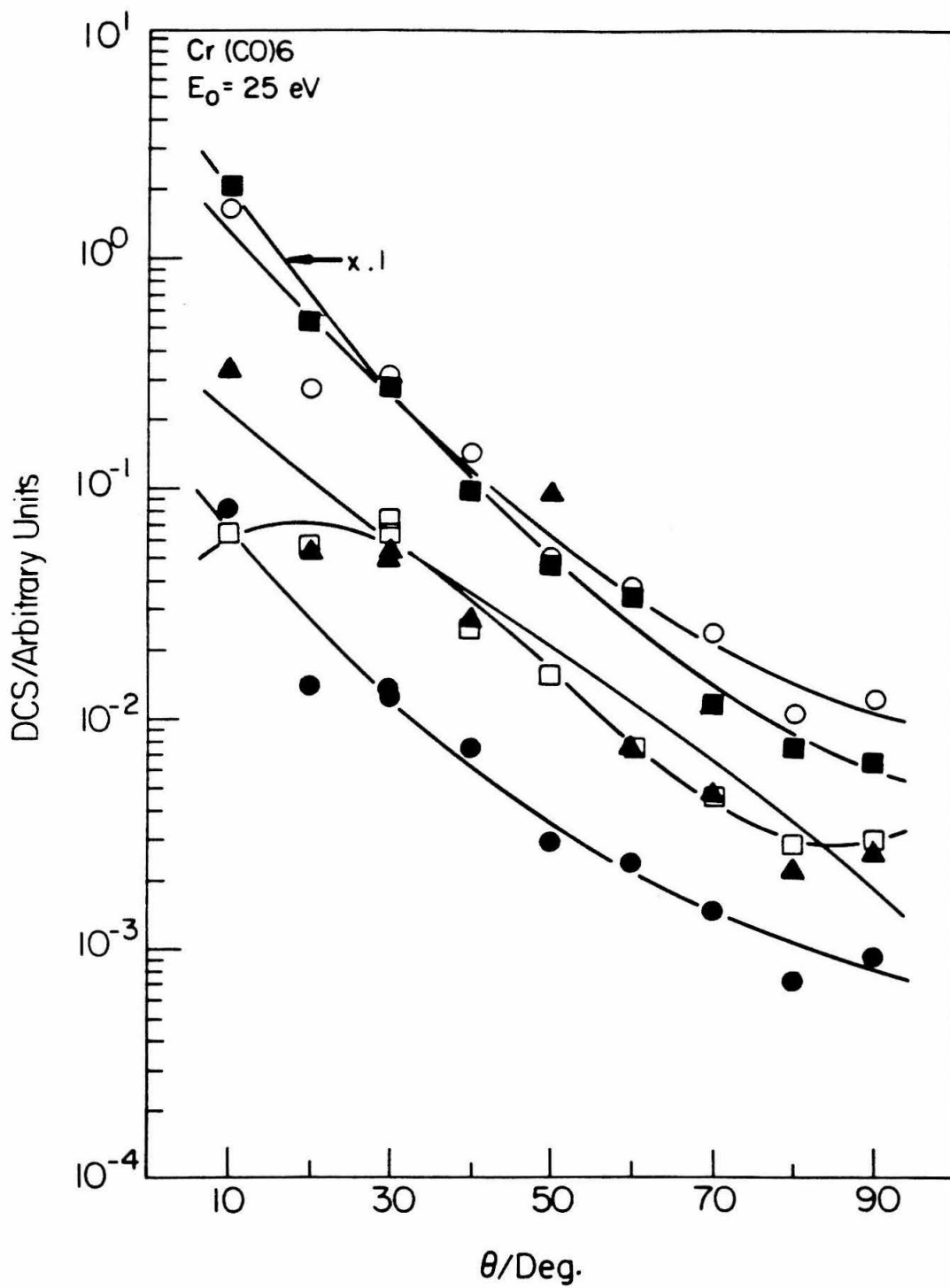


Figure 2.

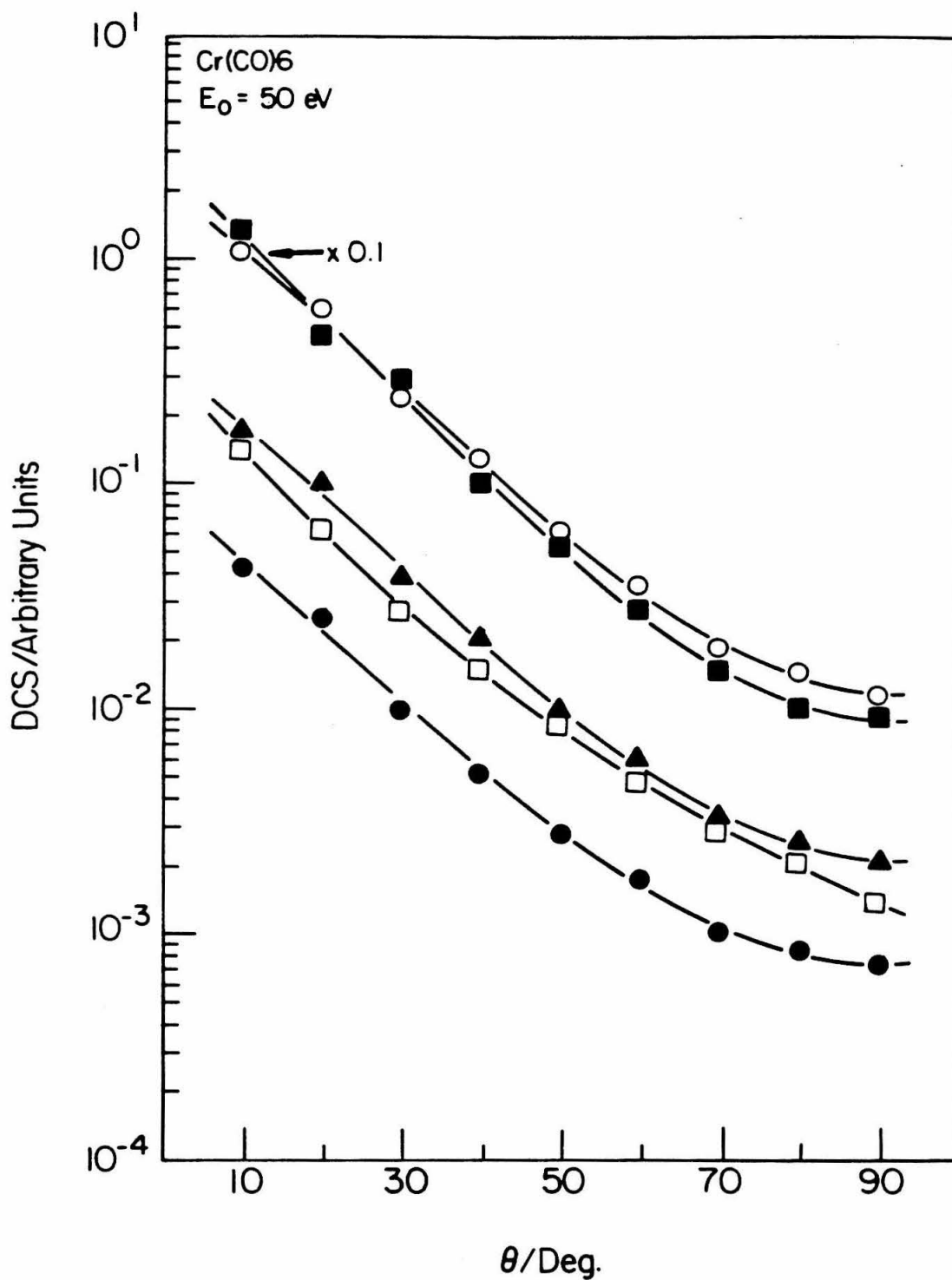


Figure 3.

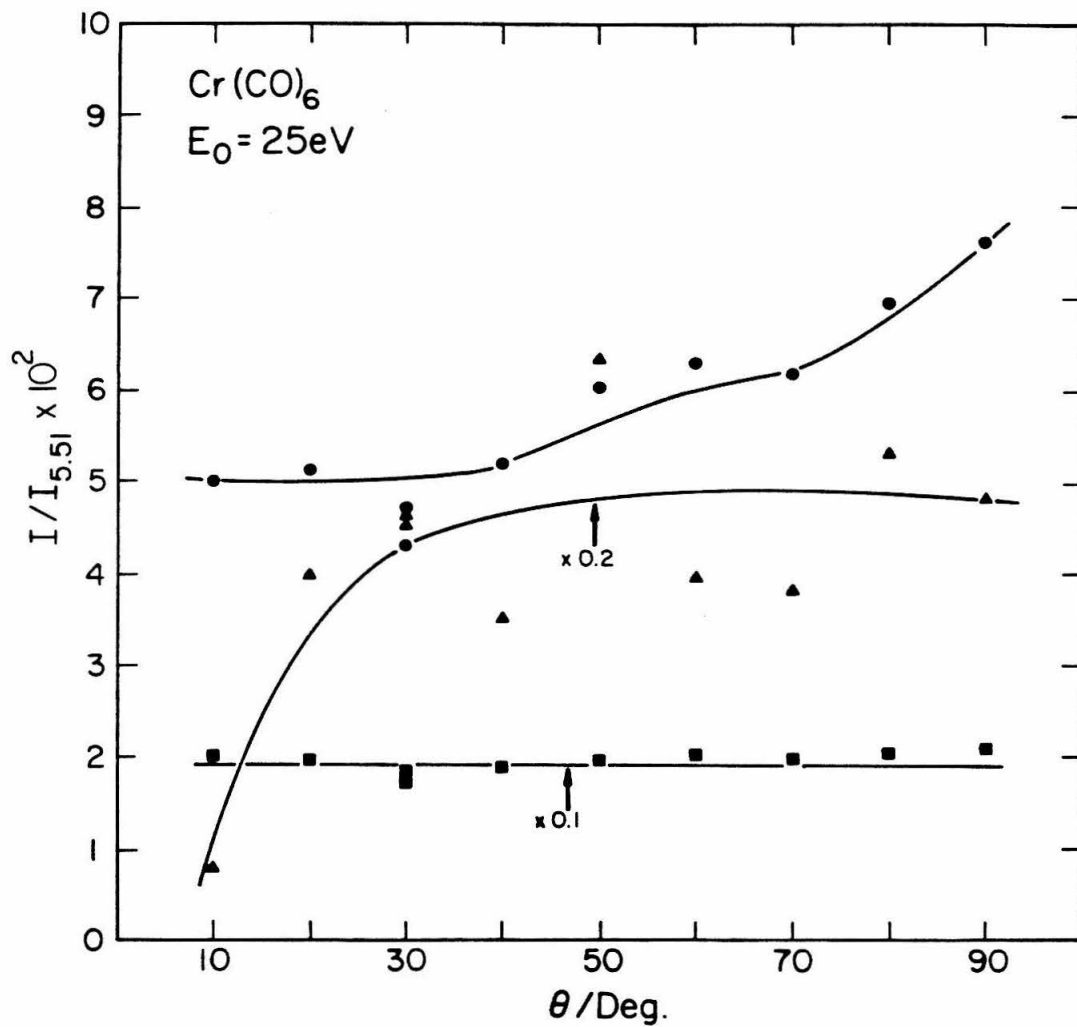


Figure 4.

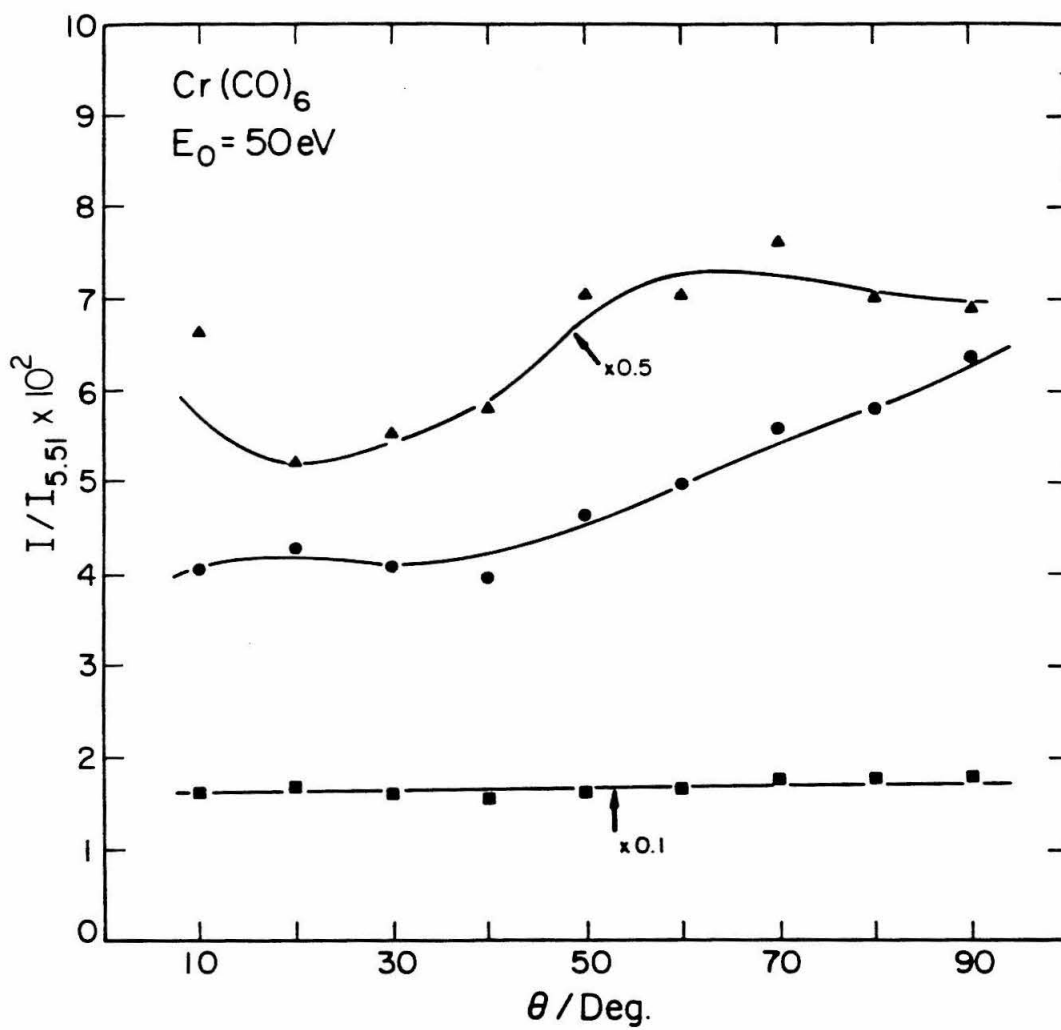


Figure 5.

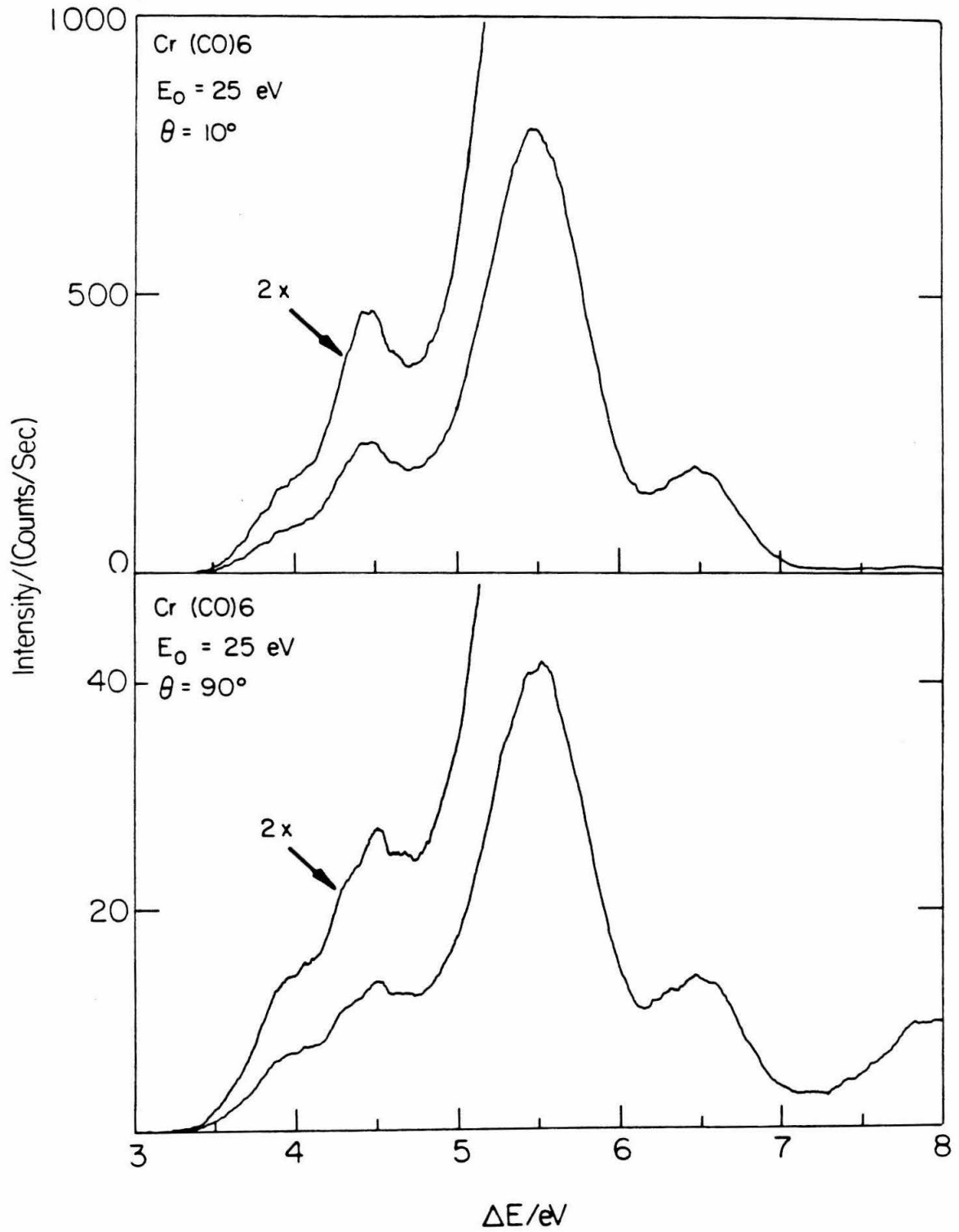


Figure 6.

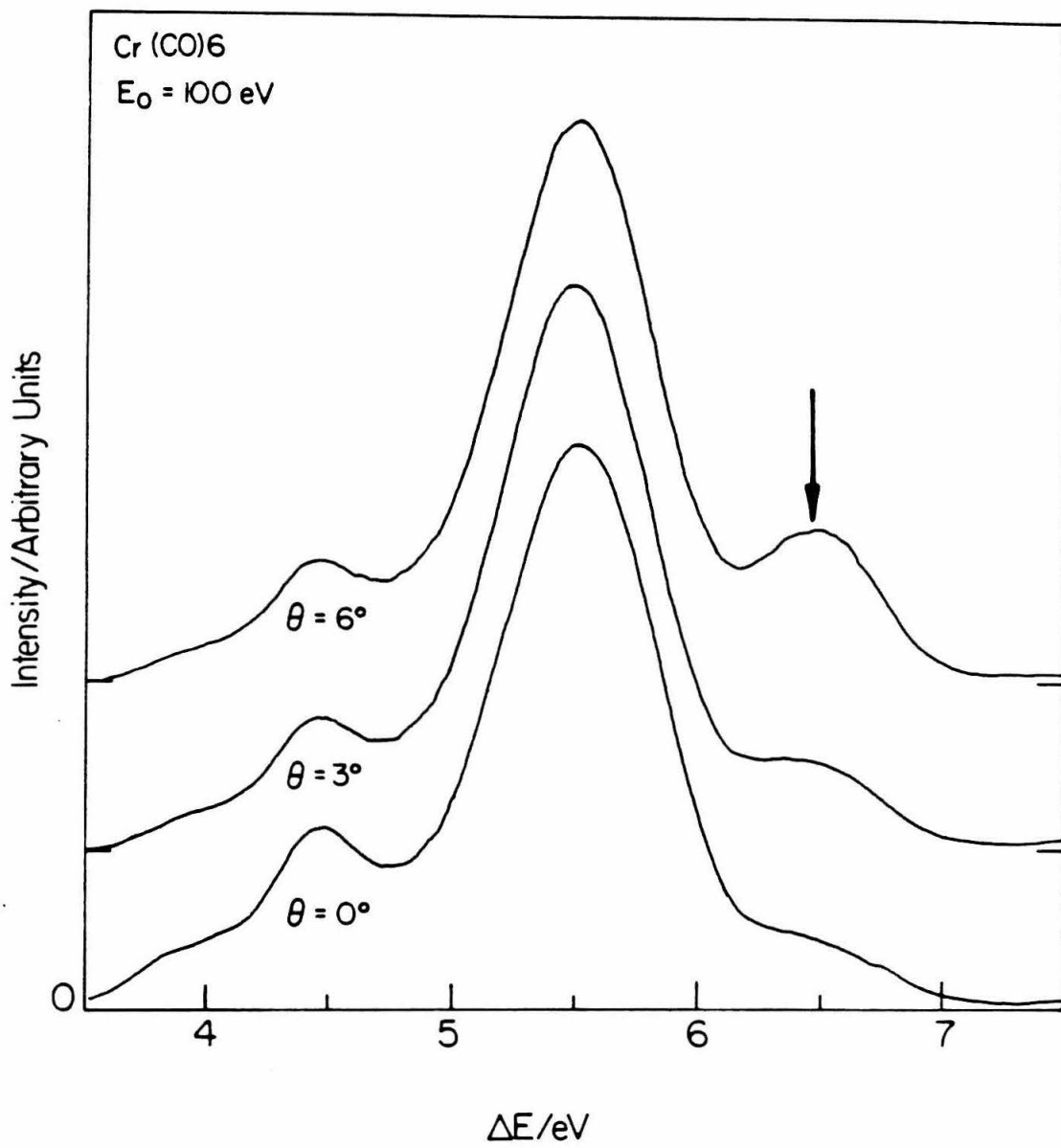


Figure 7.

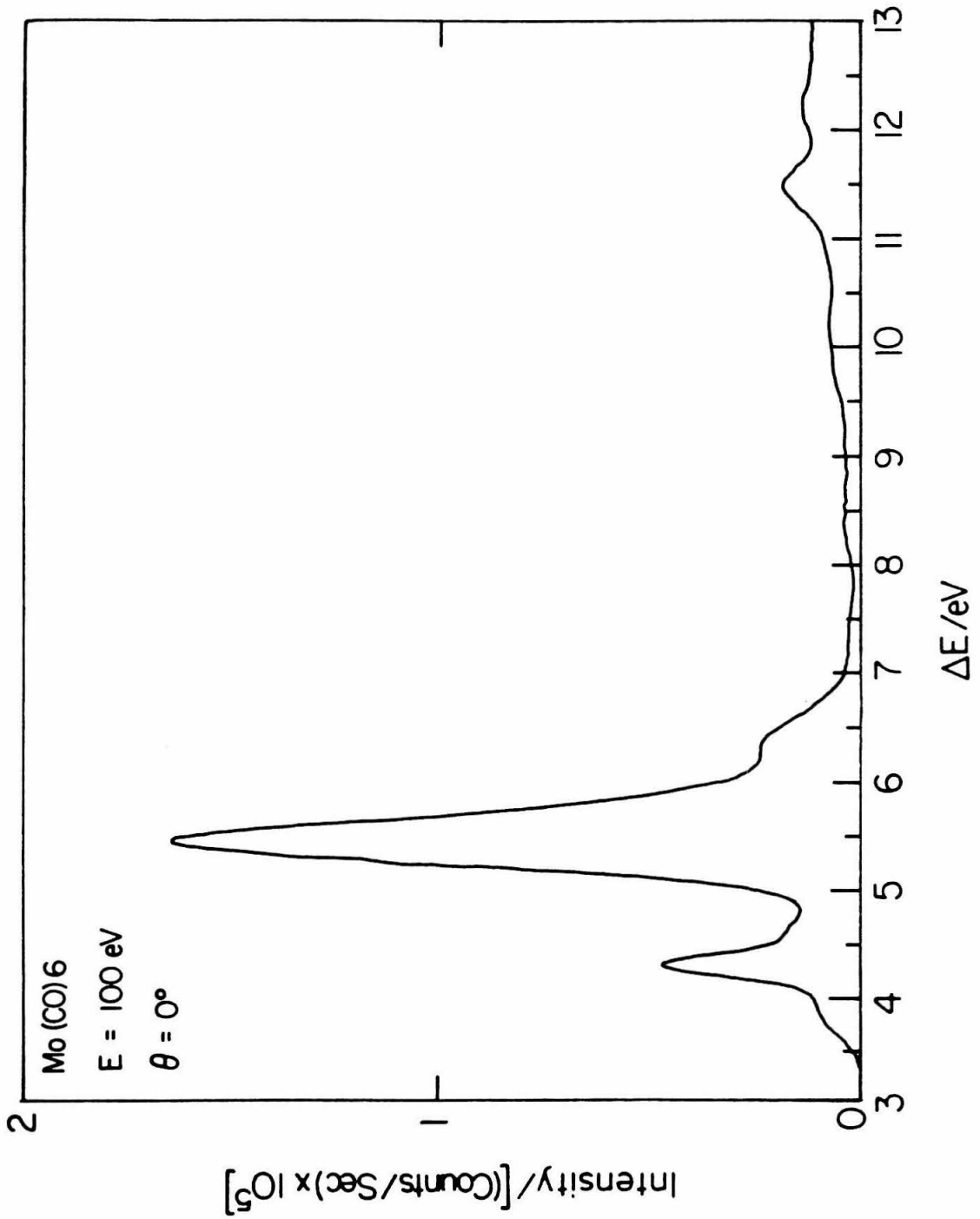


Figure 8.

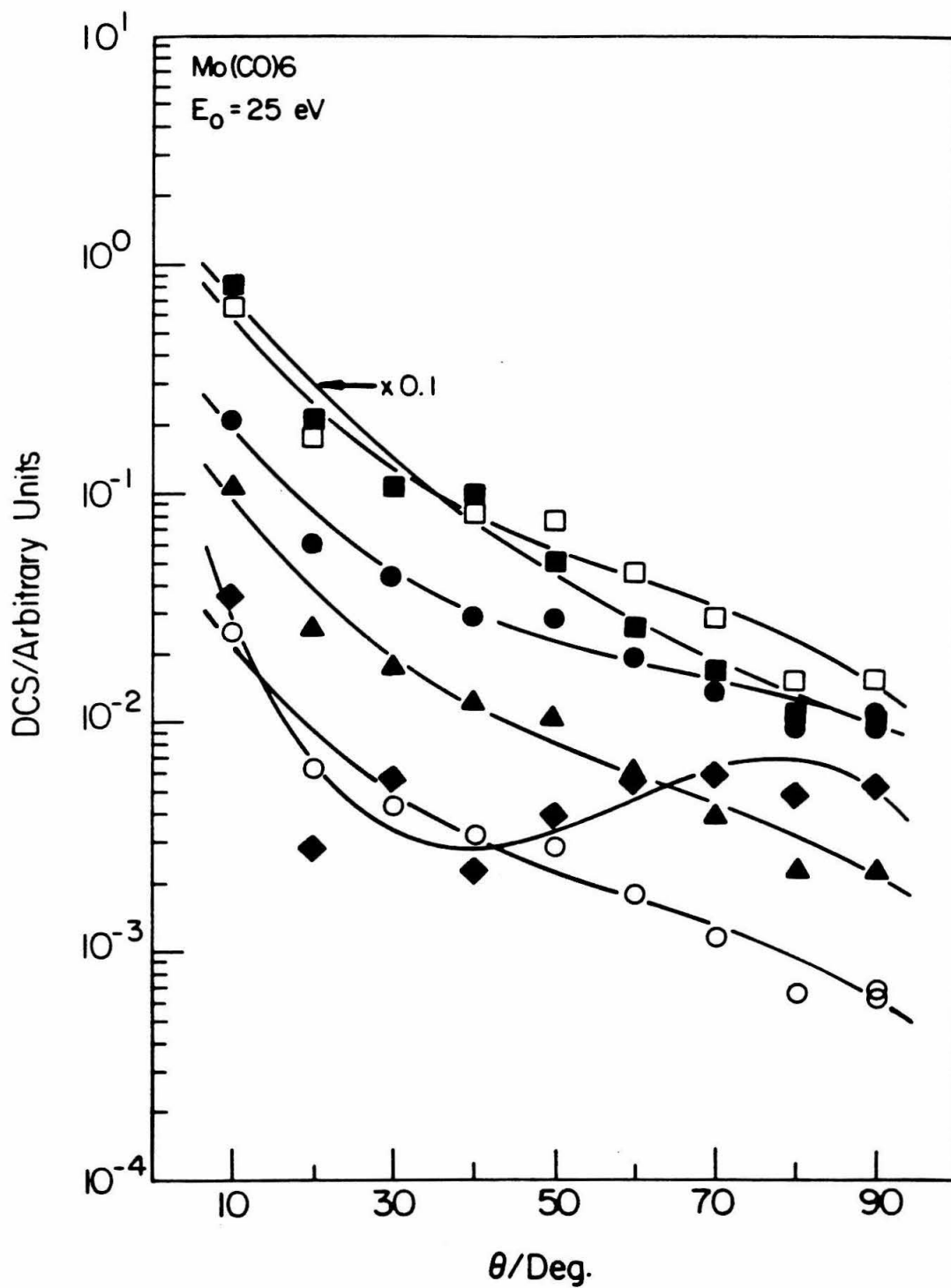


Figure 9.

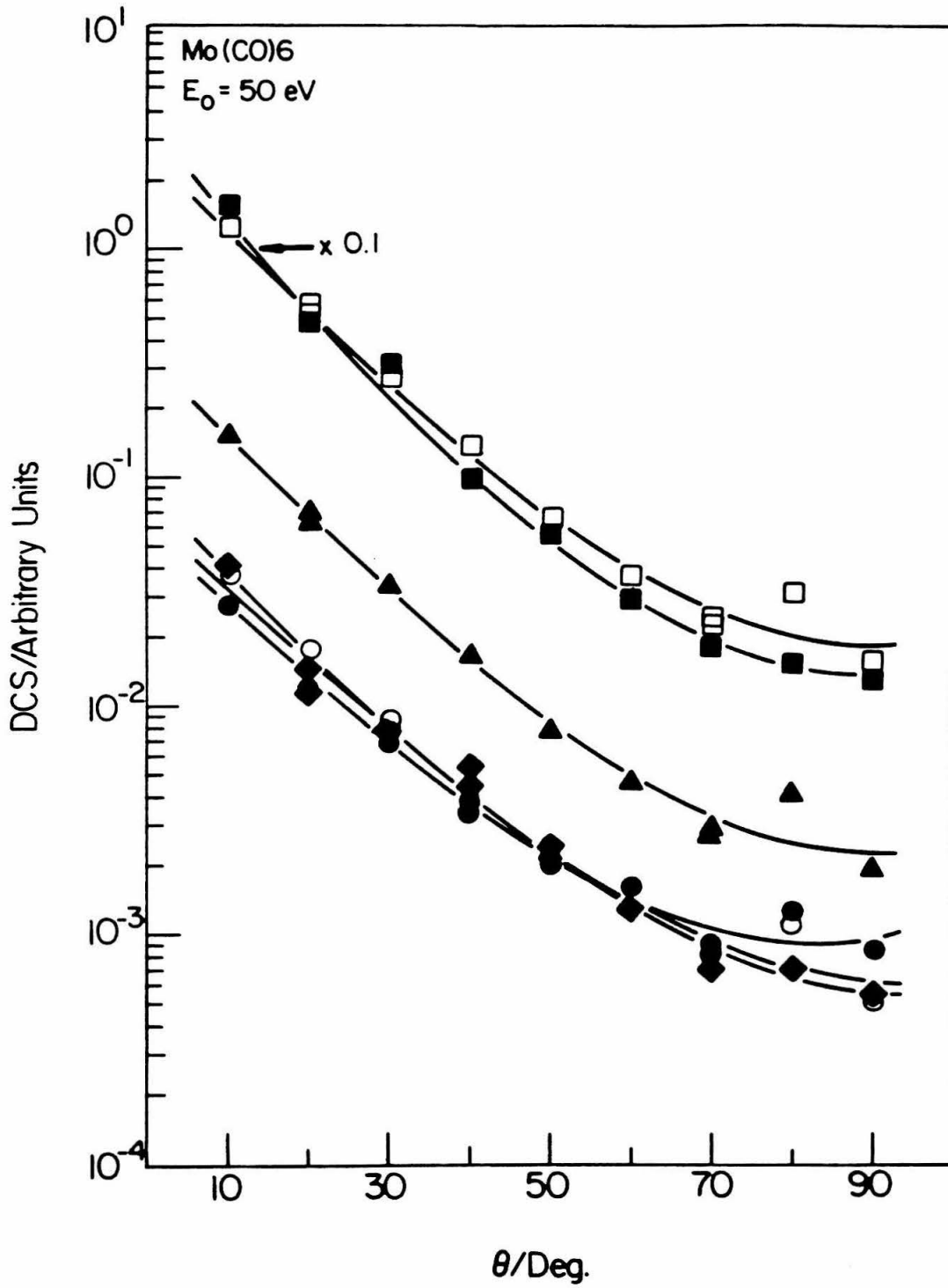


Figure 10.

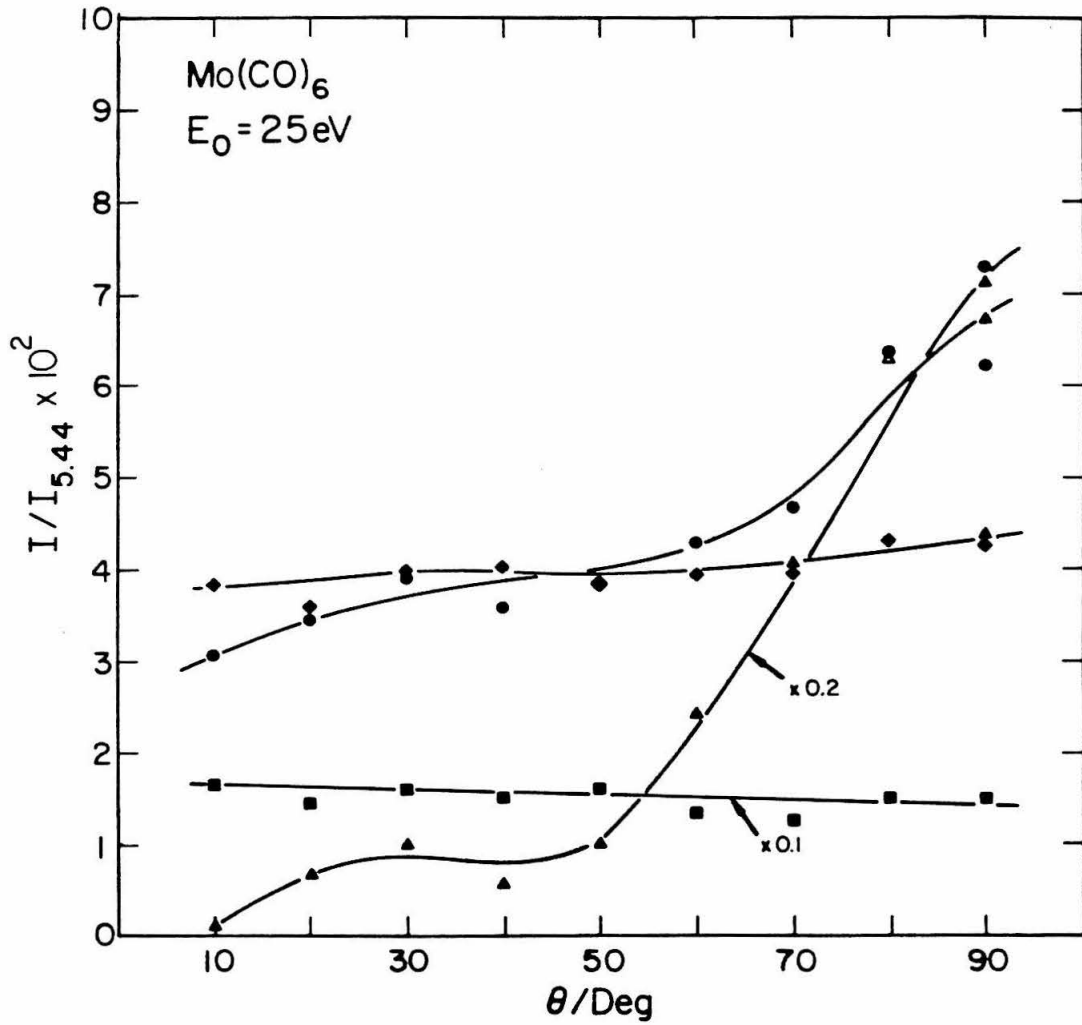


Figure 11.

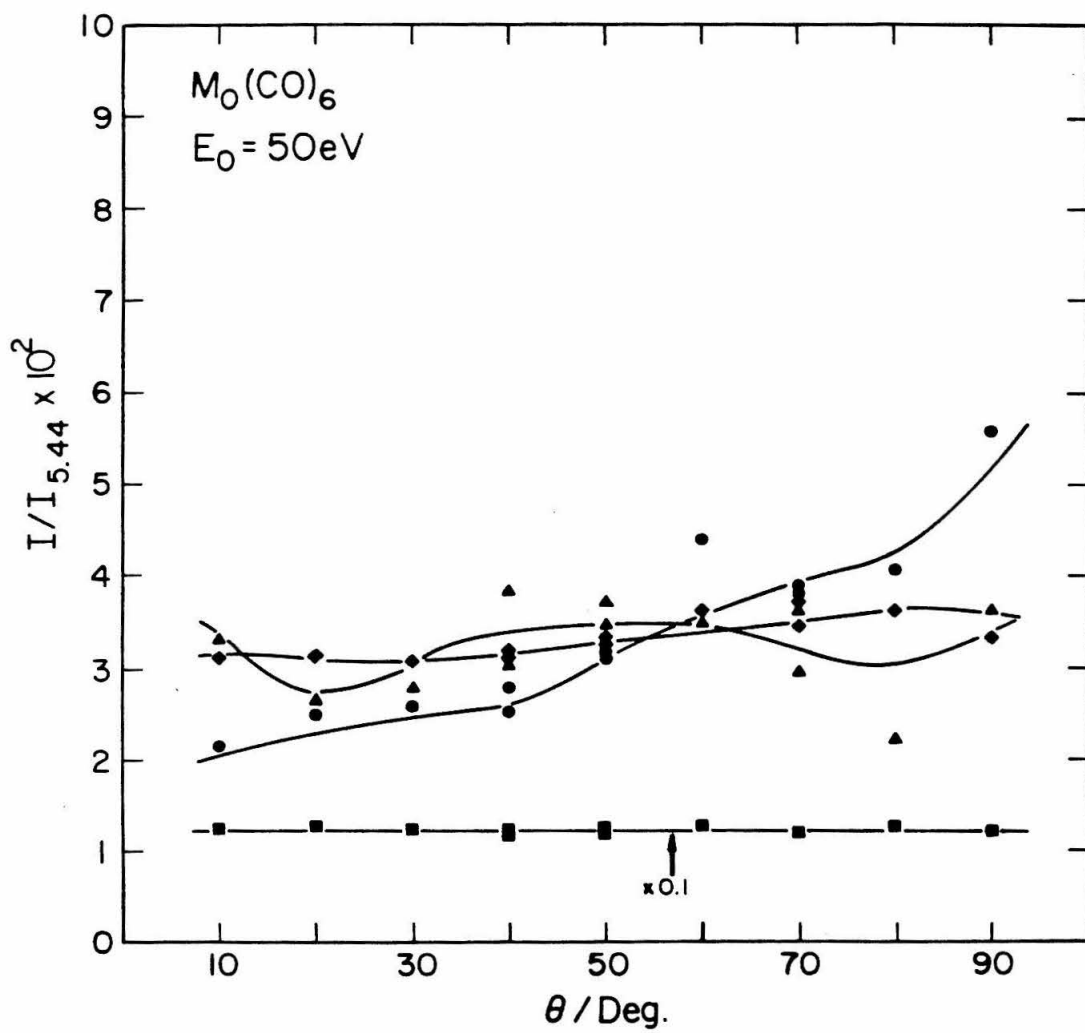


Figure 12.

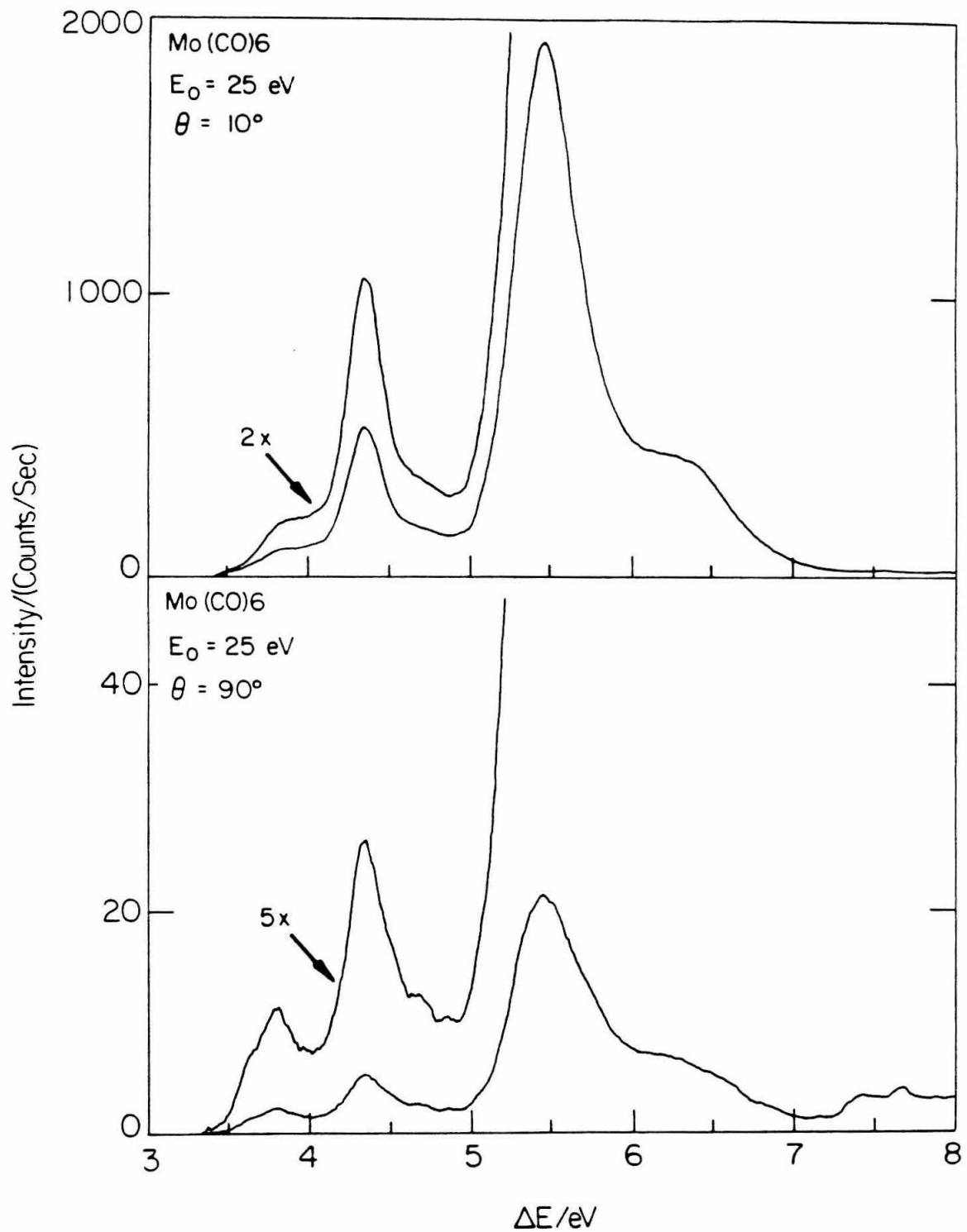


Figure 13.

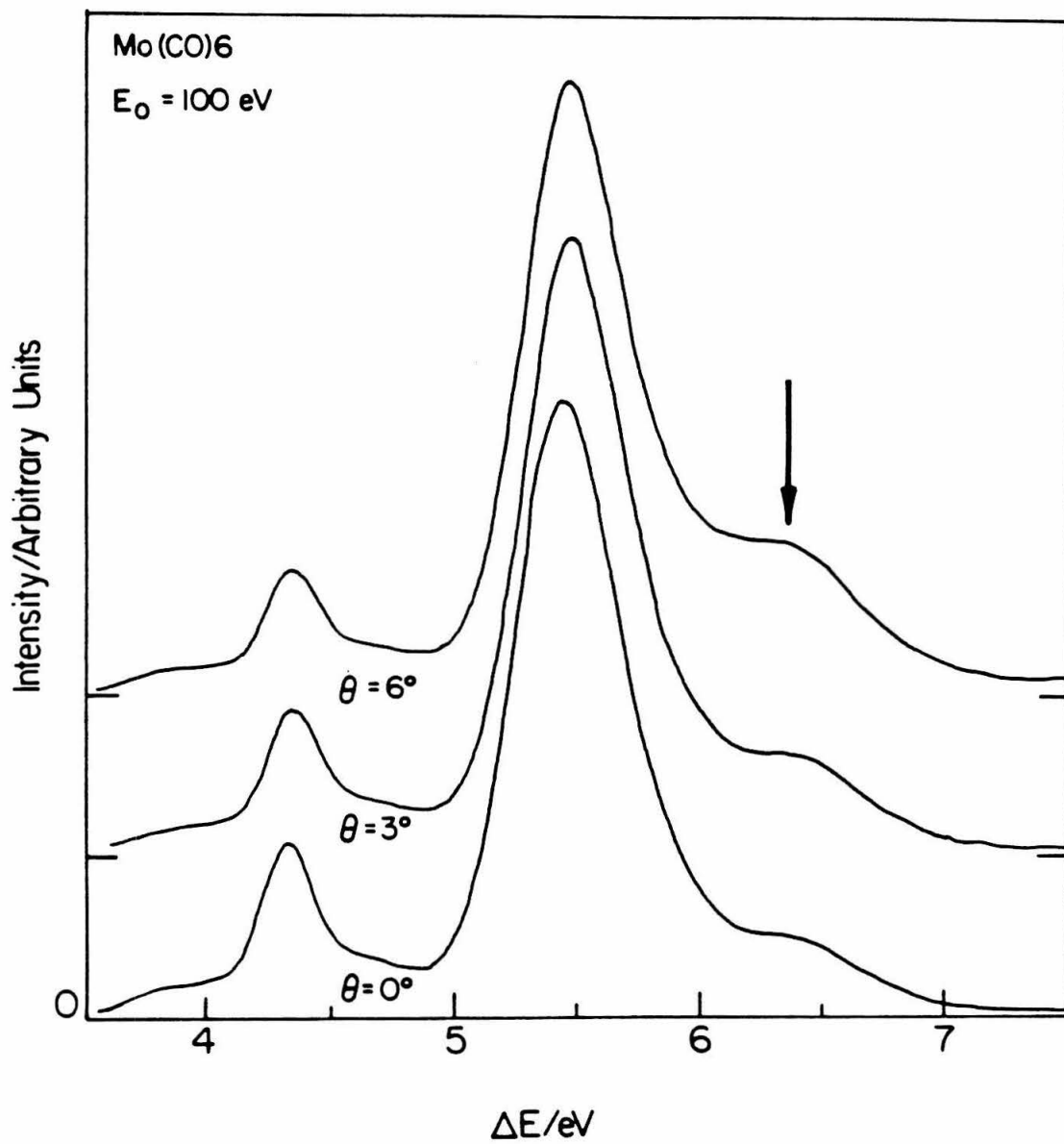


Figure 14.

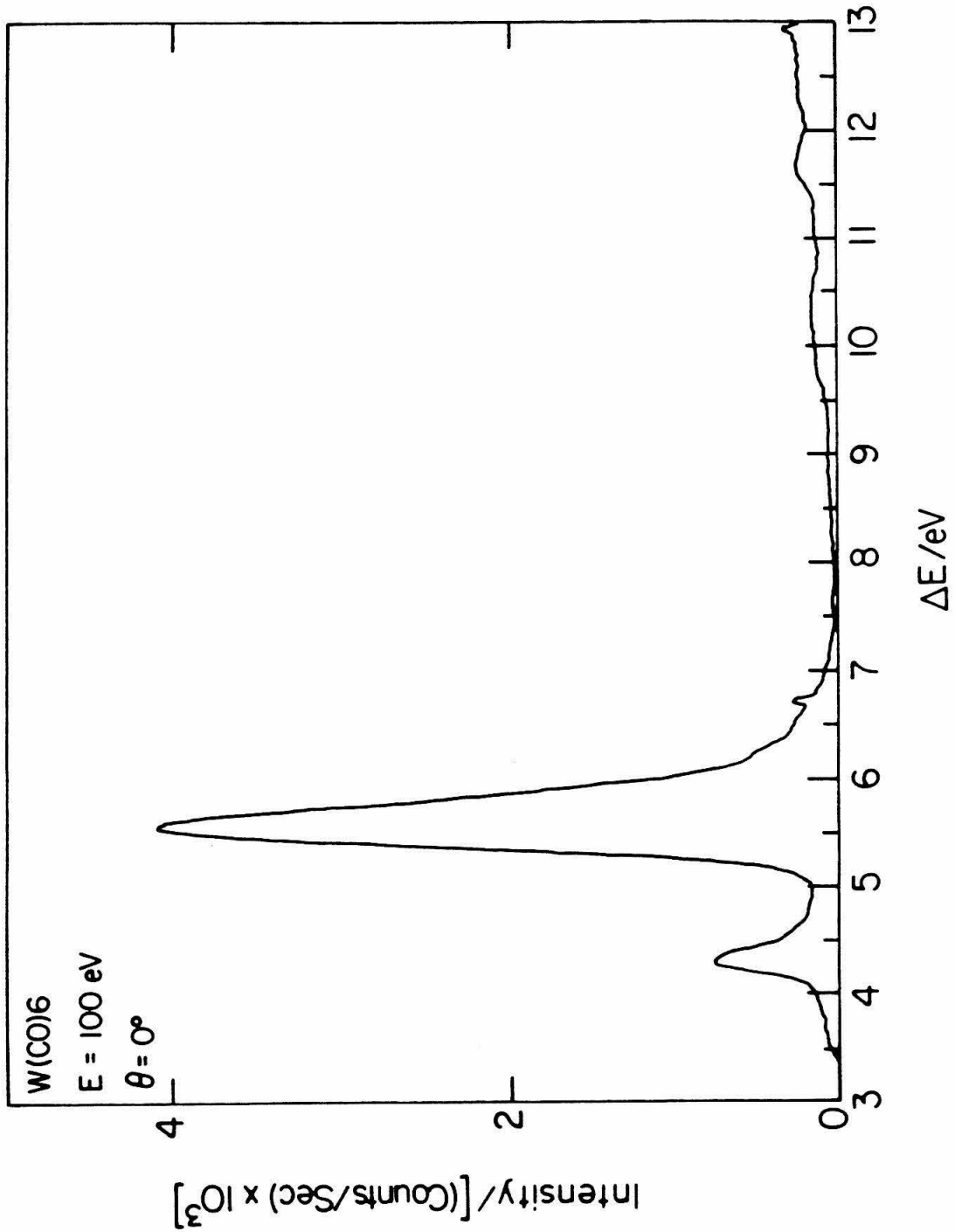


Figure 15.

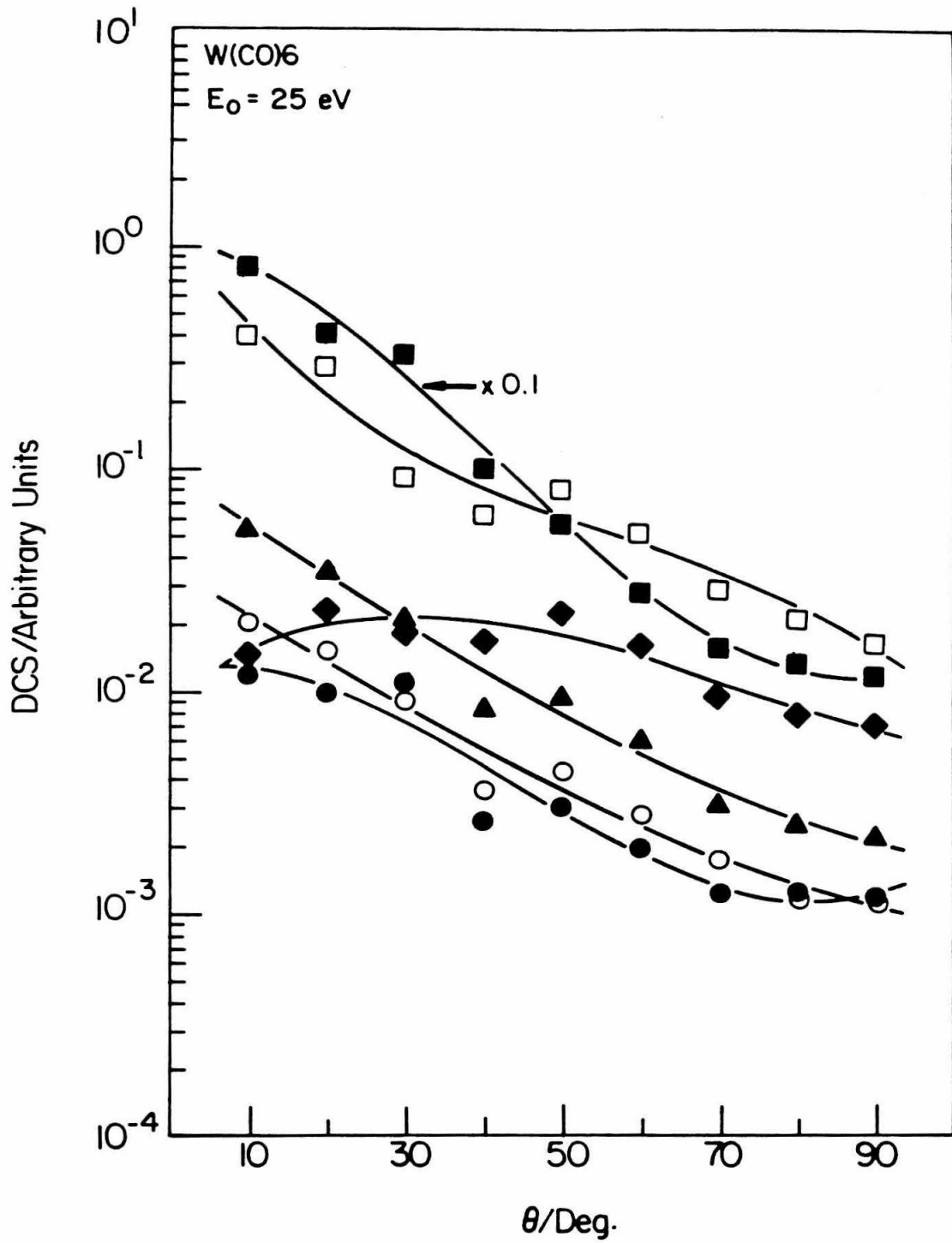


Figure 16.

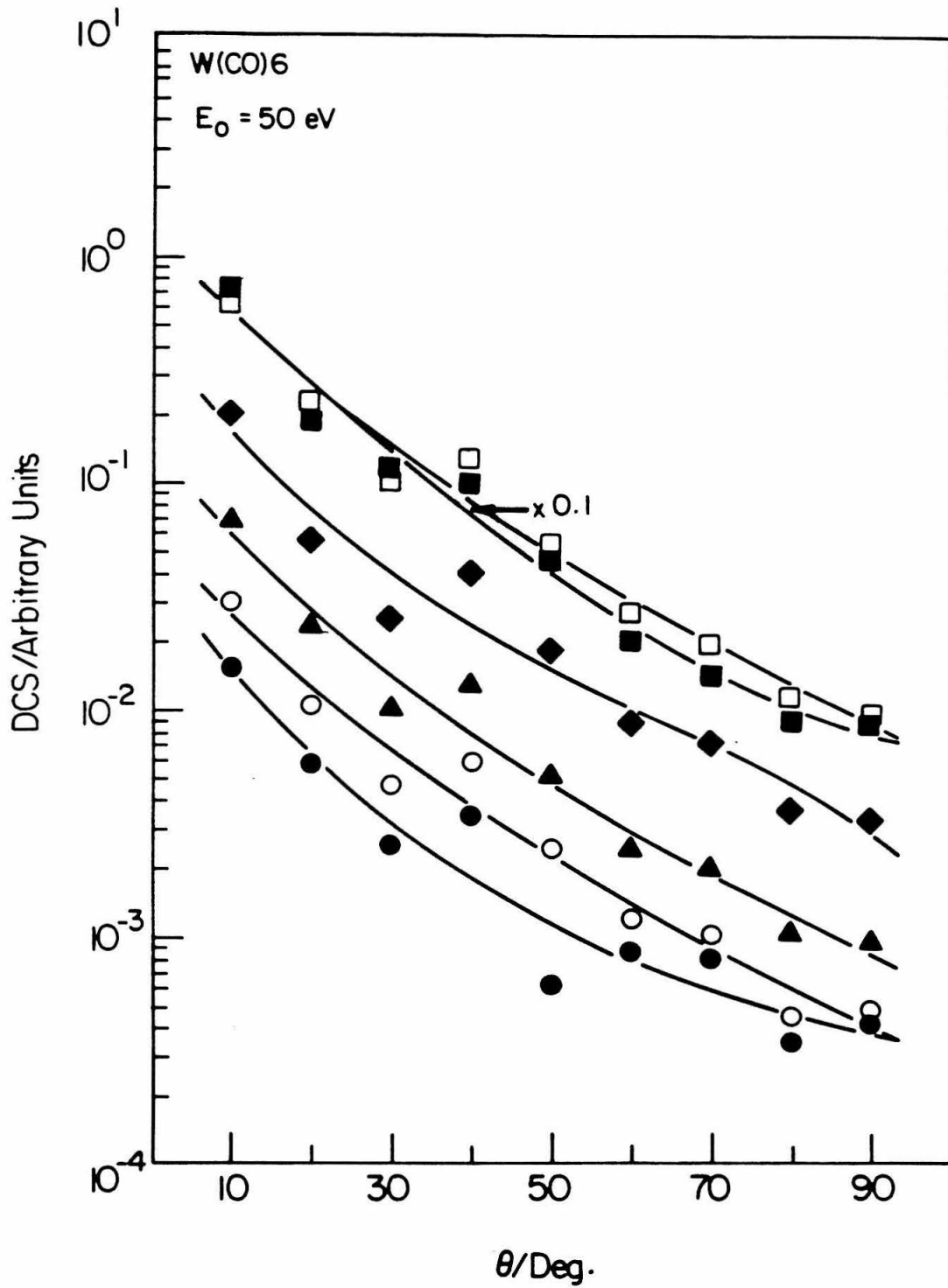


Figure 17.

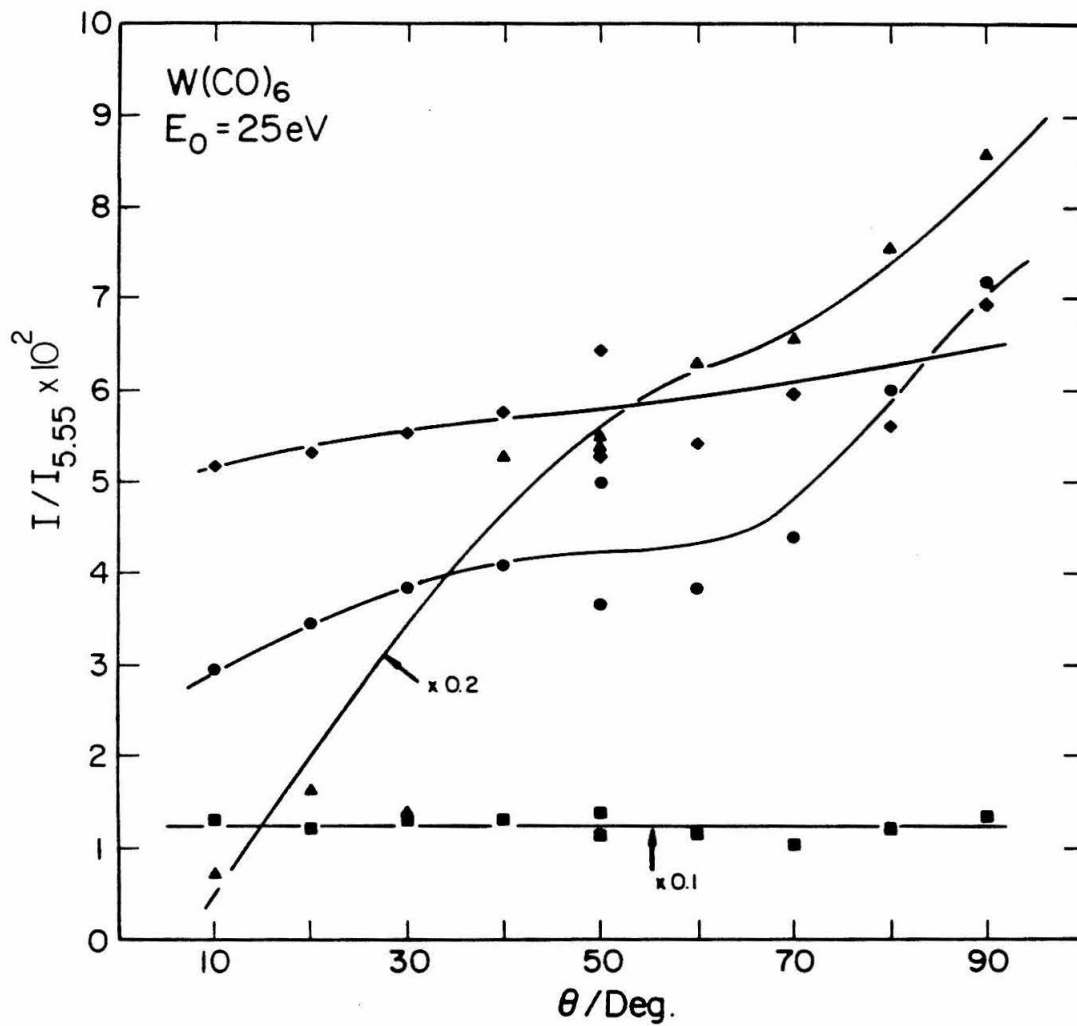


Figure 18.

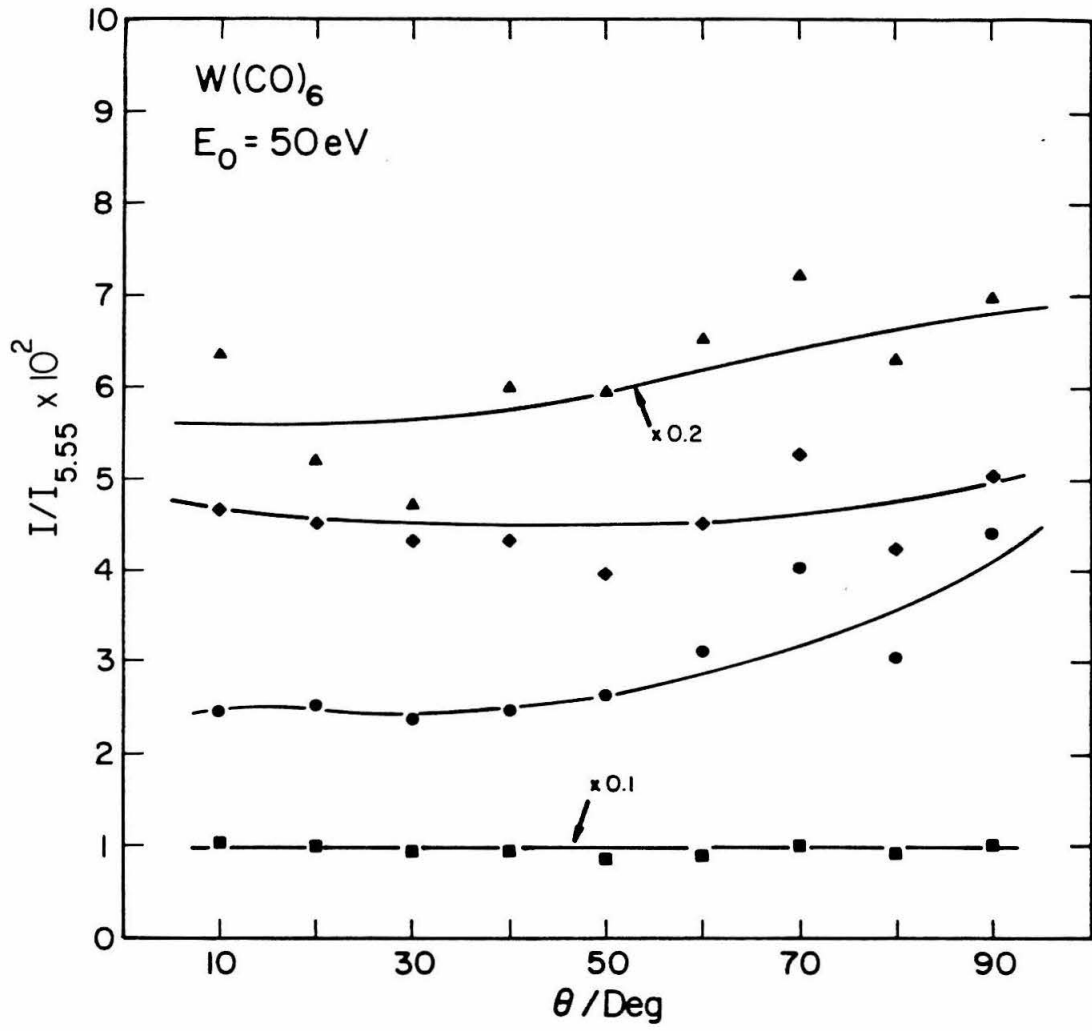


Figure 19.

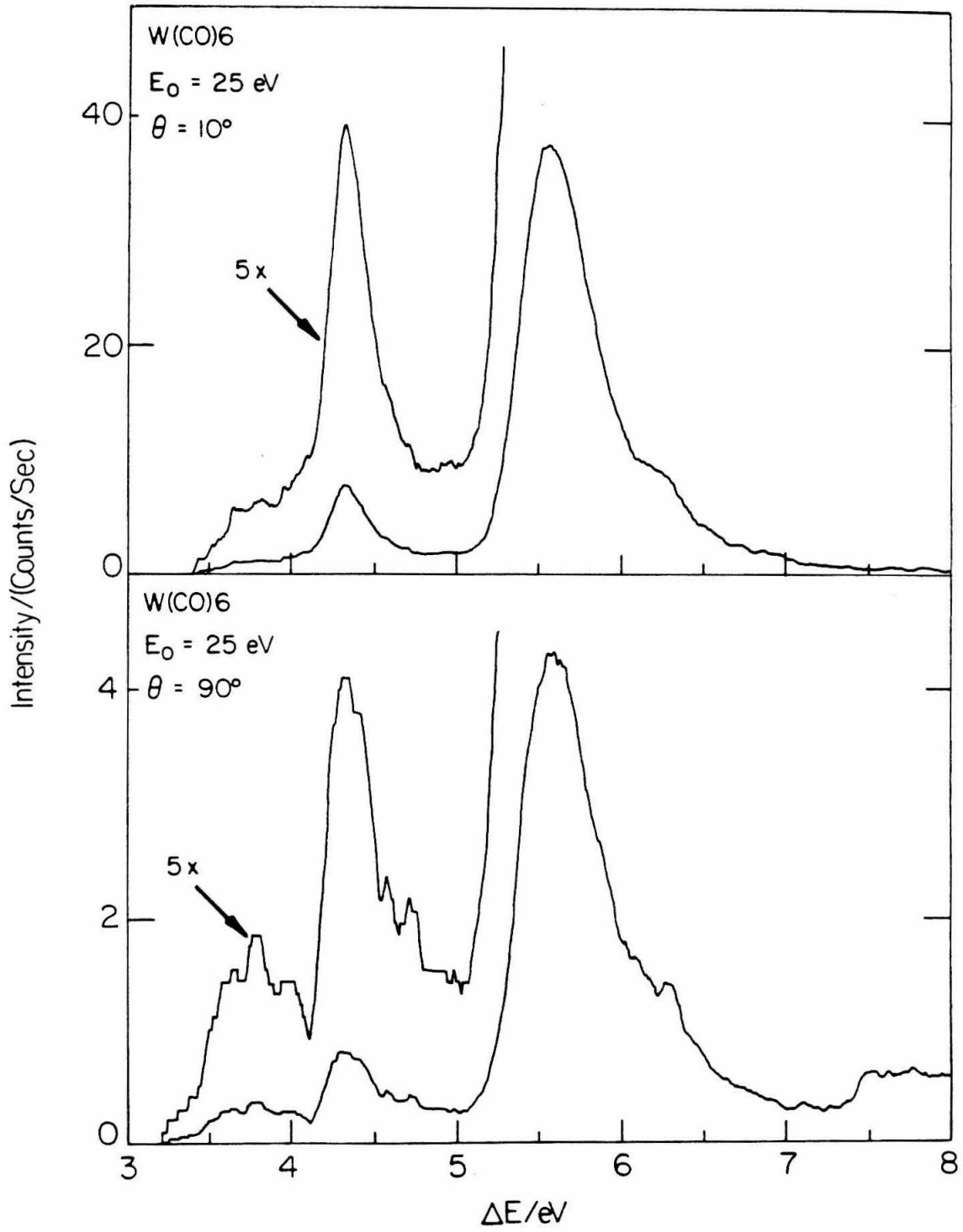


Figure 20.

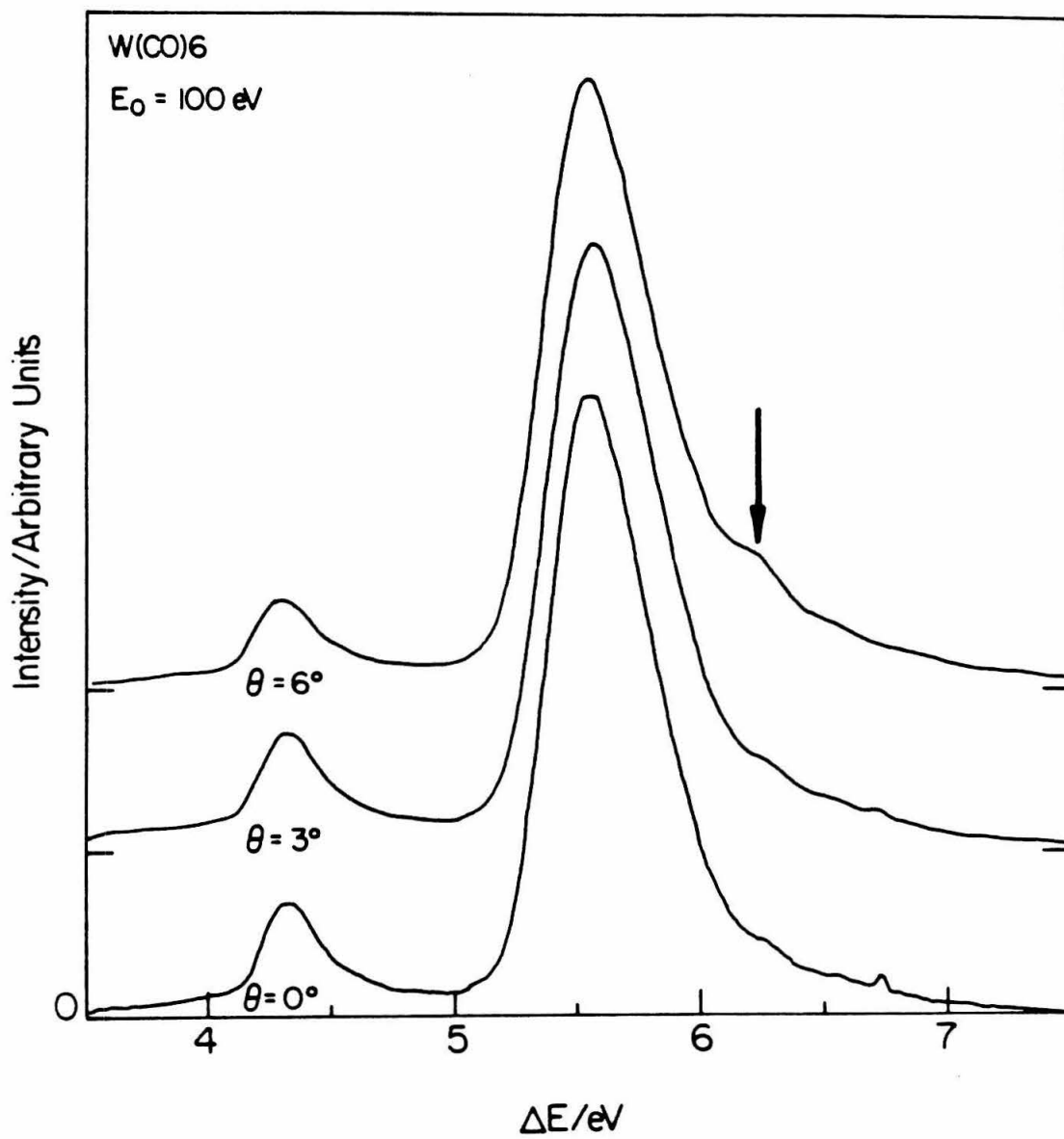


Figure 21.

CHAPTER 7

EXPLORATORY STUDIES

In this chapter we shall present the results of some of the preliminary studies which have been performed over the past few years. These studies are by no means intended to be complete investigations. Rather, they were performed in order to shed light on some of the studies presented previously or exploratory studies used to determine the spectral regions of interest and to assess the necessary conditions which will be needed to further study these molecules. These preliminary studies were performed on vinyl bromide, 1,2 dibromoethylene, iron pentacarbonyl, cyclopropane, and methyl radical. The results of these studies will be presented in the following sections on a molecule-by-molecule basis.

a) Vinyl bromide

At first glance, the energy-loss spectrum of vinyl bromide (figure 1) appears to be very similar to the energy-loss spectrum of vinyl chloride (chapter 5, figure 5). The first observed transition in vinyl bromide occurs as a broad band extending from 3.4 eV to 4.9 eV with its minimum at 4.05 eV. This band is assigned to the $\pi \rightarrow \pi^*$, $N \rightarrow T$, singlet \rightarrow triplet transition. This assignment is supported by observed enhancement of the relative intensity of this transition on going from a 20° scattering angle to a 50° scattering angle (figure 1). The next observed transition is assigned to the $\pi \rightarrow \pi^*$, $N \rightarrow V$ excitation with its maximum at 6.47 eV. One does notice that on comparison with the corresponding chloroethylenes, the bromoethylenes exhibit a much more intense shoulder on the low energy side of the $N \rightarrow V$ peak. These may be due to transitions involving σ^* orbitals. The remainder of the spectrum consists mostly of $\pi \rightarrow nL$ and $Br\ 4p \rightarrow nL$ Rydberg series converging on the various IP's of the molecule.

There is, however, a transition observed at 7.42 eV which has been assigned by Schander and Russell¹ to an $n \rightarrow \pi^*$ -type excitation. The results of the present study are listed in table 1 along with the tentative assignments of these transitions.

b) 1,2-Dibromoethylene

Figure 3 shows the energy-loss spectrum of a mixture of cis- and trans-1,2-dibromoethylene from 4.5 eV to 11.5 eV. In very general appearance the spectrum resembles those obtained optically.¹⁻³ Since a mixture of isomers was used, no specific assignments can be made. However, as seen in figure 4, one observes a transition extending from approximately 3.2 eV to 4.6 eV with a maximum around 3.8 eV which increases in relative intensity to the $\pi \rightarrow \pi^*$, $N \rightarrow V$ excitation as the scattering angle is increased from 10° to 40°. This behavior indicates that this is the $\pi \rightarrow \pi^*$, $N \rightarrow T$ excitation.

c) Iron pentacarbonyl

The spectrum of iron pentacarbonyl was measured to compare with those of the group VIb transition metal hexacarbonyls. At first glance the spectra look surprisingly similar, even though the iron is pentacoordinated, not hexacoordinated. Figure 5 shows the energy-loss spectrum of iron pentacarbonyl, taken at incident energy, $E_0 = 50$ eV and 0° scattering angle. Table 2 lists the observed transitions along with the previous work on this compound. Not many studies of the ultraviolet-visible spectroscopy of this compound exist, especially in the gas phase. Eyber⁷ first reported the absorption spectrum of this compound in 1929 but all that was observed was continuous absorption in the wavelength region he studied. Lundquist and Cais⁸ and Dartiguenae et al.⁹ have reported solution spectra for iron pentacarbonyl. The results they obtained are also

listed in Table 2.

In our work we observe two low-energy features at 3.35 eV and 3.62 eV which are not observed in the optical spectra. Impurities cannot be ruled out nor can the possibility that these are forbidden transitions. More work is needed on the energy and angle dependence of these features to verify their nature.

d) Cyclopropane

Cyclopropane is of great experimental and theoretical interest in that it is the smallest alkane ring system. The strained ring structure of cyclopropane causes it to possess a reactivity which more closely resembles an olefinic system than an alkane.¹¹ The spectroscopy of cyclopropane is not well understood. To complicate matters, the E' excited state of cyclopropane is Jahn-Teller split¹² into two components as is the lowest ionic state. Figure 6 shows the electron impact spectrum of cyclopropane at an incident energy of 50 eV and 10° in the 2 eV to 12 eV energy-loss region. The observed transitions and assignments are listed in table 3 along with the previous work on this molecule. Figure 7 compares the energy-loss region from 2.5 eV to 7.5 eV for incident energy and scattering angles of 50 eV and 10° to 25 eV and 60°. The triplet state observed by Brongersma¹³ at 5.9 eV was not observed in the present study; however, the low-energy side of the band at 6.80 eV and the spectral region from 8.0 to 9.5 eV do show some enhancement on going from 50 eV and 10° to 25 eV and 60°. Several triplet states are theoretically predicted to lie in these regions.^{14,15} So it is quite possible that the observed changes are due to one or more of these triplet states. In any case, more detailed study is required before a certain assignment of such states is possible.

e) Methyl radical

In figures 8a and 8b are shown two electron impact spectra taken at $E_0 = 100$ eV, $\Theta = 0^\circ$ between 4.5 and 9.5 eV energy-loss. Spectrum 8a is the spectrum of tetramethyl tin obtained using the pyrolysis source with no heating applied. Tetramethyl tin (TMT) was chosen as the methyl precursor due to the production of four methyl radicals for each molecule pyrolyzed.²⁵ The resultant pyrolysis spectrum should then consist of precursor (TMT), atomic tin, and methyl radical. Figure 8b shows the spectrum when the source was heated to approximately 800° C. Immediately apparent are the sharp transitions located at 5.70, 6.72, and 8.30 eV. The 5.70 eV transition correlates well with the value of 5.73 obtained by Herzberg and is assigned to the $A_2'' \rightarrow 3s$ excitation.²⁶ The 8.30 eV transition, which has been observed by Herzberg at 8.28 eV, is assigned to a $A'' \rightarrow 3d$ transition. The 6.72 eV peak is most likely due to atomic tin absorption since it is located within the metal absorption bands of the precursor molecule.

From 8 to 14 eV (figure 9) there occur a large number of relatively sharp bands superimposed on the broad, continuous bands of TMT. This structure is due to higher members of the Rydberg series converging on the first ionization potential (IP) at 9.85 eV²⁷ plus other Rydberg transitions converging to higher IP's. In addition, a number of these transitions may be due to atomic tin excitations. Further study is needed to ascertain the exact nature of these bands.

Also of interest is the shoulder extending from 4.9 to 5.75 eV. This shoulder is not present in the absence of heating (figure 8a). At first this was thought to be a band of ethane formed by methyl radical recombination but the first absorption in ethane occurs above 8 eV²⁸. Theoretically,

the first valence transition, $A_2'' \rightarrow 1E''$, has been predicted to occur at about 7.4 \rightarrow 7.6 eV.^{29,30} This transition is forbidden by symmetry in the planar configuration of the ground state and unfavorable Franck-Condon factors would preclude strong absorption into the pyramidal configuration of the valence excited state.²⁹ Unless these calculations give valence state energies which are about 1 eV too high, it is doubtful that this shoulder would correspond to the transition to this state. A study of the behavior of this shoulder relative to the 3s band as a function of angle would show if indeed this shoulder were due to a symmetry-forbidden state. It is also possible that this shoulder is due to incompletely dissociated TMT.

Operation of the source with TMT was limited to about five hours due to the beam capillary becoming obstructed by metallic tin. To the best of our knowledge this is the first electron-impact spectrum of a polyatomic free radical.

References

- 1) J. Schander and B. R. Russell, J. Amer. Chem. Soc. **98**, 6900 (1976).
- 2) W. S. Felps, K. Wittel, and S. P. McGlynn, J. Molec. Spect. **71**, 101 (1978).
- 3) K. Wittel, W. S. Felps, K. Klasinc, and S. P. McGlynn, J. Chem. Phys. **65**, 2698 (1976).
- 4) W. Von Niessen, L. Åsbrink, and G. Bieri, J. Elect. Spect. and Relat. Phenom. **26**, 173 (1982).
- 5) D. Chadwick, D. C. Frost, A. Katrib, C. A. McDowell and R. A. N. McLean, Can. J. Chem. **50**, 2642 (1972).
- 6) K. Wittel and H. Bock, Chem. Ber. **107**, 317 (1974).
- 7) G. Eyber, Z. Physik Chem. **144**, 1 (1929).
- 8) M. Dartiguenave, Y. Dartiguenave, and H. B. Gray, Bull. Chim. Soc. Fra. **12**, 4223 (1969).
- 9) R. T. Lundquist and M. Cais, J. Org. Chem. **27**, 1167 (1962).
- 10) D. R. Lloyd and E. W. Schlag, Inorg. Chem. **8**, 2544 (1969).
- 11) A. de Meigere, Angew. Chem. **18**, 809 (1979).
- 12) M. B. Robin, *Higher Excited States of Polyatomic Molecules*, vol. 1 (Academic Press, 1974) pp. 140-148.
- 13) H. H. Brongersma and L. J. Oosterhoff, Chem. Phys. Lett. **3**, 437 (1969).
- 14) D. T. Clark, Theor. Chim. Acta **10**, 111 (1968).
- 15) B. Tinland, J. Molec. Struct. **8**, 333 (1971).
- 16) P. Wagner and A. B. F. Duncan, J. Chem. Phys. **21**, 516 (1953).

- 17) J. W. Raymonda and W. T. Simpson, *J. Chem. Phys.* **47**, 430 (1967).
- 18) C. Fridh, *J. Chem. Soc. Farad. Disc.* **2 75**, 993 (1979).
- 19) H. Basch, M. B. Robin, N. A. Kuebler, C. Baker, and D. W. Turner, *J. Chem. Phys.* **51**, 52 (1969).
- 20) R. I. Schoen, *J. Chem. Phys.* **37** 2032 (1962).
- 21) M. B. Robin and N. A. Kuebler, *J. Chem. Phys.* **69**, 86 (1978).
- 22) A. Y. Meyer and R. Pasterak, *Theor. Chim. Acta* **45**, 45 (1977).
- 23) N. Ohmicki, A. Tajiri, and T. Nakajima, *Bull. Chem. Soc. Jap.* **45**, 3028 (1972).
- 24) G. Bieri, F. Burger, E. Heilbronner, and J. P. Maier, *Helv. Chim. Acta* **60**, 2213 (1977).
- 25) I. S. Zaslanko and V. N. Smirnov, *Kinet. i Kataliz* **20**, 575 (1979) (eng. trans.)
- 26) G. Herzberg, *Proc. Roy. Soc. (Lon)* **A262**, 291 (1961).
- 27) F. A. Houle and J. L. Beauchamp, *J. Amer. Chem. Soc.* **101**, 4067 (1979).
- 28) Ref. 12 pp. 120.
- 29) R. McDiarmid, *Theoret. Chem. Acta* **20**, 282 (1971).
- 30) B. H. Lengsfeld, P. E. M. Siegbahn, and B. Liu, *J. Chem. Phys.* **81**, 710 (1984).

Table 1. Vinyl Bromide

Transition Energy/eV		
Assignment	Present Results	Previous Work
$\pi \rightarrow \pi^*$, N \rightarrow T	4.05 (3.4-4.9) ^a	
	5.76	
	5.86	
	5.94	
	6.03	
$\pi \rightarrow \pi^*$, N \rightarrow V	6.47	6.47 ^b
$\pi \rightarrow 3s_1$ ^c	6.68	6.79 ^b
$\pi \rightarrow 3s_1 + 2\nu_1$	7.08 sh	
n $\rightarrow \pi^*$	7.42	7.39 ^b
n $\rightarrow \pi^* + \nu_2$	7.50 sh	
Br4p \rightarrow 5s ₂	7.75	7.78 ^b
	7.90	
	8.12 sh	
$\pi \rightarrow 4s_1$	8.43	8.40 ^b
Br4p \rightarrow 5p ₂	8.65	8.66 ^b
$\pi \rightarrow 4p_1$	8.76	8.75 ^b
$\pi \rightarrow 5s_1$	9.10	9.07 ^b
Br4p \rightarrow 5d ₂	9.28	9.26 ^b
$\pi \rightarrow 6p_1$, Br4p \rightarrow 6s ₂	9.41	9.43, ^b 9.42 ^b
$\pi \rightarrow 8s_1$	9.55	9.53 ^b
Br4p \rightarrow 6p ₂	9.81	9.77 ^b
IP1		9.9 (9.83) ^{d,e} 9.8, ^f 9.87 ^g

Transition Energy/eV		
Assignment	Present Results	Previous Work
Br4p → 6d ₂	9.98	10.00 ^b
Br4p → 7s ₂	10.10	10.06 ^b
Br4p → 9s ₂ , Br4p → 8d ₂	10.50	10.52 ^b , 10.50 ^b
Br4p → 10s ₂	10.64	10.62 ^b
	10.83	
IP2		10.9 ^{d,f} , 10.87 ^g
	11.35	
	11.55	
	11.70	
IP3		12.3 ^d , 12.28 ^f , 12.30 ^g

^a Uncertainty ±.1 eV for this band, ±.05 for all other bands. Extent of Franck-Condon envelope indicated by numbers in parentheses.

^b Ref. 1.

^c Subscript denotes IP to which Rydberg series is converging, i.e., 1 = first IP, etc.

^d Ref. 4.

^e Vertical IP's (adiabatic in parentheses)

^f Ref. 5.

^g Ref. 6.

Table 2. Iron Pentacarbonyl

Transition Energy/eV		
Assignment ^a	Present Results	Previous Work
	3.35 sh ^{b,c}	
	3.62 sh	
5e' → 5a ₁ '	4.40 sh	4.40 ^d , 4.39 ^e
5e' → 2a ₂ ', 5e' → be'	4.95	5.15 ^d , 5.06 ^e
5e' → 4e'', 3e'' → 6e', 3e'' → 4a ₂ '', 5e' → 7e', 3e'' → 4e'', 5e' → 5e'', 3e'' → 7e'	6.18	6.19 ^d
	7.22	
IP1		8.60 ^{f,g}
SES	8.77	
SES	9.63	
SES	10.24	
SES	11.46	
SES	11.78	

^a Assignments after ref. 8.

^b Uncertainties ±.05 eV for these transitions.

^c sh indicates shoulder.

^d Ref. 8.

^e Ref. 9.

^f Ref. 10.

^g Vertical IP.

Table 3. Cyclopropane

Transition Energy/eV		
Assignment ^a	Present Results	Previous Work
3e' → 3s	6.80 ^{b,c} sh	6.79 ^d , 6.53 ^j , 6.76 ^l 6.93 [?]
3e' → 3p	7.92	7.78 ^d , 7.80 ^{e,f} , 7.81 ^g 7.4 ^k , 7.77 ^m
3e' → 3p	8.72	8.56 ^d , 8.60 ^{e,f} , 8.67 ^{g,k} 8.87 ^l , 8.48 ^m
3e' → 1a ₂ '	10.18	10.32 ^d , 10.2 ^f , 10.29 ^g 10.1 ^{h,i} , 9.05 ^k , 9.73 ^l 9.72 [?]
IP1		10.6 ^{n,o}
SES	13.35	13.5 ^h , 13.0 ^f

^a Assignments after ref. 12.

^b Uncertainties ±.05 eV for these transitions.

^c sh indicates shoulder.

^d Ref. 16.

^e Ref. 17.

^f Ref. 18.

^g Ref. 19.

^h Ref. 20.

ⁱ Ref. 13.

^j Ref. 21.

- k Ref. 22.
- l Ref. 23.
- m Ref. 24.
- n Ref. 25.
- o Vertical IP.

Figure Captions

- Figure 1. Energy-loss spectrum of vinyl bromide between 5 and 11 eV with $E_0 = 50$ eV, $\Theta = 20^\circ$.
- Figure 2. Low angle (20°) and high angle (50°) spectra of vinyl bromide between 2.5 and 7.5 eV energy-loss.
- Figure 3. Energy-loss spectrum of 1,2 dibromoethylene between 4.5 and 11.5 eV with $E_0 = 50$ eV, $\Theta = 10^\circ$.
- Figure 4. Low angle (10°) and high angle (40°) spectra of 1,2 dibromoethylene between 2.5 and 7.5 eV energy-loss.
- Figure 5. Energy-loss spectrum of iron pentacarbonyl between 2 and 12 eV with $E_0 = 50$ eV, $\Theta = 0^\circ$.
- Figure 6. Energy-loss spectrum of cyclopropane between 6 and 19 eV with $E_0 = 50$ eV, $\Theta = 10^\circ$.
- Figure 7. Low angle, high energy ($10^\circ - 50$ eV) and high angle, low energy ($60^\circ - 25$ eV) spectra of cyclopropane between 6.5 and 10 eV energy loss.
- Figure 8. Energy-loss spectrum of tetramethyl tin with a) pyrolysis source off, b) pyrolysis source on, $T = 800^\circ$ C. For both spectra $E_0 = 100$ eV, $\Theta = 0^\circ$.
- Figure 9. Energy-loss spectrum of tetramethyl tin with the pyrolysis source at 800° C. $E_0 = 100$ eV and $\Theta = 0^\circ$ in the energy-loss region of 8 to 14 eV.

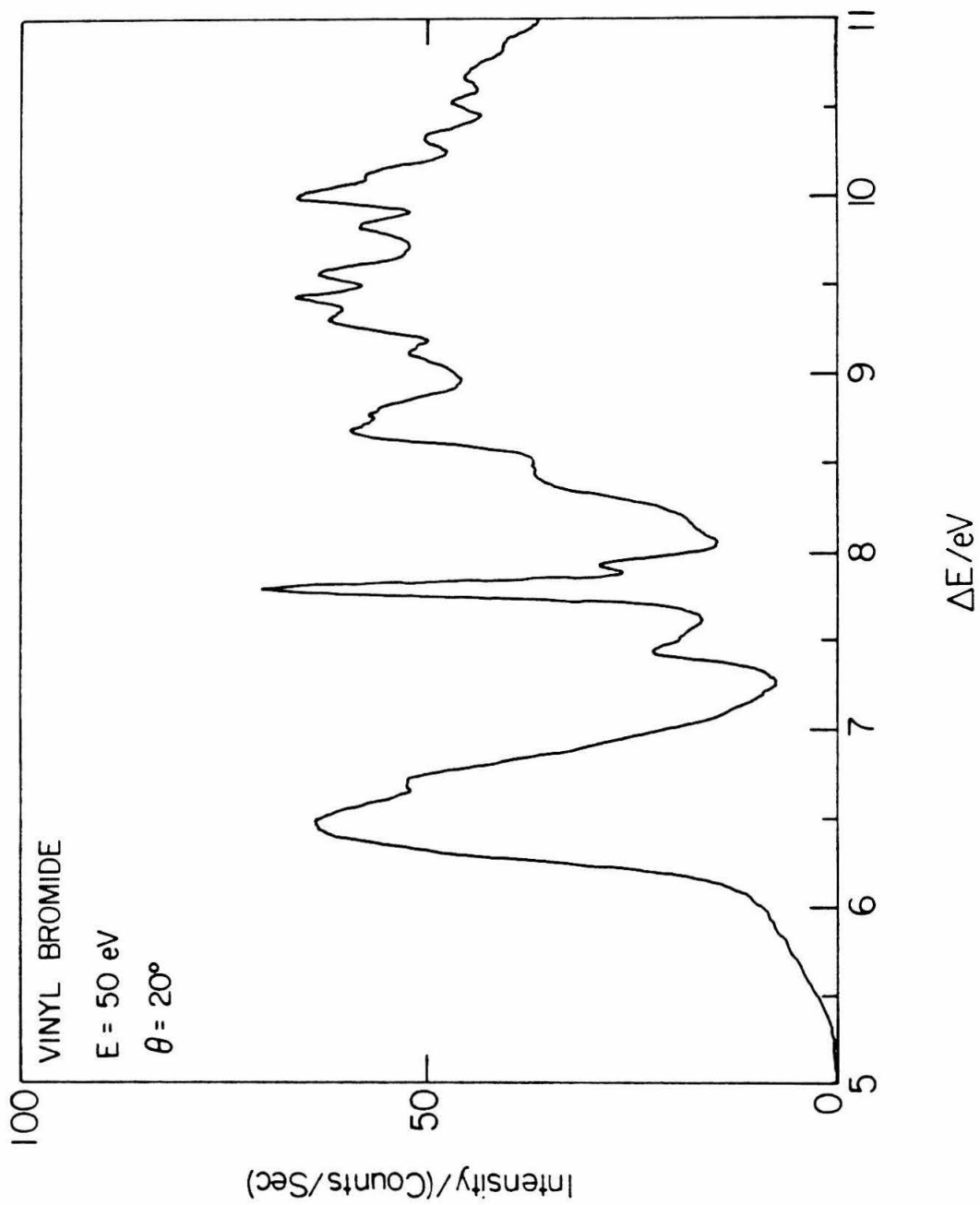


Figure 1.

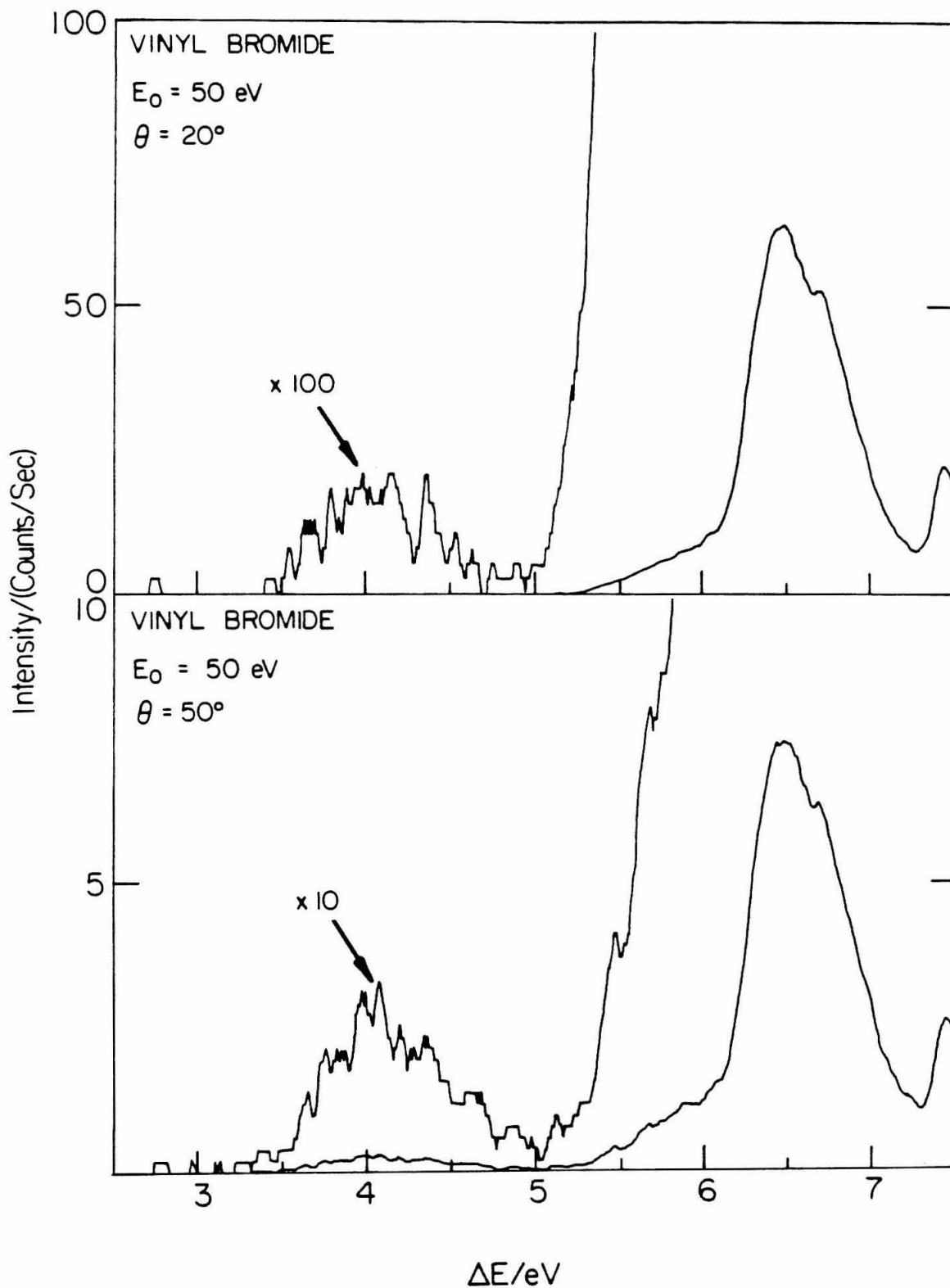


Figure 2.

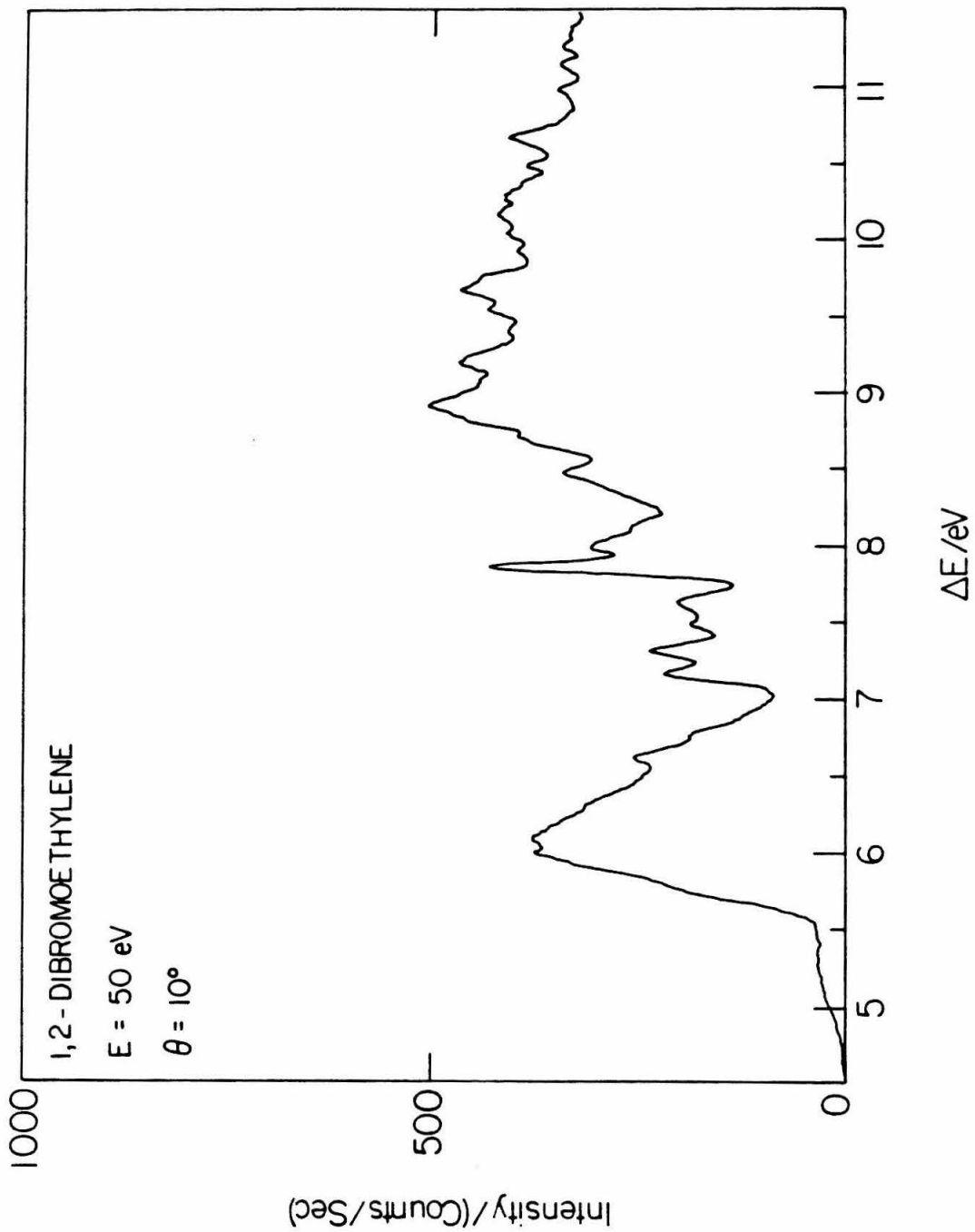


Figure 3.

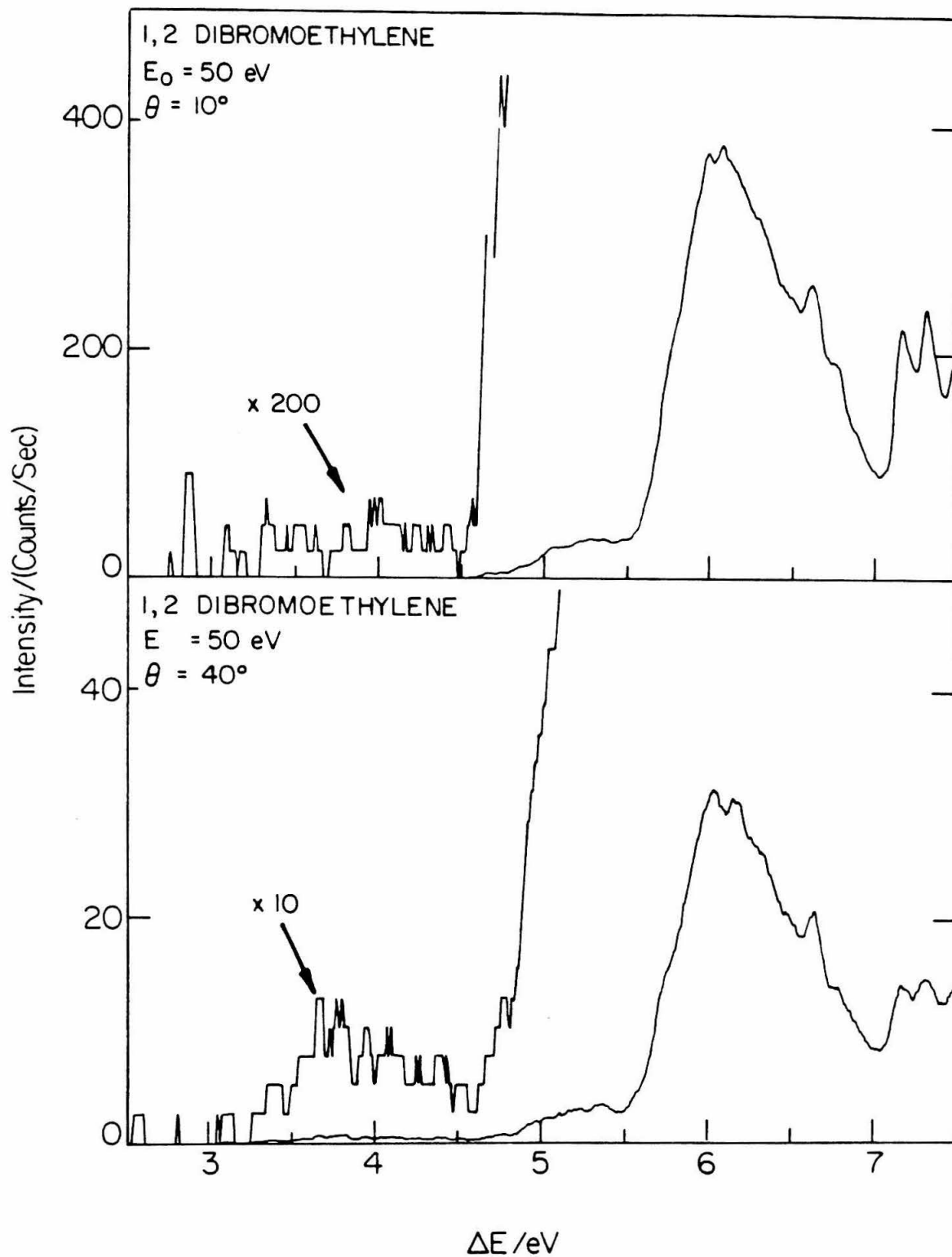


Figure 4.

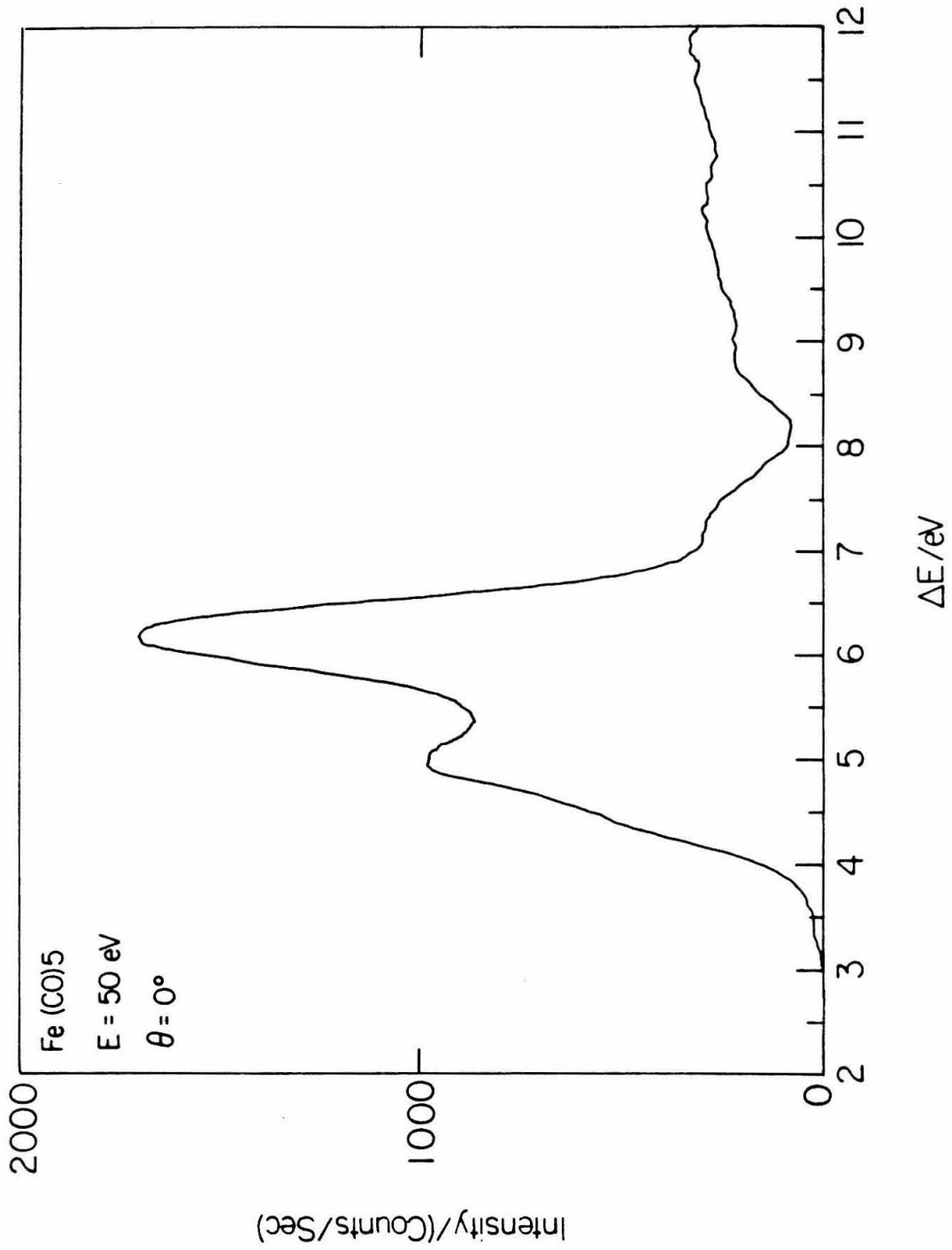


Figure 5.

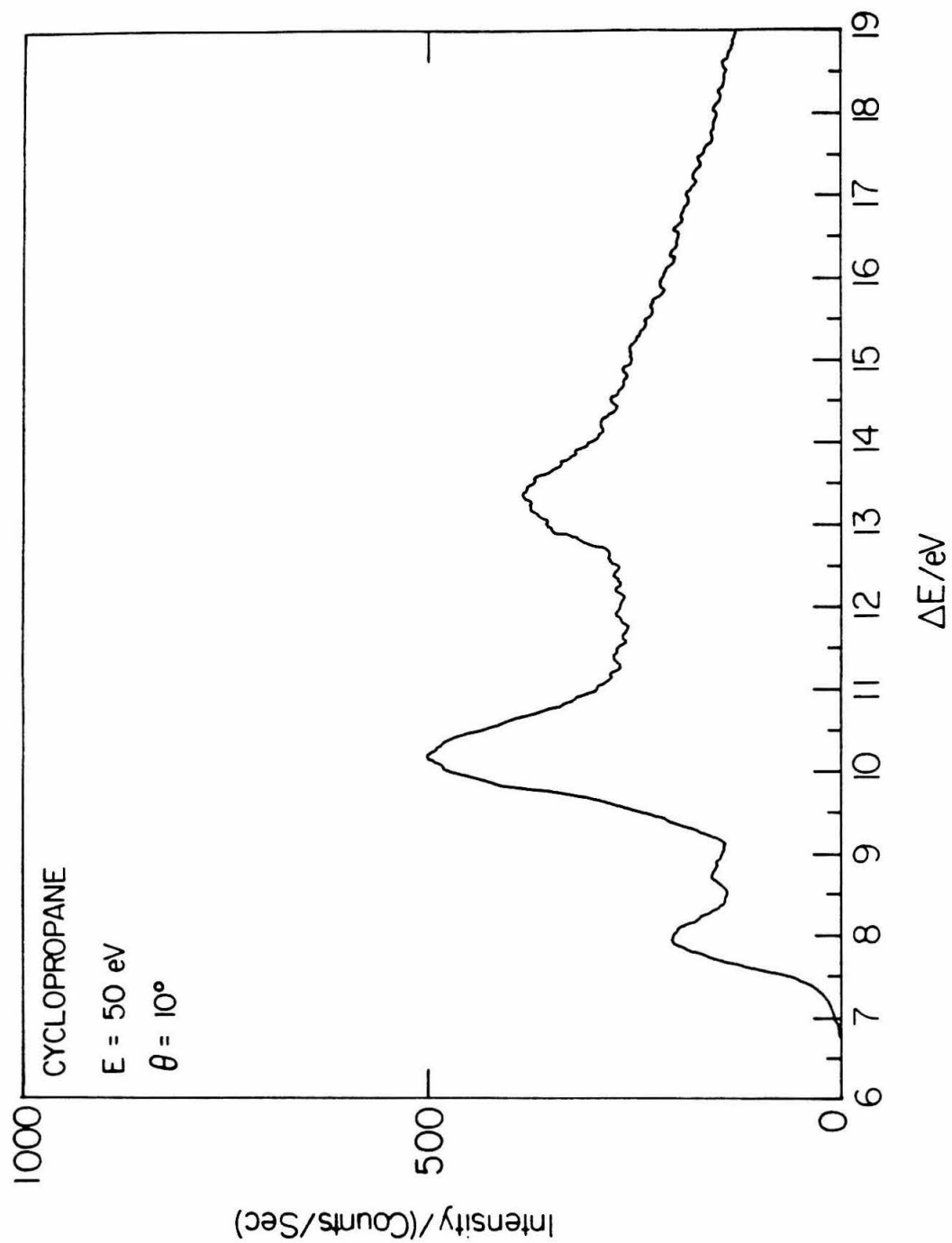


Figure 6.

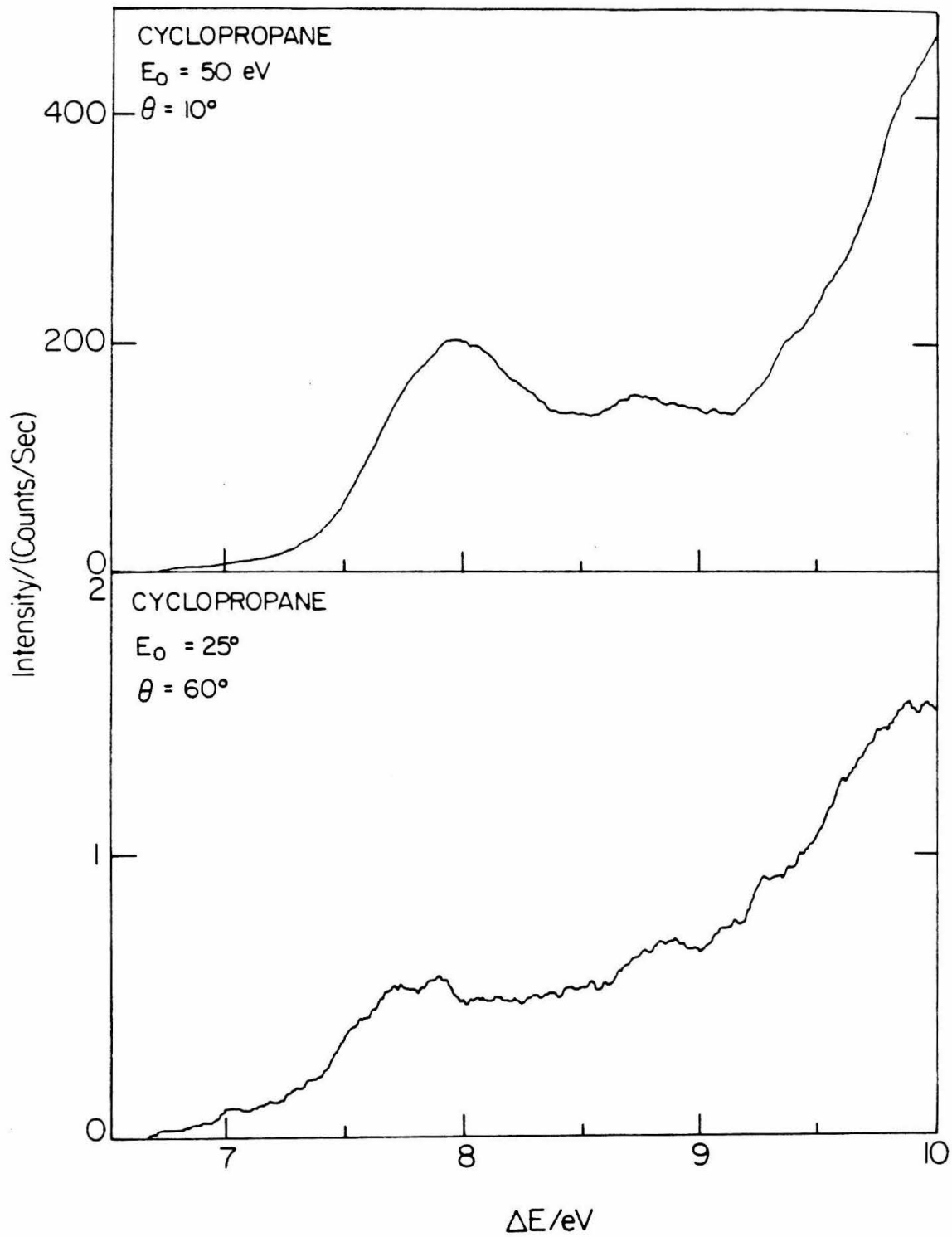


Figure 7.

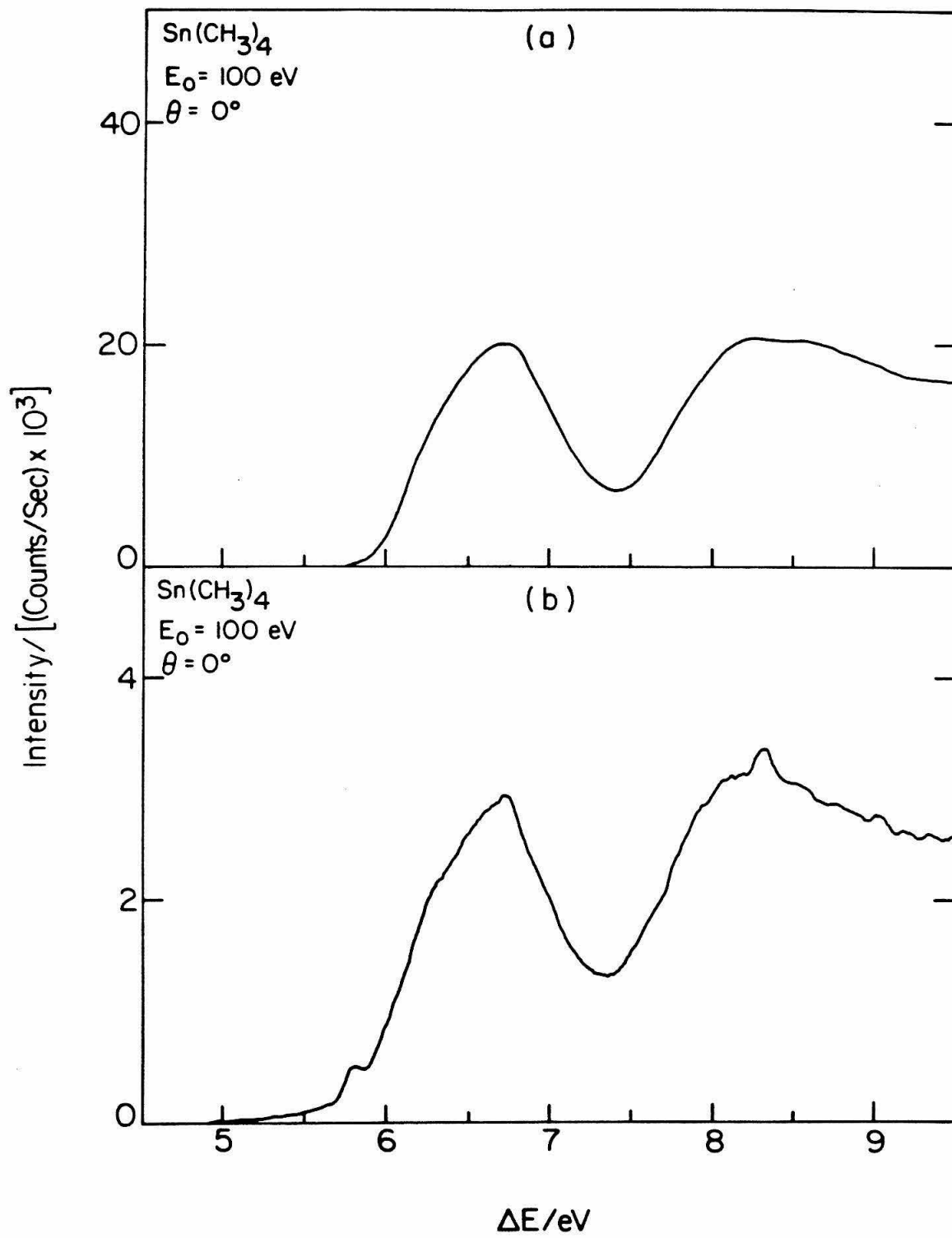


Figure 8.

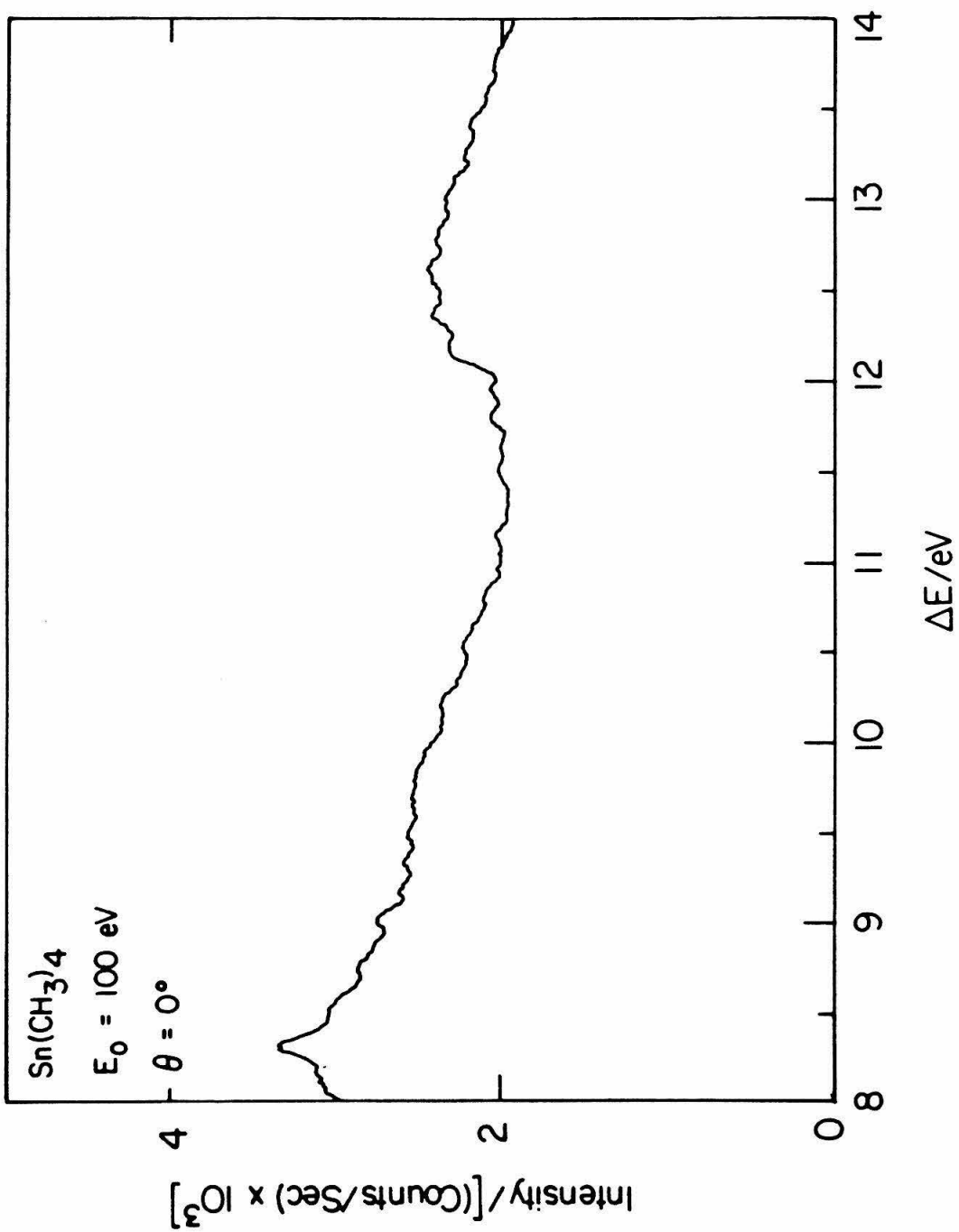


Figure 9.

CHAPTER 8

INTRODUCTION TO VARIABLE-ANGLE PHOTOELECTRON SPECTROSCOPY

In this section of the thesis (chapters 8 - 11) is introduced the technique of variable-angle ultraviolet photoelectron spectroscopy. Since its development in the early 1960's,^{1,2} photoelectron spectroscopy has been extensively used to study the electronic structure of both molecules and ions. As pointed out in the first chapter of this thesis, photoelectron spectroscopy and electron-impact spectroscopy provide mutually complementary information and as a result photoelectron spectroscopic data has found wide application in many of the same areas as electron-impact measurements.

As was the case with electron-impact spectroscopy, photoelectron spectroscopy has had a long history. Einstein³ won the Nobel prize for his work on the photoelectric effect during the early part of this century. His work was one of the cornerstones in the development of quantum theory. The relation he obtained from his work is given in equation 1,

$$E_{\text{elec}} = h\nu - IP \quad (1)$$

where E_{elec} is the kinetic energy the electron carries from the photoionization event. This expression provides the basis for the interpretation of the photoelectron spectrum.

Photoelectron spectroscopy may be performed on a wide range of targets. Typically the target consists of a gas-phase atom or molecule but it may be a solid, adsorbate on a surface, or a liquid. In this work we will be dealing exclusively with gas-phase targets.

The radiation sources for these experiments can be vacuum ultraviolet rare gas resonance lamps,⁴ synchrotron radiation,^{5,6} or lasers.⁷⁻⁹

In this set of experiments we will make exclusive use of helium resonance radiation ($h\nu = 21.22\text{eV}$). Photoionization in this energy regime probes the valence states of the molecule as opposed to the use of x-ray radiation which is generally used to examine the atomic core states. It is the valence region of the spectrum which is important in our experiment since the characteristics of the valence orbitals determine most of the chemical properties of the molecule. Orbital energies can be obtained from this experiment by the use of Koopmans' theorem¹⁰ which states that the ionization potential of the orbital is simply the negative of the orbital energy. This theorem assumes that electronic rearrangement in the ion is a slow process compared to photoionization; it has been found that in a large majority of cases this is a reasonable approximation.

Determination of the orbital energies from the photoelectron spectrum would therefore seem to be a trivial task but in practice this is not always so. Many organic compounds have photoelectron spectra in which the bands are strongly overlapped and the question arises of which band corresponds to what orbital. Methods of determining the orbitals responsible for bands in the photoelectron spectrum have included isotopic substitution, vibrational analysis, and the use of different photon energies. In many cases these techniques have aided in assigning the photoelectron spectrum but almost all dictate that one has a fairly detailed theoretical understanding of structure of the system under study. The method of variable-angle photoelectron spectroscopy has provided an additional tool for the deciphering of the PES spectrum which in many cases can be used to determine the origin of the photoelectron band without requiring such a detailed knowledge of the structure of the molecule.

It has been realized for a long time that the angular distributions of

photoelectrons from hydrogenic atoms¹¹ have the form,

$$I(\theta) = a + b \cos^2\theta \quad (2)$$

where θ is the angle between the incoming photon beam or polarization vector of the photons and the direction in which the electron is ejected. This formula was later shown to be valid for cases of more complex atomic and molecular photoionization.¹²⁻¹⁴ It will be shown in chapter 9 that the shape of the angular distribution depends on the nature of the orbital from which the electron was ejected. This in principle allows one to distinguish between types of atomic orbitals such as s, p, and d. In cases of molecular photoionization, these orbitals are no longer purely atomic in character. Thus one expects the angular distribution information to be somewhat scrambled. However, it has been experimentally verified that some of these orbital distinctions, such as between σ and π , hold true even for molecules.¹⁵⁻¹⁸ By making use of this property of the angular distributions one has a powerful tool for making orbital assignments. Determination of β not only provides information concerning the spectroscopy of the target but it also contains a good deal of dynamical information as well. The asymmetry parameter is very sensitive to dynamical phenomena such as autoionization and shape resonances.¹⁹

The first experimental work on the angular distribution of photoelectrons was performed by Chaffee in 1931.²⁰ He used a polarized ultraviolet light source to ionize a beam of potassium atoms. By varying the polarization of his light source he was able to verify the $\cos^2\theta$ dependence in the angular distributions of the ejected electrons. Little else was done in this field until Berkowitz and Erhardt²¹ studied the angular distributions of photoelectrons from rare gas photoionization using a sections grid type of analyzer. A little later Vroom et al.²² employed a single, movable

detector, as is done in this experiment, to study angular distributions.

In chapter 9 of this thesis is outlined the theoretical origin of the form of the angular distributions and in chapter 10 the instrumentation used to perform such experiments is described. Chapter 11 concerns the application of this technique to the study of the electronic structure of a series of three-membered ring heterocyclic compounds.

For further information on the techniques and applications of photoelectron spectroscopy one is referred to a few of a number of books on the subject.^{6,23-26}

References

- 1) D. W. Turner and M. I. Al-Jobuoury, *J. Chem. Phys.* **37**, 3007 (1962).
- 2) F. I. Vilesov, B. C. Kurbatov, and A. N. Terenin, *Dokl. Akad. Nauk. SSR.* **138**, 1329 (1961).
- 3) A. Einstein, *Amer. J. Phys.* trans. by A. Arons and M. Peppard **33**, 367 (1965).
- 4) J. A. R. Samson *Techniques of Vacuum Ultraviolet Spectroscopy*, (John Wiley & Sons, New York 1967) pp. 129-175.
- 5) *Topics in Current Physics: Synchrotron Radiation, Techniques and Applications*, edited by C. Kunz (Springer-Verlag, Berlin 1979).
- 6) J. Berkowitz, *Photoabsorption, Photoionization, and Photoelectron Spectroscopy* (Academic Press, New York 1979) pp. 414-425.
- 7) J. C. Miller and R. N. Compton, *Chem. Phys. Lett.* **93**, 453 (1982).
- 8) S. L. Anderson, G. D. Kubiak, and R. N. Zare, *Chem. Phys. Lett.* **105**, 22 (1984).
- 9) S. T. Pratt, P. M. Dehmer, and J. L. Dehmer, *Chem. Phys. Lett.* **105**, 28 (1984).
- 10) T. Koopmans, *Physica* **1**, 104 (1933).
- 11) H. A. Bethe in *Handbuch der Physik* vol. 24 (Springer-Verlag, Berlin 1933) pp. 483-484
- 12) J. A. Tully, R. Berry, and B. Dalton, *Phys. Rev.* **176**, 95 (1968).
- 13) J. Cooper and R. N. Zare in *Lectures in Theoretical Physics* edited by S. Geltman, K. Mahanthappa, and N. Britten (Gordon and Breach, New York 1969) p. 317

- 14) A. Buckingham, B. Orr, and J. Sichel, *Phil. Trans. Roy. Soc. (Lond.) A*, **268**, 147 (1970).
- 15) R. M. White,, T. A. Carlson, and D. P. Spear, *J. Elect. Spect.* **3**, 59 (1974).
- 16) D. Mehaffy, P. R. Keller, J. W. Taylor, T. A. Carlson, M. O. Krauss, F. A. Grimm, and J. D. Allen Jr., *J. Elect. Spec.* **26**, 213 (1982).
- 17) J. A. Sell and A. Kuppermann, *Chem. Phys.* **33**, 367 (1978).
- 18) J. A. Sell, D. M. Mintz, and A. Kuppermann, *Chem. Phys. Lett.* **58**, 601 (1978).
- 19) J. L. Dehmer, D. Dill, and A. C. Parr in *Photophysics and Photochemistry in the Vacuum Ultraviolet* edited by S. P. McGlynn, G. Findley, and R. Huebner (D. Reidal. Pub. Co., Dordecht, Holland 1983).
- 20) M. A. Chaffee, *Phys. Rev.* **37**, 1233 (1933).
- 21) J. Berkowitz and H. Erhardt, *Phys. Lett.* **21**, 531 (1966).
- 22) D. A. Vroom, A. Comeax, and A. McGowan, *Chem. Phys. Lett.* **3**, 476 (1969).
- 23) D. W. Turner, C. Baker, A. D. Baker, and C. R. Brundle, *Molecular Photoelectron Spectroscopy* (Wiley-Interscience, New York 1970).
- 24) J. W. Rabalais, *Principles of Ultraviolet Photoelectron Spectroscopy* (Wiley-Interscience, New York 1976).
- 25) J. H. D. Eland, *Photoelectron Spectroscopy* (John Wiley & Sons, New York 1974).
- 26) T. A. Carlson, *Photoelectron and Auger Spectroscopy* (Plenum Press, New York 1975).

CHAPTER 9

THEORY OF PHOTOELECTRON ANGULAR DISTRIBUTIONS

As with electron-impact in chapter 3, no attempt shall be made to present a detailed derivation of the theory of angular distributions in photoelectron spectroscopy. All that will be attempted is to show the origin of the general form of the angular distributions. We begin by describing the photoionization process in the context of the semi-classical treatment of the interaction of a radiation field with a particle.^{1,2} In this formalism the radiation field will be treated classically and the motion of the particle will be described quantum mechanically. This theory is valid for absorption and induced emission processes but is not valid for spontaneous emission where one must rely on quantum field theory for a satisfactory treatment.

We begin with the Schrödinger equation for a particle of mass m and charge q in an electromagnetic field which is described by a vector potential, \mathbf{A} and a scalar potential, φ .³

$$i\hbar \frac{\partial \psi}{\partial t} = \left[-\frac{\hbar^2}{2m} \nabla^2 + \frac{ie\hbar}{mc} \mathbf{A} \cdot \nabla + \frac{ie\hbar}{2mc} \nabla \cdot \mathbf{A} + \frac{e^2}{2mc^2} \mathbf{A}^2 + e\varphi + V(\mathbf{r}) \right] \psi \quad (1)$$

Having the quantum mechanical equation of motion for the particle, we now turn our attention to the form of the vector potential, \mathbf{A} . From the motion of a charged particle in an electromagnetic field, we can define the electric and magnetic field strengths in terms of the potentials, \mathbf{A} , and φ .⁴

$$\mathbf{E} = -\frac{1}{c} \frac{\partial \mathbf{A}}{\partial t} - \nabla \varphi \quad (2)$$

$$\mathbf{H} = \nabla \times \mathbf{A} \quad (3)$$

By choosing the proper gage transformation so that

$$\varphi = 0 \quad (4)$$

$$\nabla \cdot \mathbf{A} = 0 \quad (5)$$

and then substituting the definitions of \mathbf{E} and \mathbf{H} into Maxwell's equations we arrive at the wave equation for the vector potential, \mathbf{A}

$$\nabla^2 \mathbf{A} - \frac{1}{c} \frac{\partial^2 \mathbf{A}}{\partial t^2} = 0 \quad (6)$$

The solution to this equation has the form,³

$$\mathbf{A} = \mathbf{A}_0 \exp^{i(\mathbf{k} \cdot \mathbf{r} - \omega t)} + \mathbf{A}_0 \exp^{-i(\mathbf{k} \cdot \mathbf{r} - \omega t)} \quad (7)$$

where \mathbf{A}_0 is a complex vector which contains the information describing the intensity and polarization of the light wave and is defined as

$$\mathbf{A}_0 = |\mathbf{A}_0| e^{i\theta} \quad (8)$$

and \mathbf{k} is its propagation vector with \mathbf{r} being the position coordinate on which \mathbf{A} depends. We can now relate \mathbf{A}_0 to the intensity, I , of the incident radiation which turns out to be the Poynting vector averaged over a time $2\pi/\omega$ of the oscillation,³

$$\frac{c}{4\pi} (\mathbf{E} \times \mathbf{H}) = I = \frac{\omega^2}{2\pi c} |\mathbf{A}_0|^2 \quad (9)$$

where I is given in units of power per unit area and,

$$|\mathbf{A}_0|^2 = (\mathbf{A}_0 \cdot \mathbf{A}_0^*) \quad (10)$$

Bethe has specified the polarization of the light by realizing that \mathbf{A}_0 has a complex squared magnitude which is scalar with phase 2θ .⁵

$$\mathbf{A}_0 \cdot \mathbf{A}_0 = |\mathbf{A}_0 \cdot \mathbf{A}_0| e^{2i\theta} \quad (11)$$

He has used this relation to obtain a form of the vector potential which

explicitly includes the polarization information.⁵

$$\mathbf{A} = \mathbf{A}_0 \mathbf{P} \exp^{i(\mathbf{k} \cdot \mathbf{r} - \omega t + \theta)} + \mathbf{A}_0 \mathbf{P} \exp^{i(\mathbf{k} \cdot \mathbf{r} - \omega t + \theta)} \quad (12)$$

The first term in equation 12 represents absorption and the second term emission. Thus by realizing that photoelectron spectroscopy is an absorption process, we can write,

$$\mathbf{A} = \mathbf{A}_0 \mathbf{P} \exp^{i(\mathbf{k} \cdot \mathbf{r} - \omega t + \theta)} \quad (13)$$

We can also see that for \mathbf{A} to satisfy the relation $\nabla \cdot \mathbf{A} = 0$ and to be a solution of equation 6, the following relations must hold.

$$\mathbf{P} \cdot \mathbf{k} = 0 \quad (14)$$

$$\omega = kc \quad (15)$$

$$\mathbf{P} \cdot \mathbf{P} = \exp^{i2\theta} \quad (16)$$

where k is the magnitude of the propagation vector, \mathbf{k} , and θ is a real phase constant.

We can simplify the Hamiltonian in equation 1 by applying the results of the gauge transformation, i.e., $\nabla \cdot \mathbf{A} = 0$ and $\varphi = 0$ and by noting that the ratio of the fourth term to the second term is on the order of $e\mathbf{A}/cp$, where p is the momentum of the particle. This ratio is vanishingly small for the weak vector potentials and one electron excitation processes normally encountered in valence photoelectron spectroscopy and thus the dropping of the fourth term is justified. This leaves us with the final form of the Hamiltonian,

$$H = -\frac{\hbar^2}{2m} \nabla^2 + \frac{ie\hbar}{mc} \mathbf{A} \cdot \nabla + V(\mathbf{r}) \quad (17)$$

If we consider the vector potential to be relatively weak, we may apply first order perturbation theory in order to solve the Schrödinger

equation. We may express the zeroth order or unperturbed Hamiltonian as

$$H_0 = -\frac{\hbar^2}{2m} + V(r) \quad (18)$$

with the perturbation given by

$$H_1 = \frac{ie\hbar}{mc} \mathbf{A} \cdot \nabla \quad (19)$$

with the total Hamiltonian being

$$H_T = H_0 + H_1 \quad (20)$$

We can express the time-dependent wave function of the unperturbed Hamiltonian, $\psi(\mathbf{r}, t)$, as a superposition of the unperturbed stationary states.

$$\psi(\mathbf{r}, t) = \sum_{\mathbf{k}} a_{\mathbf{k}}(t) \varphi_{\mathbf{k}}(\mathbf{r}) \quad (21)$$

where the coefficients of the expansion are functions of time and are given by the following relation,

$$a_{\mathbf{k}}(t) = C_{\mathbf{k}}(t) \exp^{-iE_{\mathbf{k}}t/\hbar} \quad (22)$$

so that the wave function becomes,

$$\psi(\mathbf{r}, t) = \sum_{\mathbf{k}} C_{\mathbf{k}}(t) \exp^{-iE_{\mathbf{k}}t/\hbar} \varphi_{\mathbf{k}}(\mathbf{r}) \quad (23)$$

Substitution of this wave function into the time-dependent Schrödinger equation yields,

$$i\hbar \sum_{\mathbf{k}} \frac{\partial}{\partial t} (C_{\mathbf{k}}(t) \varphi_{\mathbf{k}} \exp^{iE_{\mathbf{k}}t/\hbar}) = \sum_{\mathbf{k}} \exp^{-iE_{\mathbf{k}}t/\hbar} H_1 \varphi_{\mathbf{k}} \quad (24)$$

Multiplying this equation from the right by $\varphi_{\mathbf{n}}^*$ and integrating using the fact that $\varphi_{\mathbf{n}}^*$ was picked to be orthogonal to $\varphi_{\mathbf{k}}$, then rearranging keeping

only the terms in the sum on the left-hand side of equation 24, where $k = n$, we are left with,

$$\frac{dC_n}{dt} = \frac{-i}{\hbar} \sum_k C_k(t) \langle \varphi_n | H_1 | \varphi_k \rangle \exp^{i\omega_{nk}t} \quad (25)$$

where $\omega_{nk} = (E_n - E_k) / \hbar$

Now we must specify the initial conditions, in which $\psi(\mathbf{r}, t=0) = \varphi_m$. At $t = 0$, $C_m(t) = 1$, where $C_m(t)$ is the coefficient of the initial state and $C_n(t) = 0$. Realizing that our perturbation, H_1 , is small and as a consequence that $C_m(t) \cong 1$ and $C_n(t) < 1$, we can replace C_k by δ_{mk} and integrate from time $t = 0$ to $t = t$ which yields,

$$C_n(t) = \frac{-i}{\hbar} \int_0^t \langle n | H_1 | m \rangle \exp^{i\omega_{nm}t} dt \quad (26)$$

where $\langle n | = \varphi_n^*$ and $|m\rangle = \varphi_m$.

Substituting the expressions for H_1 and the vector potential, A , yields,

$$C_n(t) = \frac{-i}{\hbar} \int_0^t \langle n | H_1 | m \rangle \exp^{i\omega_{nm}t} \exp^{-i\omega t} dt \quad (27)$$

where

$$\langle n | H_1 | m \rangle = \frac{ie\hbar|A_0|}{mc} \int \varphi_n^* \exp^{-i(\mathbf{k}\cdot\mathbf{r})} \mathbf{P}\cdot\nabla\varphi_m d^3\mathbf{r} \quad (28)$$

Upon integration of equation 27 and realizing that the probability of a transition occurring is given by,

$$Prob. = C_n^*(t)C_n(t) \quad (29)$$

we obtain the probability per unit time.

$$W = Prob. / t = \frac{1}{\hbar^2} |\langle n | H_1 | m \rangle|^2 t \frac{(\sin^2 \frac{1}{2}(\omega_{nm} - \omega)t)}{((\omega_{nm} - \omega)t/2)^2} \quad (30)$$

This expression is the transition rate from a discrete initial to a discrete final state. In photoionization it is generally assumed that there are a continuum of final states. To determine the transition rate we must integrate the probability over a density of final states, $\rho(n)$,⁶

$$W = \int |\langle n | H_1 | m \rangle|^2 \frac{t}{\hbar^2} \frac{(\sin^2 \frac{1}{2}(\omega_{nm} - \omega)t)}{((\omega_{nm} - \omega)t/2)^2} \rho(n) dE_n \quad (31)$$

where $\rho(n)dE_n$ is the number of states with energies between E_n and $E_n + dE_n$. Recognizing that $\langle n | H_1 | m \rangle$ and $\rho(n)$ can be regarded as relatively independent of E_n such that they may be removed from the integral, we obtain upon change of variable and integration,

$$W = \frac{2\pi}{\hbar} \rho(n) |\langle n | H_1 | m \rangle|^2 \quad (32)$$

which is known as Fermi's golden rule.⁶

The density of the final states may be found from the allowed values of \mathbf{k} in a box such that,

$$k_x = \frac{2\pi n_x}{L}, k_y = \frac{2\pi n_y}{L}, k_z = \frac{2\pi n_z}{L} \quad (33)$$

Since the matrix element in equation 32 is directional dependent, we can thus define a group of states, k_i , each of which correspond to an infinitesimal range of direction in which the electron is ejected.⁷ Expressing this range in terms of spherical coordinates and using the fact that $E_k = \hbar^2 k^2 / 2m$, the following expression may be obtained,

$$\rho(n) = \frac{mL^3}{8\pi^3 \hbar^2} k \sin \theta d\theta d\varphi \quad (34)$$

Substituting the expressions for H_1 and for $\rho(n)$ into the rate equation (equation 32), leaves us with

$$W = \frac{L^3 k e^2 |A_0|^2}{4\hbar \pi^2 m c} |\langle n | \exp^{i(\mathbf{k}\cdot\mathbf{r})} \mathbf{P}\cdot\nabla | m \rangle|^2 d\Omega \quad (35)$$

where

$$d\Omega = \sin\theta d\theta d\varphi \quad (36)$$

and the final state wavefunction is considered to be box normalized to $L^{-3/2}$.

This rate equation can be converted into a differential cross section in terms of the solid angle $d\Omega$ by dividing the rate by the incident current density, which is just the intensity divided by the energy per photon. Remembering that the intensity was given earlier as the time averaged Poynting vector, we may express the incident current density, I_{inc} , given by,

$$I_{inc} = \frac{\omega |A_0|^2}{2\pi\hbar c} \quad (37)$$

The differential cross section then becomes,

$$\frac{d\sigma}{d\Omega} = \frac{L^3 k e^2}{2\pi m c} |\langle n | \exp^{i(\mathbf{k}\cdot\mathbf{r})} \mathbf{P}\cdot\nabla | m \rangle|^2 \quad (38)$$

If r is taken to be the radius of the atom and $k = \omega/c$, it can be shown for photoionization by HeI radiation that $\mathbf{k}\cdot\mathbf{r} \cong 1/300$ and thus the dipole approximation allows the expression $\exp^{i(\mathbf{k}\cdot\mathbf{r})}$ to be replaced by 1.⁸ The matrix element can be further simplified by making use of the relations,⁹

$$\mathbf{P}_{op} = \frac{\hbar}{i} \nabla \quad (39)$$

$$\mathbf{P}_{op} = \frac{i\mathbf{m}}{\hbar} [H\mathbf{r}] \quad (40)$$

where H is the total Hamiltonian. This leaves us with the relation

$$\langle n | \nabla | m \rangle = \frac{i\mathbf{m}\omega}{\hbar} \langle n | \mathbf{r} | m \rangle \quad (41)$$

where

$$\omega = (E_n - E_m) / \hbar \quad (42)$$

Substitution of these expressions into equation 38 yields,

$$\frac{d\sigma}{d\Omega} = \frac{L^3 k e^2 \omega m}{2\pi c \hbar} |\langle n | \mathbf{P} \cdot \mathbf{r} | m \rangle|^2 \quad (43)$$

Recalling that the final state, $\langle n |$, was box normalized so that it was proportional to $L^{-3/2}$, allows all L dependence to be removed from the cross section. Any angular dependence of the cross section must thus originate from the matrix element,

$$\langle n | \mathbf{P} \cdot \mathbf{r} | m \rangle \quad (44)$$

To show that the form of the angular distribution is $a + b \cos^2 \theta$, we will follow the argument presented by Bethe and Salpeter¹⁰ (see figure 1), which was applied to the case of a hydrogenic atom.

If the polarization direction of the incoming beam of photons is taken to be the x-axis, the matrix element takes on the form

$$\langle n | x | m \rangle \quad (45)$$

This matrix element does not explicitly depend on the direction of the incoming light beam but it does depend on the angle, θ , between the polarization direction, \mathbf{P} , and the direction of electron ejection, \mathbf{k} . The initial state is discrete and thus depends on the quantum numbers n, m, and l. The cross section will also depend on the quantization direction of $|m\rangle$ and on the magnetic quantum number m . If the cross section is averaged over all possible values of m from -l to l, the average becomes independent of the quantization direction and thus the angular dependence of the matrix element comes from θ . For the final state, the wave

function has the form of,

$$\langle n | = N(\exp^{i(\mathbf{k}\cdot\mathbf{r})} + V(r)) \quad (46)$$

which is the sum of a plane wave and a spherical wave, $V(r)$, for a hydrogen-like atom. If the direction of \mathbf{k} is reversed then $\mathbf{r} \rightarrow -\mathbf{r}$ and $\mathbf{x} \rightarrow -\mathbf{x}$ and the direction of the quantization of $|m\rangle$ is also reversed. Since $\cos\theta = k_x/k$, changing \mathbf{k} to $-\mathbf{k}$ changes $\cos\theta$ to $-\cos\theta$. $\langle n|x|m\rangle$ also changes sign but since the cross section is proportional to the square of the matrix element, it must be an even function of $\cos\theta$. To show that the differential cross section also has the form $a + b\cos^2\theta$, we can define a new coordinate system, shown in figure 2, in which \mathbf{k} is taken to be the polar axis using the spherical coordinates, r , θ' , and φ' . From the addition theorem of spherical harmonics, x in equation 45, may be written as,

$$x = \mathbf{P}\cdot\mathbf{r} = r\cos\theta'' = r(\cos\theta\cos\theta' + \sin\theta\sin\theta'\cos\varphi') \quad (47)$$

The matrix element depends on θ only through the terms in equation 47, which are linear in $\sin\theta$ and $\cos\theta$. The cross section is obtained by summing the absolute values of the squares of the matrix elements averaged over all possible m values. From previous symmetry arguments, it is known that the cross terms in $\cos\theta\sin\theta$ must vanish and thus,

$$\frac{d\sigma}{d\Omega} \propto A\sin^2\theta + B\cos^2\theta \quad (48)$$

from which,

$$\frac{d\sigma}{d\Omega} \propto a + b\cos^2\theta \quad (49)$$

Cooper and Zare¹¹ used angular momentum coupling and vector coupling theory to calculate the differential cross sections for both atomic and molecular systems. They showed that the angular distributions of

photoelectrons for linearly polarized light have the form,

$$\frac{d\sigma}{d\Omega} = \frac{\sigma_{tot}}{4\pi} \left[1 + \beta P_2(\cos\Theta) \right] \quad (50)$$

where $P_2(\cos\Theta)$ is the second Legendre polynomial and is equal to $\frac{1}{2}(3\cos^2\Theta - 1)$ and Θ is the angle between the incident photon beams polarization vector and the outgoing electrons direction. For atomic cases they found β to have the form,

$$\beta = \frac{l(l+1)\sigma_{l-1}^2 + (l+1)(l+2)\sigma_{l+1}^2 - 6l(l+1)\sigma_{l+1}\sigma_{l-1}\cos(\delta_{l+1} - \delta_{l-1})}{2(l+1)[l\sigma_{l-1} + (l+1)\sigma_{l+1}]} \quad (51)$$

where l is the orbital angular momentum of the initial state, δ_{l+1} , δ_{l-1} are the phase shifts, and σ_{l-1} , σ_{l+1} are the radial dipole integrals for the $l-1$ and $l+1$ outgoing waves which are of the form,

$$\sigma_{l1} = \int_0^{\infty} r R_{nl} G_{kl\pm 1}(r) dr \quad (52)$$

In equation 52, $R_{nl}(r)$ is the radial wavefunction of the initial state and $G_{kl\pm 1}$ is the radial wave, divided by kr , of the continuum states. For a physically correct cross section, β may take on any values between 2 and -1. For the case of $\beta = 2$ the angular distribution is $\cos^2\Theta$ about the polarization vector, \mathbf{P} . For $\beta = -1$, it is one of $\sin^2\Theta$ and for $\beta = 0$ the distribution is isotropic. For an s type electron, β will be 2 but for a non- s type electron β will depend on the interference between the partial waves $l+1$ and $l-1$.

Cooper and Manson¹² have obtained the differential cross section for non-polarized light by considering it to be an incoherent superposition of two polarized light beams that have one polarization direction in the plane of the incident radiation and ejected electron and the other per-

pendicular to it. The expression they derived for the differential cross section is given below,

$$\frac{d\sigma}{d\Omega_{unpol}} = \frac{\sigma_{tot}}{4\pi} \left[1 - \frac{\beta}{2} P_2(\cos\Theta) \right] \quad (53)$$

where Θ is now the angle between the incident photon beam and the direction of the ejected electron.

Several groups¹³⁻¹⁵ have extended this formalism to molecular photoionization and have shown that the general form of the angular distribution derived for atoms was still valid assuming that the molecules were randomly oriented in space and that photoejection occurs on a time scale which is fast compared to molecular rotation. Buckingham et al.¹⁵ have derived a formula which explicitly includes the effects of rotation. They found that the angular distributions for rotationally resolved transitions were different than for rotationally unresolved ones. Peshkin¹⁶ has predicted the general characteristics of the angular distributions by use of symmetry arguments and again assumes unoriented targets.

Cooper and Zare¹⁴ also treated the case for two photon ionization and showed that the general form of the angular distributions to be

$$I(\Theta) = a + b\cos^2\Theta + c\cos^4\Theta \quad (54)$$

Jacobs¹⁷ has generalized this formalism to treat n photon ionizations. His expression is given below.

$$\frac{d\sigma_n}{d\Omega} = \frac{\sigma_{tot}}{4\pi} \left[1 + \sum_{i=2}^{2N} \beta_i P_i(\cos\Theta) \right] \quad (55)$$

In theory all that is needed to calculate photoelectron angular distributions are accurate initial and final state wave functions. The discrete initial state wave functions can be determined to reasonable accuracy for

many small molecules but treating the continuum final state wave functions is a difficult task. Parallel to theoretical calculations for electron scattering, (see chapter 3), a number of approximate methods have been developed to deal with this problem. We will not describe any of the methods used in calculating the angular distributions but instead we shall refer the interested reader to the appropriate reviews¹⁸⁻²⁰ and the references they contain.

References

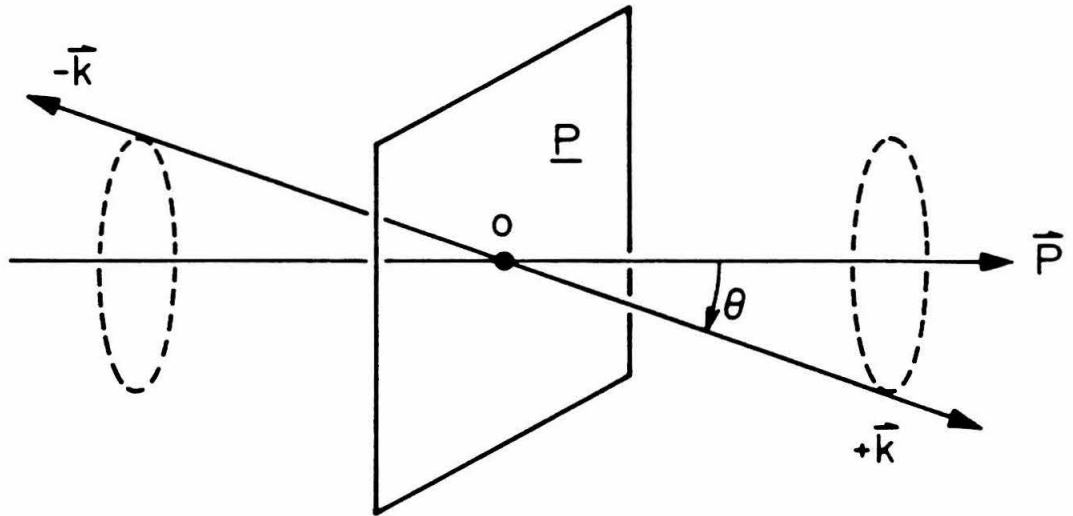
- 1) L. I. Schiff, *Quantum Mechanics*, (McGraw-Hill, New York 1968) Chapters 8 and 11.
- 2) H. A. Bethe and R. W. Jackiw, *Intermediate Quantum Mechanics* 2nd edition (W. A. Benjamin, New York 1968) chapter 12.
- 3) Ref. 1 p. 400
- 4) Ref. 1 p. 177
- 5) Ref. 2 p. 194
- 6) Ref. 1 p. 285
- 7) Ref. 1 p. 286
- 8) Ref. 1 p. 201
- 9) Ref. 1 p. 181
- 10) H. A. Bethe and E. E. Salpeter, *Quantum Mechanics of One and Two Electron Atoms* (Springer-Verlag, Berlin 1957) pp. 307-310
- 11) J. Cooper and R. N. Zare, *J. Chem. Phys.* **48**, 942 (1968).
- 12) J. Cooper and S. Manson, *Phys. Rev.* **177**, 157 (1969).
- 13) J. Tully, R. Berry, and B. Dalton, *Phys. Rev.* **176**, 95 (1968).
- 14) J. Cooper and R. N. Zare in *Lectures in Theoretical Physics* edited by S. Geltman, K. Mahanthappa, and N. Britten (Gordon and Breach, New York 1969) p. 317.
- 15) A. Buckingham, B. Orr, and J. Sichel, *Phil. Trans. Roy. Soc. (Lond.) A* **268**, 147 (1970).
- 16) M. Peshkin, *Adv. Chem. Phys.* **18**, 1 (1970).
- 17) V. L. Jacobs, *J. Phys. B.* **6**, 1461 (1973).

- 18) *Electron Molecule and Photon Molecule Collisions* edited by T. rescigno, V. McKoy, and B. Schneider (Plenum, New York 1979)
- 19) J. Berkowitz, *Photoabsorption, Photoionization, and Photoelectron Spectroscopy* (Academic Press, New York 1979) pp. 359-391.
- 20) S. T. Manson and D. Dill in *Electron Spectroscopy; Theory, Techniques, and Applications* vol. 2 edited by C. R. Brundle and A. D. baker (Academic Press, New York 1978) pp. 157-195.

Figure Captions

Figure 1. Diagram illustrating the Bethe-Salpeter¹⁰ argument for the symmetry of $\frac{d\sigma}{d\Omega}$ about a perpendicular to the light polarization axis.

Figure 2. Diagram illustrating the coordinate system used in the Bethe-Salpeter¹⁰ argument for the $a + b\cos\theta$ form of the angular distributions.



$\frac{d\sigma}{d\Omega}$ depends only on θ .

$\frac{d\sigma}{d\Omega}$ is unchanged by inversion through the origin, o .

$\frac{d\sigma}{d\Omega}$ is thus unchanged by reflection through the plane, \underline{P} which is perpendicular to \vec{P} .

Figure 1.

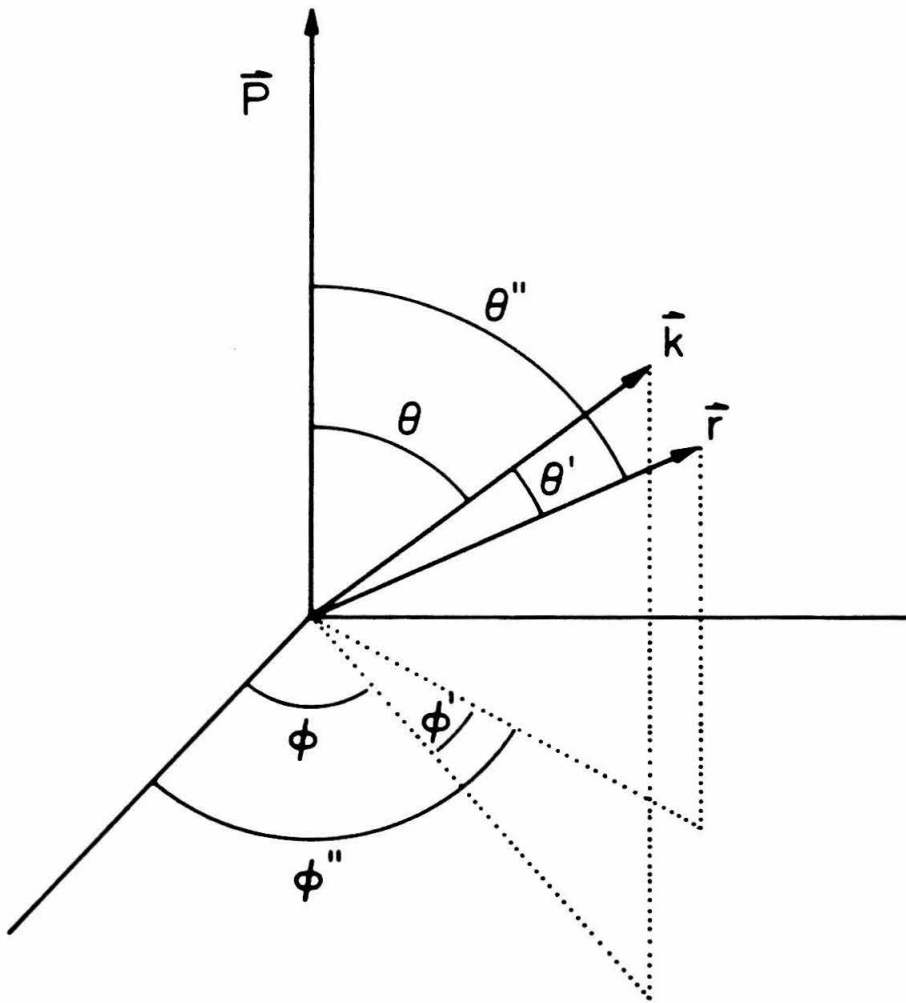


Figure 2.

CHAPTER 10

EXPERIMENTAL VARIABLE-ANGLE PHOTOELECTRON SPECTROSCOPY

This chapter will focus attention on the instrumentation of the variable-angle photoelectron spectroscopy experiment. This instrument has been described in detail previously¹⁻³ and will only be briefly described here. Emphasis will be placed on the changes made in the instrumentation since the last documentation.⁴

A block diagram of the instrument is shown in figure 1. Ultra-high purity (UHP) helium flows through a liquid nitrogen (LN₂) cooled zeolite trap into a DC discharge rare gas resonance lamp. The discharge within the lamp produces 584 Å vacuum ultraviolet (VUV) radiation which is then collimated and enters a scattering chamber where it interacts with the target gas. The target gas is usually maintained at a pressure of 1 to 10 microns, depending on the sample. Care must be taken to keep the sample pressure low enough to avoid multiple collisions. Photoelectrons produced from the target-photon interactions leave the scattering chamber through a slot and are then collimated and decelerated by a set of electrostatic lenses. The electrons enter a 180° hemispherical analyzer where they are energy selected. Electrons leaving the hemispheres are then accelerated and focused by another set of lenses onto the front cone of a spiral electron multiplier (SEM). Electrons impinging upon the SEM are multiplied and the resulting voltage pulse, usually 50 to 100 mV, is fed into a pulse amplifier-discriminator (PAD). Here the pulses are amplified and shaped before being sent to the computer interface. The electrostatic lenses, hemispherical analyzer, and the SEM are all mounted on a large rotating gear which allows the detection system to be rotated about the scattering center in a range from 40° to 120° with respect to the

incoming photon beam. The pulses generated by the PAD are then channeled into a DEC PDP8/e minicomputer which effectively functions as a programmable multi-channel scaler. Here the pulses are counted and the resulting spectra are displayed on an oscilloscope or plotted on an X-Y recorder. The spectra may also be output on punched paper tape. The entire vacuum chamber of the spectrometer sits within three pairs of Helmholtz coils which nullify the earth's magnetic field to within .2 mgauss. Each major component system of the instrument will be described in greater detail in the following sections.

a) Vacuum system

The main vacuum chamber (figure 2) is pumped by a 6" oil diffusion pump which is isolated from the main chamber by a cryotrap. Cooling for the trap is not provided by LN₂ but by a Polycold PCT-200 mechanical cold trap chiller. The diffusion pump is backed by a 6.1 liter/sec mechanical vacuum pump which has a freon baffle located between it and the diffusion pump. The pumping stack may be isolated from the main chamber by a 6" pneumatically controlled gate valve which is interlocked to isolate the pumping system in case of an overpressure.

The internal portion of the instrument is mounted on an 18" flange which in turn is mounted on a cart so that it may be rolled away from the main chamber to allow easy access for maintenance of the instrument (figure 3). This flange also contains all of the electrical and mechanical feedthroughs along with the feedthroughs for the lamp cooling, differential pumping, and He inlet lines. The pressure within the main chamber is monitored using an ionization gauge and the ionization gauge controller is connected to the main interlock, which shuts down the diffusion pump, polycold, and other equipment which might be damaged

should an overpressure occur. The pressure after one day of pumping is typically 2×10^{-6} torr, after 2 days it is about 3×10^{-7} torr. With the lamp operational and a sample gas present in the scattering chamber, typical operating pressures range from 2×10^{-6} to 1×10^{-5} torr, depending on the sample pressure being used.

b) Lamp

UHP helium first flows through a LN_2 cooled zeolite trap before entering the back of the lamp through a feedthrough on the main flange. This is done to remove any H_2O and other condensable impurities which might cause impurity lines in the lamp's spectral output. A cross sectional view of the lamp is given in figure 4. He enters the discharge region where an arc is sustained through a quartz capillary between a copper wire anode held at +300 to 550 volts and a tungsten cathode held at ground potential. The region between the discharge and the main chamber is differentially pumped by two mechanical pumps located in a lamp service stand. This is done so that the flow of He into the main chamber is reduced and so that as much He as possible is removed from the light path to minimize the losses brought on by self-absorption of the 584A light by ground state He atoms. The lamp is powered by a high voltage DC power supply which is current limited by a 300 watt network of ballast resistors. This power supply has also been tied into the main interlock in such a way that if a fail occurs, the lamp will be shut off to prevent damage. An interlock system has also been built so that loss of lamp coolant will shut off the lamp. Typical operating parameters for the lamp are 100mA and 400volts at the power supply, with a helium pressure at the inlet line of approximately 10 torr. The actual pressure within the discharge region of the lamp is not known since there is glass wool pack-

ing at the rear of the starter electrode, which was installed to prevent back-arcing. It is estimated, however, that the helium pressure in the discharge region is of the order of .5 to 2 torr. The optimum pressure for stable lamp operation is determined by monitoring the photon flux at the photocathode as a function of helium inlet pressure. The pressure is adjusted until the photon flux is maximized and is usually re-adjusted once a day when the lamp is operational. The photon flux under optimum conditions has been estimated to be on the order of 2×10^{11} photons/second. With everything functioning properly, the lamp may be run continuously for 2 to 3 weeks. The design of the lamp is such that it may be used with other rare gases such as neon, which emits light at 736 and 744 Å. The lamp does not produce significant amounts of HeII (304 Å) radiation, but it does produce small amounts of 537 Å and 522 Å light at 2% and .5% of the intensity of the 584 Å line, respectively.

Due to the low intensities of photoelectrons from many of the organic molecules now under study, it was desirable to design a new light source with increased intensity. The new VUV lamp based on the design of Heinzmann and Schönhense^{5,6} is shown in figure 5. The operating conditions of this lamp are somewhat different and will be discussed below.

The major difference in the design of this lamp from that of the previous one is the reversal of the positions of the cathode and anode. One problem with the previous lamp design was that sputtering of the cathode plugged the collimating apertures. In this design the sputtering of the cathode does not affect the collimation apertures since it is located at the He inlet end of the discharge capillary. The lamp discharge operates at a pressure of from 2 to 5 torr as measured by the gauge at the He inlet on the lamp stand. Typical operating voltages range from 600 V to 800 V

with the current varying from 75 to 150 mA. The higher operating voltages of this lamp necessitated a new power supply (3 kV, 500 mA) which could maintain the voltages needed for lamp operation. The discharge is initiated by simply applying 1.5 to 2 kV across the electrodes. The spectral purity of the VUV light under the aforementioned operating conditions is identical to that of the previous lamp.

The intensity of this lamp, as measured by the count rate of the Ar $^{2}P_{3/2}$ ionization signal is typically 5000 counts/second-micron. Under ideal conditions as many as 10,000 counts/second-micron have been obtained. This is approximately 20 to 50 times the typical intensity of the old lamp and corresponds to photon fluxes of 4 to 8×10^{12} photons/second.

There are, however, several problems which must be dealt with before the full benefits of this high intensity light source can be realized. It was found that even though the signal was increased by a factor of 20 to 50, the background also increased by the same amount. This is most likely due to photoelectrons from the target and sample chamber walls scattering about the sample chamber and then finding their way through the electron optics. It was also discovered that the angular distributions were not reliable and varied widely in the patterns of asymmetry observed. This was probably due to surface charging effects involving the photocathode and chamber walls. Both of these problems can be eliminated by going to a molecular beam type of target. The studies presented in chapter 11 of this thesis were performed using the old lamp design.

c) Scattering chamber and inlet system

The scattering chamber, figure 6, is constructed of three coaxial

shells of gold plated copper. The inner and outer shells rotate with the analyzer while the middle shell remains fixed to the base of the scattering chamber. Light enters the chamber via a small aperture and passes through the slotted inner chamber where it interacts with the sample gas. The radiation which does not interact then passes on through to a titanium photocathode, mounted on the wall of the middle chamber, where the photon flux is monitored. The sample gas enters the scattering chamber through a 1/4" diameter hole in its base. The pressure inside the chamber is continuously monitored by a capacitance manometer. The design of the scattering chamber is such that the pressure changes as a function of the detector angle. As a result, the pressure must be measured frequently since the count rate obtained must be normalized to the sample pressure. This requirement also restricts the operation of the instrument to regions of sample pressure where the count rate is a linear function of the sample pressure. With 2 to 5 microns of sample gas present in the scattering chamber, the pressure in the main chamber rises to between 2×10^{-6} and 1×10^{-5} torr.

The external portion of the inlet system consists of a glass manifold with a five liter ballast bulb. This inlet manifold is attached to a variable leak valve which controls the rate of sample flow into the scattering chamber. Usually the sample manifold is pumped down to between 5 and 10 microns before a sample gas is admitted. If the sample is a gas it is usually loaded at pressures ranging from 10 to 14 psi. If the sample is a liquid, it is subjected to vacuum distillation and degassing by freeze-pump-thaw cycles. Liquids are usually admitted directly into the manifold at their room temperature vapor pressure.

A pneumatically controlled shutoff valve was installed between the

leak valve and the sample inlet feedthrough into the main vacuum chamber. This was connected to the interlock so that if the pumping were to shut down, the sample gas flow would be cut off. This was done to avoid filling the vacuum chamber with the sample and possibly damaging some sensitive components.

d) Electron energy analyzer and detection system

The electron energy analysis and counting system consists of two sets of electrostatic lenses, a 2.5" mean radius hemispherical electron energy analyzer, and a SEM, and is shown in figure 7. The entire analysis and detection system is mounted on a 20 cm diameter gear and can be rotated through the angles of 40° to 120° with respect to the photon beam. This range is determined by the physical interactions within the vacuum chamber. All of the lens elements and hemispheres are constructed of OFHC copper and are gold plated. This inner sleeve of the scattering chamber as well as the surfaces of the electrostatic lenses and hemispheres are coated with a thin layer of graphite. This provides uniform surface potentials and helps increase the signal to noise ratio by reducing the number of electrons reflected off these surfaces.

Photoelectrons leaving the interaction region are first decelerated by the chamber side lens system to the voltage at which they are to be analyzed, usually 1.5 eV. The difference between the initial energy of the electrons and the voltage at which they are to be analyzed is referred to as the sphere center voltage and is used as the reference point for all the analyzer element voltages. The operation of the analyzer is such that it will only transmit electrons of 1.5 eV kinetic energy. Once the electrons have traversed the hemispheres, they are accelerated to about 7 volts and are focused onto the front cone of the SEM. The voltage across the

SEM is set to provide an electron gain of about 10^8 . The resulting electron pulses pass through a pulse amplifier-discriminator before being sent on to the counting electronics. Typical count rates resulting from the Ar $^3P_{3/2}$ ionization range from 250 to 400 counts/second-micron with the original lamp design.

e) Helmholtz coils

From previous experience it has been found that magnetic fields in excess of .2 milligauss within the electron energy analyzer lead to spurious angular distributions. To minimize the magnetic fields, the vacuum chamber is lined with a .050" layer of μ -metal. The entire vacuum system is also located in the center of three pairs of Helmholtz coils, measuring approximately 10 feet per side.² By adjusting the current flowing through the coils, all magnetic fields can be nullified such that the field gradient within the analyzer region of the instrument does not exceed .2 milligauss. The fields are checked by mounting the probe of a gaussmeter on the analyzer and rotating it through its operating range.

f) Computer system

The entire experiment is under the control of a PDP 8/e minicomputer with 12k bytes of memory. The peripheral devices controlled by this computer include a high speed paper tape reader, high speed paper tape punch, a 120 hz real time clock, and three channels of digital to analog conversion (DAC). Two of the DAC channels are used to drive an oscilloscope display or X-Y recorder while the third channel provides the voltage used to sweep the electron energy analyzer.

The remainder of the computer interfacing consists of three major components. The first of these is a counter with a six digit LED display. The counter accumulates the number of pulses received from the pulse

amplifier over a user specified time period, usually 1 second, and displays the number of counts on the display. The second interface unit consists of a four bit sense and 12 bit drive register. At present only the angle drive sense is in use with the remainder of the registers being disabled. The drive register controls the warning blinker, angle drive motor, multiplexer, paper tape punch, terminal, X-Y recorder pen control, and audio alarm. The third interface unit is an analog to digital converter (ADC) which allows the lens voltages, ample pressure, and lamp flux to be read into the computer via the multiplexer. The computer also has available software which allows data analysis to be carried out even though this method of data analysis is no longer in use.

g) Computer software and data handling procedures

The details of the data acquisition and analysis software of the PDP 8/e have been described in detail elsewhere,² and will only be very briefly reviewed here.

The data acquisition program in the PDP 8/e has the capability of storing spectra in up to 512 channels, each with a capacity of over 8×10^6 counts. During actual spectral acquisition, the counter accumulates counts over a fixed interval set by the user. At the end of this interval the counts are loaded into memory and the DAC voltage, which controls the electron energy analyzer, is incremented. When a scan is completed, the sample pressure is measured and the process repeated until the preset number of scans set by the user is reached. After the last scan is complete, the computer calculates the average sample pressure and prints this out on the terminal. The computer also performs a partial analysis of the spectrum by applying a smoothing routine devised by Savitsky and Golay.⁷ A derivative algorithm is also applied to the spectrum

to determine the locations of the peaks present. All of this information is then punched out on paper tape and printed on the terminal.

Formerly, the data was analyzed using the available software on the PDP 8/e but this was a very time-consuming procedure. Data is now transferred from punched paper tape to a PDP 11/03 located in 05 Noyes where it is stored on floppy diskettes. The program which accomplishes this transfer was written by D. J. Flanagan and will be described in detail in her thesis. The data is transferred from floppy diskette to the departmental VAX 11/780 computer where the data analysis and plotting is carried out. The data analysis programs for the VAX were also written by D. J. Flanagan and will be described in detail in her thesis.

h) Data acquisition procedure

Once the magnetic fields have been zeroed and the performance of the instrument checked by its ability to reproduce the Ar $^2P_{3/2}$ β value of $.88+.02$, the instrument is ready for operation. First a sharp or intense feature in the spectrum is found and the dependence of the count rate on the sample pressure is determined. The results are plotted and the sample pressure adjusted by means of the leak valve such that it falls within the region where the count rate is still linear with the sample pressure. Once this is done, a scan over the entire electron energy range, usually about 12 eV, of the spectrum is performed. This is always done at the magic angle, $\Theta = 54.7^\circ$, since at this angle the relative intensities of the features of the spectrum are independent of β . The resolution of the instrument during operation is typically set between 35 and 50 meV as measured by the FWHM of a rare gas ionization peak. Once the location of the bands has been determined from the full scan, spectra are taken over each band, usually 1 - 2 eV in width, at 9 angles ranging from 45° to

120°. The channel spacing is typically set at 15 meV with a dwell time of around 30 seconds for most bands of the molecules studied here. The computer may accept instructions read in on paper tape, which is necessary since a full set of spectra comprising an angular distribution measurement may take anywhere from 4 to 12 hours.

After each band is completed, a short scan is taken over a sharp or otherwise prominent feature in the spectrum for energy calibration purposes. When all of the bands are completed, an energy calibration is usually performed by adding some Ar to the sample gas and measuring the spectrum of the mixture. If a more complete energy calibration is desired one may add a calibration mixture consisting of Ar, Kr, Xe, and ethylene. Generally this has been found to be unnecessary since any contact potential shift is almost always linear over the entire spectrum. Once the energy calibration has been completed, background spectra are taken with no sample gas present. If any bands display resolvable structure, high resolution spectra are measured at $\theta = 54.7^\circ$ with $\Delta E = 15 - 10 \text{ meV}$.

References

- 1) D. C. Mason, M.S. Thesis, California Institute of Technology, Pasadena, CA. (1973).
- 2) D. M. Mintz, Ph.D. Thesis, California Institute of Technology, Pasadena, CA. (1976).
- 3) D. C. Mason, D. M. Mintz, and A. Kuppermann, *Rev. Sci. Instr.* **48**, 926 (1977).
- 4) J. A. Sell, Ph.D. Thesis, California Institute of Technology, Pasadena, CA. (1979).
- 5) U. Heinzmann and G. Schönhense in *Vith International Conference on Vacuum Ultraviolet Radiation* (Plenum Press, New York 1980)
- 6) G. Schönhense, Thesis Westfälische Wilhelms-Universität, Münster (1978).
- 7) A. Savitsky and M. J. E. Golay, *Anal. Chem.* **36**, 1627 (1964).

Figure Captions

- Figure 1. Block diagram of the variable-angle photoelectron spectrometer. He, cylinder of UHP helium. ZT, liquid nitrogen immersed zeolite trap for lamp helium supply. RB, lamp ballast resistor. LPS, lamp power supply. SC, sample chamber. PC, photocathode for light flux measurement. CL, electrostatic lens elements before the hemispherical analyzer. ANALYZER, 180° hemispherical electrostatic electron energy analyzer. ML, electrostatic lens elements between hemispherical analyzer and detector. S, Spiraltron electron multiplier. CPS, power supply to spiraltron cathode. APS, power supply to spiraltron anode. R,C, differentiating network for Spiraltron pulses. PDP 8/e, Digital Equipment Corporation PDP 8/e minicomputer. INTER, counting system interface to experiment. OUTPUT, computer output devices to user.
- Figure 2. General view of variable-angle photoelectron spectrometer vacuum system.
- Figure 3. Side view of apparatus where the main flange is separated from the vacuum chamber (not drawn to scale).
- Figure 4. Section view of lamp. Hatched and stipled parts, except for the stainless steel lamp anode, A, are of aluminum and constitute the lamp body. K, tungsten cathode. C, quartz discharge capillary. HV, high voltage power lead. S, starter electrode. He, helium inlet. OA, lamp flux outlet capillary. DP, differential pumping connections. WAT, water cooling inlet (outlet not shown). M, Mica spacer. CE, water cooling envelope inside lamp body. Flows of Helium and water are

indicated by the arrows.

Figure 5. Section view of new lamp. Hatched and stipled parts of lamp show the different materials from which the lamp is constructed and are explained in the legend on the figure. He, helium inlet. H_2O , water inlet. K, beryllium-copper cathode. A, beryllium-copper anode. DC, quartz discharge capillary. CCh, cooling channels. CC, light collimation capillary. Direction of flows of helium and water are indicated by the arrows.

Figure 6. Sectional and external views of sample chamber. Hatched areas are sections of the inner and outer shells. OS, outer shell. MS, middle shell. IS, inner shell. GI, gas inlet. HS, helical slot. GS, guide screw for helical slot. LI, light inlet. Motion of OS and flow of samples are shown with vertical arrows.

Figure 7. Section view of electron energy analyzer and sample chamber in the plane of the electron trajectories. Hatched areas include BN, a boron nitride mounting block for S, the Spiraltron, and part of CIS, the inner shell of the sample chamber. COS, outer shell of sample chamber. PC, photocathode. LE, light entrance. C1, HC, HM, and M1 lens elements. LS, aluminum supports for lens elements. IS, inner hemisphere. OS, outer hemisphere. ISC, corrector electrode for inner hemisphere. OSC, corrector electrode to outer hemisphere. AL, aluminum enclosure for Spiraltron. CF<AF, electrical feedthroughs for Spiraltron. AR, resistor from Spiraltron anode to anode plate A.

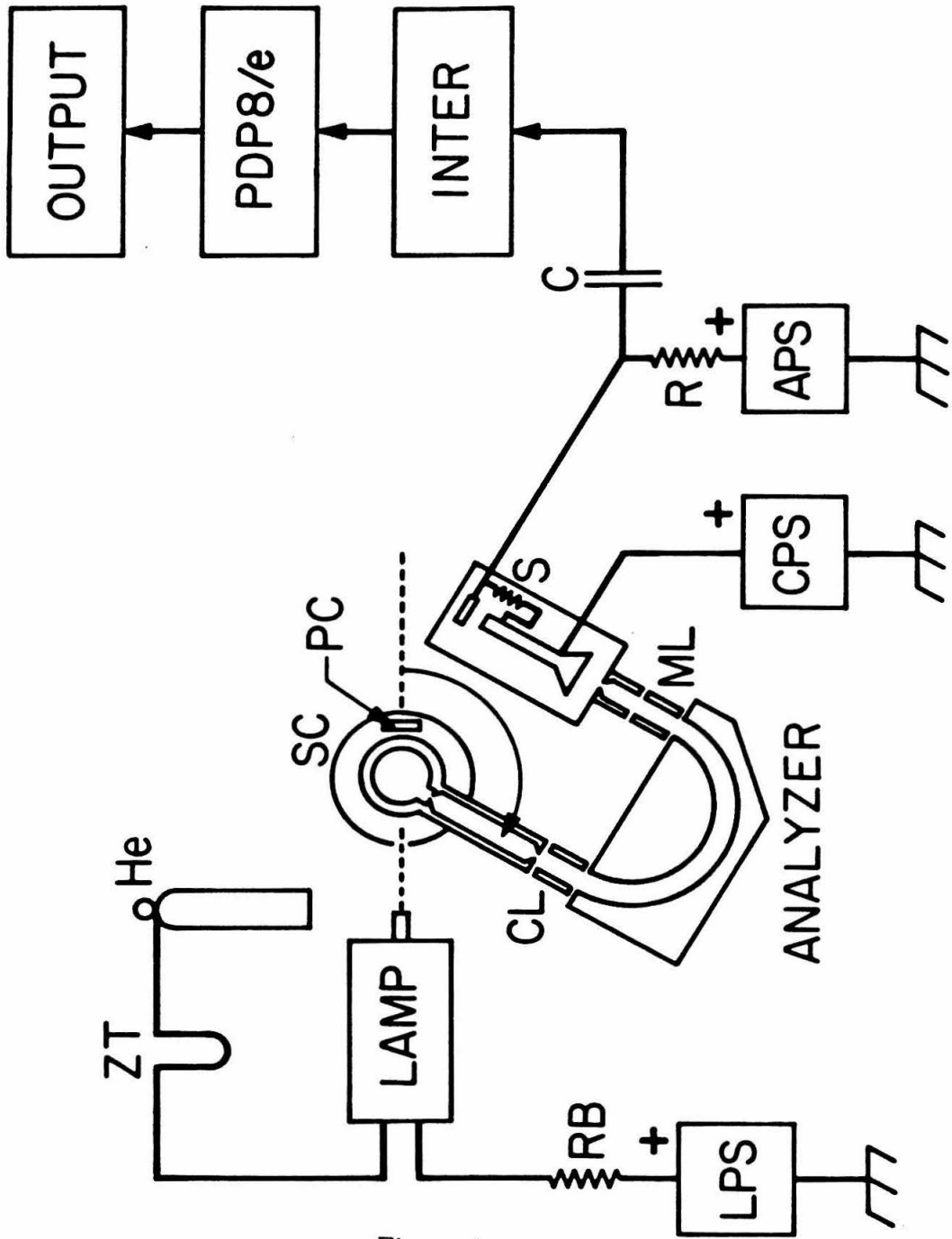


Figure 1.

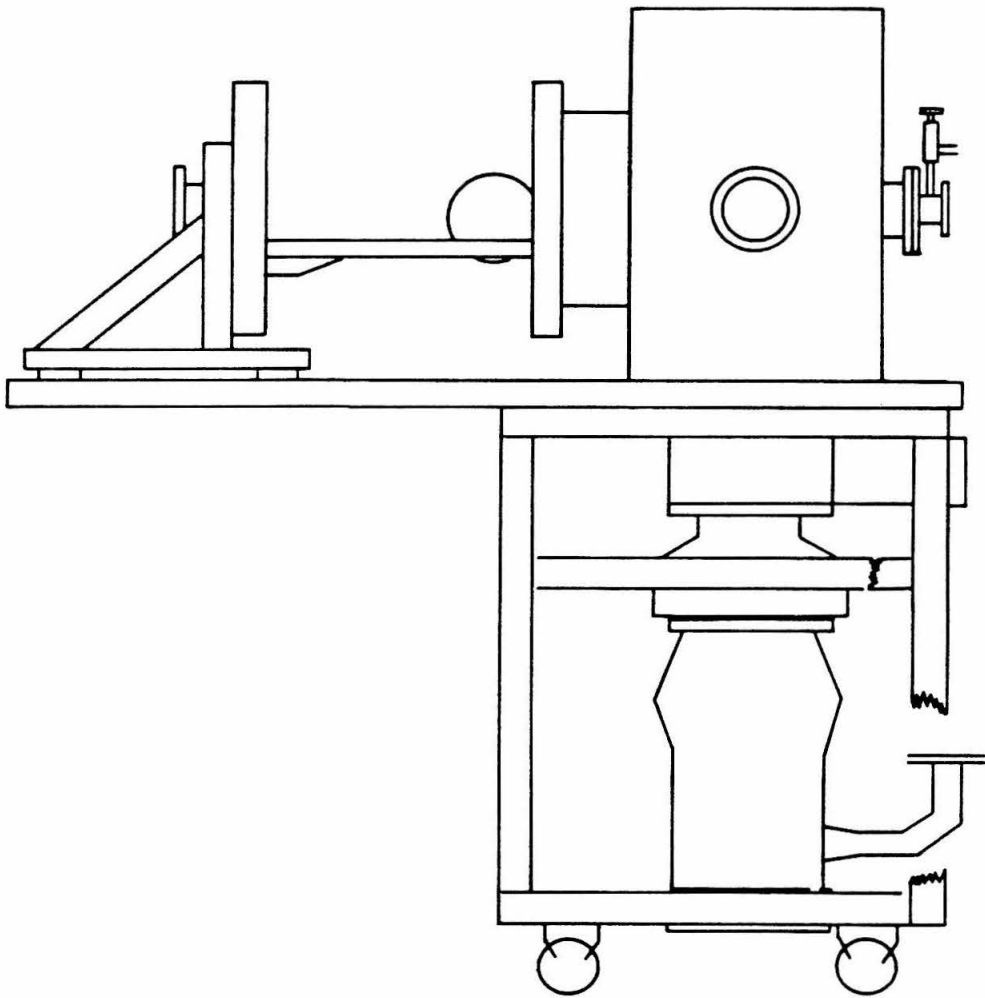


Figure 2.

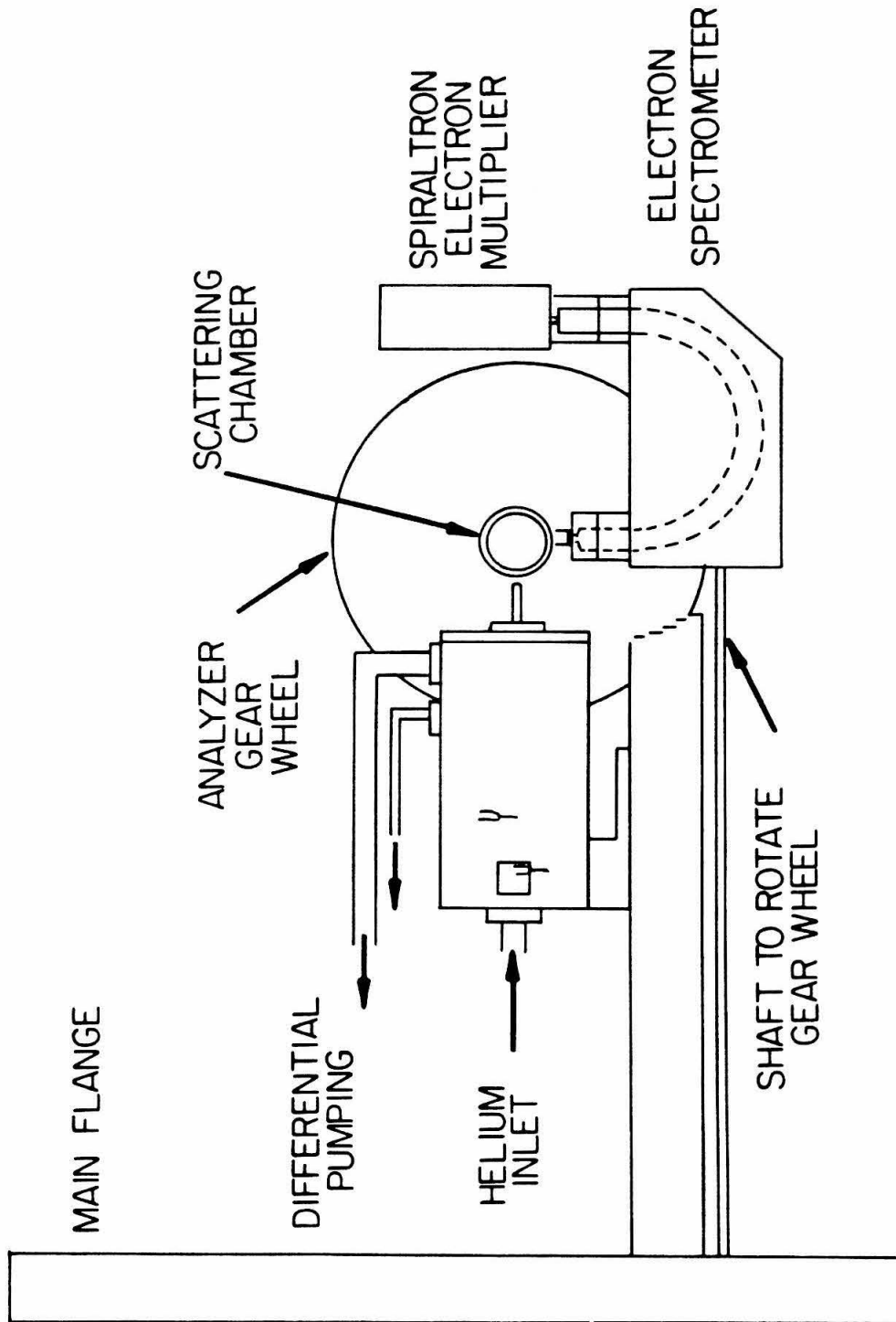


Figure 3.

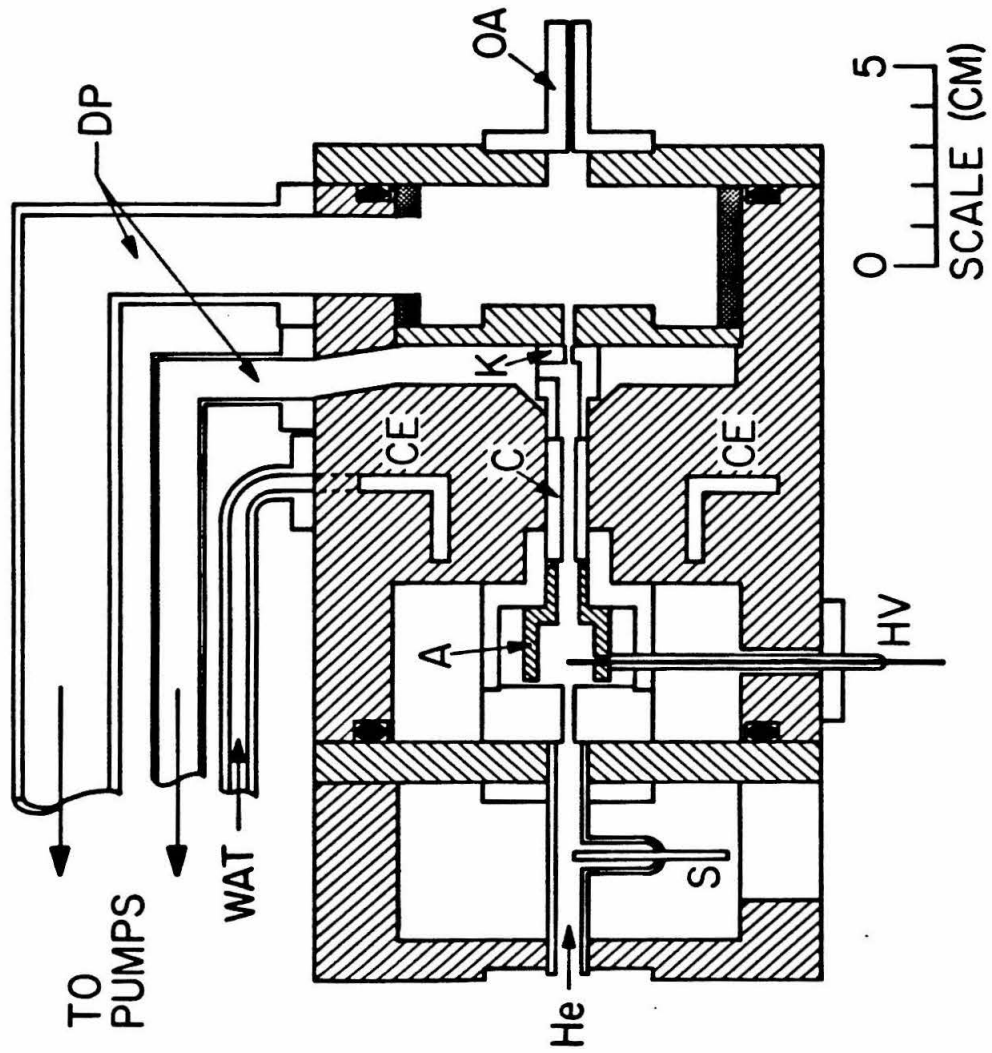


Figure 4.

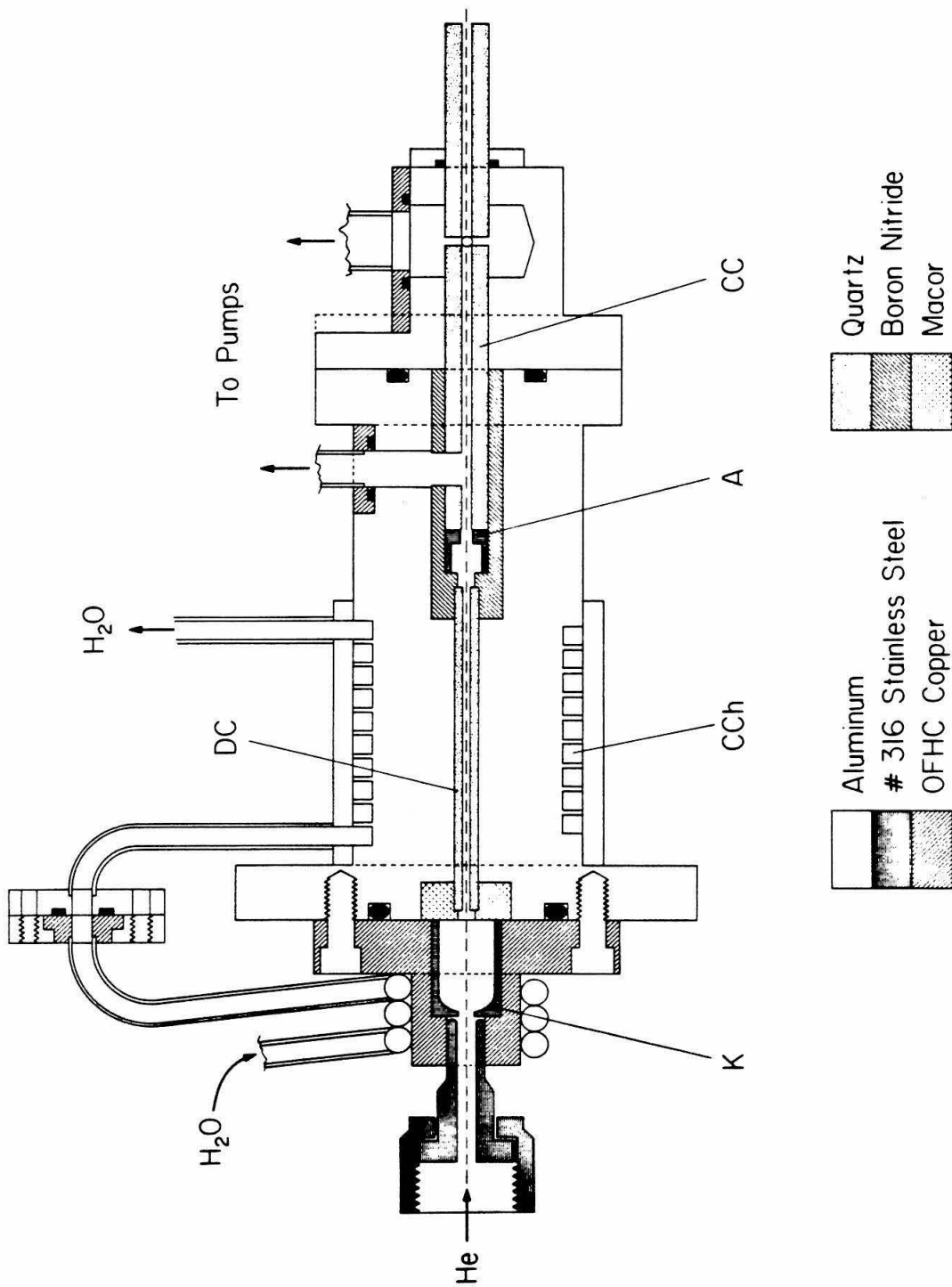


Figure 5.

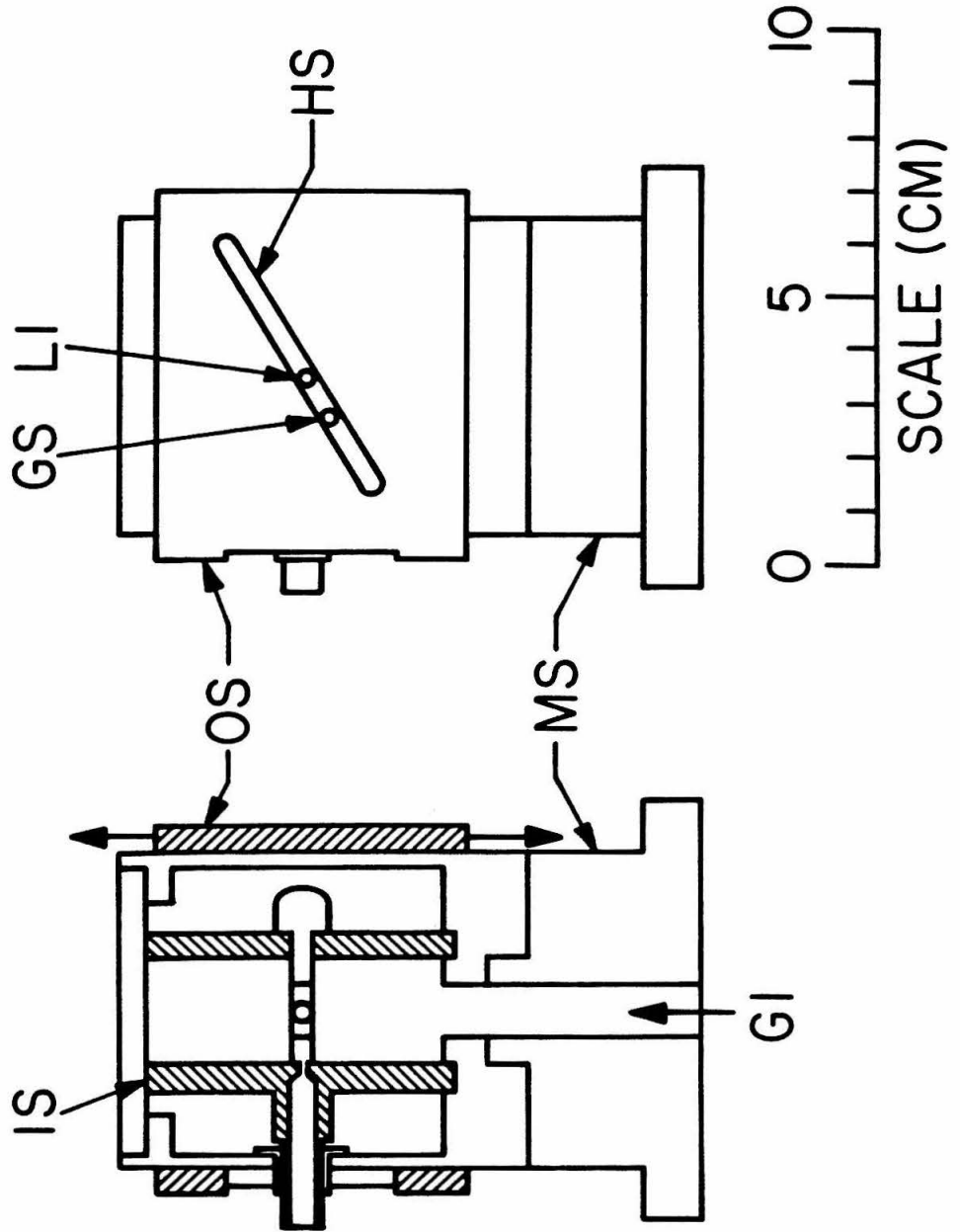


Figure 6.

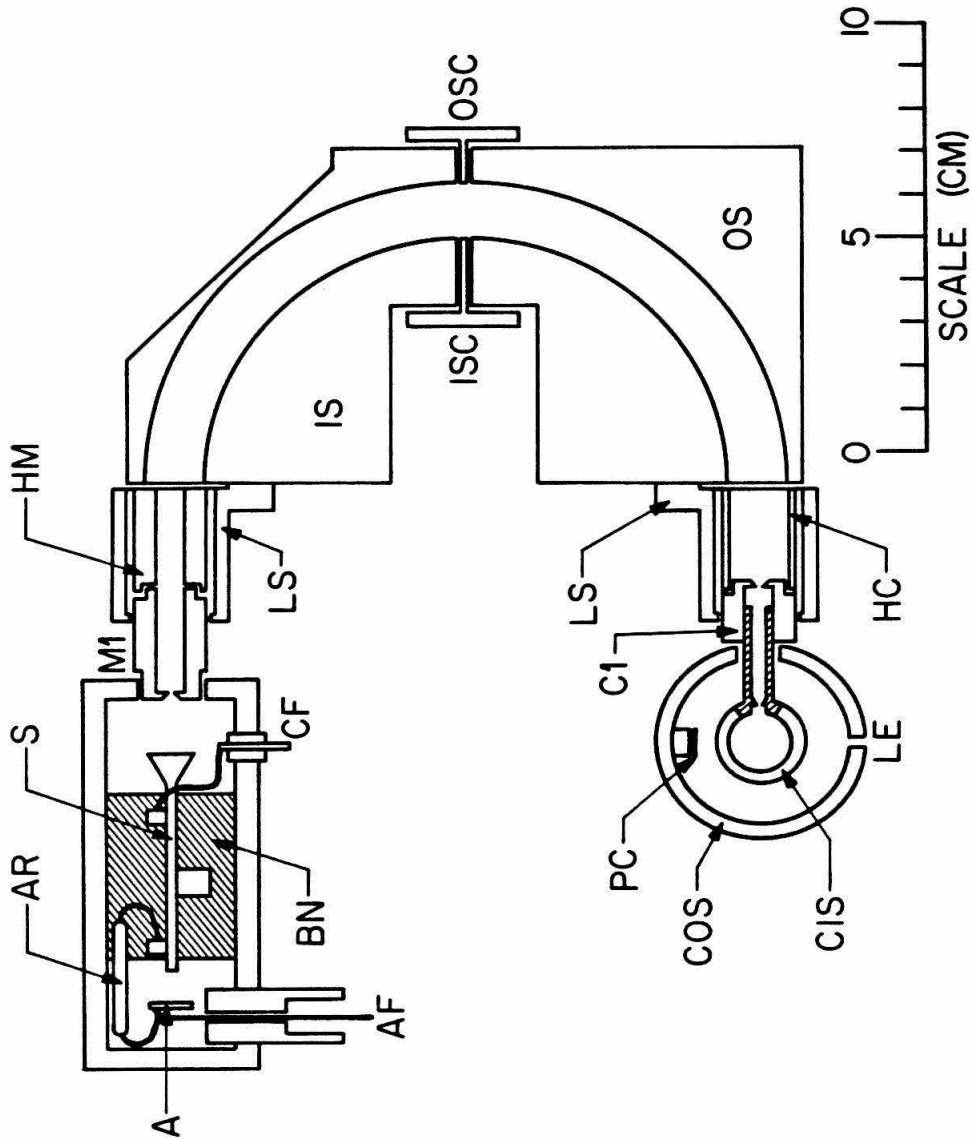


Figure 7.

CHAPTER 11

Paper III:

**The Angle Resolved Photoelectron Spectroscopy of
Cyclopropane, Ethylene Oxide, and Ethyleneimine**

I. INTRODUCTION

It has been previously shown that the measurement of the angular distributions of photoelectrons can be used to analyze the orbital assignments of the corresponding photoelectron.^{1,3} These angular distributions furnish more information about the electronic structure of the molecules than do the fixed angle photoelectron spectra alone.

The angular distribution of the photoelectrons resulting from the interaction of unpolarized light with a randomly oriented target can be described in terms of the differential cross section $d\sigma_{if}/dr$ of the process which is given as^{4,5}

$$\frac{d\sigma_{if}}{dr} = \frac{\sigma_{TOT\,if}}{4\pi} \left[1 - \frac{\beta_{if}P_2}{2} (\cos \theta) \right]$$

where $\sigma_{TOT\,if}$ is the total ionization cross section from initial target state i to the ionic target state f , θ is the angle between the directions of the ejected electron and the incident photon beam, β_{if} is the asymmetry or anisotropy parameter for the process, and $P_2(\cos\theta)$ is the second Legendre polynomial. β_{if} is restricted by the fact that the cross section must be positive to values between -1 and 2. β is dependent on the kinetic energy of the photoelectron as well as the characteristics of the orbital from which it was removed, including its angular momentum.⁶ This makes β a sensitive probe of some of the details of the electronic structure of the target molecule. Previous work has shown that differences in β can be used to distinguish between ionization processes involving σ - and π -type orbitals.^{1,7-11}

The three-membered ring compounds possess unusual chemical and structural properties. Much work has been done in exploring the conjugative properties of cyclopropane.^{12,13} In these studies, much has been

said about the similarities between cyclopropane and alkenes in terms of reactivities. Even the Auger electron spectra¹⁴ of cyclopropane more closely resemble that of an alkene than of an alkane. Several bonding schemes have been proposed by Walsh,¹⁵⁻¹⁷ Förster¹⁸ and Coulson and Moffitt.¹⁹⁻²⁰ Their schemes have been examined in detail by Honegger et al.²¹⁻²² who have come to the conclusion that the alkene-like behavior of cyclopropane is due to the high orbital energies of its highest occupied molecular orbitals.

In this work we present the results of measurements of the asymmetry parameters for the HeI photoionization of cyclopropane, ethylene oxide, and ethyleneimine. The photoelectron spectra of these molecules have been published previously²⁶⁻⁴⁰ but it is hoped that asymmetry parameter measurements will provide additional information concerning the bonding in this series of compounds as well as elucidate the similarities and differences in this series of molecules.

II. EXPERIMENTAL

The apparatus used in these studies is basically the same one described previously,¹⁰ and we will only briefly describe it here. A block diagram of the instrument is given in figure 1. A helium discharge lamp is used to produce the 584 Å radiation which then interacts with the sample gas present in the scattering chamber. The pressure of this gas is on the order of a few millitorr and is continuously monitored via a calibrated capacitance monometer. The electrons resulting from the photoionization of the sample gas are then energy-analyzed by a 6.8 cm mean radius hemispherical electrostatic energy analyzer, and detected by a spiraltron electron multiplier. The detector and analyzer are mounted on a gear and can be rotated from 45° to 120° with respect to the incident photon

beam. The entire spectrometer is located within a vacuum chamber lined with a single layer of 0.050" μ -metal and surrounded by three pairs of square Helmholtz coils. These coils and the μ -metal serve to lower the residual magnetic field to less than 0.2 milligauss. The entire instrument is under the control of a PDP 8/e minicomputer which stores the counts from the electron multiplier, increments the analyzer voltages, monitors the sample pressure, and scans the scattering angle. Background counts are subtracted before β is calculated and the performance of the instrument is checked by its ability to reproduce the β for the $^2P_{3/2}$ state of argon which has previously been reported as being 0.88¹⁰ using this instrument. The typical energy resolution of the work presented here is between 40 and 50 meV as measured by the FWHM of the $^2P_{3/2}$ peak of argon.

Samples of cyclopropane and ethylene oxide were obtained as gases from Matheson Gas Products and had stated purities of 99% and 99.7%, respectively. These were used without further purification. Ethyleneimine was obtained from Columbia Organics and had a stated purity of >97%. This liquid was degassed by application of several freeze-pump-thaw cycles and vacuum distilled prior to use. No extraneous peaks due to impurities were observed in any of the spectra.

III. RESULTS AND DISCUSSION

a) *Cyclopropane*

Cyclopropane has been the most studied member of the three-membered ring series. A number of previous PES studies exist^{23-29,37,38,40} for this molecule and the relevant ones are summarized in table 1 along with the results of the present work. The asymmetry parameters for cyclopropane have been previously determined²³ and are also

summarized in table 1. The HeI spectrum along with the β spectrum are shown in figure 1. The HeI spectra agrees well in general appearance with published HeI spectra.^{23,24,26,36,37,39} Minor differences exist in the relative intensities of some of the bands but this is most likely due to the varying electron transmission functions of the electron energy analyzers used in the various studies. The other cause of this difference is that the published spectra were all recorded at a 90° angle. The spectrum we display in this paper are recorded at 54.7°, the so-called "magic angle" as $\frac{d\sigma_{if}}{dr}$ is proportional to $\sigma_{if\ tot}$ because $P_2(\cos\theta)$ in equation 2 vanishes at $\theta = 54.7^\circ$.

The first band of the cyclopropane photoelectron spectrum is Jahn-Teller split into two components⁴¹⁻⁴³ having a vertical ionization potential (IP) at 10.51 and 11.26 eV, respectively. We have measured β for these two components to be $0.46 \pm .07$ and $0.44 \pm .10$, respectively, and observed no appreciable change in β across the two components of this band. This is similar to the results reported by Carlson for the Jahn-Teller split first band of methane⁴⁴ where no significant variation of β over the split band was observed. This result is different from benzene where a significant variation over a Jahn-Teller split band was observed.⁸ This result also confirms the observations of Leng and Nyberg²³ even though their values for β are higher than ours, possibly due to instrumental artifacts.

The second band in the spectrum is also theoretically predicted to be Jahn-Teller split.^{42,43} The calculated splitting is small and has so far been observed, because of overlapping vibrational progressions. Hasselbach⁴² has also concluded that since the $1e''$ orbital is primarily composed of $p_\pi(\text{C-H})$ -type "outer" orbitals, the distortion of the carbon skeleton will

affect it to a much lesser extent than it will the $p_{\sigma}(\text{C}-\text{C})$ "inner" orbitals which compose the $3e'$ orbital. β has been determined to be 0.32 ± 0.5 for this band in crude agreement with the value of 0.43 ± 0.05 obtained previously.²³

There is some question regarding the assignments of the overlapping bands observed at 15.74 and 16.66 eV. All of the theoretical calculations done so far,^{27,45-54} both semi-empirical and *ab initio*, assign the lower electron energy band to ionization from the $1a_2''$ orbital. Evans et al.³⁶ have suggested that the assignments of the third and fourth bands should be reversed. This was done on the basis of comparison with the PES spectra of P_4 and a vibrational analysis of the fourth band. Schweig and Theile²⁸ have also supported this assignment on the basis of intensity variations between the He I and He II spectra of cyclopropane and some of its heterocyclic derivatives. Our measured β 's are quite different for the two bands, 1.18 ± 0.05 and 0.67 ± 0.04 for the third and fourth bands, respectively. This agrees with the values of 1.26 ± 0.05 and 0.65 ± 0.10 obtained by Leng and Nyberg²³ for the same bands supporting the initial assignments on the basis of their measurements. Their argument was based on the nodal properties of the two orbitals involved. The $3a'$ orbital is "internal" C-C bonding and may contain appreciable carbon $2s$ character.³⁶ The nodal properties of this orbital resemble closely an atomic s -type orbital which would account for the high β observed for this C-C σ type orbital. This argument seems to be supported by the orbital diagrams of Jorgensen and Salem⁵⁵ We concur with the conclusions reached by Leng and Nyberg²³ that support the theoretical predictions of the order of these two states.

For the fifth band at 19.51 eV we obtain a β of 0.40 ± 0.08 which is

substantially lower than the value of 0.90 ± 0.10 observed previously.²³ Measurements in this region of the spectrum are difficult since the background is large and signals small. This band lies in the low electron energy portion of the spectrum where differing instrumental effect can become more pronounced and produce a large difference in the values obtained for β . No autoionization effects as postulated by Lindholm⁵² manifested themselves in the angular distributions. A need for a thorough study of β vs. photoelectron energy is needed for the third and fourth bands in order to further clarify their assignments.

b) *Ethylene oxide*

The observed IP's and β 's are summarized in table 2. The PES spectrum and β 's are shown in figure 3. This spectrum agrees quite well with previous ones.^{27,33,38-40} The first band appears as a sharp set of vibrational progressions with its vertical IP at 10.57 eV. This band has been assigned to the $2b_1$ orbital since it is non-bonding in character and calculations show that it is primarily localized on the lone-pair orbitals of the oxygen atom. The vertical β for this band has been measured to be 0.36 ± 0.05 which is reasonably close to that obtained for the lone-pair ionization in furan ($\beta_{\text{vert}} = 0.56 \pm 0.11$). Band II occurs at 11.77 eV and has a $\beta_{\text{vert}} = 0.38 \pm 0.7$. The originating orbital has been assigned as the σa_1 orbital. According to Basch's et al.²⁷ correlation diagram, this orbital correlates with the $3e'$ orbital in cyclopropane which is primarily $\sigma(\text{C}-\text{C})$ in character. The β 's would then be expected to be similar, which they are, 0.38 vs. 0.45 in cyclopropane. Bands III and IV occur between 13.5 and 15.5 eV and are strongly overlapped. These bands have been assigned to the $3b_2$ and $1a_2$ orbitals, respectively. The orbitals are primarily $\sigma(\text{C}-\text{O})$ and $\pi(\text{C}-\text{H})$, respectively. They are correlated with the $3e'$ and

1e' states of cyclopropane, respectively. We have measured β_{vert} for the two bands as 0.11 ± 0.06 and 0.27 ± 0.03 . As seen from figure 3 there is no appreciable variation in β across both bands with β ranging from 0.1 to 0.3 over the entire region. The assignment for band III is consistent with the β 's observed in cyclopropane. β as a function of energy over the first band of cyclopropane gives a slope of $-0.14/\text{eV}$. Extrapolating to the IP of $3b_2$ orbital of ethylene oxide gives a β of about 0.1 which is what is observed. This argument makes the assumption that β is a smooth function of energy over this photoelectron energy range. For the second band of cyclopropane the slope is $0.05/\text{eV}$ giving a β of ≈ 0.37 which is slightly higher than observed for the $1a_2$ orbital but not inconsistent with its assignment. Bands V and VI occur between 16 eV and 18 eV. In appearance this band is very similar to the 15-17 eV band system in cyclopropane. As in cyclopropane the β 's vary widely; 0.99 ± 0.06 for the first band dropping to 0.65 ± 0.10 for the second band. The value for the first band is about 0.2 units of β lower than the equivalent cyclopropane orbitals. Since there are two overlapped bands, accurate slopes for β as a function of energy were not determined so the lower β of the V band may be due to the variation of β with photoelectron energy. It is also possible that this is a manifestation of the influence of the oxygen atom; in either case, we cannot clearly distinguish between the two effects. The $5a_1$ orbital density contours show great similarity to the correlated $3a'$ orbital of cyclopropane.⁵⁵ The β 's of band VI are virtually identical for the $^1b_1\pi(\text{C-H})$ orbital of ethylene oxide and the $1a''_2 \pi(\text{C-H})$ orbital of cyclopropane to which it is correlated 0.65 ± 0.1 vs. 0.68 ± 0.04 , respectively. This indicates that either β is independent of energy in this region or that the effect of oxygen substitution fortuitously cancels the energy

variation of β , the data is not sufficiently clear to distinguish between the two effects. As in cyclopropane Schweig and Thiel²⁸ have used intensity arguments to suggest that the assignment of the last two bands be reversed, but by analogy to cyclopropane we concur with the generally accepted assignments as predicted by both *ab initio* and semiempirical calculations.^{27,48,50,51,54,56}

c) *Ethyleneimine*

With ethyleneimine even more symmetry is removed when compared to cyclopropane or ethylene oxide. Accordingly the photoelectron spectrum shown in figure 4 becomes more complex. Table 3 summarizes the IP's and β 's as determined by the present study.

Band I of the ethyleneimine spectrum appears at 9.85 eV with a measured $\beta_{\text{vert}} = 0.43 \pm 0.09$ and has been assigned to the 8a' orbital. This correlates with the 1e'' state of cyclopropane and displays a similar value of β . The value of β reported for this band is much lower than that reported for the analogous band in pyrrole¹ ($\beta_{\text{vert}} = 1.09 \pm 0.06$). This difference may be due to lack of π contributions to the orbital which may be present in pyrrole.

From approximately 11 eV to 14 eV there is a broad band with three distinct maxima at 11.81, 12.70 and 13.47 eV, respectively. These have been assigned to the 4a'', 7a', and 3a'' orbitals, respectively. β drops over this region with the β_{vert} being 0.55 ± 0.06 , 0.55 ± 0.03 , and 0.17 ± 0.07 for the three bands, respectively. The 4a'' and 7a' σ -type orbitals both correlate with the cyclopropane 3e' band and thus it is not unreasonable to expect them to display similar β 's. The β 's for the first two bands in this region also agree with that for the cyclopropane 3e' band if one takes into account the energy-dependence of β observed in the latter. The

predicted value of the ethyleneimine β using an energy extrapolation of the cyclopropane results is about 0.59 which is within the experimental error of the observed value. Band III has been assigned to the $3a''$ $\pi(\text{CH})$ orbital and displays a β of 0.17 ± 0.07 . This measurement is lower than the value of 0.32 ± 0.05 for the $1e''$ cyclopropane band to which it is correlated but is closer to the 0.27 ± 0.03 observed for the $1a_2$ band in ethylene oxide to which it is also correlated. From the molecular electron density diagrams⁵⁵ one can see that their orbitals are almost exclusively localized on the CH_2 groups and one would suspect that the hetero atoms would have little effect on it. It may be that this is just a manifestation of the dependence of β on electron energy although the small energy change between the correlated states in this series is rather small (~ 1.1 eV).

Bands V and VI correlate with the $3a_1'$ and $1a_2''$ states in cyclopropane and the $5a_1$ and $1b_2$ states in ethylene oxide. These states have been assigned to the $6a'$ and $5a'$ orbitals, respectively. These states are not overlapped in this molecule in contrast to cyclopropane and ethylene oxide. The β 's for these bands are 0.83 ± 0.04 and 0.84 ± 0.07 respectively. Surprisingly, the large contrast observed in the β values for the other two molecules in this series is not present here. These states correspond to internal $\sigma(\text{C}-\text{C})$ and $\sigma(\text{CH}_2)$ orbitals, respectively. Observation of the orbital diagrams⁵⁵ shows similar behavior to the states to which they correlate in cyclopropane and ethylene oxide. It is possible that this is due to the energy dependence of β but is most likely due to some as yet undetermined effect of the NH group on these orbitals. Again we concur with the energy ordering predicted by the theoretical calculations.^{27,45,48,50,51,54}

IV. SUMMARY AND CONCLUSION

We have obtained the photoelectron spectra of cyclopropane, ethylene oxide, and ethyleneimine using HeI radiation and at scattering angles ranging from 45° to 120°. The anisotropy parameter, β , has been determined for ethylene oxide and ethyleneimine for the first time and has been used to confirm the previous orbital assignments and correlation diagrams within this series, suggesting that π -type bonding does not contribute significantly to the overall structure of this molecule. This is consistent with the idea that many of the "conjugative" properties observed for these three-membered rings may be purely due to the high energy levels of the orbitals involved. No effects of autoionization on the angular distributions were observed.

REFERENCES

- 1) J. A. Sell and A. Kuppermann, Chem. Phys. **33**, 367 (1978).
- 2) C. Utsunomiya, T. Kobayashi, and S. Nagakura, Bull. Chem. Soc. Jap. **51**, 3482 (1978).
- 3) M. N. Piancostelli, P. R. Keller, J. W. Taylor, F. A. Grimm and T. A. Carlson, J. Amer. Chem. Soc. **105**, 4235 (1983).
- 4) J. Cooper and R. N. Zare, J. Chem. Phys. **48**, 942 (1968).
- 5) J. Cooper and S. T. Manson, Phys. Rev. **177**, 157 (1969).
- 6) J. Cooper and R. N. Zare in *Lectures in Theoretical Physics*, edited by S. Gelfman, K. Mahanthappa, and N. Britten (Gordon and Breach, New York, 1969) p. 317.
- 7) R. M. White, T. A. Carlson, and D. P. Spears, J. Electron Spect. **3**, 59 (1974).
- 8) T. A. Carlson and C. P. Anderson, Chem. Phys. Lett. **10**, 561 (1971).
- 9) D. M. Mintz, Ph. D. Thesis, California Institute of Technology, Pasadena, CA (1976).
- 10) D. C. Mason, D. M. Mintz, and A. Kuppermann, Rev. Sci. Inst. **48**, 926 (1977).
- 11) D. Mehaffy, P. R. Keller, J. W. Taylor, T. A. Carlson, M. O. Kraus, F. A. Grimm and J. D. Allen, J. Elect. Spect. **26**, 213 (1982).
- 12) A. de Meigere, Angew. Chem. Int. Ed. **19**, 809 (1979).
- 13) R. Gleiter, Topics Curr. Chem. **86**, 197 (1979).
- 14) J. E. Houston and R. R. Rye, J. Chem. Phys. **74**, 71 (1981).
- 15) A. D. Walsh, Nature **159**, 167 (1947).

- 16) A. D. Walsh, *Nature* **159**, 712 (1947).
- 17) A. D. Walsh, *Trans. Farad. Soc.*, **45**, 179 (1949).
- 18) Th. Förster, *Z. Phys. Chem.*, **B43**, 58 (1939).
- 19) C. A. Coulson and W. E. Moffitt, *J. Chem. Phys.* **15**, 151 (1947).
- 20) C. A. Coulson and W. E. Moffitt, *Philos. Mag.* **40**, 1 (1949).
- 21) E. Honegger, E. Heilbronner, A. Schmelzer, and W. Jian-Qi, *Isr. J. Chem.* **22**, 3 (1982).
- 22) E. Honegger, E. Heilbronner, and A. Schmelzer, *Nouv. Chem.* **6**, 519 (1982).
- 23) F. J. Leng and G. L. Nyberg, *J. Elect. Spect.* **11**, 293 (1977).
- 24) D. W. Turner, C. Baker, A. D. Baker, and C. R. Brundle, *Molecular Photoelectron Spectroscopy*, (Wiley-Interscience, New York, 1970) pp. 203-213.
- 25) G. Bieri, F. Burger, E. Heilbronner and J. P. Maier, *Helv. Chim. Acta.* **60**, 223 (1977).
- 26) M. J. S. Dewar and S. P. Worley, *J. Chem. Phys.* **50**, 654 (1969).
- 27) H. Basch, M. B. Robin, N. A. Kuebler, C. Baker, and D. W. Turner, *J. Chem. Phys.* **51**, 52 (1969).
- 28) A. Schweig and W. Thiel, *Chem. Phys. Lett.* **21**, 541 (1973).
- 29) A. W. Potts and D. G. Streets, *J. Chem. Soc. Farad. Trans. II* **70**, 875 (1974).
- 30) A. W. Potts, T. A. Williams, and W. C. Price, *Farad. Disc. Chem. Soc.* **54**, 104 (1972).
- 31) N. Bodor, M. J. S. Dewar, W. B. Jennings, and S. D. Worsley, *Tetrahedron* **26**, 4109 (1970).

- 32) K. Yoshikawa, M. Hashimoto, and I. Morishimo, *J. Amer. Chem. Soc.* **96**, 288 (1974).
- 33) D. S. C. Yee, A. Hamnett, and C. E. Brion, *J. Elect. Spec.* **8**, 291 (1976).
- 34) M. I. Al-Joboury and D. W. Turner, *J. Chem. Soc.* 4434 (1964).
- 35) D. H. Ave, H. M. Webb, W. R. Davidson, M. Vidal, M. T. Bowers, H. Goldwhite, L. E. Vertal, J. E. Vertal, J. E. Douglas, P. A. Kollman, and G. L. Kenyon, *J. Amer. Chem. Soc.* **102**, 5151 (1980).
- 36) S. Evans, P. J. Joachim, A. F. Orchard and D. W. Turner, *Int. J. Mass. Spec. and Ion Phys.* **9**, 41 (1972).
- 37) E. Lindholm, C. Fridh, and L. Åsbrink, *Farad. Disc. Chem. Soc.* **54**, 127 (1972).
- 38) G. Bieri, L. Åsbrink, and W. Von Niessan, *J. Elect. Spect.* **27** 129 (1982).
- 39) R. Krässig, D. Rienke and H. Barmgärtel, *Ber. Buns. Gells.* **79** 116 (1975).
- 40) K. Johnson, I. Powis, and C. J. Danby, *Chem. Phys.* **70**, 329 (1982).
- 41) J. R. Collins and G. A. Gallup, *J. Amer. Chem. Soc.* **104**, 1530 (1982).
- 42) E. Haselbach, *Chem. Phys. Lett.* **7**, 428 (1970).
- 43) C. G. Rowland, *Chem. Phys. Lett.* **9**, 169 (1971).
- 44) F. A. Carlson, G. E. McGuire, A. E. Jonas, K. L. Cheng, C. P. Anderson, C. C. Lu, and B. P. Pullen in *Electron Spectroscopy*, edited by D. A. Shirley (North-Holland, Amsterdam 1972) p. 207.
- 45) D. T. Clark, *Theor. Chim. Acta* **15**, 225 (1969).
- 46) E. Kochanski and J. M. Lehn, *Theor. Chim. Acta* **14**, 281 (1969).
- 47) A. Skancke, *J. Molec. Struct.* **30**, 95 (1976).

- 48) W. Von Niessen, L. S. Cederbaum, and W. P. Kraemer, *Theor. Chim. Acta* **44**, 85 (1977).
- 49) H. Marsman, *Tetrahedron* **27**, 4377 (1971).
- 50) D. T. Clark, *Theor. Chim. Acta* **10**, 111 (1968).
- 51) C. Fridh, *J. Chem. Soc. Farad. Disc. 2* **75**, 993 (1979).
- 52) E. Lindholm, C. Fridh, and L. Åsbrink, *Farad. Disc. Chem. Soc.* **54**, 127 (1972).
- 53) G. Bieri, L. Åsbrink, and W. Von Niessen, *J. Elect. Spect.* **27**, 129 (1982).
- 54) P. D. Mollere and K. N. Houk, *J. Amer. Chem. Soc.* **99**, 3226 (1977).
- 55) W. L. Jorgensen and L. Salem, *The Organic Chemistry Book of Orbitals* (Academic Press, New York 1973) pp. 153-159.
- 56) D. P. Chang, F. G. Herring, and Denis McWilliams, *J. Chem. Soc. Farad. Trans. 2* **70**, 193 (1974).

TABLE I. Cyclopropane

Orbital Assignment	Vertical IPs (eV)		β		β_{vert} (previous work) ^a
	This work	Previous work	β_{vert}	β range across band	
Band I 3e'	<10.51, 11.26 ^b	<10.53, 11.3 ^c <10.6, 11.3 ^{d,e} <10.3, 11.3 ^f	.46 \pm .07 .44 \pm .10	.21 \pm .09 - .71 \pm .15	.60 - .50 \pm .05
Band II 1e''	12.94	13.2 ^{c,d} 13.0 ^{e,f}	.32 \pm .05	.23 \pm .08 - .56 \pm .10	.43 \pm .05
Band III 3a'	15.74	15.7 ^{c,d,e} 15.6 ^f	1.18 \pm .05	.43 \pm .15 - 1.31 \pm .159	1.25 \pm .05
Band IV 1a' ₂	16.66	16.7 ^c 16.5 ^d 16.6 ^{e,f}	.67 \pm .04	- - -	.65 \pm .10
Band V 2e'	19.51	19.3 ^d 19.5 ^{e,f}	.40 \pm .08	.25 \pm .10 - .64 \pm .10	.90 \pm .10

a) ref 23

b) numbers in brackets refer to both components of Jahn-Teller split band

c) ref 27

d) ref 36

e) ref 25

f) ref 37

g) range is for both bands III and IV since they overlap

TABLE 2. Ethylene Oxide

Orbital Assignment	Vertical IPs (eV)		β		β_{vert} (previous work)
	This work	Previous work	β_{vert}	β range across band	
Band I 2b ₂	10.57	10.57 ^{a,b} 10.56 ^c	.36±.05	.31±.04 - .40±.06	---
Band II 6a ₁	11.77	11.7 ^a 11.85 ^{b,c}	.38±.07	.08 - .52±.14	---
Band III 2b ₁	13.75	13.7 ^a 14.0 ^b 13.73 ^c	.11±.06	.02±.09 - .26±.14 ^d	---
Band IV 1a ₂	14.23	14.2 ^a 14.0 ^b 14.16 ^c	.27±.03	---	---
Band V 5a ₁	16.51	16.6 ^{a,b} 16.52 ^c	.99±.06	.40±.04 - 1.17±.09 ^e	---
Band VI 1b ₂	17.31	17.4 ^{a,b} 17.2 ^c	.65±.10	---	---

a) ref 27

b) ref 38

c) ref 35

d) range is for both bands III and IV since they overlap

e) range is for both bands V and VI since they overlap

TABLE 3. Ethylene Imine

Orbital Assignment	Vertical IPs (eV)		β		β_{vert} (previous work)
	This work	Previous work	β_{vert}	β range across band	
Band I 8a'	9.85	9.8 ^a 9.85 ^{b,d} 9.83 ^c	.43±.09	.13±.23 - .65±.05	---
Band II 4a"	11.81	11.8 ^a 11.9 ^{b,d} 11.79 ^c	.55±.06	.08±.11 - .71±.05 ^e	---
Band III 7a'	12.70	12.5 ^a 12.16 ^c 12.7 ^d	.55±.03	---	---
Band IV 3a"	13.47	13.5 ^a 13.45 ^c 13.6 ^d	.17±.07	---	---
Band V 6a'	15.93	15.9 ^a 15.69 ^c 16.0 ^d	.83±.09	.50±.10 - .83±.09	---
Band VI 5a'	17.47	17.4 ^a 17.19 ^c 17.5 ^d	.84±.07	.65±.07 - .86±.06	---

- a) ref 27
- b) ref 32
- c) ref 35
- d) ref 38
- e) range is for bands II, III, and IV since they overlap

FIGURE CAPTIONS

Figure 1. Block diagram of the variable-angle photoelectron spectrometer. He, cylinder of ultra-high purity helium; ZT, liquid nitrogen cooled zeolite trap for lamp helium supply; RB, lamp ballast resistor; LPS, lamp dc power supply; SC, sample chamber, PC, photocathode for light flux measurements; CL, electron lens elements; ANALYZER, hemispherical electron energy analyzer; ML, electron lens element; S, Spiraltron electron multiplier; CPS, Spiraltron cathode power supply; APS, Spiraltron anode power supply; R. C., resistance and capacitance of differentiating network for Spiraltron.

Figure 2. Photoelectron spectrum (b) and variation of β with ionization potential (a) for cyclopropane using HeI (21.22 eV) radiation. The spectrum was obtained at a detector angle of 54.7 degrees.

Figure 3. Photoelectron spectrum (b) and variation of β with ionization potential (a) for ethylene oxide using HeI (21.22 eV) radiation. The spectrum was obtained at a detector angle of 54.7 degrees.

Figure 4. Photoelectron spectrum (b) and variation of β with ionization potential (a) for ethylene imine using HeI (21.22 eV) radiation. The spectrum was obtained at a detector angle of 54.7 degrees.

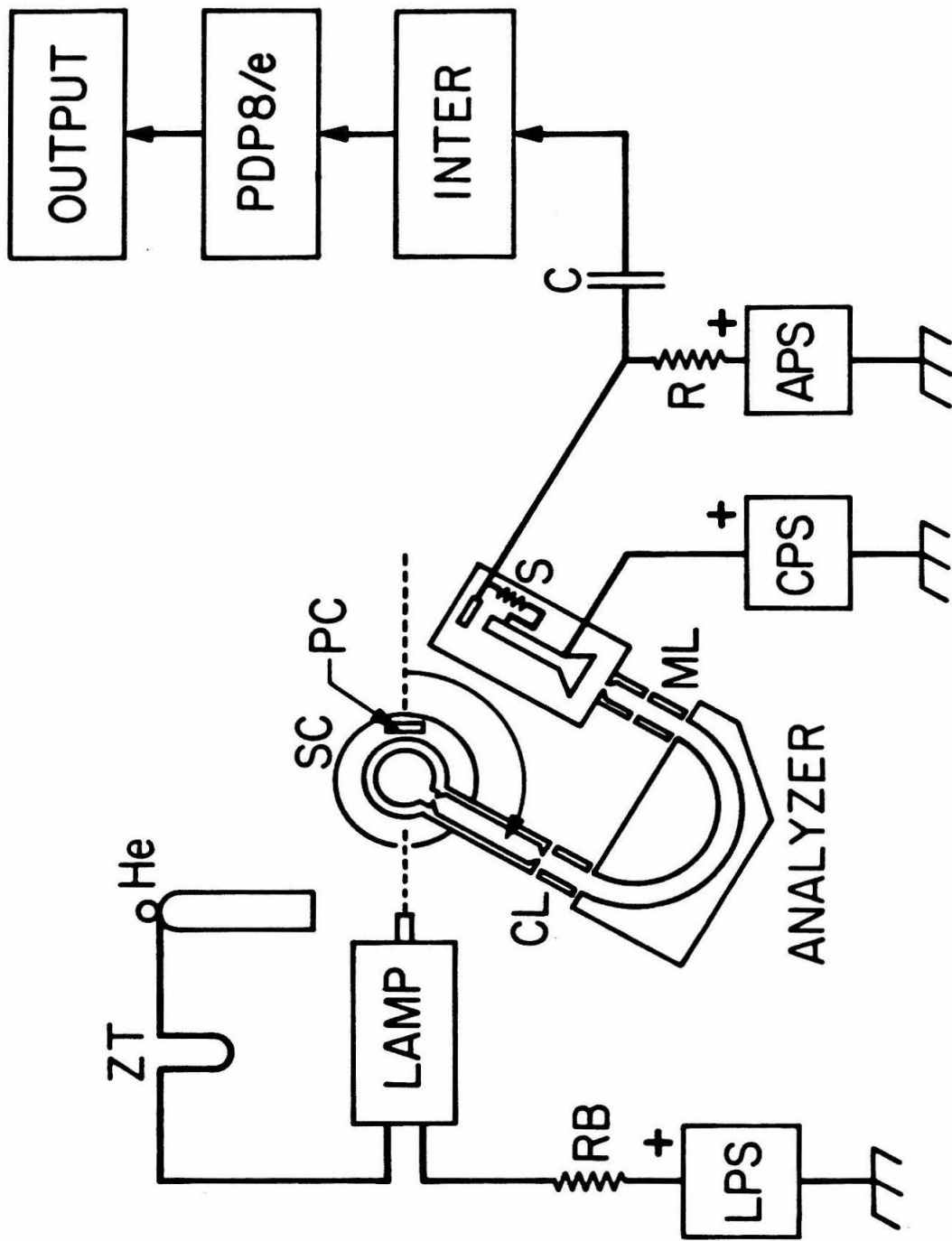


Figure 1.

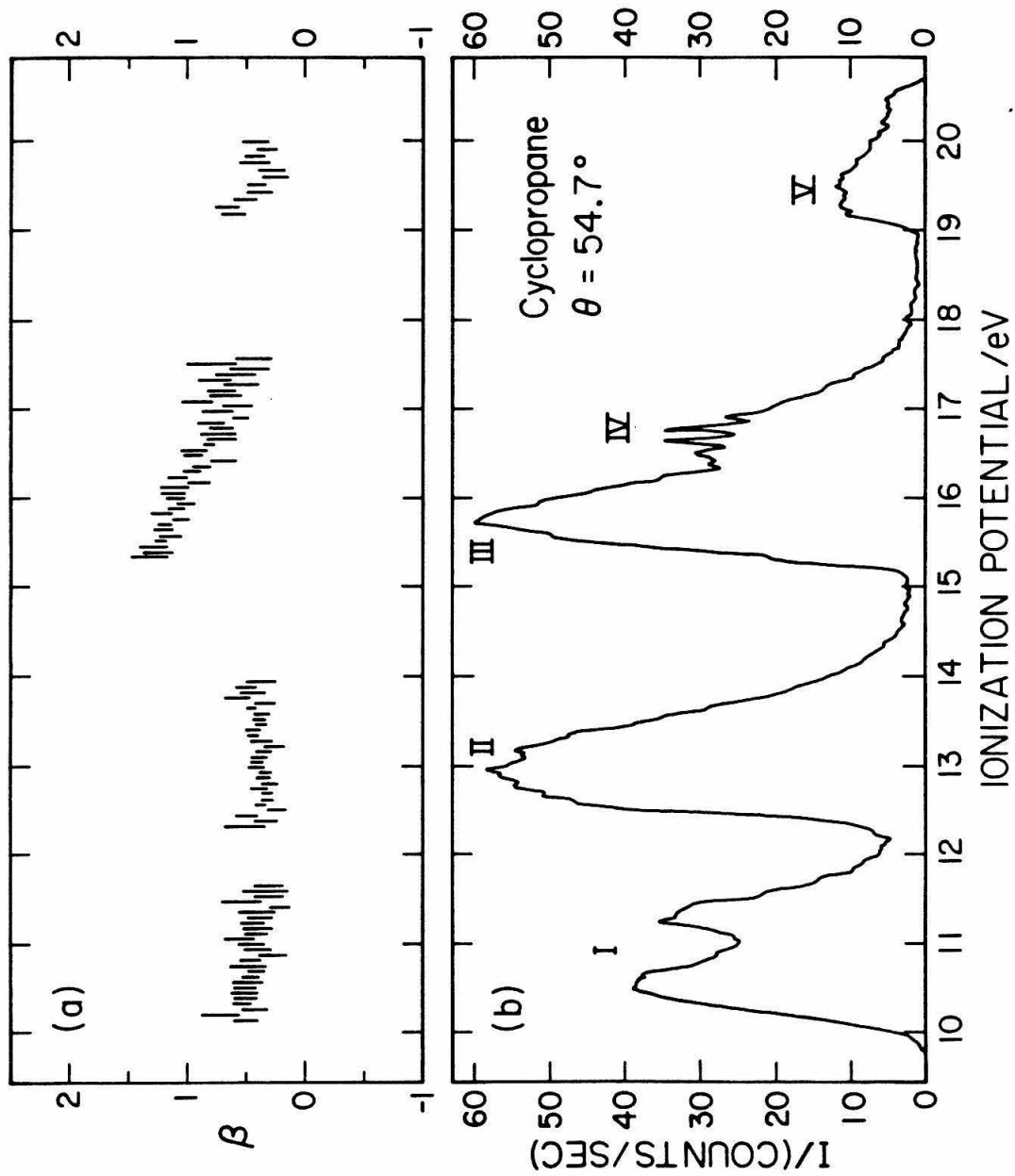


Figure 2.

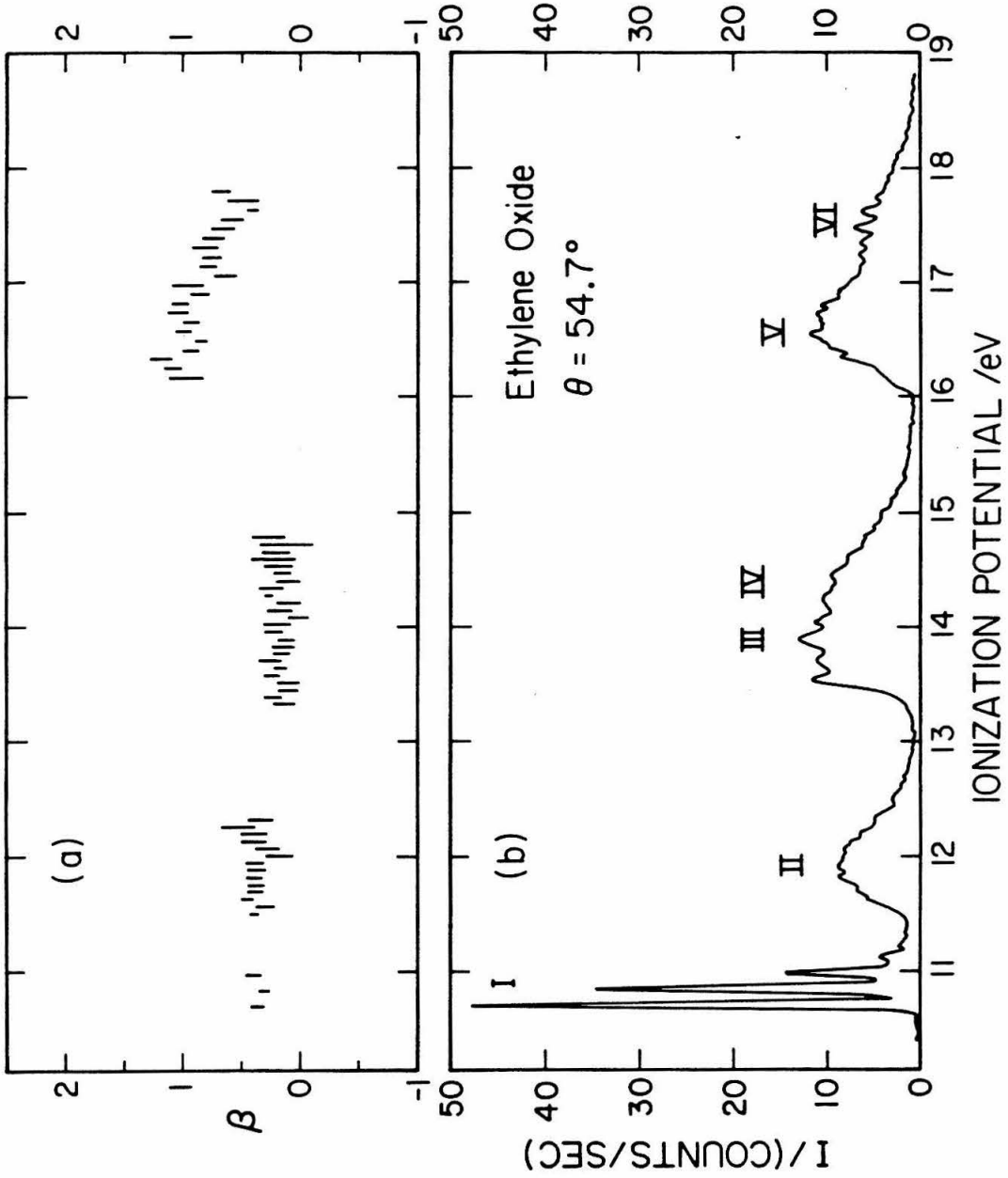


Figure 3.

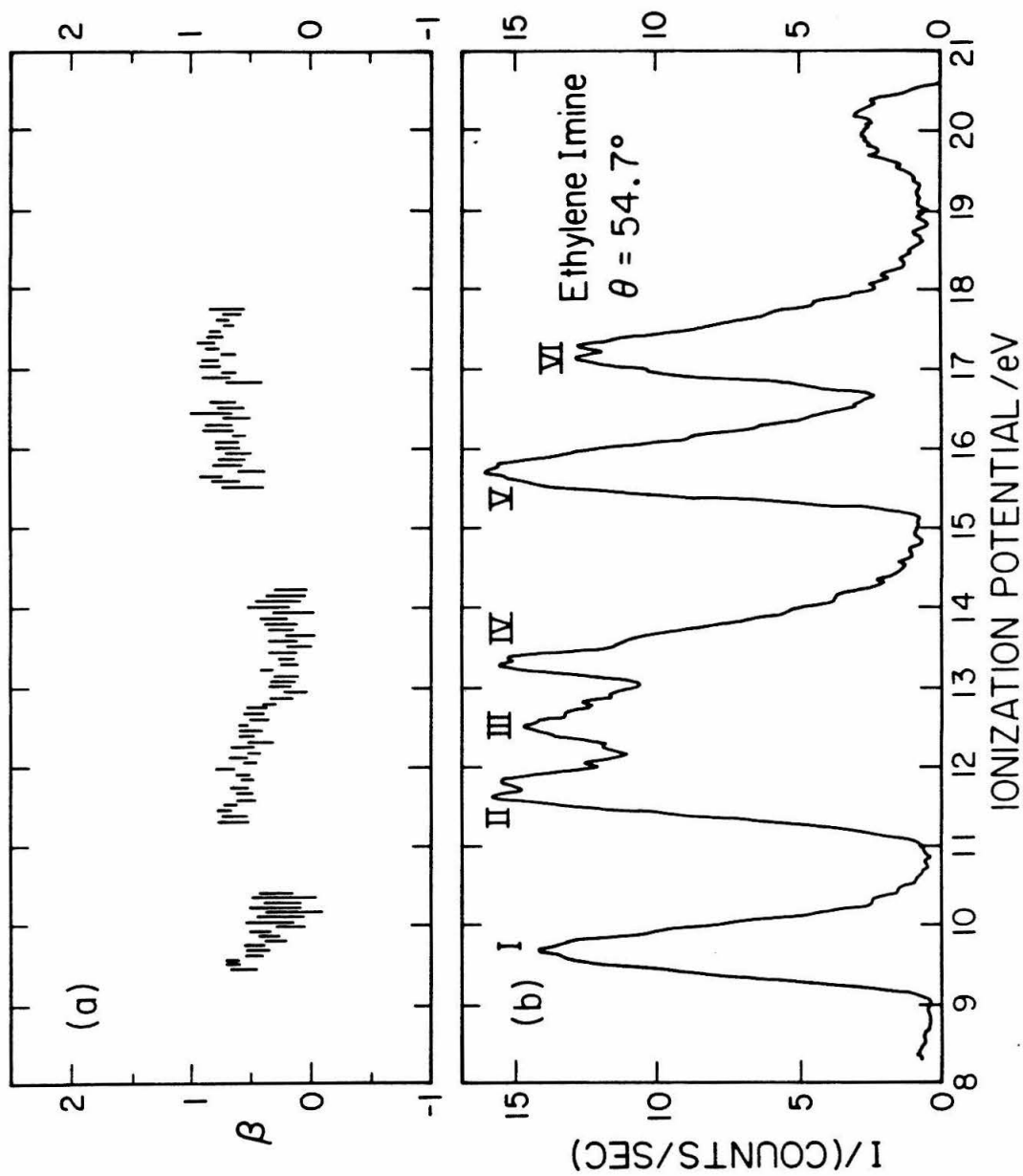


Figure 4.